Curtin University

WASM: MECE

"Monoethylene Glycol Distillation System Design Validation, Operation and Effluent Treatment".

**Sami Mohammed Zaboon Zaboon**

**This thesis is presented for the Degree of**

**Doctor of Philosophy**

**Of**

**Curtin University**

December 2019

This thesis contains no material which has been accepted for the award of any degree or diploma in any university or institution

Sami Mohammed Zaboon Zaboon

# Abstract

A regenerated MEG (Monoethylene Glycol) closed loop is a complex system involving various chemical and physical processes. The Chevron sponsored bench-top scale closed loop MEG distillation regeneration/reclamation unit located at Curtin University can bridge the gap between individual laboratory scale tests to a comprehensive testing protocol that will enable laboratory scale testing to be correlated to field conditions, thus improving confidence in the selection of production chemical additives.

The facility is designed and operated to use realistic approximations of production fluids, such as condensate mixtures and formation water/brines to simulate conditions representative of an industrial MEG system. To avoid Health and Safety considerations no hydrocarbon gases, mercury or NORMs are simulated. Many parameters such as MEG inlet concentration, temperature of feed, rebiler temperature, MEG inlet mass flowrate and reflux ratio have been experimentally examined in order to reach the optimum conditions for the MEG distillation regeneration process. These results were then compared with the results obtained from HYSYS simulation.

A distillation unit was used to avoid losing MEG and reconcentrate it (i.e. > 80 wt. %). This process named Meg regeneration process that operates at atmospheric pressure. This study was planned to achieve number of experiments to optimize the operating conditions. The separating experiments of monoethylene glycol (MEG) from the water by using batch distillation has been focused on the relation between temperature and final MEG concentration. The experiments have covered a range of temperatures between (125-145 °C) in the presence of MEG solution at different concentrations, around (35-75%). These conditions can show and explain the influence of temperature on the final concentrations of MEG that discharges from the boiler, and minimize the MEG compound in the distilled water from the top. The reflux ratio is constant at total reflux rate. In addition, the pH values were at 7.6 – 8.4 for all experiments for the feed, distillate, and reboiler. The experiments at 55% wt. (MEG + water) operate ideally at 135°C, while 65% wt. (MEG + water) operated ideally at 140°C, finally at 75% wt. (MEG + water) operated ideally at 140°C. The analysis method used to recognise the final MEG concentration in the reboiler has showed values of 81, 84 and 86% respectively.

This work includes the building and operation of a packed bed distillation column system (bench scale laboratory plant), The components of the distillation system consist of, Carbon steel frame structure (3618mm height, 1250mm width, 685mm length), reboiler heater 5 KW, reboiler vessel 8-10 litre capacity, Two glass columns were connected in series one mater

each, condenser unit (60cm height, 2″ dimeter), reflux drum 5 litre, (feed, reflux and bottom product) pumps, solid filtration system 10 µ, Rich and Lean MEG tank 160 litre each and Measurement Systems.

The MEG benchtop facility was also used to simulate a number of different scenarios that are likely to occur in the field such as switchover between different corrosion management strategies. Four experiments with respect to switching over between corrosion control strategies have been executed. These strategies included:

1) Gorgon: pH stabilisation using MDEA to film forming corrosion inhibition (FFCI)
2) Gorgon: pH stabilisation using MDEA to film forming corrosion inhibition (FFCI) using an additional HCl dosing point to modify the reboiler feed's pH.

On the other hand, in case of the distillation column failures, monoethylene glycol passes into the Reflux drum unit leading to environmental issues. The wastewater has been treated with some active chemicals via adsorption process to remove the MEG before being disposed. Metal-organic frameworks (MOFs) (modified UiO-66* and UiO-66-2OH) were used for the effective removal of MEG waste from effluents of distillation columns (MEG recovery units). Batch contact adsorption method was used to study the adsorption behavior toward these types of MOFs. The experimental results were fitted by Langmuir and Freundlich models to describe the adsorption isotherms while the experimental results were fitted by pseudo-first order and pseudo-second order to describe the adsorption kinetic.

# Acknowledgement

# Table of Contents

# List of Figure

# List of Tables

# List of publications

*1.* *Recovery of mono-ethylene glycol by distillation and the impact of dissolved salts evaluated through simulation of field data.*

*Sami Zaboon, Adam Soames, Varun Ghodkay, Rolf Gubner and Ahmed Barifcani.*

*In Journal of Natural Gas Science and Engineering. Volume 44, August 2017, Pages 214-232 (Chapter 4).*

*2.* *Removal of Monoethylene Glycol from Wastewater by Using Zr-Metal Organic Frameworks.*

*Sami Zaboon, Hussein Rasool Abid, Zhengxin Yao, Rolf Gubner, Shaobin Wang and Ahmed Barifcani.*

*In Journal of Colloid and Interface Science. Volume 523, 1 August 2018, Pages 75-85 (Chapter 7).*

*3.* *Modelling and optimization of MEG recovery by distillation process.*

*Sami Zaboon, Fires Alnilam, Hasan Almohmmadawy, Rolf Gubner and Ahmed Barifcani,*

*Submitted to the journal, for publication (Chapter5)*

# Other publication

*1.* *Operation of a MEG pilot regeneration system for organic acid and alkalinity removal during MDEA to FFCI switchover.*

*Adam Soames, Edith Odeigah, Sami Zaboon, Stefan lglauer, Ahmed Barifcani,  and Rolf Gubner.*

*In Journal of Petroleum Science and Engineering. Volume 169, October 2018, Pages 1-1*

# 1. Introduction

The formation of the hydrates in pipelines that are transporting hydrocarbons represent a big concern for petroleum and gas processing industries, with vigorous economical impacts. Compounds of the hydrates are solid materials that are formed by hydrogen bonding and cage formation of light hydrocarbons, included acid gases like $H_2S$ and $CO_2$ pulled within the consolidated structure[1, 2]. The makeup of hydrates happens at low temperatures and high pressures environments when adequate water is present; these conditions are common for gas pipelines in offshore due to temperatures decreasing at sea bed and pipeline working under high pressures [3, 4]. Formation of the hydrate in gas processing systems can cause significant disarray for the process and flow assurance because of possible blockages with ripping on internals and installation [1, 5]. Figure 1-1 shows the formation of hydrate for natural gas transferred through pipeline.



Figure 1-1: Hydrate formation in natural gas transmission pipeline [6].

The frozen water crystalizes to form ice at temperature 0ºC or below. While hydrates are produced at temperatures above 0ºC under high pressures [7].
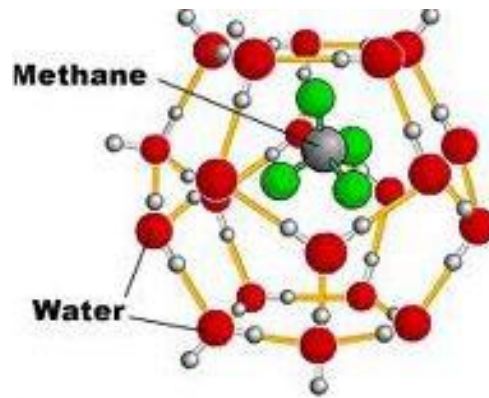
Figure 1-2: Example of the molecular structure of methane clathrate hydrate[8]

On the account of the hardness to eliminate the conditions needed for the formation of hydrates nowadays gas processing and transportation involves utilization of anti-hydrate agent as industrial application to prevent using the hydrate inhibitor injection at the well head in the upstream direction [5, 9]. Monoethylene glycol (MEG) is desirable thermodynamic inhibitor considered the best industry for hydrate prevention in the petroleum, with methanol being of a secondary choice [3]. The preference of MEG as inhibitor is because of operational, environmental and safety issues related to methanol. In addition, MEG is stable retrieved, and also recyclable back to the well head for extra hydrate prevention. Monoethylene glycol possesses the chemical formula $C_2H_6O_2$ and it can be synthesised from the ethylene oxide hydrolysis, while ethylene oxide is produced from oxidation of ethylene [10]. It is reported that production of monoethylene glycol is 20 million tons annually in the world, based on demand it will increase to reach 28 million tons/year by Shell Global [11]. MEG is mainly utilized in the production of polyester fibres. Furthermore it is applied in industrial application as anti-freeze agent and flow insurance factor. For Chevron's Gorgon project in WA, MEG use represents approximately 10% of the world's monoethylene glycol production that is produced from ethylene oxide hydrolysis. The cost of MEG as anti-hydrate agent is reported by Sloan [1].

Monoethylene glycol regeneration is as a required step because of the quantities consumed for providing control of the hydrates, in the downstream sector [5]. MEG is mainly recycled in a process of two-steps, implemented by recycling and retrieval. During this process, the MEG saturated with water gets heated to remove any extra water purifying MEG to 80-90%[12]. The most basic regeneration unit consists of a flash drum, re-boiler, a fixed tower and on top a condenser [13]. After regeneration,

recovery is performed on the MEG to eliminate the dissolved salts prior to MEG recycling process back to the well head upstream.

The processing and the running of monoethylene glycol recovery system can incorporate three steps depending on the amount of salts present in the rich MEG solution. When no salts separate during these processes a distillation tower is used. For regeneration when salts precipitate, either a MEG distillation plus reclamation unit is used according to the amount of rich MEG to be treated [12, 14]. During MEG recovery process, a tower typically uses inner packing because of the pressure dropping and high performance of separation. The packing tower design can be carried out either by units transferring ideal or estimation of height equivalent versus to theoretical panels joined with a standard carrier tower assessment of the required number over equilibrium steps. The main scope of the current research is design. The goal of simulation and corresponding computer work was to assess the efficiency of the laboratory scale MEG tower along with the dissolved salts effect on the tower efficiency to achieve pure MEG. The importance of this work a corresponds to industrial MEG restore by distillation wherever these salts are usually experienced. HYSYS simulation precisely predicts the action of these salts on the lean MEG purity and this is significant for MEG processing systems design and maintain also its purity during the processes.

## 1.1 Outline of Thesis

This thesis contains nine main chapters. Each of the chapters is started with a brief introduction to outline the contents and closes with a concise summary to highlight the major points. These are followed by nomenclature, references, and appendices.

Chapter 1: Introduction

This chapter gives an overview, the objectives of the project and the background of the study which describes the contribution of previous researchers in this area as well as the present knowledge about the topic. It ends with an outline of the thesis chapter.

Chapter 2: Literature Review

This chapter reviews the literature related to the design of the distillation unit, number of theoretical stages, minimum reflux, optimum reflux ratio, packed column and types of packing. This chapter also reviews the literature on the stages of the manufacturing and uses of monoethylene glycol as well as the process of recovery.

Chapter 3: MEG Regeneration Pilot Plant and Equipment details

This chapter focuses on the design and construction of the distillation unit. The column was designed and constructed by the Curtin Corrosion Engineering Industry Centre (CCEIC). It was also simulated using HYSYS software to suit the operating conditions of the Distillation column, Re-boiler vessel and the Reflux drum.

Chapter 4: Recovery of monoethylene glycol by Distillation Column.

This chapter is related to investigate the operation of a packed distillation column and analyse its performance during the separation of mono-ethylene glycol from water. Related to this chapter a research paper was published titled (Recovery of mono-ethylene glycol by distillation and the impact of dissolved salts evaluated through simulation of field data).

Chapter 5: Modelling and optimization of MEG recovery by distillation process.
In this chapter the study of operational conditions for the recovery of monoethylene glycol are studied through changes in temperature, concentration, feed and reflux rate by HYSYS simulation and then followed by Practical experimental data.

Chapter 6: Case Studies

In this chapter, four different experiments with respect to switching over option among a number of corrosion control strategies were performed as follow:

1. Gorgon: pH stabilisation using MDEA to film forming corrosion inhibition (FFCI)
2. Gorgon: pH stabilisation using MDEA to film forming corrosion inhibition (FFCI) using an additional HCl dosing point to modify the reboiler feed's pH.

The switching experiment between FFCI and MDEA in the case of Gorgon has been successfully achieved. The results have indicated that 50% of the MDEA was removed in the reclamation unit.

Chapter 7: Water treatment

In case of distillation column failures, mono ethylene glycol passes into the Reflux drum unit leading to environmental issues. The wastewater has been treated with some active chemicals via adsorption process to remove the MEG before being disposed. Further details will be discussed in this chapter. In this chapter a research paper was published under the title (Removal of Monoethylene Glycol from Wastewater by Using Zr-metal Organic Frameworks).

Chapter 8: Conclusions.
This chapter presents the Conclusions and summarises all the overall result achieved by the experiments.

# 2. Literature Review

## 2.1 Principles of Distillation

Distillation is one of the most useful chemical engineering separation methods. It is a process to separate a component from a mixture of components depending on their difference in the boiling points or volatility. The heating of volatile components in a mixture leads to vapour formation with a higher concentration of the lowest boiling point component (more volatility) compared to the liquid in which it is evolved [15]. However, when the vapour phase is to be brought to a low temperature by condensation, the less volatile component condenses with large ratio compared to more volatile component and this leads to be the feed contains higher boiling point material. The separation towers design precisely to the kind of component and the required product composition that would be practiced throughout the process. One of the main concerns with regards to the design is a proper selection of the kind of distillation tower. There are two common categories of towers, packing and tray towers. Both types have subdivisions according to the sort of using: for tray could be sieve valve or bubble cap among others, and random or structural packing for packed. Some design methodology, operations and drawbacks in packing and tray distillation tower will be mentioned in the following sections.

### 2.1.1. Vapour-Liquid Equilibrium (VLE)

Vapour-liquid equilibrium (VLE) records are imperative aspects of information about the behaviour of vapour and liquid levels all through distillation and forms the basis of calculations of towers works [16]. Vapour-liquid systems are classified either as non-ideal or ideal. Ideal liquids are common for homologous series having analogous molecular weights [16]. While at lower pressures, a mixture of the vapour phase can be approached following the ideal conditions. The idea of vapour-liquid equilibrium may be expressed numerically based on the relative volatilities or k-valves. In case of two components, the higher boiling point is taken as the reference. K value concept is to know the component tendency (i) to be vaporised as defined in eq (2-1), and evaluated k-value is indicative of the material that will be in high concentration in the vapour [15]. Reciprocally, the material in low level of K point has an extra capability to be in the liquid phase. The elements evaluated by the k-values inside a distillation

tower evaluate one volatile constituent relatively in relation to the other, this relation is defined by eq (2-2). The subscript i and j typically symbolize compounds within a multi-component distillation process, for two component system they are distinctive 1 and 2 for the lower and heavier elements.

$$Ki = \frac{mole\ fraction\ of\ compnent\ i\ in\ vapour\ phase}{mole\ fraction\ of\ component\ i\ in\ liquid\ phase} \qquad (2\text{-}1)$$

$$\alpha = \frac{Ki}{Kj} \qquad (2\text{-}2)$$

The relative volatility of binary systems with respect to each other can be used to obtain numerical benefits in distillation. The α is expressed via eq (2-2) as the ratio between K values for the higher and lower volatile components and as such has to be equal to or greater than one [15]. Means isolation of more volatile components will be facilitated for performing via distillation. Moreover, a low α reaching unity will imply the difficulty of separation. For two component systems the relative volatility can be defined as in eq (2-3). Furthermore, eq (2-4) gives the VLE curve production. Eq (2-4) refers to greater mole fraction of volatile components within the gas phase as function of the liquid phase and relative volatility. This relation is shown in two component design strategies via x-y diagram.

$$\alpha 1,2 = \frac{K1}{K2} = \frac{y1}{x2}\left(\frac{1-x1}{1-y1}\right) \qquad (2\text{-}3)$$

$$y1 = \frac{\alpha 1,2 x1}{1+(\alpha 1,2-1)\,x1} \qquad (2\text{-}4)$$

### 2.1.1.1. Phase diagrams

The development of phase diagrams may be used to define the vapour-liquid interaction inside two phase systems with the aid of plotting 2 of the 3 variables, pressure. Temperature or composition requires a constant number of the third [15]. Phase schemes are shown in Figure 2-1 including temperature versus mole fraction values. This can be facilitated to extract x-y plots for example. Figure 2-2, shows components system with the absence of relatively volatile two components. The scheme of P-xy and T-xy is mainly dependent on the composition of the volatile component in a dual system. This includes a view of x-y scheme that is obtained from both Px-y and Tx-y values of mole fractions for liquid and vapour components, x and y that are specific to temperature or pressure.

This has been achieved by a straight line plot from the y axis (specific pressure and temperature) to the dew point curve through the bubble point curve. A vertical line is drawn from each intercept point toward the x-axis. The intercept point that is determined by the vertical line on the x-axis corresponds to the fraction of liquid and vapour with specific temperature or pressure.
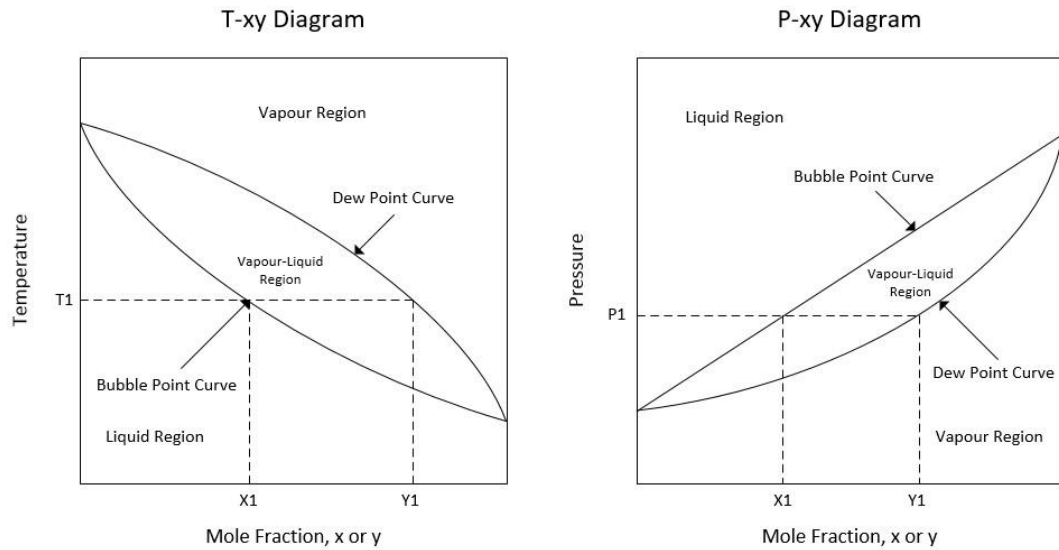


Figure 2-1: Pressure and Temperature (x-y) diagrams [15]
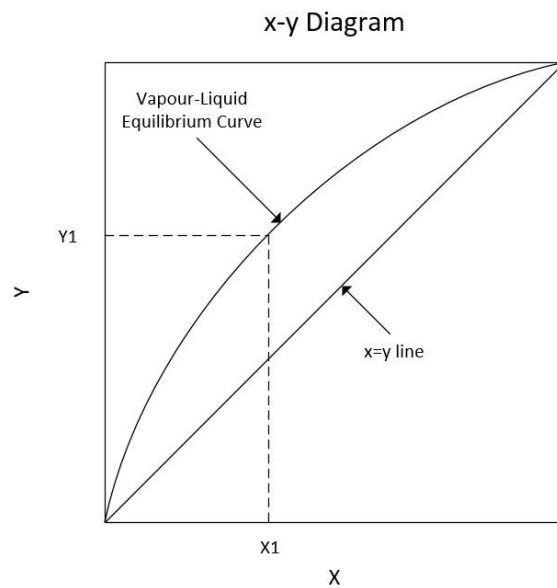


Figure 2-2: (X-Y) composition diagram [15]

### 2.1.2. Flash Distillation

Flash distillation method includes one separation step in which a portion of liquid feed vaporises via reducing its pressure. In this method, vapour is liberated from the liquid in an equilibrium state [17]. Mixture of liquid will be pumped over a hot plate to activate enthalpy and temperature of the liquid mixture prior to reducing its pressure via flowing through a valve. This will lead to partial liquid vaporization into a flash container. Flash distillation method is used in oil refineries heavily by flashing fluids into residual liquid and vapour flow [17]. In some applications, a liquid flow is flashed prior to an extra extension isolation method to avoid additional processing. For instance, light hydrocarbons in a rich MEG solution can be flashed before MEG recovery step in order to maintain hydrocarbons recovery in the top of the vapour.

### 2.1.3. Continuous Distillation with Reflux rate

In an effort to attain better purity products that can't be typically separated through flash or one stage distillation, the technique of continuous distillation throughout a multistage to be done. A flow diagram of a typical distillation tower equipped with a multistage needs is shown in Figure 2-3 (a) making use of withdrawal streams and multiple feed as shown in Figure 2-3 (b). In the distillation tower, mass transfer between the vapour and liquid phases, occurs through the vapour and liquid flows. By the tower, the vapour and liquid stream to an equilibrium state on packing, or plates, to achieve the mass transfer between the phases. Furthermore, throughout the distillation some parts of the bottom product and top product (distillate) are sent back to the tower through refluxes in an effort to achieve the counter-current flow of vapour and liquid inside the tower [18]. The procedure of reflux in the course of distillation permits non-stop mass transfer among the stages resulting in better purity of the bottom products and distillate. Additionally, distillation tower can be divided into sections referring to the rectifying and stripping divisions. The entered feed is called the stripping phase where high lighter materials are stripped from the liquid phase while the higher volatile materials are concentrated through the vapour phase and the heavier materials are recycled from the condenser by reflux [19].

### 2.1.3.1. Distillation column total and component mass balance
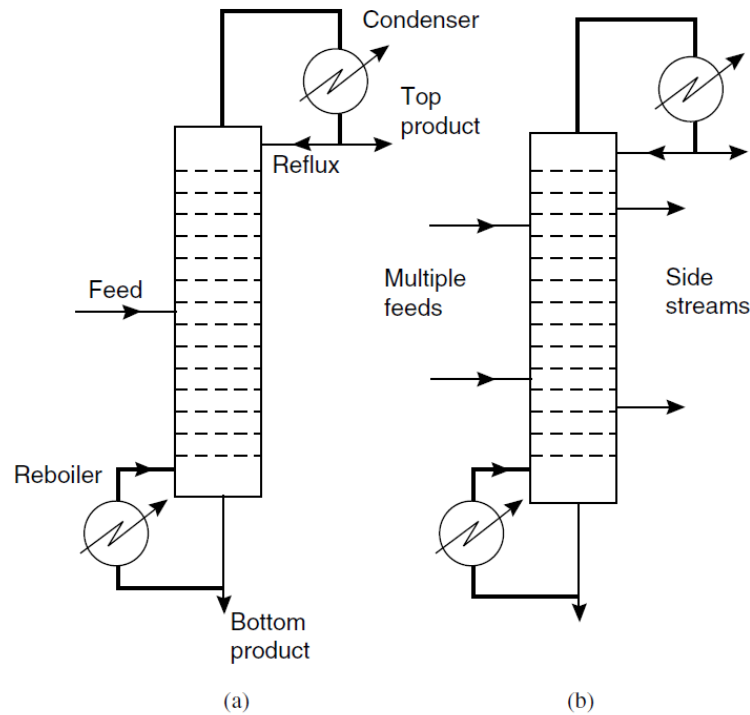


Figure 2-3: Continuous-multistage distillation tower, (a) basic tower, (b) side streams and multiple feed [19]

Inside the distillation towers, the procedure for design is calculation of the flow rates of the feed and product streams to the tower. Such estimation may be done by the use of the idea of the overall components or mass balance in the system. The feed rate and the more fraction of components of the inlet bottom and top products can be evaluated to know the overall material balance as shown in the following equations: eq (2-5) and (2-6) represent to a complete systems material and the component material equilibrium state respectively.

$$F = D + B \tag{2-5}$$

$$FXF = DXD + BXB \tag{2-6}$$

### 2.1.4. Reflux ratio (RR)

The RR is expressed to condense flow ratio by reflux to the very last product rate leaving the tower. This relation is represented by eq. (2-7). According to the R equation, the minimum required quantity of the RR value will be used in the process

at different stages. So the evaluation of the optimum RR is important to the optimization of a tower operation. In distillation towers which might be poorly insulated, unexpected changes within the outside surroundings such as surprising rain, could have direct effects on the internal RR of a tower and will have consequences to the overall performance of a tower and its manipulated systems [20].

$$R = \frac{\text{Flow returned as reflux, L}}{\text{Flow of distillate product, D}} \qquad (2\text{-}7)$$

### 2.1.4.1. Total Reflux

Overall reflux is the circumstance in which nothing of the tower product is removed throughout the work, as an alternative, the condensate is totally returned to the tower as reflux. Also, there is no feed enters to the tower while operating and the tower works as a batch tower. In total reflux operation, the number of separating stages needed to obtain a special purity is the minimum required to gain the separation [20].

### 2.1.4.2. Minimum Reflux

The minimal RR is the minimal quantity of reflux that needs to be supplied for the distillation to have a specific separation. The minimum RR is related to as optimum point at which the separation can be done with an unlimited number of theoretical stages [21]. The lowest reflux evaluates continuous distillation operation for multiple component via a design method known as Underwood shortcut. For a simple two components distillation system, the lowest reflux can be assessed, using the McCab-Thiele method as mentioned in eq. (2-8).

$$R_{min} = \frac{1}{\alpha-1}\left[\frac{X_D}{X_F} - \alpha\left(\frac{1-X_D}{1-X_F}\right)\right] \qquad (2\text{-}8)$$

### 2.1.4.1. Optimum Reflux Ratio (ORR)

In an industrial operation, the most effective RR is related to the ratio at which efficient separation may be done while minimising the overall cost. For a system, the elevation of the RR will coincide to a lowering in the number of theoretical stages needed to

obtain separation, also the cost related to tower production will decrease. Then again, a high RR will lead to excess vapour flow in the tower. Such increase could lead to growth within the utilities of each the condenser and re-boiler and so reason operating cost[16]. The exchange between operating cost and capital with regards to RR is illustrated in Figure 2-4. From it, can be seen that the best RR takes place while the total cost of a distillation tower is brought to minimum. Coker (2010) gives numerous policies by rule of thumb for evaluating the most advantages of the RR.
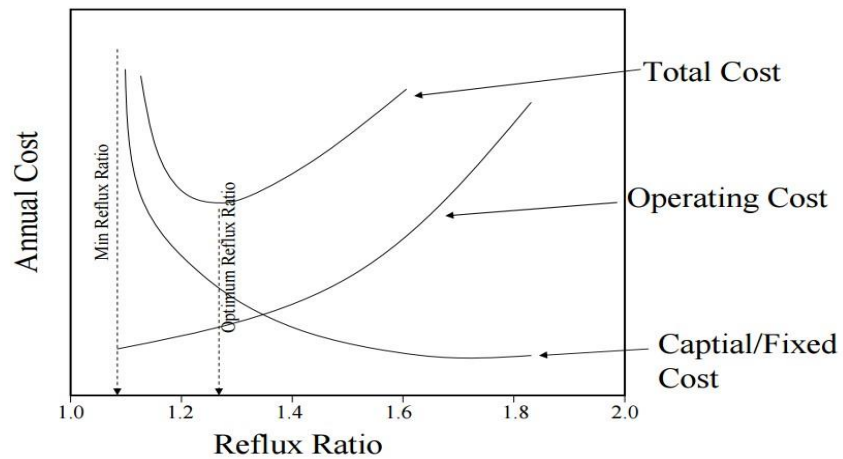


Figure 2-4: Scheme shows ratio for optimum reflux [17]

### 2.1.5. Choosing of Condenser Unit

Sometimes a partial type condenser is preferred when top product of vapour is required in the system and the minimal liquid feed is also required to achieve sufficient component to be condensed via reflux. Reflux forming through partial condenser reaches equilibrium state with vapour product flow and there will be an additional equilibrium step that separates within towers layout [19].

### 2.1.6. Design Methods of Binary Distillation

Sorel [22] improved the first theoretical equations for the analysis of easy, non-stop, steady state distillation process. This equation permits the evaluation of simple stage by stage two components distillation towers. Figure 2-5 (a) and limiting the system

boundary to consist of n stages and the material balance condenser the plate n is given with the aid of eq. (2-9).
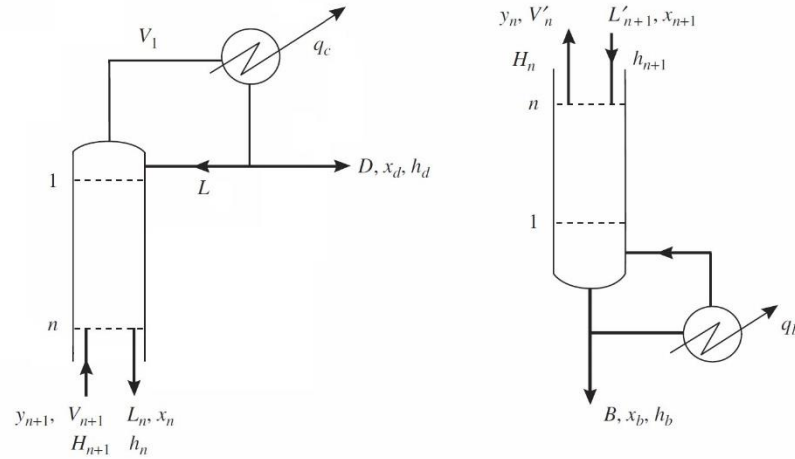


Figure 2-5: Tower compositions and flows, (a) above feed and (b) below feed [20]

$$Vn + 1 = Ln + D \qquad (2\text{-}9)$$

Where D represents to the distillation of the flow rate

$$Vn + 1yn + 1 = LnXn + DnXd \qquad (2\text{-}10)$$

Also Energy Balance, for total enthalpy stream is:

$$Vn + 1Hn + 1 = Lnhn = Dhd + qc \qquad (2\text{-}11)$$

Where $q_c$ is the removed heat from the condenser

Combining eqns. (9) and (10) we get:

$$y_{n+1} = \frac{Ln}{Ln+D}Xn + \frac{D}{Ln+D}X_d \qquad (2\text{-}12)$$

And Combining eqns. (9) and (11) we get:

$$V_{n+1}\ H_{n+1} = (Ln + D)\ H_{n+1} = L_nh_n + DhD + q_c \qquad (2\text{-}13)$$

The same procedure is used to the stripping part Figure 2-5 (b), eqns. (2-14) and (2-15).

$$n + 1 = \frac{Vn'}{Vn'{}_{l+B}} \, yn + \frac{B}{Vn'+B} \tag{2-14}$$

$$L'_n +1 h_{n+1} = (Vn' + B)h_{n+1} = V_{n'} H_n + Bh_B + q_b \tag{2-15}$$

Where B value is corresponding to the bottom quantity flow rate and qb represents the added heat via the re-boiler.

Sorel's [22] suggestions have been improved by Lewis [23] using the hypothesis of fixed molar over flow for avoiding the balanced heat equations evaluation. However, Sorel's proposal was not applied widely therefore it has been qualified with a quick graphical technique for binary systems developed by Ponchon [24]. The graphical evaluation idea was further improved to be more simple unless used for two components system where graphical evaluation is restricted. The significance of the graphical calculations strategies is the potential to understand by vision the mole fractions of materials for each stage compared to Sorel's suggestions, using x-y diagram as shown in Figure 2-6.
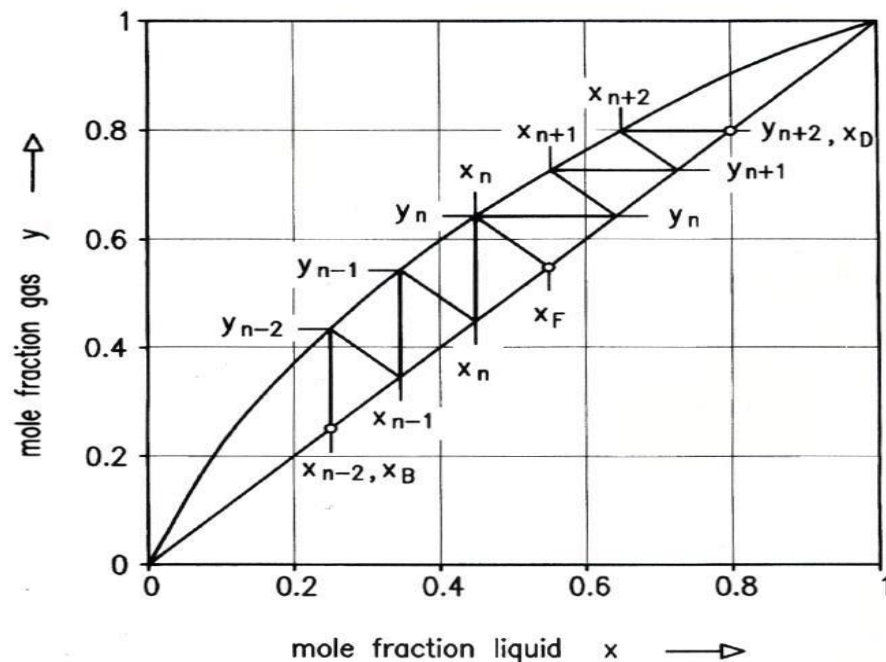


Figure 2-6: Diagram of mole fractions at vapour and liquid stage [18]

14

### 2.1.6.1. Lewis-Sorel Method

According to the developed equations by Sorel [22], at constant molar overflow, the liquid and vapour flow from each stage are assumed to be constant and the material balance equations may be used as follows in eqns. (2-16) and (2-17). Furthermore, eq. (2-17) can be written as eq. (2-18), where L and L' represent to Liquid flow rate constant, while V and V' refer to the vapour flow rate constant in stripping and rectifying parts respectively.

$$_{n+1} = \frac{L}{L+D} X_n + \frac{D}{L+D} X_d = \frac{L}{V} X_n + \frac{D}{V} X_D \tag{2-16}$$

$$X_{n+1} = \frac{V\prime}{V\prime+B} y_n + \frac{B}{V\prime+B} X_B \tag{2-17}$$

$$y_n = \frac{L\prime}{V\prime} X_{n+1} - \frac{B}{V\prime} X_B \tag{2-18}$$

The equations were based on the means of the Lewis-Sorel technique. Eqns. (2-16) and (2-18) supply the connection of the vapour with liquid components during equilibrium states corresponding to the stripping and rectifying sections. For any equilibrium state, the departing degree for the vapour and liquid components is evaluated by those relations [21]. Using the Lewis-Sorel technique for two component distillation calculations needs firstly to achieve fixed molar overflow rate to avoid heat equilibrium requirement for each state. Based on the constant of the molar overflow rate, mixture of the distillation components possesses a steady state of vaporization heat and its molar heating is to the feed components. Furthermore, the heating effects on the solution mixture can be ignored. In case of the molar over flow rate constant, every mole of the vaporized liquid from an equilibrium state requires an equal quantity of the vapour that is condensed at the same time. It has been reported that almost the constant of the molar flow rate is achieved when the two components are of the same nature, molecular weights and in case the heat solution is low [15]. The hypothesis of molar flow rate constant and the implementation of the Lewis-Sorel technique for designing secondary systems and it may be evaluated by inherent molar ratio heating for the pure components. The molar heating proportion gives a safe indicator to the degree of the heating impacts which limits the precision of the Lewis-Sorel technique [15]. In case of benzene-toluene or isobutane-butane with the equivalence of inherent heat proportions, the hypothesis of molar flow rate is acceptable, while it is less

acceptable for components with greater heat ratio like acetone-water and ammonia-water systems.

### 2.1.7. Design Methods of Shortcut Distillation

#### 2.1.7.1. Fenske Equation: Minimum Number of Stages

Fenske [25] found an equation for calculation of the minimal number of theoretical steps that is required for distillation tower operating at total reflux. This equation applies for binary and multi component systems and one model is shown in eq. (2-19). Derivation was based on the assumptions that the tower's Fenske equation stages were at equilibrium and α is constant [26].

$$N_{min} = \frac{\ln\left[\left(\frac{X_A}{X_B}\right)_{dist}\left(\frac{X_B}{X_A}\right)_{bot}\right]}{\ln\alpha_{AB}} \tag{2-19}$$

Where $X_A$ the more volatile material is mole fraction

$X_B$ refers to mole fraction for the less volatile material

$\alpha_{AB}$ is α component A relative to component B

#### 2.1.7.2. Underwood Equation: Minimum Reflux

An equation was derived by Underwood (1948) to estimate the minimum reflux ratio for more than one component distillation systems. Same as Fenske's equation, using Underwood equation can be applied for the case of two components system. Underwood equations results are consistent with the systems in which hypothesis of steady molar flow is valid and α value is constant [26]. Finding of the minimum RR, $R_{min}$ via eq (2-20) may be made by means of first evaluating eq (2-21) for the equation roots θ by a trial and error method.

$$\sum \frac{\alpha_i X_{i,D}}{\alpha_i - \theta} = R_{min} + 1 \tag{2-20}$$

$$\sum \frac{\alpha_i X_{i,F}}{\alpha_i - \theta} = 1 - q \tag{2-21}$$

Where *αi* denote to the proportional volatility of material (i) versus reference one.

Xi, D and Xi, F represented to the material concentration (i) at overheating and feeding and feeding respectively while θ is the equation's root.

On the other hand, for two components systems, the minimal reflux calculation is obtained from eq (2-22):

$$R_{min} = \frac{1}{\alpha-1}\left[\frac{X_D}{X_F} - \alpha\left(\frac{1-X_D}{1-X_F}\right)\right] \tag{2-22}$$

### 2.1.7.3. Gilliland Correlation: Number of Stages at Finite Reflux

So as to decide the ideal number of stages needed, an empirical correlation has been developed by Gilliland [27] to link the number of theoretical steps with limited RR to the minimal number of steps and the minimum RR [26]. Gilliland proposed a relationship graphically between $\{N-N_{min}\}/\{N+1\}$ as the y-axis values and $\{R-R_{min}\}/\{R+1\}$ as the x-axis values and the results can be analysed using stage by stage method. This relationship was improved by Liddle [28] ( see Figure 2-7) and illustrates Gilliland's preliminary calculation data for stage-by-stage and the fitted curve evolved is by using Liddle eqn. Molokanov [29] further refined Gilliland's graphical correlation expressing it in eq. (2-23).

$$\frac{N-N_{min}}{N+1} = 1 - \exp\left[\left(\frac{1+54.4(R-R_{min})/(R+1)}{11+117.2(R-R_{min})/(R+1)}\right)\left(\frac{(R-R_{min})/(R+1)}{\{(R-R_{min})/(R+1)\}^{0.5}}\right)\right] \tag{2-23}$$
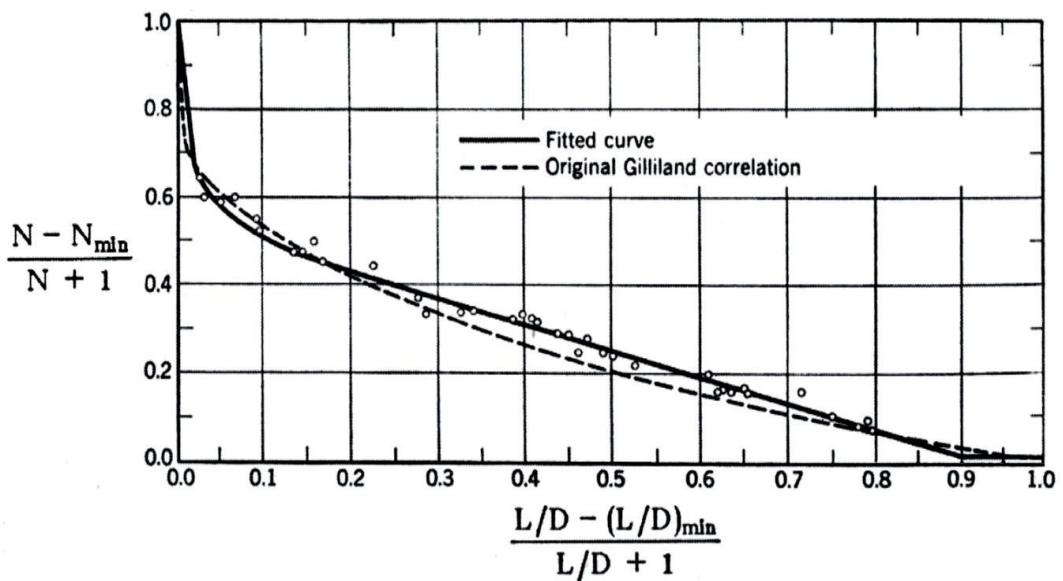


Figure 2-7: Diagram shows Gilliland's graphic correlation [28]

An assessment of the location of ideal feeding plate is performed by using the empirical correlation founded by Kirkbirde [30]. Calculation of the number of steps below and above the feed entering point step in combination with the number steps calculated by Gilliland can be applied to find the best feeding plate to go into the tower through eq. (2-24) and (2-25).

$$\log \frac{N_R}{N_S} = 0.2061 \log \left[ \left( \frac{X_B}{X_A} \right)_{Feed} \left( \frac{X_{A,bot}}{X_{B,dist}} \right)^2 \left( \frac{B}{D} \right) \right] \tag{2-24}$$

$$N_R + N_S = N \tag{2-25}$$

Where $N_s$ and $N_R$ refer to the number of steps in the stripping and rectifying sections respectively.

### 2.1.7.4. Erbar-Maddox Correlation: Number of Stages at Finite Reflux

The number of steps at limited reflux has been predicted by the Erbar-Maddox relationship that is considered to be a very accurate correlation [26]. Similarly to the Gilliland relationship, the Erbar-Maddox relationship needs to find the minimal reflux and the minimal number of steps through Underwood equation. The minimum number of stages may then be found by using Figure 2-8. Gilliland's proposal is more accurate and more proper to be used because it can be simply applied for computer calculations [see modified Molokanov eq. (2-23)].
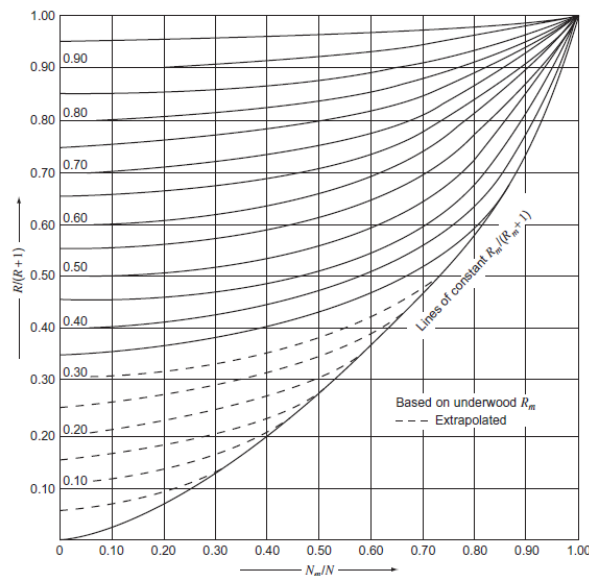


Figure 2-8: Correlation of Erbar-Maddox [31]

### 2.1.7.5. Optimum Reflux Ratio

A short-cut approach for finding the most appropriate RR may be achieved with the aid of evaluating the number of theoretical steps at a range of RRS. By drawing the number of steps needed for a known RR an obvious relationship may be found by means of Figure 2-9, where the number of stages needed reduces exponentially as the RR increases. A material balance among the number of stages the re-boiler and the condenser should be carried out and so an intermediary RR must be chosen. Figure 2-9 illustrates a simplified way to find the best reflux proportional by plotting the number of states versus RR plot in connection with a horizontal and vertical lines referring to the minimal RR and the number of steps at the overall reflux. A line with 45° is drawn from the intercept point of the vertical to the horizontal line and this point is the best RR value which may be determined that represents the number of steps.
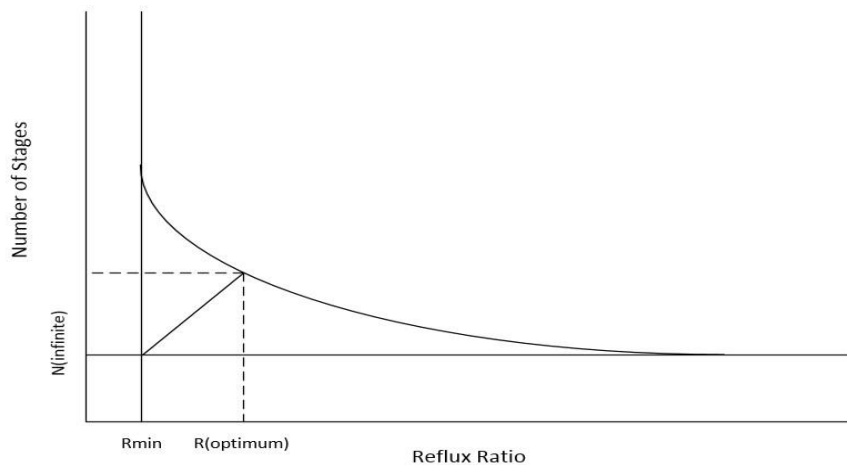


Figure 2-9: Optimum RR graphical representation

### 2.1.8. Packed Distillation

The use of packing in separation devices has come to be more and more common for distillation, gas absorption and liquid-liquid extraction operations. Packing method is another option for towers which give a considerable surface area for more efficient contact between the liquid and gas phases [15]. Packing distillation tower selection as opposed to trays is better and the isolation of the materials is fairly simple or the proper diameter tower is definitely small [17]. Packing is considered to be substantial for

small distillation towers including less than 75 cm diameter in which there is no installing and repair requirement for trays are not practicable because of safety restrictions of personnel working inside the tower for maintenance [32]. Moreover, packing is taken in to consideration of more benefit where corrosion control is important during the operation of the tower [15].

### 2.1.9. Packing Types

Packings used in distillation can be labelled into three types: dumped packings or random, structured or systematically organized packing and grid ones. Various packing designs have been used to meet the overall performance targets [15] such as:

- Giving a large surface area to give rise to the interfacial contact between the liquid phases and gas to ensure better efficiency of separation.

- Providing an open way to lower the gas flow resistance.

- Enhancing homogeneity distribution of liquid and vapour in the packing structure for obtaining high surface area and total area of packing to increase tower efficacy.

- Improving steady flow of vapour throughout the tower cross section.

Packing type used in a distillation system relies closely upon the goal to be achieved. Normally random packing is the better known and commonly used type of packing because of its overall reasonable costs and performance. Structured packing has been documented to increase mass transfer surface area at very high flow rates leading to an extra cost, therefore modification of structured packing may be required.

### 2.1.9.1. Random Packing

Random packing is composed of individually discrete fashioned pieces of different materials which can be 'dumped' or randomly packed into the tower to shape a random arrangement [15]. The packing is particularly designed in geometrical shapes that offer contact for mass transfer among phase surfaces between vapour and liquid. Random packing is frequently used within the tower by means of allowing the free-fall resting of the packing to float lightly in place in a tower filled with water [16]. Another option

of packing it can be by installing by hand into place without water filling in to the column depending on the size and the sort of packing. Packing randomly are available in different structures (see Figure 2-10) which range from saddles to rings for packing effectiveness enhancement. Packing size randomly is usually at the range of $1/8^{th}$ of the packing towers with diameter by 5 cm and this packing is considered to be the biggest recommended [20].
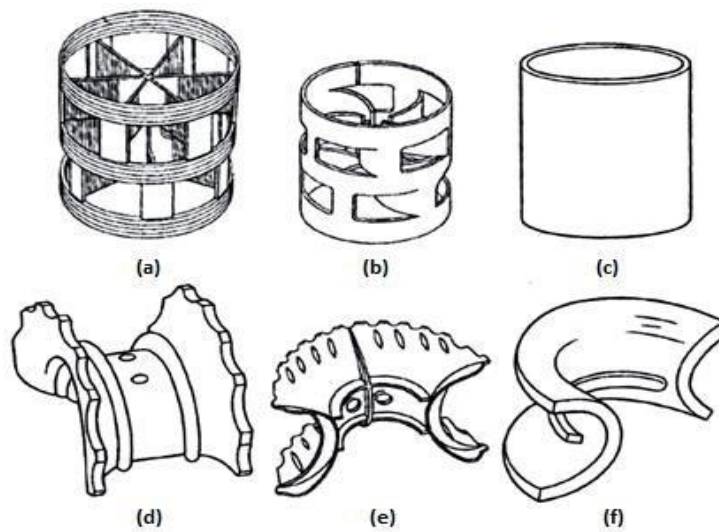


Figure 2-10: Random packing (a) plastic pall rings. (b) Metal pall ring. (c) Raschig rings. (d) Intalox saddles. (e) Intalox saddles of plastic. (f) Intalox saddles [33]

### 2.1.9.2. Structured Packing

By comparison structured packing are fabricated from corrugated metal sheeting arranged with a regular shape or wire mesh (gauze). The structured form is improved to give an excessive mass transfer area with an excessive void fraction [20]. Structured packing is usually made from either plastic or metal with 2 examples shown in Figure 2-11. Gauze packings are considered to be more effective than regular structured sheet metal packing supplying a step forward height which is equivalent to theoretical plate (HETP) and permit a totally low flow rate wetted surface [17]. To guarantee the maximum efficiency of packing structure, it is made in parts and positioned in the tower in a rotated way to make certain of homogeneity vapour and liquid flow cross mixing [16].

The utilization of structured packing method in distillation systems is desired when liquid loading is sufficient, low pressure is reducing and high efficiency is obtained, another use may exist in different absorption processes [34]. Normally, structured packing is utilized in systems which have an excessive number of theoretical stages for hard separations, like isomers separation. As an alternative, structured packing is suitable for high vacuum distillation systems and within the old trayed revamping towers to raise the tower capacity and reduce RR necessities [20].



(1)                                                            (2)

Figure 2-11: Structured Packing (1) Metal packing. (2) Plastic Packing

### 2.1.10. Packing Materials

Materials types utilized for packing are mostly dependant on the corrosion resistance needed over the work. Regular packing can be fabricated from either plastics, ceramic or metals. In case of no corrosion, carbon steel (CS) packing is considered as the most effective for higher ability and performance in comparison with plastic or ceramic options [15]. Similarly, carbon steel can give a higher turndown in a wider practical range of packing geometries, it also has an excessive compression resistivity. When corrosion is anticipated and steel packing is required, stainless steel (SS) packing can be alternatively utilized in spite of it been more expensive. For corrosion conditions, both plastic and ceramic substances are popular, while ceramic became popular rapidly because it is available and cheap [15].

Plastic packing option is also restrained for using in oxidised media and at very low temperatures leading to degrade and loss its flexibility. Furthermore, many organic

solvents significantly deteriorate plastic through packing usage, so it has limited use [20]. Using medium and high temperature during plastic packing operation should be performed with high care and under supervision to avoid any change of plastic material properties as heating for long periods can affect the plastic packing efficiency. Operating at high temperatures can also resulted in plastic material deterioration. which leads to converting packing traits and in turn tower pressure drop [16]. Coker [16] advised that plastics must not be used within 50°F of its deflection or softening temperature to be safe from changes.

### 2.1.11. Structured Packing and Random Comparison

Using structured packing or random inside a distillation tower relies strongly upon the sort of isolation that is carried out and the desired process performance. In general, random packings have higher (HETP) than structured packings although the high efficiencies of structured packings is offset through the significantly expanded cost of structured packings in each cubic metre [20].

### 2.1.12. Packing Efficiency

#### 2.1.12.1. Transfer Unit Concept

The packed tower layout method is based on the idea of transfer units that may be applied to find the required packing height to attain the wanted separation. This is actually suitable when using ordinary trayed tower design steps because of the vapour and liquid compositions that takes place in packed tower for liquids differently compared to stepwise style as traying towers [35]. The elevation of the packing, $Z$, is calculated based on any of the liquid phase or gas by eqs (2-26), (2-27) or (2-28) the calculation of the height of a single transfer unit HTU and the number based on transfer units $N_{TU}$.

$$Z = HTU \times N_{TU} \qquad\qquad (2\text{-}26)$$

$$Z = HOG \times N_{OG} \qquad\qquad (2\text{-}27)$$

$$Z = HOL \times N_{OL} \qquad\qquad (2\text{-}28)$$

Number of plates required theoretically in a specific isolation process in a traying tower, like a high number of transferral units is required to obtain a better purification. However, the height of the transferral unit immediately measures the packing performance that is required to achieve an identical isolation of tray performance [15]. The HTU mainly relies on mass transfer performance between vapour and liquid phases, the more effective mass transferral has the least number of HTU and requires the least packing option.

- Height of Transfer Unit (HTU)

Mass transferral between liquid and vapour phases during distillation process are considered to be more managed by using the resistance of vapour phase [36]. Commonly, the desired height of packing evaluated depends on the performance of gas transferral unit, using $N_{OG}$ and $H_{OG}$ from eq. (2-27). $H_{OG}$ refers to height level of gas phase transferral unit which is computed by eq. (2-29) depending on two resistance ideas by the use of the individual liquid and the height of gas transferral units. Gas transferral units $H_L$ and $H_G$ can be calculated by the coefficient of the individual mass transferral for the liquid and gas phases, while the $K_G$ and the active interfacial area for the packing option $a_e$ are calculated from eqns. (2-30) and (2-31). Many correlations have been suggested in the literature some of them are tabulated in Table 2-1 and Table 2-3 for the calculations of the effective interfacial area of packing and the mass transfer coefficients.

$$H_{OG} = H_G + \lambda H_L \qquad (2\text{-}29)$$

$$H_G = \frac{U_G}{K_G a_e} \qquad (2\text{-}30)$$

$$H_L = \frac{U_L}{K_L a_e} \qquad (2\text{-}31)$$

$$\lambda = m \frac{G_m}{L_m} \qquad (2\text{-}32)$$

Where m equals the average of slope on the equilibrium curve that is measured by eq. (2-33).

$$M_{ave} = \frac{\sum_{i=1}^{n} m_i}{n} \qquad (2\text{-}33)$$

- Transferral unit number (TUN)

The TUN or $N_{OG}$ versus the vapour can be referred to the total number of the gas phase transferral units and may be calculated by eq. (2-34). To evaluate this number, the motivation force through the gas film is decided to be first. This motivation force refers to the difference between the actual (y) vapour concentration and the equilibrium (y*) at a corresponded X point as shown in

Figure *2-12* [37]. The $N_{OG}$ can be evaluated by way of both graphical integration through the integral number result of the $\frac{1}{(y^*-y)}$ values.

$$N_{OG} = \int_{y_B}^{y_D} \frac{dy}{(y^* - y)} \tag{2-34}$$
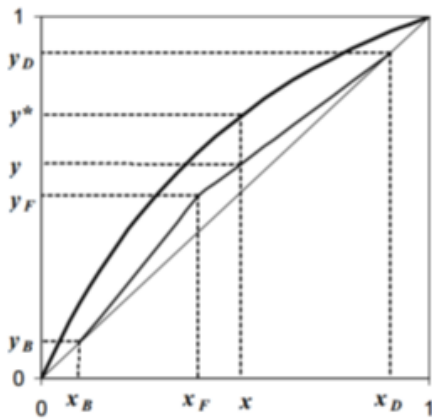


Figure 2-12: Scheme of the relation between y* and y.
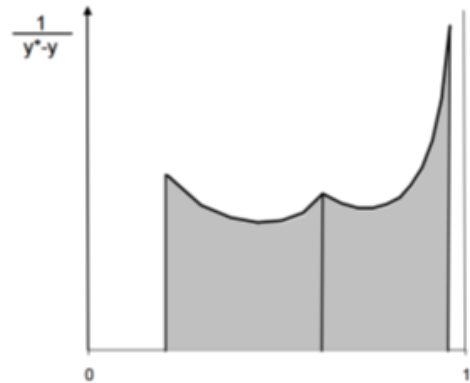
Figure 2-13: Shows graphic integration values

### 2.1.12.2. Height Equivalent of Theoretical Plate (HETP)

The (HETP) refers to a relationship between the needed packing height and the envisioned theoretical steps number essential to obtain a preferred isolation [16]. The design of column compared to the performances among traying packed towers and it can be expressed in eq. (2-35). Throughout a distillation column, the HETP for a given size and type of packing has been shown to be basically constant as long as that good distribution of liquid that is preserved in the course of operation [21].

$$HETP = Z/N \qquad (2\text{-}35)$$

- Factors Affecting HETP

The calculated data of HETP for a given type of packing can be influenced by some factors. These factors have been investigated to understand packed column design results. These factors affect the HETP of packing as follow:

- Surface area of packing in volume units: An amazing packing surface area leads to further activity of packing efficacy (lower HETP). The activity of random packing will increase as the size of the packing decreases while for structure packing option, as the channels among sheet materials decrease accomplishment of further efficacy can be obtained [16].
- HETP drops when the symmetry of the packing surface is increased [15].
- The homogeneity of vapour and liquid spread throughout the packing body significantly affects the packing performance. The mal-distribution of vapour and liquid flow rates become lower.
- In the structure packing option, as the loaded fluid in the tower rises, the HETP of packing will also rise. This loaded influence will be further effective in case of wire mesh style. However, it is less influenced for wavy sheet packing [15].

- HETP Prediction- Mass Transfer Models

The former strategies discussed height calculation of a transferral unit and the coefficients of liquid phase mass transferral can also be used in calculating the packing HETP. The relationship among the overall gas phase transferral unit and HETP is given through eq. (2-36) or eq. (2-37) in accordance with the two-film theory [38]. Where $\lambda$ is described as the slope ratio of the equilibrium curve to the operation curve. The precision of the HETP evaluation by mass transferral models count highly on the precision of the relation applied for the interfacial area prediction of packing and the mass transferral coefficients. Kister [15] used the mass transfer relations evolved for structured packing based on the two-film theory by Bravo [39]. Those correlations are represented by eqns. (2-40) and (2-41).

$$\text{HETP} = \frac{H_{OG}\ln\left(m\frac{G_m}{L_m}\right)}{m\frac{G_m}{L_m-1}} = H_{OG}\frac{\ln\lambda}{\lambda-1} \qquad \text{for } \lambda \neq 1 \qquad (2\text{-}36)$$

$$\text{HETP} = H_{OG} \qquad \text{for } \lambda = 1 \qquad (2\text{-}37)$$

- HETP Prediction- Rules of Thumb

The packing HETP also can be evaluated by many rules of thumb used by plenty of authors' personal practices and tests. Due to there being just a few variables that decide the packing HETP together with the unreliability that's associated with the most of mass transferral models, Kister indicated [15] that thumb rule is regularly more precise and is credible for predicting HETP. The primary rule of thumb was advised by Kister [15] as shown in eq (2-38) that is dependent upon rule of thumb released by Harrison and France [40]. This rule can obtain structure packing performance as function of packing corrugation [15]. Furthermore, it evolves to accommodate a much broader range packing configurations with angle of crimp more than 45° and later further progressed  (see eq. 2-39) [41].

$$\text{HETP} = \frac{100}{a_p} + 0.01 \qquad (2\text{-}38)$$

$$\text{HETP} = \frac{100C_{XY}}{a_p} + 0.01 \qquad (2\text{-}39)$$

For calculating the HETP of packing by the thumb rule, hydrocarbon and organic systems with surface tension of liquid are put lower than 25 mN/m. In case of higher surface tensions such as water-rich or amine-glycol systems can be achieved respectively employed. [41].

- Prediction- Data interpolation of HETP

The calculation of a packing HETP may also be done by the insertion of experimental HETP information. Kister [15] showed that estimation of HETP using data interpolation is considered to be one of the most dependable methods to obtain values of HETP design. This included the calculation of HETP extracted from experimental data in respect to thumb rule. However, many precautions have been applied to assess the required packing height. The scale–up for packing distillation size towers in industrial field data is normally lower 1 metre and this is doubtful according to Coker [16]. Coker recommends to attain their advocated HETP calculation from the packing producers.

### 2.1.12.3. HETP and Transfer Unit Concept Comparison

Although each of the applicable methods to design packing distillation towers have given large benefits for transferral units and HETP packing calculations, there are some shortcomings in their methods.

- The usage of HETP for both secondary and multi-component distillation columns employing transferral units is basically restricted to two components systems. Therefore for multi component systems its application is limited.

- According to Kister [15], the usage of transferral units is unable to improve good accuracy compared to the HETP method as it is more complicated.

- The assessment of a packed tower HETP leads to also rapprochement evaluation to plate towers than the NTU'S.

- The application of the NTU'S permit more facile analysis in packing tower properties related to mass transferral coefficients. Consequently transferral unit idea is more appropriate for essential model and analysis evolution [15].

Table 2-1: Coefficient correlations of gas and liquid mass transferral in structured packing design

| Author | Correlation |
|---|---|
| Bravo [39] | $K_G = 0.0338 \left(\dfrac{D_G}{d_{eq}}\right) \left[\dfrac{\rho_g d_{eq}(u_{Le}+u_{Ge})}{\mu_G}\right]^{0.8} Sc_G^{0.33}$     (2-40) |
| | $K_L = 2\sqrt{\left(\dfrac{D_L}{\pi s}\right)\left(\dfrac{9\Gamma^2 g}{8\rho_L \mu_L}\right)^{\frac{1}{3}}}$     (2-41) |
| | Where $u_{Ge} = \dfrac{u_G}{\epsilon \sin\alpha}$ and $u_{Le} = \left(\dfrac{9\Gamma^2 g}{8\rho_L \mu_L}\right)^{\frac{1}{3}}$ |
| Nawrocki [42] | $K_G = 0.0338 \left(\dfrac{D_G}{d_{eq}}\right) \left[\dfrac{\rho_g d_{eq} u_{Ge}}{\mu_G}\right]^{0.8} Sc_G^{0.33}$     (2-42) |
| | $K_L = 2\sqrt{\dfrac{D_L 3 V_L}{\pi s 2 w \delta_{dyn}}}$     (2-43) |
| Billet [43] | $K_G = \sqrt{\dfrac{4 D_G}{\pi \tau_L}}$     (2-44) |
| | $K_L = \sqrt{\dfrac{4 D_G}{\pi \tau_G}}$     (2-45) |
| | Where $\tau_G = \dfrac{(\epsilon - h_L)l}{u_G}$ , $\tau_L = \dfrac{h_L l}{u_L}$ |
| Hanley [44] | $K_G = \dfrac{D_G}{d_{eq}}\left[\dfrac{d_{eq} K_V \left(\dfrac{\rho_L}{\rho_g}\right)^{0.5}}{\epsilon \mu_L \left(1-\dfrac{f}{f_c}\right)^P}\right]^{0.8} Sc_G^{0.33}$     (2-46) |
| | $K_G = \dfrac{D_L}{d_{eq}}\left[\dfrac{d_{eq} u_L \rho_L}{\epsilon \mu_L}\right]^{0.5} Sc_L^{0.33}$     (2-47) |
| Rocha [45] | $K_G = 0.054 \left(\dfrac{D_G}{s}\right)\left[\dfrac{\rho_G S(u_{Le}+u_{Ge})}{\mu_G}\right]^{0.8} Sc_G^{0.33}$     (2-48) |
| | $K_L = 2\sqrt{\dfrac{0.9 D_L u_{Le}}{\pi S}}$     (2-49) |
| | Where $u_{Ge} = \dfrac{u_G}{\epsilon(1-h_L)\sin\alpha}$ , $u_{Le} = \dfrac{u_L}{\epsilon h_L \sin\alpha}$ |
| Brunazzi [46] | $K_G = 0.054 \left(\dfrac{D_G}{d_h}\right)\left[\dfrac{(\rho_g d_H)(u_{Le}+u_{Ge})}{\mu_G}\right]^{0.8} Sc_G^{0.33}$     (2-50) |
| | $K_L = A\left(\dfrac{D_L}{d}\right)\left(\dfrac{\mu_L^4 g}{\sigma^3 \rho_L}\right)^{B_1}\left(\dfrac{\delta \sin\alpha_L}{Z_t}\dfrac{u_{Le}d}{D_L}\right)^{B_2}$     (2-51) |
| | Where $u_{Ge} = \dfrac{u_G}{\epsilon(1-h_L)\sin\alpha}$ , $u_{Le} = \dfrac{u_L}{h_L \sin\alpha_L}$ |
| Shetty [47] | $K_G = 0.054 \dfrac{D_G}{s}\left[\dfrac{\rho_G S(u_{Le}+u_{Ge})}{\mu_G}\right]^{0.8} Sc_G^{0.33}$     (2-48) |

$$K_L = \frac{0.4185 D_L}{b} \sqrt{\frac{\sin\alpha}{1_{ratio}}} \left(\frac{4\rho_L q}{\mu_L}\right)^{\frac{1}{3}} \left(\frac{\rho_L^2 g b^3}{\mu_L^2}\right)^{\frac{1}{6}} Sc_L^{\frac{1}{2}} \qquad (2\text{-}52)$$

| | | |
|---|---|---|
| Olujic [48] | $K_G = \sqrt{\left(\frac{Sh_{G,lam} D_G}{d_{hG}}\right)^2 + \left(\frac{Sh_{G,turb} D_G}{d_{hG}}\right)^2}$ | (2-53) |

$$\text{Where } Sh_{G,lam} = 0.664 Sc_G^{\frac{1}{3}} \sqrt{\frac{Re_{Grv} d_{hG}}{1_{g,pe}}}$$

$$Sh_{G,turb} = \frac{\left(\frac{Re_{Grv} Sc_G \xi_{GL}\varphi}{8}\right)\left[1+\left(\frac{d_{hG}}{1_{G,pe}}\right)^{\frac{2}{3}}\right]}{1+12.7\sqrt{\frac{\xi_{GL}\varphi}{8}\left(Sc_G^{\frac{2}{3}}-1\right)}}$$

$$K_L = 2\sqrt{\frac{D_L u_{Le}}{0.9\pi d_{hG}}} \qquad (2\text{-}54)$$

| | | |
|---|---|---|
| Xu [49] | $K_G = \sqrt{\frac{4 D_G u_G}{\pi I\left[\in -\left(\frac{4Ft}{S}\right)^{\frac{2}{3}}\left(\frac{3\mu_L u_L}{\rho_L \in g_{eff}\sin\alpha}\right)^{\frac{1}{3}}\right]}}$ | (2-55) |

$$K_L = \sqrt{\frac{4 D_L u_L}{\pi I\left[\in -\left(\frac{4Ft}{S}\right)^{\frac{2}{3}}\left(\frac{3\mu_L u_L}{\rho_L \in g_{eff}\sin\alpha}\right)^{\frac{1}{3}}\right]}} \qquad (2\text{-}56)$$

Table 2-2: The mass transferral evaluation of a packing column using shortcut methods.

| Author(s) | Correlation | |
|---|---|---|
| Murch [50] | $HETP = c(\rho_G u_G)^a d_G^b Z_T^{\frac{1}{3}} \left(\frac{\alpha \mu_L}{\rho_L}\right)$ | (2-57) |
| Harrison [40] | $HETP = \dfrac{100}{a_p}$ for 45° crimp angle | (2-58) |
| Kister [15] | $HETP = \dfrac{100}{a_p} + 0.10$ | (2-59) |
| | $HETP = \dfrac{100 C_{XY}}{a_p} + 0.10$ | (2-60) |
| Lockett [51] | $HETP = \dfrac{1.54 g^{0.5}(\rho_L - \rho_G)^{0.5} \mu^{-0.06}}{a_p\left[1 + 0.78 \exp(0.00058 a_p)\left(\frac{\rho_G}{\rho_L}\right)^{0.25}\right]^2}$ | (2-61) |
| Carillo [52] | $HETP = \dfrac{1.54 g^{0.5}(\rho_L - \rho_G)^{0.5} \mu^{-0.06}}{a_p\left[1 + 0.78 exp(0.00058 a_p)\left(\frac{\rho_G}{\rho_L}\right)^{0.25}\right]^2}$ Sheet packing | (2-62) |
| | $HETP = \dfrac{P\sqrt{\rho_L F_V^{0.42}}}{(2712 + 82.0P)\left[1 + 1.505\left(\frac{\rho_G}{\rho_L}\right)^{0.25}\right]^2}$ Gauze Packing | (2-63) |
| Coker [16] | $HETP = (HTU)_{OG}\left(\frac{ln\lambda}{\lambda - 1}\right)$   $\lambda \neq 1$ | (2-64) |
| | $HETP = (HTU)_{OG}$   $\lambda = 1$ | (2-65) |

Table 2-3: Efficient interfacial spaces correlations of a structured packing design.

| Author(s) | Correlation | |
|---|---|---|
| Shi [53] | $\frac{a_e}{a_p} = 0.76 m d_{pe}^{1.1} \frac{u_L^{0.4} V_L^{0.2}}{1-0.93\cos\theta} \left(\frac{\rho_L}{\sigma_L g}\right)^{0.15} \left(\frac{a_p^{0.22}}{\epsilon^{0.6}}\right)$ | (2-66) |
| Fair [54] | $\frac{a_e}{a_p} = 0.50 + 0.0058 \qquad Fr \leq 0.85$ | (2-67) |
| | $\frac{a_e}{a_p} = 1 \qquad Fr < 0.85$ | (2-68) |
| Henriqus [55] | $\frac{a_e}{a_p} = 0.465 \left(\frac{\rho_L u_L}{\mu_L a_p}\right)^{0.3}$ | (2-69) |

| Billet [43] | $\frac{a_e}{a_p} = 1.5 \left(a_p d_h\right)^{-0.5} (Re_L)^{-0.2} (We_L)^{0.75} (Fr_L)^{-0.45}$ | (2-70) |

In case of negative system, surface tension will be as follow:

$$\frac{a_e}{a_p} = \left(\frac{a_e}{a_p}\right)_{Eq.71} (1 - 2.4 * 10^{-4} |Ma_L|^{0.5}) \qquad (2-71)$$

$$Re_L = \frac{\rho_L u_L}{(\alpha_p u_L)}, \quad Fr_L = \frac{u_L^2 \alpha_p}{g}, \quad We_L = \tilde{n}_L u_L (\sigma_L \alpha_p)$$

| Hanley [44] | $\frac{a_e}{a_p} = \frac{\left[1-\left(\frac{f}{f_c}\right)^P\right]}{(1-f)^{-1}} \left\{1 - \exp\left[-\omega \left(\frac{d_{eq} u_L^2 \rho_L}{\epsilon \sigma_L}\right)\right]^2\right\}$ | (2-72) |
| Brunazzi [56] | $\frac{a_e}{a_b} = \frac{d_{eq}}{4} \left(\frac{h_L}{\epsilon}\right)^{1.5} \left[\frac{\rho_L g \epsilon (\sin\alpha)^2}{3\mu_L u_L}\right]^{0.5}$ | (2-73) |

| Rocha [45] | $\frac{a_e}{a_b} = F_{se} \left[\frac{29.12 u_L^{0.4} V_L^{0.2} S^{0.159}}{(1-0.93\cos\theta)(\sin\alpha)^{0.3} \epsilon^{0.6}} \left(\frac{\rho_L}{\sigma_L g}\right)^{0.15}\right]$ | (2-74) |

| Gualito [57] | $\frac{a_e}{a_b} = \left(\frac{a_e}{a_b}\right)_{eq (76)} \left[\frac{1.2}{1+0.2\exp\left(\frac{15 u_L}{u_G}\right)}\right]$ | (2-75) |

$$\frac{a_e}{a_b} = (1-\Omega)\left\{1 - \exp\left[-1.45 \left(\frac{\sigma_c}{\sigma_L}\right)^{0.75} Re_L^{0.1} Fr_L^{-0.05} We_L^{0.2}\right]\right\} \left(\frac{\sin 45}{\sin\alpha_L}\right)^n \quad (2-76)$$

Olujic [58]

$$0.04 < Re_L < 500; \qquad 1.2 * 10^{-8} < We_L < 0.272$$

$$5 * 10^{-9} < Fe_L < 1.8 * 10^{-2}; \qquad 0.3 < \frac{\sigma_c}{\sigma_L} < 2$$

### 2.1.13. Fluid Distribution Systems in Packed Columns

According to Coker [16] distribution of liquid is one of the very important factors to make sure of efficient separation using packed towers. The activity of internal packing will hardly be decreased by means of weak liquid distribution throughout the top of its higher surface, or throughout the packing parts under any reflux or feeding [16]. The impact of bad distribution was outlined in the discussion of mal-distribution which can cause a less wetted area of packing and the enhancing of channelling of liquid. This is widely accepted for vacuum under distillation process in which low levels of liquid are predictable. Furthermore the preliminary distribution of liquid is considered to be crucial for the separation performance within the entire of tower [18]. Thus distributor choices rely on the tower size, the sort of packing option in terms of configuration availability and surface area in addition to the capability of flow in the direction of the walls of the tower. Structured packing with an excessive surface area usually have a higher sensitivity to non-uniform liquid distribution than those of lower surface area [16]. Stichlmair [18] also reported some necessities for a good distributor of liquid:

- Uniform liquid distribution through the whole sections of the tower

- Wide flexibility for liquid flow

- Less resistance for gas flow ($\Delta P$)

- Less potential for fouling

For standard applications, liquid distributor involves weirs, perforated or nozzle plates using troughs for element dispensing. Commonly diameter up to 0.8 m is well known for orifice distributor uses. The orifice distributor consists of a plate with small holes to flow liquid and chimneys to flow the upward vapour [18]. Bigger diameter towers normally need more complicated liquid distribution systems to include troughs or pipes. Furthermore, to avoid an excessive degree of liquid mal-distribution alongside the packed bed, the utilization of liquid redistributors is frequently needed to straggle the liquid flow toward the tower wall. Generally, liquid re-distributors additions every one metre (3 feet) is adequate to avoid mal-distribution situations. A combination of liquid distributors with collectors is more likely to be needed for larger diameter towers an example can be seen in Figure 2-14. Proper liquid collector designs are used to break liquid flow without impact on the vapour flow and to allow sufficient liquid mixing prior to redistributing to achieve large differences in the concentration of the

liquid through flow part [18]. Despite the hazard of mal-distribution of the gas flow is notably very less compared to the liquid flow, gas homogeneity flow distribution throughout the tower cross section is counted as critical as liquid homogeneity flow while it is regularly over notable [16]. This is acceptable in particular for more modern structured packing option in which precise attention is necessary for the preliminary gas distribution. [18]. For tower diameters in the range of 2.5m Stichlmair [18] indicated that a common inlet pipe is enough, but for bigger ones a more complicated distribution mechanism could be required.

### 2.1.14. Packed Column Design
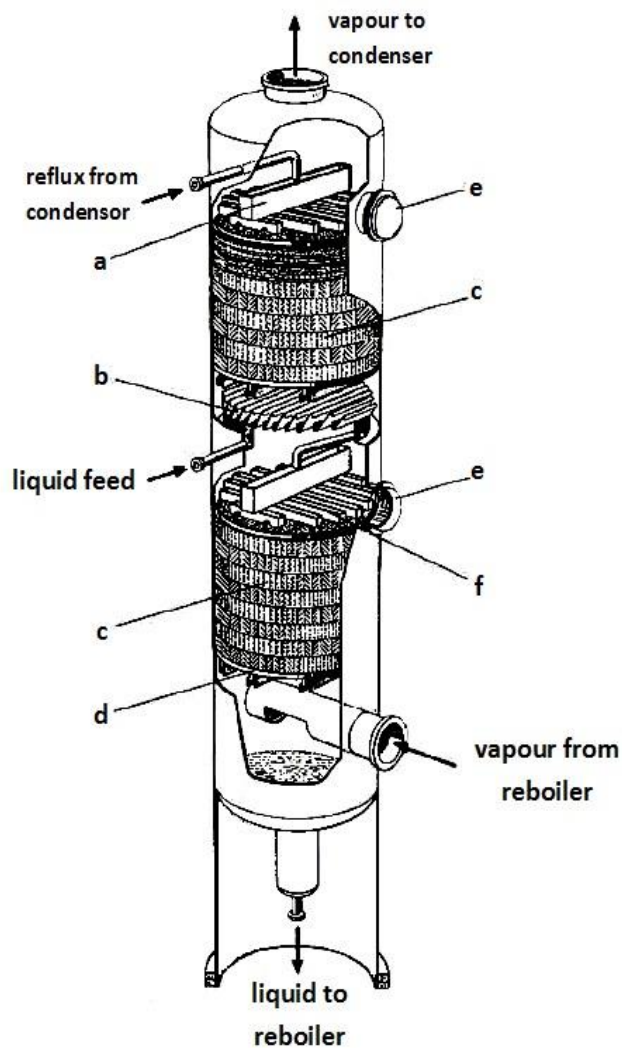


Figure 2-14: Packing column image shows tower inner walls,  a; liquid collector, c; Structured packing, d; Support grid, e; Manway and f; Liquid redistributor [18]

### 2.1.14.1. Packed Column Diameter

The evaluation of the diameter of packed towers may be done by the use of the design technique mentioned by Towler and Sinnott [20]. The tower diameter is approximated by knowing the gas mass flow rate per unit tower cross sectional area $V_W$, calculation of this value may be done by the use of eq (78). Together with the vapour-liquid flow factor $F_{LV}$, eq (2-79) along with Figure 2-15 relate the vapour and liquid flow rates. Properties of the system and packing with the flow rate of gas mass per unit area with the flow lines of constant $\Delta P$ as a parameter [20].

$$K_4 = \frac{13.10(V_W)^2 F_P \left(\frac{\mu_L}{\rho_L}\right)^{0.1}}{\rho_V(\rho_L - \rho_V)} \tag{2-78}$$

$$K_{LV} = \frac{L}{V} \sqrt{\left(\frac{\rho_V}{\rho_L}\right)} \tag{2-79}$$

Towler and Sinnott [20] adviced the use of a $\Delta P$ of 40-80 mm $H_2O$/m of packing for the introductory packing distillation towers design work at atmospheric pressure to pressures of moderate. If we use a liquid of a high tendency to foam, calculation of $\Delta P$ according to the mentioned rules must be reduced to half. Typical distillation towers are usually designed to be worked in flooding conditions at the range of 30-95%; flooding and may be evaluated via eq (83) based on the $K_4$ variable at the predicted $\Delta P$ and line of flooding (see Figure 2-15) [26]. To calculate the needed tower diameter by eq. (2-78), preliminary estimation of the towers packing factor has to be made if it is unknown. Eq. (2-80) to evaluate the factor of packing based upon the size typical factors mentioned in Table 2-4 a size factor of 8 will be employed for structured packing. The other variable ($\delta_p$) is a descriptive of dimensional property packing by the height of corrugation in structuring packing or the nominal diameter for packing randomly in inches.

$$F_P = C_{p,size}(\delta_p)^{-1.1} \tag{2-80}$$

Table 2-4 : Sizes Factors for eq. (2-80) [26]

| Packing Type | Cp:size |
|---|---|
| Raschig Ring | 140 |
| Metal Pall Ring | 62 |
| Intalox Metal Tower Packing | 39 |
| Hiflow Ring | 34 |
| Packing of Structured | 8 |

Cross Sectional Area of Column, $\qquad AC = \dfrac{V}{V_W}$ $\qquad\qquad$ (2-81)

Column Diameter, $\qquad\qquad\qquad d_c = \sqrt{\left(\dfrac{4}{\pi}\right) * A_C}$ $\qquad\qquad$ (2-82)

$\qquad$ Flooding of Percentage $= \left[\dfrac{k_4 \text{at disign } \Delta P}{k_4 \text{at flooding}}\right]^{1/2} * 100$ $\qquad$ (2-83)
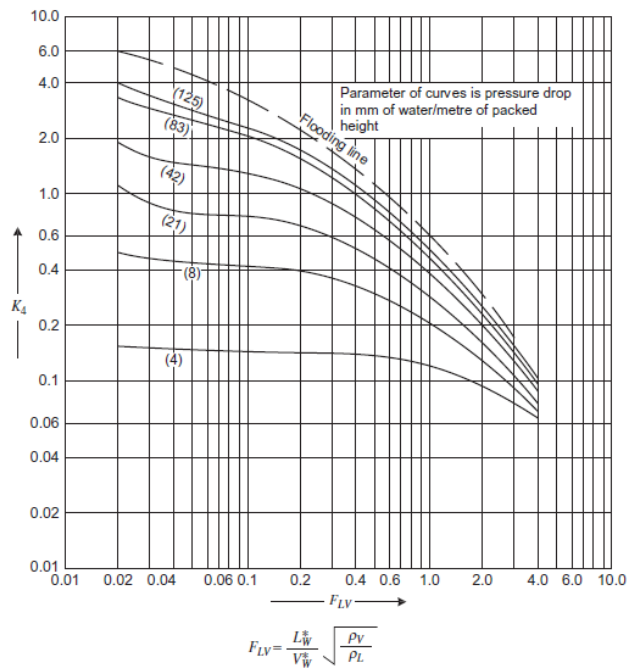


Figure 2-15: Correlation of the generalized pressure drop [20]

For laboratory sized distillation columns it is usual to use column diameters in the range 20-50mm for vacuum distillation and 10 to 30 mm for column atmospheric pressures [59]. Krell [59] also recorded that the separation stage height will increase with the increasing of tower diameter if the internal packing size remains the same. Even though, there is limited reports for type structured wire mesh packing compared to randomly packing kind such as Rasch saddle or ring packing [59]. As such this impact must be taken into consideration while employing the packing performance

36

evaluated from the laboratory sized pilot towers to the layout of industrial scale distillation towers.

### 2.1.14.2. Packed Column Pressure Drop (ΔP)

Based on Stichlmair [18] one of the maximum essential parameters inside the distillation tower operation is the gas phase ΔP. The gas phase ΔP symbolizes the losses of kinetic energy and friction forces that are spent on the gas phase by the liquid holdup across the packed bed [16]. The ΔP inside a tower is basically affected by; the dimensional type of the tower, the used type for packing, the gas flow rate, counter current liquid flow rate and characteristics of fluids [18, 59]. In a large scale distillation system, distillation towers are usually monitored by ΔP controlling systems to discover the starting of flooding point. An evaluation of the ΔP in the tower was done to calculate the tower diameter needed by using the generalized correlation graph of ΔP. Realistically, the estimation of ΔP can be more precisely done by the use of ΔP correlations developed with the aid of many authors. The ΔP inside a packed bed distillation could be predicted for both wetted and dry packing with both sort capable to be calculated via particle or channel models [18].
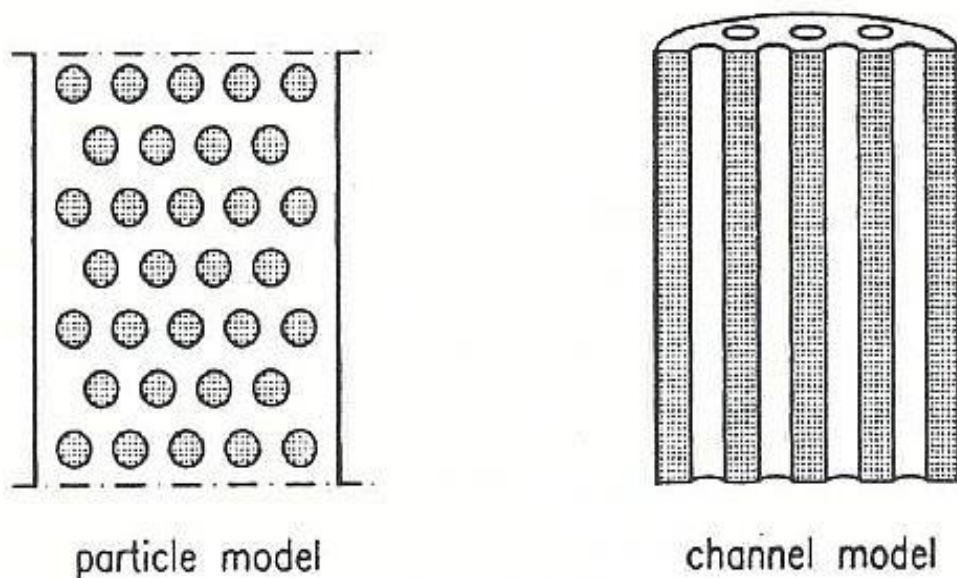


Figure 2-16: Channel packing and Particle models [18]

- Pressure Drop of Dry Packing

• Structure of the channel model:

In case of the model of channel, the idea of ΔP is calculated by the use of drop gas pressure in a pipe length, H. The ΔP across a pipe may be defined by the following eq. (2-84).

$$\frac{\Delta P_d}{H} = f\left(\frac{\rho_G}{2}\right)\left(\frac{u^2}{d}\right)$$   (2-84)

Where the velocity of the gas in the channel, $u$ can be envisioned primarily based on the flowing gas superficial velocity of across the tower by the use of eq. (2-85):

$$u = \frac{u_G}{\epsilon}$$   (2-85)

The channel diameter, $d$ can be predicted based on the given packing equivalent diameter by eq. (2-86) in which the term $d_p$ symbolize the packing particles diameter [18]:

$$d_{eq} = \frac{\epsilon}{1-\epsilon} d_p$$   (2-86)

Gathering of eq. (2-85) and (2-86) with eq. (2-84) permit the formulization of Ergun Equation that is usually used in the calculations of pressure drop in packed towers [18].

$$\frac{\Delta p_d}{H} = \xi_E \frac{1-\epsilon}{\epsilon^3} \rho_G u_G^2 \left(\frac{1}{d_p}\right)$$   (2-87)

The variable symbolizes to the resistant vapour of flow rate inside the packed bed and should to be specified experimentally.

• Particle model Structure:

The development of the relation of ΔP by the use of the particle model in the ΔP equation founded for fluidized beds. The essential equation for ΔP in dry beds by the use of the particle model is given by Stichlmair [18] as eq. (2-88).

$$\frac{\Delta p_d}{H} = \frac{3}{4}\xi_{Eo}\left(\frac{1-\epsilon}{\epsilon^{4.65}}\right)\rho_G u_G^2 \left(\frac{1}{d_p}\right)$$   (2-88)

Friction factor for one species not all is represented by $\xi_E$. The ΔP in a bed of spheres is anticipated based on a single sphere friction factor compared to the structure of

38

channel model [18]. The porosity term is expressed by that is widely specified via experimental data for fluidised beds at range of porosities from 0.4 to1 [18]. As such, the term porosity in eq. (2-88) is counted to be more accurate compared to those obtained from eq. (2-87). Moreover, not like the variable used for the friction factor in evaluating the ΔP in channel model, friction factor can be extracted from experimental data that gives a good agreement with the Reynolds number for different kinds of packing. These relations are stated by Figure 2-17 where literature information was mentioned about the dry ΔP for a single species represented to packing option.
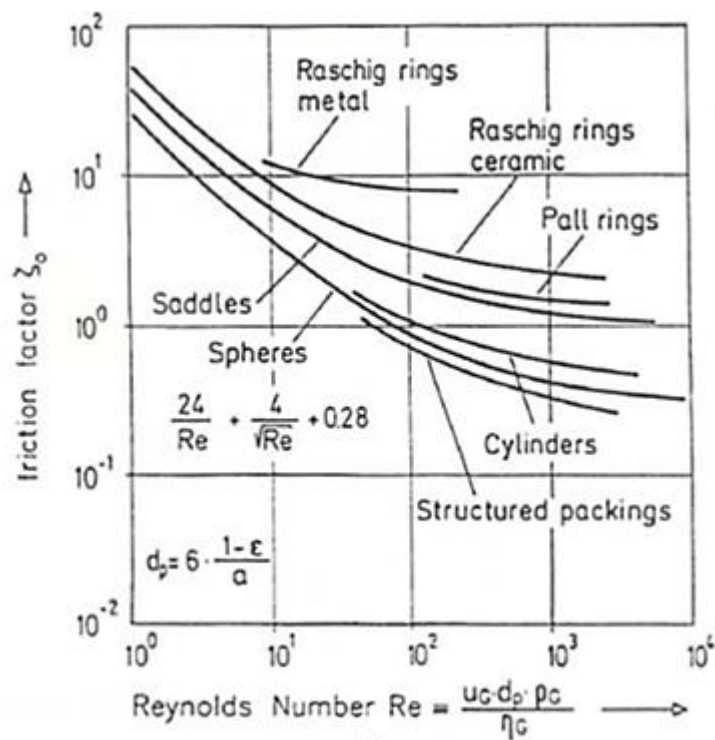


Figure 2-17: Correlation of friction factor (single particles) [18]

- ($\Delta P$) Of Wet Packing

In the calculations of packing pressure drop, the ΔP related with a wet bed is normally anticipated to be higher compared with that of the dry one. Stichlmair [18] assigned the rise of ΔP of wet packing liquid aggregation inside the bed through the work. A large quantity of liquid directly holds up in the packed bed increasing in the voidage of packing and in turn gas velocity increased [18].

- Channel Model Structure:

It was reported in the literature by Stichlmair [18], that the $\Delta P$ can be evaluated using the relation of the wet packing of the channel model to the dry packing as expressed by eq. (2-89):

$$\frac{\Delta p_{wet}}{H} = \left(\frac{\Delta p_d}{H}\right)\left(\frac{1}{(1-C_h.h_L)^5}\right) \tag{2-89}$$

Consequently, the wet packing can be described as shown in eq. (2-90):

$$\frac{\Delta p_{wet}}{H} = \xi_E \frac{1-\epsilon}{\epsilon^3} \rho_G u_G^2 \left(\frac{1}{d_p}\right)\left(\frac{1}{(1-C_h.h_L)^5}\right) \tag{2-90}$$

Here $C_h$ is an empirical factor that relies on the sort of the used packing with assets of values published by Stichlmair [18]. And $h_L$ symbolize the liquid holdup during the packing.

- Structure of Particle Model:

In case of using particle model for dry and wet packings, eq (2-88) may be applied too. But, the impact of the wet packing on the variables $d_{pwet}$, $\epsilon_{wet}$ and $\xi_0$, should be considered for corrosion issues. Correction factors for every variable explained by Stichlmair [18] outlined by eq (2-92) to (2-94) respectively.

$$\frac{\Delta p_{wet}}{H} = \frac{3}{4}\left(\xi_{0,wet}\right)\left(\frac{1-\epsilon_{wet}}{\epsilon_{wet}^{4.65}}\right)\rho_G u_G^2 \left(\frac{1}{d_{pwet}}\right) \tag{2-91}$$

$$\epsilon_{wet} = \epsilon - h_L \tag{2-92}$$

$$d_{pwet} = d_p \left[\frac{1-\epsilon\left(1-\frac{h_L}{\epsilon}\right)}{1-\epsilon}\right]^{\frac{1}{3}} \tag{2-93}$$

$$\xi_{0,wet} = \xi_0 \left[\frac{1-\epsilon\left(1-\frac{h_L}{\epsilon}\right)}{1-\epsilon}\right]^{\frac{c}{3}} \tag{2-94}$$

Where c = 0 for turbulent flow and -1 for laminar flow

Instead, the wetted packing ΔP may also be represented to the dry packing in terms of the dry packing ΔP, using eq. (2-95). This derived equation associated with wetted and dry packing pressure drop is counted as simplified theoretical model and it recommends that any calculated ΔP value from its application has to verified by experimental work data [18].

$$\frac{\Delta p_{wet}}{\Delta p_d} = \left[\frac{1-\epsilon\left(1-\frac{h_L}{\epsilon}\right)}{1-\epsilon}\right]^{\frac{2+c}{3}} \qquad (2\text{-}95)$$

### 2.1.15. Batch Distillation

In some chemical separations, the technique of continuous distillation is not always suitable and the method of batch distillation can be an extra appropriate option. That is well known for the isolation processes of some special chemicals substance due to the versatility and flexibility of batch distillation method in isolating small quantities of materials that are costed, or in the recovery of compounds that might be dangerous if lost [16]. Coker [16] indicated that batch distillation is more desirable to continuous distillation when little excessive technological materials or expensive chemicals are required. Batch distillation is usually carried out for the following: [15, 21]:

- Distillation of small amounts, example small-scale of commercial facilities.
- For a broad range of products.
- The feed is generated at unequal intervals or isolation requires to be done from time to time like in pilot type-plant operations.
- The materials compositions to be isolated, change over a broad range.
- The feed includes just small quantities of heavy and light impurities.

## 2.2.   Monoethylene Glycol (MEG)

### 2.2.1      Production of MEG

The feed gas use for MEG manufacturing approach used in industry is based on ethylene oxide by hydrolysis that is acquired during the direct oxidation process for feeding ethylene with air or oxygen [60] without using any catalyst or new processes such as sliver oxide reaction as described in eq. (2-96). Figure 2-18 shows a simple flow scheme of the production plant of ethylene glycol using the hydrolysis method. Through the reaction di, tri-, tetra- and polyethylene glycols can be also generated as by-products. The generation of the by-products takes place because ethylene oxide (EO) reacts to generate ethylene glycols that happens more easily than the primary reaction with water [60].

$$C_2H_2O + H_2O \rightarrow HOC_2H_4OH \tag{2-96}$$
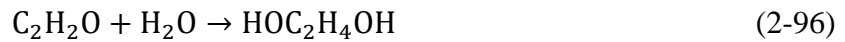
Following the ethylene glycol formation and its variables can be fed to the drying unit including water recovering. The produced glycols are then isolated through a series of distillation towers working under vacuum pressure with every sequential tower working at a lower pressure [60].
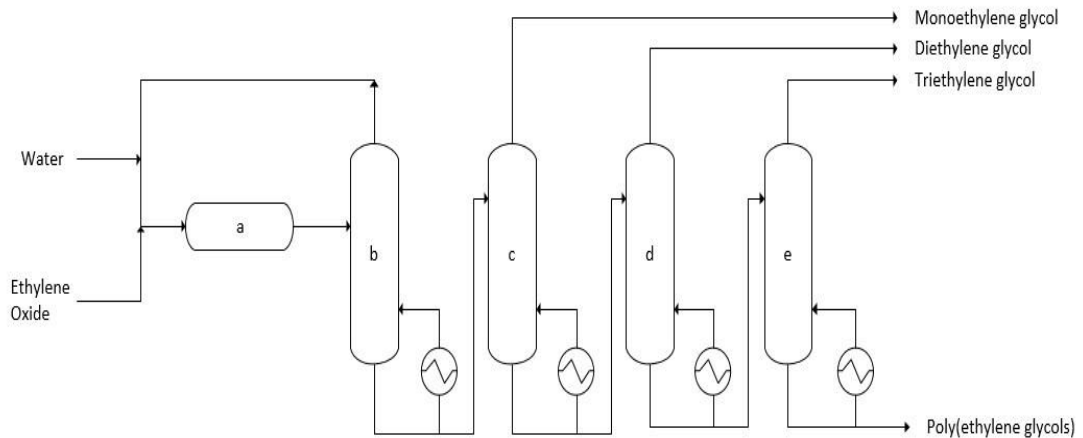


Figure 2-18: Flow scheme for glycol plan: a; Reactor, b; Tower for drying, c; MEG column, d; DEG tower, e; TEG tower [60]

### 2.2.2    MEG Economic Data

The usage of MEG is not only restricted to hydrate inhibition in industrial process of hydrocarbon but also as a major raw material within the production of polyester (PE) fibres [60]. The primary PE fibre made from MEG is polyethylene terephthalate (PET) generally used in the manufacturing of bottles and packaging. Shell Global (2005) have assigned 55% of the global consumption MEG to the manufacturing of PE fibres with 25% only utilized to produce PET. Another industrial application for MEG is engine anti-freeze for vehicle to avoid engine damaging under condition of low temperature [60]. Shell is one of the main producers of MEG, with about 40% of global MEG manufacturing assigned to methods using Shell technologies [61]. Shell possesses three MEG synthetic facilities using the newly advanced OMEGA production technique in Singapore, Saudi Arabia, and South Korea with capacities of 400, 600, and 750 kilotons each year respectively [61]. In total, China takes 45% of the worldwide consumption of MEG and it is expected  that its needs to be growing annually by about  7% [61]. Furthermore, it is predicted that Chevron's project in WA will use about 10% of the global production of MEG for hydrate inhibition during operation.

### 2.2.3    MEG Physical Properties and Cost

MEG is a clear, odourless, colourless liquid which has by a sweet taste if it is ingested [60]. Figure 2-19 (a) shows MEG structure. MEG is assorted as a hygroscopic material that is totally miscible in many polar solvents such as water, glycol ethers, alcohol and acetone, but the MEG solubility is low for non-polar solvents [60]. The MEG physical properties are outlined in Table 2-5 and their freezing points of MEG mixed with water are presented in Figure 2-19 (b).

The cost of MEG per metric tonne has increased from $900 USD in 2005 [14]. The rising price of MEG has been attributed to increasing demand for MEG for hydrate inhibitor and polyester production in markets specially China and India. A cost trend of MEG over 2012 and 2013 is displayed indicating a fluctuating price between approximately $1250 to $800 USD per ton [14].
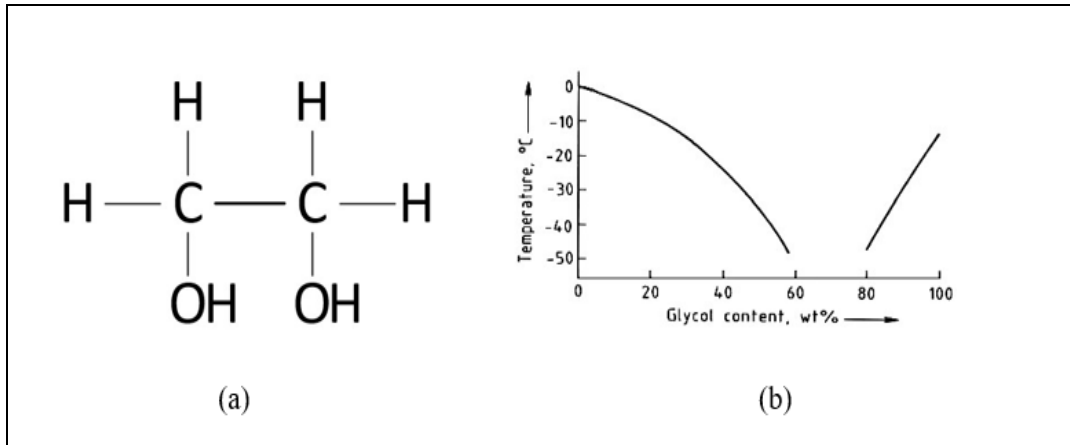
Figure 2-19: (a) MEG structure, (b) Freezing point of water and MEG mixture

Table 2-5: Physical properties of MEG [60, 62]

| | |
|---|---|
| Boiling point (1 atm) | 197.5°C |
| Density (20 °C) | 1.1134 g/ml |
| Molecular Weight | 62.07 |
| Specific heat (kJ/kg.K) | |
| 20 °C | 0.560 |
| 0 °C | 0.545 |
| Viscosity (Cp) | |
| 10 °C | 33.60 |
| 20 °C | 19.82 |
| 25 °C | 17.40 |
| 35 °C | 12.30 |
| 60 °C | 5.20 |
| Combustion Heat | 19.05 MJ/kg |
| Critical Values | |
| Temperature | 372°C |
| Pressure | 6515.73 kPa |
| Volume | 0.186L/mol |

### 2.2.4    MEG Recovery Processes

In the industry of hydrocarbon processing, MEG recovery from water is mostly by distillation in order to vaporize surplus water commonly generating a lean MEG by 80-90% wt. MEG [12, 63]. The most common MEG recovery technique may be broadly categorized into two important process types consisting of re-concentration and regeneration [3]. The simplest restoration approach is the re-concentration where a distillation tower is used to vaporize a solution of the rich MEG to produce the desired lean MEG specification.

Re-concentration is usually used when no corrosion or salts products are predicted through the recovery process [2]. This is typical during the early production stages where the formation water produced if any, contains little to no dissolved salts [3, 14]. As the reconcentration process only removes water from the rich MEG, any dissolved salts, corrosion products and additional chemical used in processing will accumulate inside the closed MEG loop. This assembly  of salts higher than the saturation limits inside the MEG system may additionally bring about severe fouling and plugging of device and flow-lines, as such the salt have to be either eliminated or the MEG must be replaced from time to time[2].

MEG regeneration may be done using two exceptional methods relying on the desired final lean MEG salt composition, by either slip stream salt elimination or full stream regeneration. Full stream regeneration is applied when large quantities of dissolved salts can be produced in the course of processing or when an efficacious salt free lean MEG is required. Another option, slip stream regeneration can be carried out when a specific amount of dissolved salts sustain during the closed MEG cycle.

### 2.2.4.1. Full Stream Regeneration

For systems wherein huge amounts of water production are anticipated during the facility lifetime or the rich MEG feed which has great amount of corrosion products and dissolved salts full stream regeneration ought to be used [2, 3]. As an alternative, full stream regeneration can be chosen if a totally salt free lean MEG product is the desired option. Commonly, other solids and salts have to be eliminated before MEG reinjection at the well head to avoid pipe scaling and damaging other system devices.

the full stream regeneration of MEG is carried out in 2-step system in which The rich MEG component can be vaporized using low pressure of (0.1-0.15 bara) which leaves non-volatile and salts solids residual in a flash drum [3, 14]. The MEG solution free from salt is then re-concentrated using the distillation process to obtain the specified lean MEG. A scheme of the MEG full stream regeneration method is illustrated in Figure 2-20.

Other techniques for MEG recovery included a simple re-concentration and slip-stream regeneration to enable getting rid of the excessive salt amount encountered throughout the formed water manufacturing. As such, full stream regeneration should be carried out to avoid long term harm to the processing facility via high solid build-up system devices and in pipelines.
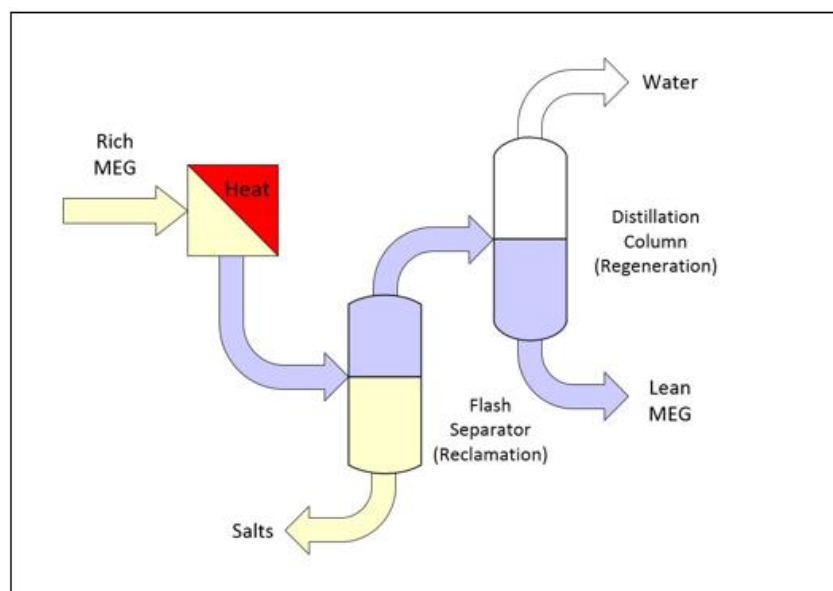


Figure 2-20: Full stream regeneration for MEG [3]

### 2.2.4.2. Slip Stream Regeneration

For low to moderate water formation rates it is usually more desirable to use the split-stream salt removal technique to lower the cost of operation and size of equipment [12]. In using split stream regeneration, the rich MEG solution is initially subjected to treatment to take out the light hydrocarbons, salts of low solubility and corrosion products prior to the conventional distillation stage. Traditional re-concentration is done by the use of a distillation tower as per the re-concentration approach to get rid

of excess water to gain the wanted MEG purity. Following the distillation, most of the lean MEG is subjected to salt elimination through an ion exchange unit or reclaimer to eliminate the remaining soluble salts. However, part of the salty lean MEG stream by-passes the salt elimination unit and mixes with the very last salt free lean MEG. The rate of the slip-stream is usually specified by the permissible quantity of soluble salts in the required lean MEG product needed to avoid pipeline scaling [3, 14]. The flow scheme of regeneration system for an ordinary slip stream is presented in Figure 2-21.

The main advantages of running a split stream is to reduce the needed power throughout the work due to smaller fractions to be vaporized. Furthermore, the distillation system may be operated under atmospheric pressure that replaces the vacuum conditions requirements and this saves more power costs for the process [12]. However, under atmospheric pressures, the MEG evaporation will require higher temperatures which can cause more thermal degradation of the MEG with respect to its effectiveness of inhibition and overall performance. As such, care ought to be taken with MEG 160 °C to avoid thermal degradation [5].

The reclaimer system is used to eliminate salts which is only desired throughout the manufacturing of formation water that contains salts, therefore, when there is no water formation, the reclaimer system can be bypassed to lower operating costs. Whereas the long term operation leads to accumulation of impurities inside the closed loop of MEG which may cause additional problems which will need additional treatment to avoid solid precipitation in system devices and flow-lines [14]. This may be basically prevented with good control to the flow rate from by-pass stream to make sure that the amount of salts in the MEG product stays less than the saturation point downstream.
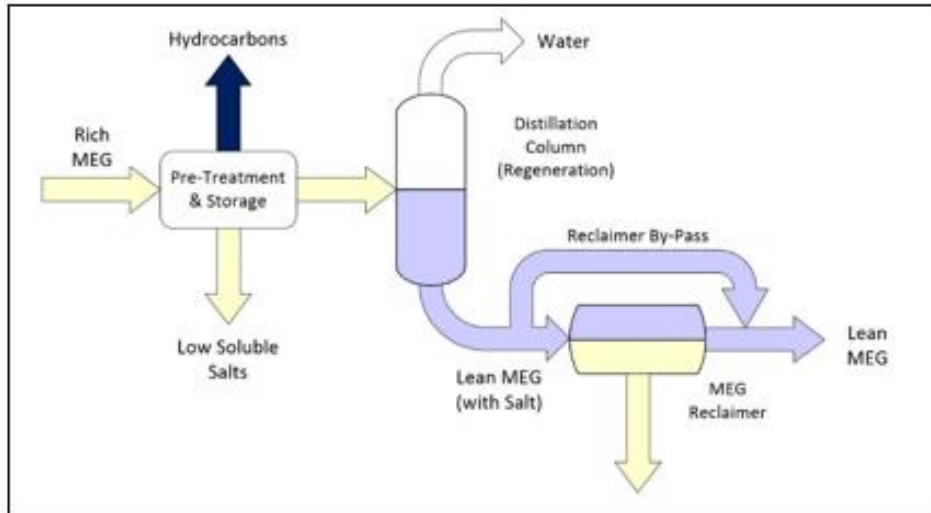
Figure 2-21: Flow scheme for stream regeneration[3]

## 2.3. Salts, Scaling and Precipitation

Many sources of rich MEG pollution are common during the regeneration process, with the higher predominant of which being the supersaturated salts precipitation in the MEG system giving rise to fouling of process devices and pipes. The main origin of salt cations in MEG regeneration process are generated from the associated water. The formed water is represented by the liquid water enclosed in the pores of reservoir [64]. Formation water usually hold dissolved solids which are of low divalent solubility cations mainly, $Mg^{2+}$ and $Ca^{2+}$ and very soluble mono-valent cations like $Na^+$ and $K^+$. Formed water breakthrough may not arise till many years after the initial processing have started which ought to be taken into consideration in the recovery system design of MEG [64]. Typically, an assessment will be made for the reservoir production profile and the MEG recovery system designed to treat the most awful case of the scenarios of salt loading to ensure of minimum salt precipitation during system processing time.

Many other contamination sources of MEG normally involve corrosion products like $Fe^{2+}$ ions and many other chemical materials injected into the MEG system such as corrosion inhibitors, also scale inhibitors and oxygen scavengers. Also hydrocarbons in vapour and liquid phase can exist in the rich MEG stream that follows upstream 3 phase isolation. Dissolved cations and salts in the rich MEG can be taken away by the

use of several processing strategies like using chemical precipitation, filters, vessel of MEG reclaimer and centrifuges, with the removal type method dependant on the amount and kind of contaminant that exist. Eliminations of contaminants, mainly salts is essential to avoid build-up of solid and damaging of sensitive parts of the MEG regeneration plant.

Figure 2-22 shows a serious fouling case of a MEG regeneration kettle re-boiler caused from the excess iron carbonate precipitation during the course of operation. The forming of such solids gives rise to a remarkable reduction in the efficiency which needs permanent maintenance and cleaning to avoid its occurrence.



Figure 2-22: MEG Regeneration Kettle re-boiler tube bundle $FeCO_3$ fouling [64]

### 2.3.1 Divalent Salts

#### 2.3.1.1 Calcium Carbonate ($CaCO_3$)

$CaCO_3$ precipitation in gas manufacturing pipelines can take place when water from a tank that holds calcium interacting with the injected MEG as anti haydrate agent throughout transportation [65]. In the gas production, the $CaCO_3$ precipitation is thought to be one of the most regular sources of scaling and mineral precipitation [66]. The hazard of $CaCO_3$ precipitation throughout work is accelerated if the conditions are alkaline in the pipes, while they are normal when using MEG combined with the pH stabilisation. The MEG alkalinisation is done by the use of pH stabilisation to enhance

the film formation of iron carbonate at the interior surface of the pipes in order to control corrosion [65, 67, 68]. Calcium carbonate crystallisation may happen to produce 3 different structures of anhydrous polymorph such as, aragonite, vaterite and calcite with the proportion to be the highest thermodynamically stable phase [65, 66]. Shapes of aragonite calcite crystals collected as shown in Figure 2-23. The minimum stable polymorph structures of $CaCO_3$ have the best solubility but will convert by dissolution and re-crystallisation to a calcite of greater stability structure with time [69]. In aqueous solutions of MEG, the calcium carbonate precipitation at low temperatures is mostly in the shape of calcite, while at higher temperatures the aragonite precipitation will take place [65]. Typically, the third kind of $CaCO_3$, vaterite exists at higher supersaturation situations and is not often observed in MEG processing.
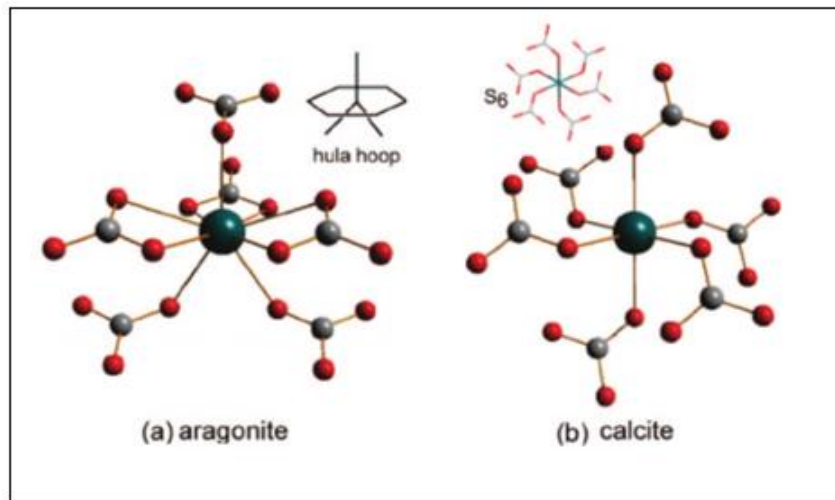


Figure 2-23: Crystal Structure for Aragonite and Calcite [70]

$CaCO_3$ precipitation throughout the recovery of MEG is the result of the $CaCO_3$ super-saturation in the solution. According to Flaten [65], the origin of calcium carbonate super-saturation in MEG processing is the high quantities of Ca cations within the created formed water. This is related to the $CO_2$ concentration in the hydrocarbons and the alkaline media happening in the pipes because corrosion control leading to $CaCO_3$ via steps as follow:

$$CO_{2(g)} \rightarrow CO_{2(aq)} \qquad (2\text{-}97)$$

$$CO_{2(g)} \rightarrow CO_{2(aq)} \qquad \text{(2-98)}$$

$$CO_{2(g)} + H_2O \rightarrow H^+ + HCO_{3(aq)}^{-2} \qquad \text{(2-99)}$$

$$Ca_{(aq)}^{+2} + CO_{3(aq)}^{-2} \rightarrow CaCO_{3(s)} \qquad \text{(2-100)}$$
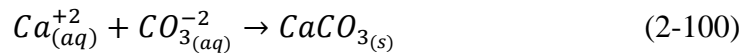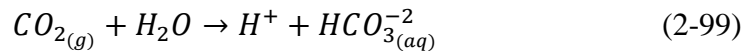
According to Flaten [65] the calcium carbonate solubility is reduced with increasing MEG concentration. This is explained by the experiments accomplished by Kassa [71] related to calcium carbonate solubility at different concentration of MEG and different temperatures. From the experiments, it was discovered that a noted reduction in $CaCO_3$ was seen with the rise of MEG concentration at various temperatures of three levels. Figure 2-24 shows the experimental measurements against the theoretical model evolved by Kassa [71] to evaluate the solubility of calcium carbonate (calcite) in MEG. This depression in the solubility of $CaCO_3$ at higher concentration of MEG, together with the rise in the activity of carbonate in alkaline conditions enhance the $CaCO_3$ precipitation in recovery system of MEG.
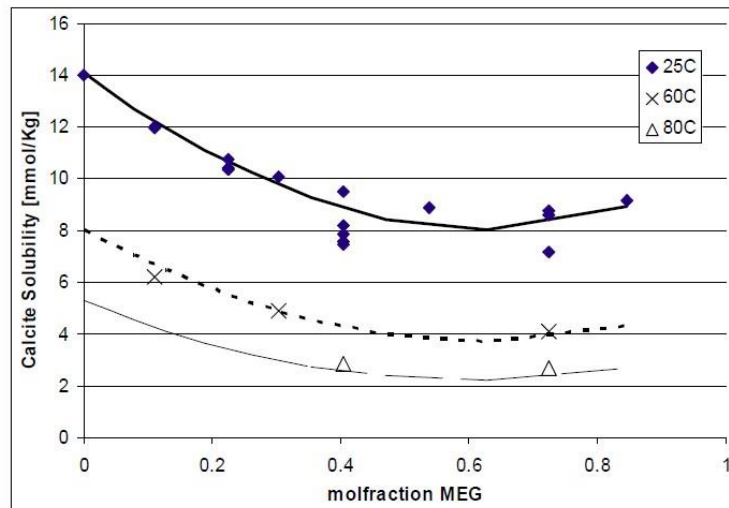


Figure 2-24: Solubility of $CaCO_3$ in MEG water solution [71]

The $CaCO_3$ precipitation can just happen when the limits of saturation are achieved. Precipitation is thermodynamically preferred when the ratio of saturation is more than one and it is specified from eq (103). $K_{sp}$ represents to thermodynamic solubility product of a polymorph for known composition of solvent [66]. The terms $Ca^{+2}$ and

$CO_3^{-2}$ are the activity of $Ca^{+2}$ and $CO_3^{-2}$ which can be predicted by the use of thermodynamic software packages. Before the occurrence of the precipitation of $CaCO_3$ once super-saturation has been accomplished, a specific time should be passed over super saturation and the $CaCO_3$ physical precipitation during the nucleation of solid stage. This period is called the induction time and is determined by noticing the solution physical changes like conductivity, turbidity and pH [66]. The complete induction time is a summation of the nucleation time and the time of growth to an observable size of the nucleus [65, 66].

$$SR = \sqrt{\frac{a_{Ca^{+2}} \cdot a_{CO_3^{-2}}}{K_{sp}(CaCO_3)}}$$ (2-101)

The rate of nucleation of crystal precipitation may be predicted by the use of eq. (2-102). This rate is controlled by 3 important factors which are the super-saturation ratio (SR), the interfacial tension ($\gamma$), and absolute temperature (T). Generally, a high rate of nucleation will result in the production of small crystals in huge amounts, whereas a low rate of nucleation will result in the formation of bigger crystals in a smaller amount [68]. The nucleation rate is normally an indication of super saturation level of solution resulting in large quantity crystal formation.

$$J = A \, exp \left[\frac{16\pi\gamma^3 v^2}{3K^3 T^3 (\ln SR)^2}\right]$$ (2-102)

It has been reported by Flaten [66] that the existence of MEG will expand the required induction stage for the precipitation of $CaCO_3$. Their presence in pipelines lead to the decrease of nucleation and the growth rate of all the three kinds of $CaCO_3$ polymorphs. The rise in the induction time of calcium carbonate crystallisation with the rise in the concentration of MEG was assigned to the delay of the growth of the crystal and not to the decreased rate of nucleation [68]. Also it has been noted that the existence of $Fe^{2+}$ ions additionally caused an increase in induction period for the precipitation of $CaCO_3$ with the consequence of concentration increasing [66, 68]. More induction time researches of $CaCO_3$ in solutions of MEG has been done by Flaten [72] concluding the super-saturation ratio will fall between the limits of 3-10 and once more showing the delay of crystal growth by MEG.

### 2.3.1.2    Iron Carbonate (FeCO₃)

As formerly discussed, the (FeCO₃) formation in the MEG regeneration system is produced by the formation of an iron carbonate protective layer against corrosion which are known as corrosion products. FeCO₃ together with CaCO₃ are the most abundant forms of carbonate precipitating inside the regeneration process of MEG [73]. The stability of the protective film of iron carbonate on the surface of the pipes is immediately related to FeCO₃ solubility [68]. This solubility of FeCO₃ controls the quantities of salts that are dissolved in the rich MEG as it flows in the pipe with the generation of FeCO₃ happening by a similar reaction to CaCO₃. Other factors affecting the extent of dissolving iron are the alkalinity, the pipe length and the corrosion rate [73].

$$Fe^{+2}_{(aq)} + CO_3^{-2}{}_{(aq)} \rightarrow FeCO_{3(s)} \tag{2-103}$$

Although it is helpful in resisting corrosion of pipes, high production of iron carbonate will result in precipitation of solids in the regeneration process of MEG, particularly in the re-boiler. The ferrous cation, $Fe^{2+}$, formed in the course of corrosion can gather downstream of the aqueous phase of the pipeline and might react with the carbonate anions and sulphide to make severe mineral scaling [64]. When corrosion rate is low, the iron concentration in the outlet part of the pipeline will be in the range of 1-100 ppm [68, 73]. The deposition of iron carbonate mostly takes place in 'sweet' systems with low content of hydrogen sulphide, however, the deposition of iron sulphide might take place when there is sufficient concentration of hydrogen sulphide [73].

A considerable part of the suspended iron carbonate in the rich solution of MEG does not commonly form upstream of the MEG regeneration process, but iron carbonate typically stays as dissolved ionic species at supersaturated conditions, typically precipitating within the MEG regeneration unit where the greater temperatures accelerate precipitation [64]. As such, using a system of filtration for the feed is usually not a possible method to prevent iron carbonate crystallisation. Also chemical deposition may rather be found as a possible choice relying on the conditions of the systems [64]. However, according to Latta [64], precipitating factors are significant for reduction the device cleaning and fouling needs because of the chemical additives that may produce further contaminating from the lean MEG. The research published

by Figueiredo [73] presents an opinion for the growth kinetics of $FeCO_3$ in Water - MEG solutions.
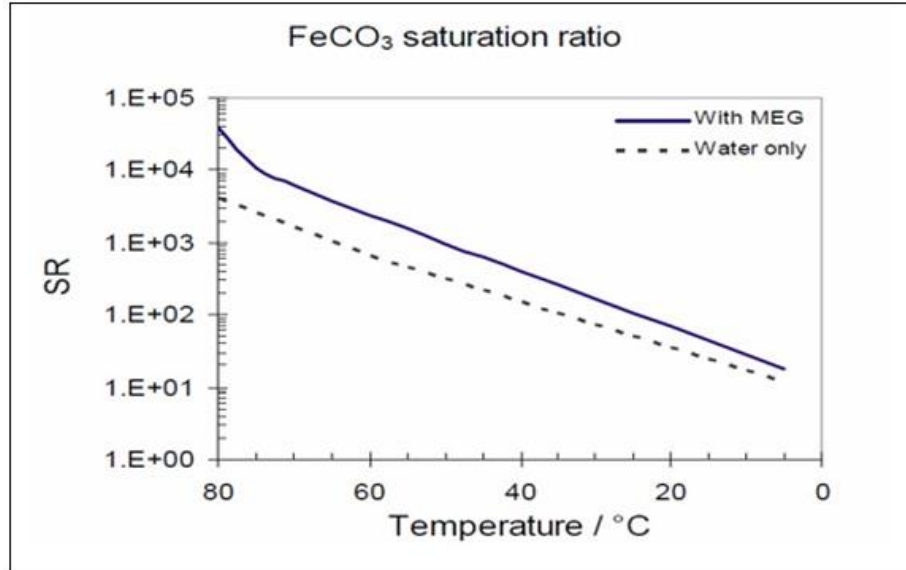


Figure 2-25: Iron carbonate saturation ratio as a function of temperature over a pipeline.

### 2.3.1.3  Iron Sulphide (FeS)

FeS formation throughout MEG processing may arise when considerable concentration of hydrogen sulphide ($H_2S$) exists through processing. Similar to the formation of iron carbonate, dissolved ferrous cations are required for producing the iron sulphide. The mixing of $Fe^{2+}$ and $H_2S$ will bring about the formation of many FeS species with the ratio of $Fe^{2+}$ to sulphide (S) inside these species conditioned by temperature, pressure, pH, and the concentration of $H_2S$ [74]. The ratio of sulphide to iron has a crucial action in selecting the best technique for removing of FeS scaling from pipes and vessels [74]. The existence of FeS inside piping and MEG systems can be a source of fundamental troubles due to the possibility of the occurrence of crevice or bimetallic corrosion particularly when water is present [75].

### 2.3.2    Monovalent Salts

The existence of monovalent salts in rich MEG systems is usually $Na^+$ and $K^+$ cations founded by the processing of formed water. Sodium ions account for about 90-95% of total dissolved ions in formed water as given by Latta [64]. Potassium is generally considered to be the remaining monovalent cation in the formed water with lithium feasible but of low concentration. Na+ and K+ cations particularly form salts with the existence of chlorine anions by the subsequent reactions:

$$Na^+_{(aq)} + Cl^-_{(aq)} \rightarrow NaCl_{(s)}$$

$$K^+_{(aq)} + Cl^-_{(aq)} \rightarrow KCl_{(s)}$$
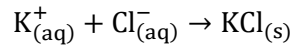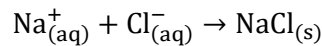
Because of large amount of $Na^+$ cations normally existing in the rich MEG stream, sodium chloride is considered as one of the essential salts formed inside the reclaimer process [76]. Figure 2-26 shows graphically the solubility of KCl and NaCl at 25°C both measured experimentally and by using a solubility model suggested by Kaasa [71]. It can be clearly seen that salts decrease steadily with the MEG ratio. Typically large MEG ratio inside the re-boiler unit it probably change the super-saturation of both salts which will lead to their precipitation inside the re-boiler. The reduction in the solubility of these salts with the rising MEG content may be assigned to water amount reduction in the rich MEG composition, in which there is high solubility of these salts in water compared to MEG. So the rich MEG solution will be heated by the reboiler and water boiling off leading to increased concentration of the salts in solution. This leads to a precipitation consequence because there is not sufficient water for dissolving these salts.
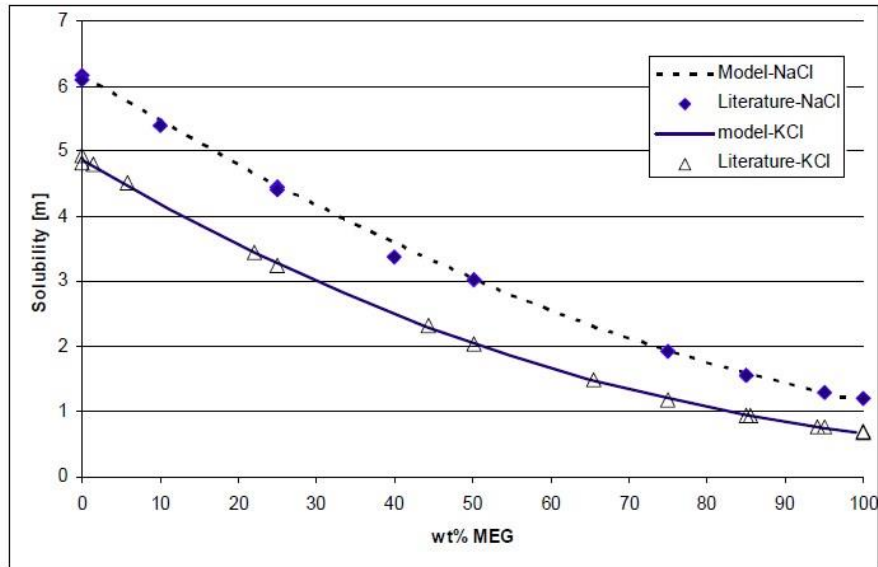
Figure 2-26: KCl and NaCl Solubility at 25°C [71]

### 2.3.3 Scale Formation

The build-up of scale within MEG process and pipes is a big issue for recovery of MEG, it is specifically troublesome inside re-boilers and the heat exchangers operating at high temperatures. $CaCO_3$, one of the maximum regularly experienced scaling products, is in particular at risk of causing fouling in heat exchanger devices because of its solubility decrease with temperature increase [12]. The scale formation inside the heat exchanging units of MEG process may result in a depression in the efficiency of heat transferral. Moreover, the scale formation downstream in system piping flow schemes can cause severe flow limitations, which could lead to blockages that may severely obstruct process operation and control as shown by Figure 2-27.
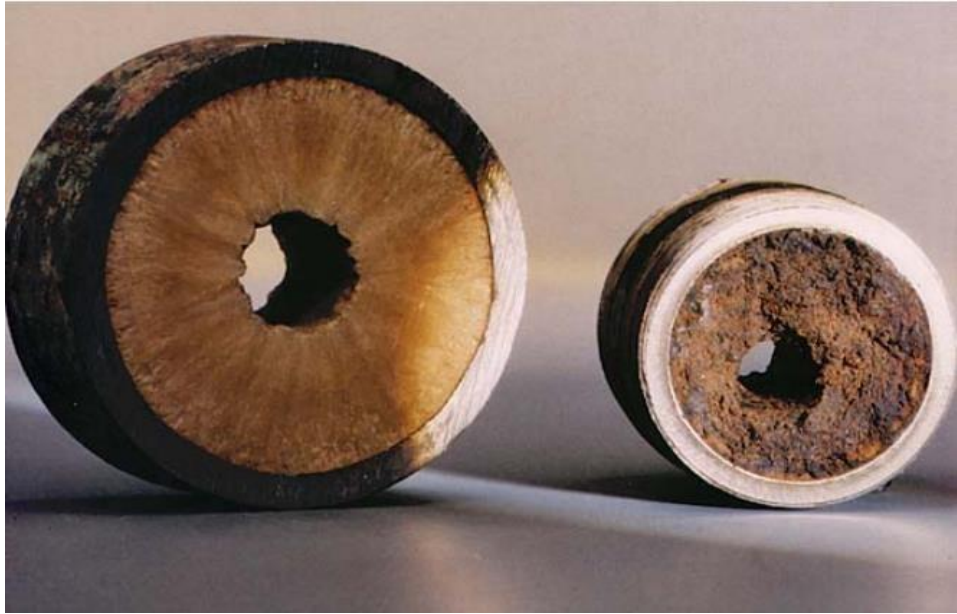
Figure 2-27: Scale formation in process piping [77]

Excessive scaling of downstream heat exchanger devices may be elevated with the aid of precipitation upstream to permit the elimination of divalent salts before getting into the MEG regeneration tower. NaOH is usually added to simplify the divalent salts precipitation, mostly calcium carbonate, $MgCO_3$ and to smaller degree corrosion products like $FeCO_3$ [78]. As soon as super-saturation of the salt products has happened which results in salt precipitation, filtration may be used to get rid of solids before the rich MEG undergoes regeneration in the MEG tower. The improvement of monitoring programs and the use of corrosion inhibitors will also be done to restrict the formation of scale as a result of corrosion products like iron carbonate and iron sulphide [79].

### 2.3.4 Other Contaminants

#### 2.3.4.1. Hydrocarbon Contamination (HC)

Before the MEG recovery with the aid of distillation, the water - MEG solution needs to be isolated from the HC vapours and liquid streams by using a 3 phase separation vessel. Throughout the processing, the rich MEG stream is possibly contaminated by the liquid HCs. Numerous sources of HC pollution can arise by the two popular soluble HC liquids like benzene, toluene, ethylbenzene and xylenes (BTEX) and with HC

liquids that would be emulsified in the rich MEG [64]. The immiscible HC liquids may in addition be categorised as light HC, commonly $C_{17}$ or lighter which are of higher volatility and contaminate the stream of water product, also the heavier HCs, $C_{18+}$, which usually pollute the MEG and salt final streams [64].

- Impact on MEG Regeneration Systems

The excessive entrainment of HCs in the rich MEG stream may cause huge quantities of light HCs being flushed inside the MEG regeneration tower. Light HCs flushing inside the unit of distillation may cause a big damage to the unit's internals and an excessive disruption to the MEG recovery. Moreover, if considerable liquid HCs exist in the regeneration of MEG unit, heavier HC having boiling points more than the range of 150-160 would stay in the MEG product.

- Impact on MEG Salt Reclamation System

The effect on reclamation process of MEG salts mostly results from pollution due to the heavier hydrocarbons that are not eliminated by means of pre-flashing or by way of distillation. Figure 2-28, picture shows a comparison between heavy HC contaminated salt cake and a clean one that was recovered throughout the removal of MEG salts. The existence of heavy HCs retard the salt composition that make a paste which is difficult to be isolated from the glycol and can lead to blockage of downstream separation equipment [64]. Latta [64] indicated that despite the fact that just a small quantity of heavy hydrocarbons might exist in the salt recovery process, it might have a significant impact on the MEG reclaimer and the following monovalent salts separation.

The existence of HC in the final product of lean MEG if not separated may have a severe impacts on the quality of product. High increase in viscosity of MEG and its density may result in reduction of re-boiler recirculation rate and decrease the heat transfer rate of the boiler because of the increase in liquid viscosity that could affect the distillation towers efficiency.

Figure 2-28:  (a) Hydrocarbon contaminated salt cake  (b) Clean Salt Cake [64]

- Removal of Hydrocarbon Contamination

The hydrocarbon contamination removal in the rich MEG stream may be carried out by the use of a pre-treatment vessel that is designed for the purpose of elimination of light HCs. The location of the pre-treatment flash vessel is just before the MEG regeneration tower and it is operated under vacuum in an effort to flash light HCs contained within the liquid feed rich MEG. As an alternative, the regeneration tower of the MEG and the related reflux drum can be designed to include decanting provisions capable of liquid HC separation [64]. Liquid HC will make an emulsion by its reaction with the attached water with MEG. However, by good designing for tower internals of the MEG distillation and reflux drum separation of the liquid HC phase may be accomplished.

## 2.4. Water Treatment

MEG is widely used in the gas and oil industries as an anti-hydrate agent and its availability in wastewater is considered as hazardous. During natural gas processing for industrial production, the wastewater is contaminated by MEG leading to increase oxygen requirement in water [80]. Furthermore, the wastewater may contain MEG due to the distillation column failure and this could occur as follows: The lack of the reflux ratio, re-boiler doesn't work properly and in case of distillation process running under vacuum. It is reported that the MEG content in drinking water should not be more than 7 mg L$^{-1}$ [81, 82]. The most reliable and economical method to remove MEG from wastewater is by the adsorption method [83]. The removal methods by adsorption will be discussed as follow.

### 2.4.1 Adsorption

Adsorption is a separation process where the solute existing in a gas phase or liquid can be adsorbed onto solid substrates, consequently they are eliminated from the gas or liquid. Typical applications of this include purification of drinking water and pollutants removal from effluents. Adsorption process can occur because of the linking forces between ions. Adsorption nature can be classified to physisorption and chemisorption process [84]:

In physisorption, the adsorbent is connected to the surface by physical forces like Van der Waals and $H_2$ lining. Multi-layers can be generated by similar adsorption heating. There is no electron exchange between adsorbent and the substrate. This kind of adsorption is considered to be reversible.

For chemisorption there is chemical bonding by electrons sharing between the adsorbent and substrate. This chemical bond is stronger compared to the Van der Waals forces in physisorption. This adsorption counts as stable and has high value of adsorption heating. Furthermore, multilayers are not available in this adsorption [84]**.**

Among the treatment and separation techniques that are available for water and waste water treatment, adsorption process indicates the probability to be one of the most effective applications for contaminates removal in wastewater. The major advantage of adsorption technique is considered as an economical method.

### 2.4.1.1 Adsorption Thermodynamics

Adsorption processes similar to any chemical system reaches an equilibrium step. To meet the basic design and practical purposes, this technique requires a clear concept of temperature effect in addition to thermodynamic parameters. There are two kinds of thermodynamic characteristics; Gibb's free energy entropy and enthalpy. These parameters count as significant variables for design, performance evaluation, mechanism prediction and adsorption characterisation.

The thermodynamic parameters can be determine using the following relations.

$$LnK_d = ln\frac{C_a}{C_e} = \frac{-\Delta G^\circ}{RT} \tag{2-104}$$

$$\Delta G^\circ = \Delta H^\circ - T\Delta S^\circ \tag{2-105}$$

$$LnK_d = \frac{\Delta S^\circ}{R} = \frac{\Delta H^\circ}{RT} \tag{2-106}$$

Where:

$K_d$ = Equilibrium constant.

$C_a$ = Adsorbent concentration in solid state mg/L.

$C_e$ = Adsorbent concentration at equilibrium state in aqueous solution mg/L.

$\Delta S°$ = Entropy Change J/mol.

$\Delta G°$ = Gibb's free energy change J/mol.

T = Enthalpy change J/mol.

R = Universal Gas Constant 8.314 J/mol.

The linear relationship between Ln K and 1/T as shown in eq. (2-104) can be of benefit to calculate the values for each temperature using Helmholtz relation eqns. (2-105) and (2-106).

### 2.4.1.2 Adsorption Kinetics

The kinetic study has the important practical task to determine the degree of utilization of the adsorption capacity as a time function of contact between the liquid and the solid. Therefore, different models can be used for fitting the obtained kinetic curves to

define the rate parameters and explain the mechanism of mass transfer [85]. First order rate pseudo equation can be expressed as follows [86]:

$$\frac{dq_t}{dt} = K_1(q_e - q_t)$$ (2-107)

Where $q_t$:  Capacity of adsorption at time t (mg/g)

$q_e$:  Capacity of adsorption at equilibrium state (mg/g)

$K_1$:  first order rate pseudo constant (min$^{-1}$.)

In case of integration and application of boundary conditions t=0 and $q_t$ =0 to t=t and $q_1$=$q_e$ at equilibrium, the above equation can be expressed as follow:

$$ln(q_e - q_t) = lnq_e - K_1.t$$ (2-108)

The second order pseudo is described according to [86]

$$\frac{dq_t}{dt} = K2(q_e - q_t)^2$$ (2-109)

Where $K_2$: pseudo second order rate constant.

In the case of applying the same boundary conditions, the integration in eq. (2-109) expresses as follow:

$$\frac{t}{q_t} = \frac{1}{K_2 q_e^2} + \frac{t}{q_e}$$ (2-110)

The Elovich's equation is expressed as follows [87]

$$q_t = \frac{1}{\beta} ln(\alpha\beta) = \frac{1}{\beta} ln(t)$$ (2-111)

Where $\alpha$ is the initial adsorption rate (mg/g) and $\beta$ is adsorption constnt (mg/g.min).

The model of intraparticle diffusion can be expressed according to the literature [87]:

$$q_t = K_p t^{0.5} + C$$ (2-112)

Where $k_p$ is the diffusion rate intraparticle constant (mg/g.min$^{0.5}$).

The dynamic process that is produced from liquid solid contact by adsorption process may be described as follow:

- 1$^{st}$ diffusion of the film that refers to adsorbent molecules transferring from the bulk onto the substrate.

- 2nd diffusion of intraparticle that expresses the adsorption molecules movement from the substrate to the active centers.
- 3rd the interaction that involves between active centers and adsorption molecules.

### 2.4.1.3    Adsorption Isotherm

The adsorption isotherm can be defined as the relationship between adsorbent concentration in the particle and the adsorbent concentration in the fluid phase at specific temperature. It is classified to four major classes based on the initial part of isotherm graph.  The isotherm graph refers to the adsorbent concentration in returns to the capacity of the adsorption process as shown in

Figure *2-29*. The linear relationship is found for C isotherm and this linearity starts from the original value. This is referred to that the adsorbent concentration on the solid surface and the adsorbent concentration in the liquid phase are the same for any initiation concentration. L curve represents to the reduction of the adsorbent concentration in solid and liquid with adsorbent concentration increasing. However, it is been noted that slope on H was started hard when the adsorption operating began and this described as high tendency for adsorbent. Typically this kind of isotherm results from at least two opposite mechanisms calling cooperation adsorption [84].
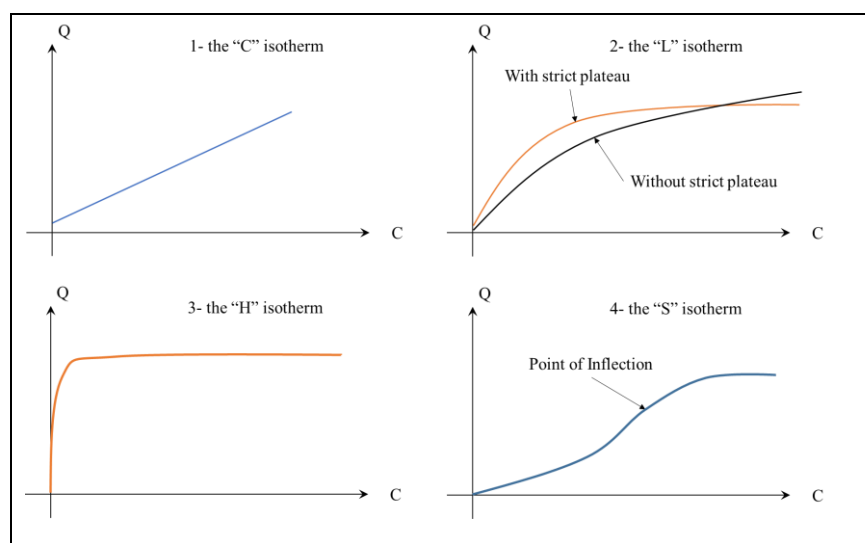


Figure 2-29: Type of Isotherm shapes [84]

- Langmuir model

The relationship between the amount of adsorbed gas on the substrate and pressure has been developed by American chemist Irving Langmuir.

The hypothesis of Langmuir isotherm can be described as follow:

- After the monolayer is formed, adsorption cannot occur.
- All active centres for adsorption possess the same change in Gibbs energy values.
- The activity of adsorbent molecules is not reliant on neighbour active center occupation.

The Langmuir concept can be represented as in eq. (2-113) [88].

$$q_e = \frac{q_{max} \times K_L \times C_e}{1 + (K_L \times C_e)}$$  (2-113)

Where:

$q_e$ : Adsorbed amount per sorbent unit (mg/g)

$q_{max}$ : Maximum capacity of adsorption (mg/g)

$C_e$ : Solute concentration in solution at equilibrium state (L/mg)

$K_L$ : Constant of Langmuir adsorption (L/mg)

- Freundlich's model

Freundlich's hypothesis is described as the adsorbent active centres that have different energy values (inhomogeneous surfaces). It has been used widely because constant centre energy value requirements and monolayer forming on the surface are not sufficient for the majority of adsorbents [89]. It can be expressed by eq. (2-114):

$$q_e = K_f . C_e^{1/n}$$  (2-114)

Where $K_f$ : Capacity parameter of Freundlich adsorption $\{(mg/g)(L/mg)^{1/n}\}$ .

1/n : Intensity parameter of Freundlich adsorption n>1.

- Model of Temkin

Model of Temkin is considered to be a development of the Langmuir hypothesis by combining the variation in linearity of adsorption energy as described in eq. (2-115):

$$q_e = \frac{RT}{b}(lnAC_e) \qquad (2\text{-}115)$$

Where; A; is the constant of equilibrium linking referring to the maximum linking energy.

RT/b: Corresponds to the Temkin constant associated with sorption heating (J/mol).

# 3. MEG Regeneration Pilot Plant and Equipment Details.

## 3.1 Introduction

Monoethylene glycol (MEG) closed loop system is complex using various chemicals and physical processes. A better understanding of these processes and their consequences on the process equipment can be useful to plant operation and management throughout the world. A closed pilot scale loop MEG regeneration/reclamation unit was designed and constructed at Curtin University. The pilot unit was aimed at mimicking field conditions for bridging gaps between laboratory scale testing, thus improving confidence in the selection of production chemical additives and implementing hydrate inhibition and corrosion mitigation strategies. The facility is designed to use realistic approximations of production fluids, such as condensate mixtures and formation water/brine to simulate conditions representative of an industrial MEG system.

The use of MEG for gas hydrate control in production pipelines has been established and seen favourably in the recently. Lean-MEG is injected at the well head and travels through the production pipeline providing the necessary hydration inhibition to avoid plugging. The lean-MEG solution comes into contact with the formation water / produced water, and salts as it flows through the transport and production pipe lines. Through the regeneration and reclamation stages of the MEG operation, the water and dissolved salts are removed from the rich-MEG solution thus re-purifying the solution to lean-MEG quality. The regenerated lean-MEG is then rerouted to the wellhead by specific pipelines for re-use as hydrate inhibitor. A simplified MEG closed loop process flow diagram representing the major process units is shown in Figure 3-1.

Even though the uninterrupted use and re-purification of MEG for reuse is a favorable solution that is reliable and least costly in terms of hydrate control, it is however, a sophisticated process consisting of numerous chemical and physical processes. The extent of complication in a MEG operation becomes even more significant owing to factors such as the existence of numerous chemicals, other additives, like scale inhibitors, corrosion inhibitors, plus the presence of salt in solution. The joint effects of all these factors (specifically salts in solution) have resulted in issues that have played a vital role in the operation shut downs resulting in loss of production.

## 3.2  MEG Pilot Plant

Corrosion and scale formation are major challenges being faced by the gas processing industries. These challenges are being addressed with the use of chemical inhibitors however, extensive studies beyond the benchtop experimentation are required before actual implementation in the field can be successfully achieved. For this purpose, pilot plants mimicking field-like operations and plants are required to better understand the dynamics of corrosion and scale inhibition strategies. The MEG plant was designed for the purpose of testing and validating industry operations and providing expert insights and recommendations. Below are listed the capabilities of the MEG Pilot Plant:

- Simulating condensate carryover into the MEG pre-treatment vessel – to address carryover issues leading to operational disruption.
- Mud clean-up experimentation – the removal of mud from MEG solution during start-up.
- Verifying the compatibilities of chemical additives.
- Simulating corrosion control strategies and switching overs– adopting amines for pH stabilization and corrosion inhibitors for film formation.
- Undertaking corrosion studies throughout the MEG plant – risk of corrosion on various parts of the plant due to various applications.
- Optimizing salt removal processes – the presence of salt can increase scale formation.
- Corrosion and scale inhibitor testing – new and innovative formulations can be pre-tested before actual field operations.

### 3.2.1  MEG process flow scheme

This process flow scheme was developed to achieve a closed loop system capable of simulating field conditions and appropriate process conditions. The MEG pilot plant has been divided into the following systems:

- Feed preparation and blending system (Area 100)
- Pre-treatment system (Area 200)
- MEG Regeneration system (Area 300)
- MEG Reclamation system (Area 400)
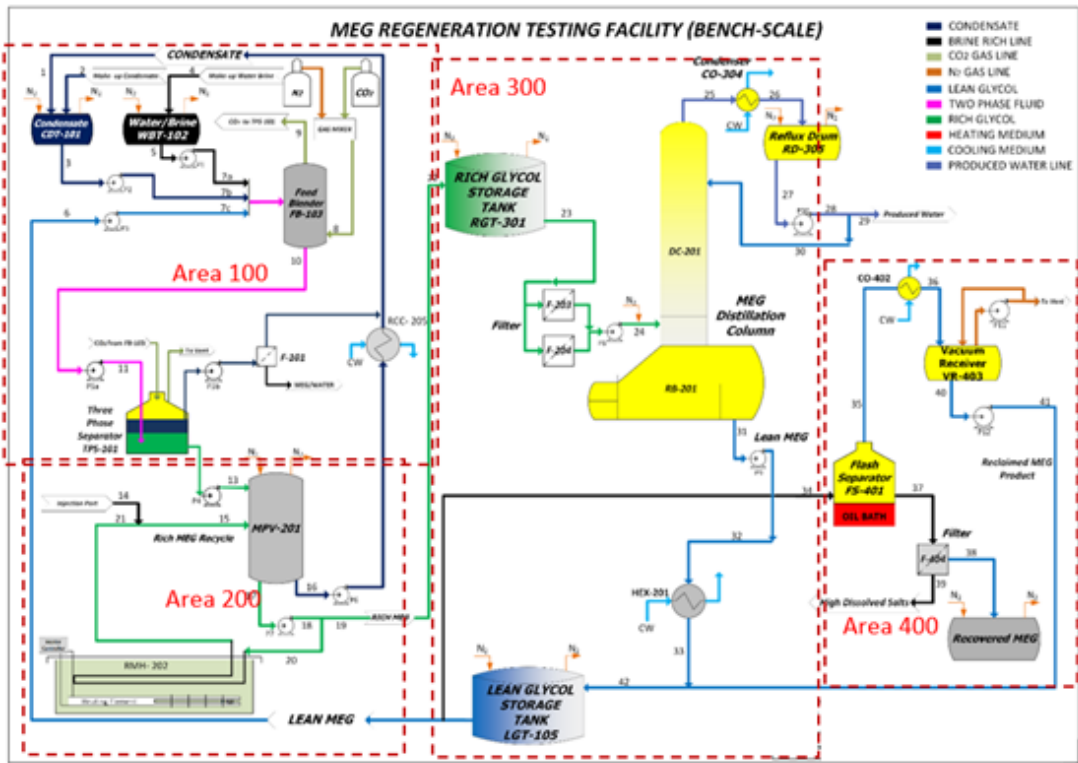
Figure 3-1: PFD of the MEG benchtop facility

## 3.3 Process Description

The MEG bench top testing loop consists of a MEG Pre-treatment system, MEG regeneration system and a reclamation system. The desired feed composition is achieved in the feed blending system. Typically, this consists of MEG, condensate and brine which may be saturated with $CO_2$. The resultant rich MEG feed is treated in the pre-treatment vessel to precipitate out salts with lower solubility. Concurrently, MEG-water separation is carried out through conventional distillation in the MEG regeneration unit. A stream of lean MEG is tapped off from the MEG distillation column and directed towards the MEG reclamation unit where MEG is flashed in a flash separator and recovered leaving behind the high soluble salts as a slurry.

## 3.4 MEG Regeneration System:

Rich MEG of a lower concentration (35 wt% - 65 wt%) is reconcentrated to achieve the desired lean MEG product specification (>85 wt.%) at the MEG regenerator. The MEG regeneration system consists of a packed distillation column, reflux condenser, reflux drum, reflux pump, and MEG reboiler (Kettle Type),

## 3.5 Piping and Instrumentation diagram (Distillation section)

Below shown in Figure 3-2 is the piping and instrumentation diagram (P&ID) based on the operating philosophy for the MEG regeneration system. A detailed step-by-step operating instruction for start-up / shut down for the regeneration system is as listed in Appendix 1.
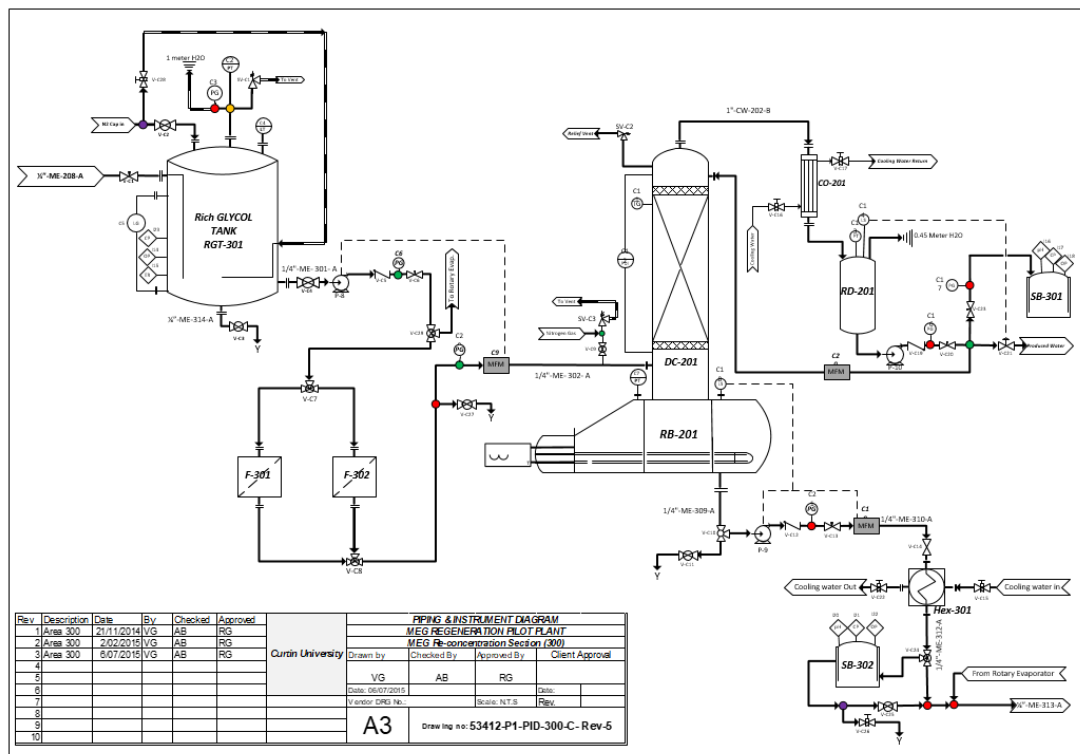


Figure 3-2: The Piping and Instrumentation Diagram (P&ID) of distillation column.

Based on the operating philosophy sizing of the associated equipment i.e. rich and lean glycol tanks, distillation column – reboiler, column and reflux drum was carried out. A detailed description of the distillation column's equipment are as listed on the

equipment data sheets listed in Appendix 2. Line sizing was also carried out which resulted in the selection of ¼" stainless steel tubing to connect the equipment together. A valve selection process was also carried out based on the specific requirements and a list of the valves installed as shown in Appendix 3.

### 3.5.1.  PLC (process logic control)

Figure 3-3 below shows the control system of the pilot plant, every instrument in the MEG plant was controlled by the PLC that was developed using LabView software. The computer, with a touch screen, was installed near the plant and it is able to transmit and read all the data from the plant instruments such as pH, conductivity, and oxygen sensors as well as operating the pumps and the re-boiler heater to attain the temperature depending required on the operating conditions. The collected data is to be saved collected, and analysed at the end of operation.
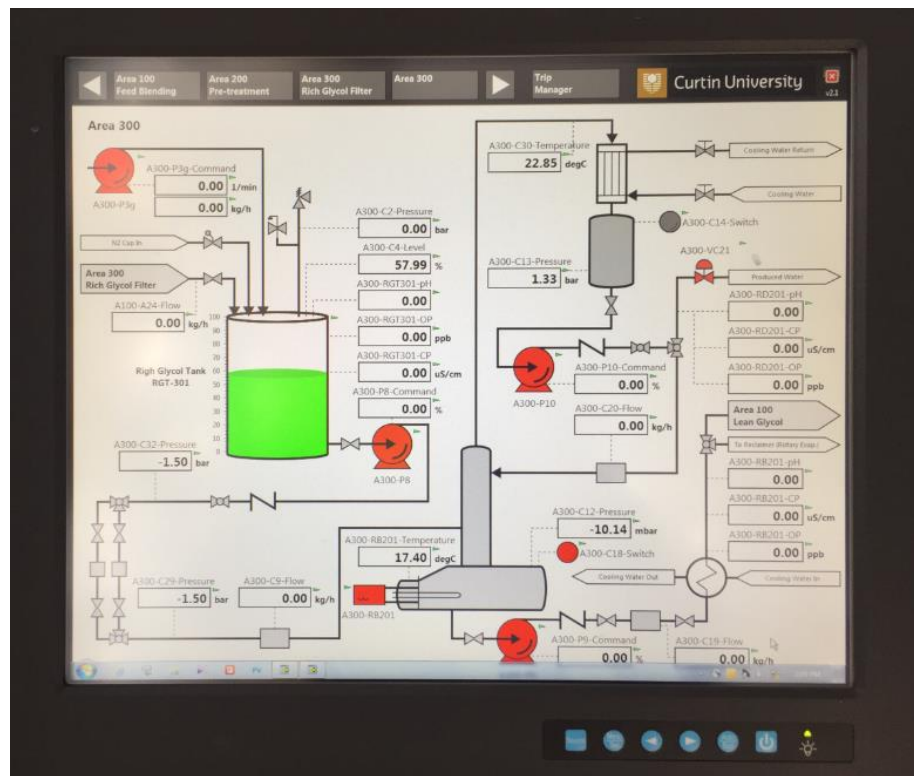


Figure 3-3: Control system of the plant, PLC (process logic control)

## 3.6. Description of probes, instrumentation and equipment controlled/monitored through the PLC

### 3.6.1. Multi-Parameter Transmitter M800 (Simultaneous monitoring to achieve maximum flexibility and control)

The M800 multi-parameter transmitter can be used to provide ongoing monitoring of one, two or four in-line sensors. It measures resistivity, pH/ORP, flow and turbidity in pure water, amperometric oxygen ($O_2$ gas as well as DO), TOC, conductivity, optical DO, dissolved ozone, and process applications [90].



Figure 3-4: Multi-Parameter Transmitter M800 [90]

- Application

The M800 multi-parameter transmitter also offers tailored solutions for ultrapure water and process applications in a big variety of industries. The combination of convenient multi-channel/multi-parameter measurement, best-in-class measurement performance and predictive diagnostics makes it a strong analytical transmitter for processes and pharmaceutical waters, microelectronics manufacturing, power generation water cycle chemistry monitoring and brewing.

### 3.6.1.1.  InPro 4850i pH Probe

The InPro 4850i combination probe for pH/ORP measurement in chlor-alkali processes, combines accurate measurement with durability and efficiency. The probe's sodium concentration of the chlor-alkali process is used as a reference for the probs glass membrane which is sensitive to sodium. This reference system is protected from chlorine and other oxidizing agents to protect it from failure. The high quality pH-sensitive glass membrane ensures precise measurement of pH as it is extremely resistant to chlor-alkali process conditions. The Features and Benefits are shown in Appendix 4.1 [91].



Figure 3-5: InPro 4850i pH Probe [91]

Table 3-1: Specifications - InPro 4850i pH Probe[91]

| Short description | Dual-membrane pH Electrode |
|---|---|
| pH-range | 0-14 |
| Temperature range | -10-120 °C (14-248°F) |
| Pressure resistance (bar) | 0-13 bar at 120 °C |
| Pressure resistance (psi) | 0-188 psi at 248°F |
| Reference system | Sodium sensitive glass membrane |
| ISM | yes |
| Length | 125mm, 230mm |
| Accuracy | +/- 0.001 |

3.6.1.2.  InPro 6850i polarographic oxygen sensor

The intelligent all-rounder InPro6850i uses the new 3-electrode system. Low level oxygen signal stability can be increased by a separate platinum anode. The integrated ISM technology makes installation much simpler with Plug and Measuring capability. Automated self-diagnosis and asset management provides more possibilities for maintenance planning together with the iSense [92]. Features and Benefits as shown in Appendix 4.2 [92].



Figure 3-6: InPro 6850i polarographic oxygen sensor [92]

Table 3-2: Specifications - InPro 6850i polarographic oxygen sensor [92]

| Segment /Application | Wide application range in Pharmaceutical, Food and Beverages and chemical applications |
|---|---|
| Accuracy | +/-1 % +6 ppb |
| Sterilizable | yes |
| Autoclavable | yes |
| Material in contact with medium | stainless steel (AISI 316L) with 3.1B certificates |
| Response time at 25 °C (air --> N2) | 90 sec |
| Mechanical pressure resistance | max. 12 bar (174 psi) absolute |
| Detection Range | 6 ppb to saturation |
| Accuracy | +/-1 % |

### 3.6.1.3. InPro 7100 Conductivity Meter

A reliable and adaptable conductivity sensor, InPro 7100, provides easy integration intothe process with substantial conductivity. The sensor is sufficient and reliable in the CIP & pulp & paper, chemical industry and food & beverages. Resistant against aggressive solutions by the shaft material PEEK, especially with the frequent SIP / CIP cycles. It has wide measurement range from 0.02 – 500mS/ cm making it a valuable solution for a wide range of applications. features and benefits are shown in Appendix 4.3 [93].



Figure 3-7: InPro 7100 Conductivity Meter [93]

Table 3-3: Specifications - InPro 7100 Conductivity Meter[93]

| Max. pressure (bar) | 0 -20 bar at 135 °C0 -10 bar at 150 °C |
|---|---|
| Max. pressure (psi) | 0 - 290 psi at 275 °F0 -145 psi at 302 °F |
| Temperature range | -20...150 °C (-4...302 °F) |
| Design | PEEK (body) <br> 316L (electrodes) <br> Hastalloy (electrodes) |
| Segment /Application | Chemical, pharmaceutical and F&B processes |
| Measurement Range | 0.02-500 mS/cm |
| Accuracy | $\pm$ 0.1 °C ( $\pm$ 0.1 °F) |

### 3.6.2. Gear Pump – Micro pump

A gear pump uses the meshing of gears to pump fluid by displacement. They are one of the most common types of pumps for hydraulic fluid power applications.

Gear pumps are also widely used in chemical installations to pump high viscosity fluids. There are two main variations; external gear pumps which use two external spur gears, and internal gear pumps which use an external and an internal spur gears (internal spur gear teeth face inwards, see below). Gear pumps are positive displacement (or fixed displacement), meaning they pump a constant amount of fluid for each revolution. Some gear pumps are designed to function as either a motor or a pump.

To achieve the desired mass balance in the system a detailed pump selection process was carried out which resulted in the identification of gear pumps as the ideal pump due to high reliability and accuracy.



Figure 3-8: Gear Pump

### 3.6.3. Mass flow meter – Coriolis force

The Coriolis measuring principle is used in a wide range of different branches of industry, such as the life sciences, chemicals, petrochemicals, oil and gas, food, and – no less importantly – in custody transfer applications. Coriolis flowmeters can measure virtually all fluids: cleaning agents, solvents, fuels, crude oil, vegetable oils, animal fats, latex, silicon oils, alcohol, fruit solutions, toothpaste, vinegar, ketchup, mayonnaise, gases or liquefied gases.

75

Each Coriolis flowmeter has one or more measuring tubes which an exciter causes to oscillate artificially. As soon as the fluid starts to flow in the measuring tube, additional twisting is imposed on this oscillation due to the fluid's inertia. Two sensors detect this change of the tube oscillation in time and space as the "phase difference." This difference is a direct measure of the mass flow [94].

**Device properties**

- Nominal diameter: DN 1 to 4 (1/24 to 1/8")
- Process pressure up to 400 bar (5800 psi)
- Medium temperature up to +205 °C (+401 °F)



Figure 3-9: Mass flow meter – Coriolis force

3.6.4. Level measurement (Liquicap FMI21)

A cost-effective and simple rod probe for constant level measurement for conductive liquids is (Liquicap FMI21). High quality non-corrosive materials (stainless steel, carbon fibre) make it suitable even for aggressive liquids such as alkalis and acids. Liquicap is an ideal solution for Inventory Management Solutions when used in conjunction with the Fieldgate FXA320 [95].

Figure 3-10: Level measurement

(Liquicap FMI21)[95]

**Measuring principle**

Probe rods have an existing alternating voltage. A measurable current flows and the Liquipoint T switches, the moment a connection is created by the conductive liquid between the ground probe rod and, as an example, the MAX probe rod. With point level detection, once the liquid clears the MIN probe the device switches back. With two-point control, the device does not switch back until the MIN and MAX probe is cleared. Corrosion of the probe rods and electrolytic destruction of the product is prevented through the use of alternating voltage. The system is designed as a closed, potential free circuit between the electronics and the probe rods so therefore the material used for the tank walls is not relevant.

3.6.5. Differential pressure (Deltabar PMD75)

Pressure differences can be measured through the metal sensors in the Deltabar PMD75 differential pressure transmitter. This transmitter has welded metallic membrane and piezoresistive sensors is used in industries for continuous measurement in vapours, liquids and gases. It has reliable and simple for commissioning and operation through the use of the 3-key operation. Management of device parameters and process are much easier by using the integrated HistoROM data module. It is designed according to IEC 61508 for use in SIL2/3 safety applications [96].

Figure 3-11: Differential pressure (Deltabar PMD75) [96]

**Field of application**

For level, mass or volume measurement in liquids, flow measurement monitoring as well as differential pressure (mass volume or flow) in conjunction with primary elements in liquids, gases and vapours.

- Process temperature: -40 to +85°C (-40 to +185°F)
- Measuring ranges: 0.25mbar to 40bar (0.0036 to 600psi)
- Accuracy: ±0.05%, "Platinum" ±0.025% (optional)

3.6.6. Bimetal thermometer (top of the column)

Bimetal thermometer is an instrument which can be used in the chemical and petrochemical industries, oil and gas industries. It can be used mainly to measure temperature that ranges from -70 to +600 °C and Accuracy (class 1 per EN 13190). The individual stem length is from 63 to 1,000mm with in all stainless steel construction.

Figure 3-12: Bimetal thermometer (Top of the column) [97]

### 3.6.7. Point level detection, FTL51 (Re-boiler)

International certificates for hazardous areas mostly use Liquiphant FTL51, which is a point level switch with extension tube. Availability and safety of the device can be guaranteed by the use of FTL51 which offers functional safety SIL2/SIL3. It provides reliable measurement values, not affected by: flow, changing media properties, gas bubbles, turbulences, foam, build-up or vibrations.



Figure 3-13: Point level detection, FTL51 [98]

**Field of application**

Point level switch with extension tube for all liquids.

- Process connections: Threads, flanges and hygienic process

- Connection (Tri-Clamp)

- Temperature: -50 to +150°C (-58 to +302°F)

- Pressure: -1 to +100bar (-14.5 to +1,450psi)

- Sensor material: 316L, Alloy


## 3.6 Environmental Impact Analysis (EIA)

The importance of preserving the environment has led to processes and policies that must be implemented before commissioning and executing any proposal. The Environmental Impact Analysis (EIA) is a procedure to assess and document the environmental impacts (severity and type) of the MEG Pilot Plant operations as listed in Appendix 7. All the activities as part of the MEG Pilot Plant have undergone an EIA and the environmental impacts are documented in this chapter as per regulations and operational approvals.

Table 3-4: Description of types of EIA impact

| Type of impact | Definition | Corresponding table colour |
|---|---|---|
| Short term impact | Temporary, likely to occur during construction phase (based on approximates construction time of 12-24 hours. These impacts and their associated effects are expected to no longer exist once construction and assembly are complete | Green |
| Long term impact | Likely to occur frequently, or in sustained manner for certain durations over course of plant's life, as result of activities and operations associated with plant | Yellow |
| Permanent impact | Impacts that cause permanent/irreversible damage to environment surrounding plant, seen well after plant is in-operational | Red |

## 3.7 Hazard

A Hazard Identification (HAZID) assessment was undertaken for the initial phase of the entire process design. This assessment evaluates the risks and determines hazards related to the process, environment and plant operation based on a qualitative method utilizing a risk matrix. The risk matrix identifies the estimated consequences and their probability of occurrence. The potential hazards resulting from events such as human factors (i.e. safety gear, human error and miscalculations), operation activities (i.e. MEG Re-concentration and Reclamation, waste disposal, start/shutdown procedures, and leaks), and environmental/natural factors (i.e. storms, cyclones, and earthquakes). As listed in Appendix 5 and 6, the HAZID risk matrix is shown in Table 3-5 .

Table 3-5: Qualitative risk matrix

|                | Insignificant | Minor | Moderate | Major | Catastrophic |
|----------------|---------------|-------|----------|-------|--------------|
| Almost certain | M             | H     | H        | E     | E            |
| Likely         | M             | M     | H        | H     | E            |
| Possible       | L             | M     | M        | H     | E            |
| Unlikely       | L             | M     | M        | M     | H            |
| Rare           | L             | L     | M        | M     | M            |

# 4. Recovery of Mono- Ethylene Glycol by Distillation and the Impact of Dissolved Salts Simulating Field Data

## 4.1.    Introduction

Mono-ethylene glycol (MEG) is an important raw material having numerous research and industrial applications, one such example is its application as a hydrate inhibitor in the hydrocarbon processing industry [99]. MEG is one of the most favoured thermodynamic hydrate inhibitors used in hydrocarbon transportation pipelines and processing facilities due to its low volatility, low toxicity, low flammability, favourable thermodynamic behaviour, simple and proven technology requirements and high availability [100, 101]. Furthermore, the preference for using MEG over other traditional thermodynamic hydrate inhibitors such as methanol stems from several operational, environmental and safety issues imposed by the use of methanol and MEG's ability to be effectively recovered, regenerated and reused [5, 9]. Due to the high cost of MEG and significant volumes required to provide effective hydrate control, following the hydrate inhibition process it is essential to separate MEG from the produced water so that it can be recycled and reused to minimize operating costs. The most prevalent MEG recovery methods have been broadly categorised into two main process types, (i) reconcentration and (ii) regeneration [100]. The reconcentration process is the most basic MEG recovery method and is comprised of a simple distillation column where the water rich MEG is concentrated to form lean MEG by vaporisation of the excess water. Typically, the distillation column is operated to regain a MEG purity within the range of 80-90% by weight as the bottoms product [102, 103]. The reconcentration method for MEG recovery is applicable when no salts are expected to precipitate out during recovery, typically during the early production stages when the produced water contains just low amounts of dissolved salts [100, 104]. As the reconcentration process only removes water from the MEG solution, any dissolved salts, pipeline corrosion products and additional non-volatile chemicals will accumulate inside the closed MEG loop. The accumulation of salt beyond saturation limits within the MEG system may result in severe fouling and plugging of equipment and flowlines, as such the salt must be either removed or the MEG periodically replaced [105].

For cases where the rich MEG contains high quantities of dissolved salts, reclamation must instead be performed before the MEG can be reinjected at the well head to prevent damage to process equipment through excessive solid build-up. The reclamation of MEG can be performed using two different methods depending on the required final lean MEG salt concentration, by either full reclamation or slip-stream salt removal. The process of full reclamation entails a two-step process where the rich MEG solution is initially vaporized at low pressure (0.1-0.15 bara) leaving the salts and non-volatile solids remaining within a flash drum [100, 104]. The salt free MEG solution is then reconcentrated by distillation to the required lean MEG specifications by the removal of water. Full reclamation is generally performed when high rates of formation water are expected over the lifetime of the processing facility.

Alternatively, slip stream regeneration may be performed when a certain level of dissolved salts can be tolerated within the closed MEG loop during processing. For low to medium formation water rates it is often more attractive to use the split-stream salt removal process to minimise operating costs and equipment size [102]. In performing split stream regeneration, the rich MEG solution first undergoes pre-treatment to remove light hydrocarbons, low soluble salts and corrosion products before conventional distillation is performed to remove excess water to achieve the desired MEG purity. Following distillation, the majority of the lean MEG undergoes salt removal via a reclaimer or ion exchange system to remove the remaining highly soluble salts. However, a fraction of the salty lean MEG stream by-passes the salt removal operation and mixes with the final salt free lean MEG. The slip-stream rate is typically determined by the allowable amount of soluble salts in the final lean MEG product required to prevent scaling in pipelines [100, 104].

The typical design and construction of MEG recovery columns utilize packed internals for columns of diameter 0.7m and below due to the low pressure drop and high efficiency of separation [106, 107]. For columns operating with higher vapour loads, trays may be more suitable and as such must be considered during the design phase. The design of a packed column can be performed through either the concept of transfer units or the evaluation of the height equivalent to theoretical plates (HETP) in combination with standard estimation of the number of required equilibrium stages. The number of equilibrium stages required can be determined through either graphical methods such as McCabe-Thiele or short-cut distillation column design methods such

as the Fenske-Underwood-Gilliland (FUG) method. Further evaluation of a packed columns design can be performed using mass and heat transfer coefficients through non-equilibrium rate based models and is recommended for highly non-ideal, polar or reactive systems [107]. Additionally, simulation software, such as ASPEN HYSYS or ASPEN Plus may also be used for the design or evaluation of distillation systems.

The operating conditions of a MEG recovery column can vary depending upon the operating envelope of the individual distillation unit [5]. Some MEG recovery units operate at temperatures as low as 95°C [108], 140°C [109] and up to temperatures of 160°C [110], with Psarrou et al (2011) recommending operation between 120°C to 160°C within the reboiler. Standard industrial operating practice for both the regeneration and reclamation process typically sees the operation of the MEG distillation column at atmospheric to vacuum pressures [111]. The operating temperature and pressure of the reboiler depends highly on the temperature to which MEG will begin to experience thermal degradation. Under excessive temperatures, MEG may begin to break down to form organics acids including glycolic, acetic and formic acids leading to higher operating costs through MEG makeup, impacts on system pH requiring additional adjustment and the potential increase in carbon steel corrosion through the presence of acetic acid. To combat MEG thermal degradation the reboiler may be operated at lower pressures to reduce the required temperature to achieve boiling in order to decrease the likelihood of the MEG degrading [5].

In this study, the primary focus of investigation is the recovery of MEG from water at varying temperatures and feed concentrations under both batch and continuous operation at a fixed reflux ratio. A secondary investigation has then been performed to investigate the impact salts present within the rich MEG feed on the MEG regeneration process through analysis of experimental and simulated results.

## 4.2.      Salt Precipitation within MEG Systems

The prevention and mitigation of salt precipitation within process piping and equipment is a crucial aspect of effectively designing a MEG regeneration system. Typically, the most frequently encountered salts in MEG processing occur from the presence of the monovalent cations sodium, $Na^+$ potassium, $K^+$ and the divalent cations calcium, $Ca^{2+}$ iron, $Fe^{2+}$ and magnesium, $Mg^{2+}$ [112, 113]. Within the

confines of the MEG regeneration column, the primary impact of salt occurs due to the precipitation of the divalent salts, $CaCO_3$, $FeCO_3$, $FeS$ and $Mg(OH)_2$ within the columns internals and reboiler unit. Due to the high solubility of monovalent cations, they typically remain dissolved in the MEG solution by-passing the regeneration column only precipitating once reaching the downstream MEG reclamation unit [112].

In hydrocarbon gas processing, the participation of $CaCO_3$ is considered to be one of the most frequently experienced sources of mineral precipitation and scaling [114]. The presence of $Ca^{2+}$ in the MEG solution originates from the breakthrough of formation water during processing alongside $Mg^{2+}$ and the previously mentioned monovalent cations. Conversely, the presence of $Fe^{2+}$ within an MEG recovery system primarily stems from the development of an iron carbonate film upon the inside of piping for corrosion control and is such referred to as a corrosion product [65]. The precipitation of $FeCO_3$ primarily occurs within 'sweet' systems with low $H_2S$ content, however, the precipitation of $FeS$ is possible when the $H_2S$ concentration is sufficient [115]. As carbon steel piping is used in most if not all MEG recovery systems, pipeline corrosion products will always be present to some degree in both solid and dissolved forms. Alongside $CaCO_3$, $FeCO_3$ is one of the most abundant carbonates precipitating within MEG distillation systems [112, 115].

The effect of salt precipitation upon MEG regeneration columns is most prevalent within a columns reboiler unit and associated piping. The precipitation of divalent salts, in particular $CaCO_3$ and $FeCO_3$ is promoted by the high fraction of MEG in the bottom product [112]. This effect is shown by the solubility studies performed by Kassa and co-workers who observed decreasing solubility of various salts in increasing MEG content solutions. The precipitation of salts within the columns reboiler can cause severe fouling and the accumulation of suspended solids in the lean MEG bottoms product [112]. The overall influence of fouling may lead to the reduced heat transfer efficiency of the reboiler resulting in a poor separation of the MEG from water. The presence of iron sulphide within piping and MEG systems can cause major issues due to its ability to cause crevice or bimetallic corrosion in the presence of water [117].

## 4.3.    Process Design Configuration

As shown by the process flow scheme in Figure 4-1, the distillation system is comprised of a feed pre-treatment section followed by a packed distillation column. Initially, a feed tank is used for the preparation of the MEG-Water solution using MEG supplied by Chem Supply Australia with the typical composition shown in Table 4-1. Once prepared, the rich MEG feed is pumped through a filtration system to remove solid particulates and is subsequently measured by a mass flow meter (MFM) to monitor inlet flow. The MEG-Water feed to the column was maintained at 30°C, 1.4 bar at a mass flow rate of 6.5 kg/hour and fed directly into the re-boiler unit. Prior to operation, the MEG feed tank is blanketed with nitrogen gas to prevent oxygen ingress within the vessel (see Table 4-2).

Table 4-1: MEG Composition

| No. | Composition | % |
|---|---|---|
| 1 | Minimum Assay (%) | 99.0% |
| 2 | Water | 0.5% |
| 3 | Diethylene Glycol (DEG) | 0.02% |
| 4 | Ash Content | 0.001% |
| 5 | Acidity (as Acetic Acid) | 0.001% |
| 6 | Aldehyde (as Formaldehyde) | 0.0008% |
| 7 | Chlorine (Cl) | 0.00001% |
| 8 | Iron (Fe) | 0.000005% |

The distillation system employs a 10 litre glass re-boiler at the base of the column heated by a 5kW insertion heater. The power of the re-boiler's heater is directly controlled by a programmable logical controller (PLC) to maintain the desired reboiler temperature during operation. The bottoms product of the re-boiler is removed through the MEG pump and the flow rate measured by a MFM, the product is then cooled by a plate heat exchanger operated using cooling water at 15°C.

The main section of the distillation column itself is comprised of two individual sections, each one metre in height. The sections are connected and fitted with structural packing of diameter 80 mm DN (3"). The column operates with a pressure differential indicator and temperature gauge to monitor the conditions within the column during processing. The final section of the distillation system encapsulates the vapour condensation and reflux systems. The condenser unit acts as a total condenser and is operated using cool water provided by a chiller system at approximately 15°C with the

flow rate of cooling water manually controlled. A glass reflux drum is located directly below the condenser unit to collect the liquid reflux by gravitationally induced flow. The reflux is then fed back into the distillation columns by pump and measured by a MFM, if required, a water product stream can also be operated during continuous operation.

Additional measurements are performed by means of pH, $O_2$ and conductivity probes located at the re-boiler and reflux product line. Further monitoring of the process is performed by level and pressure gauges installed in the locations shown by Figure 4-1, with an additional level sensor installed on the re-boiler unit
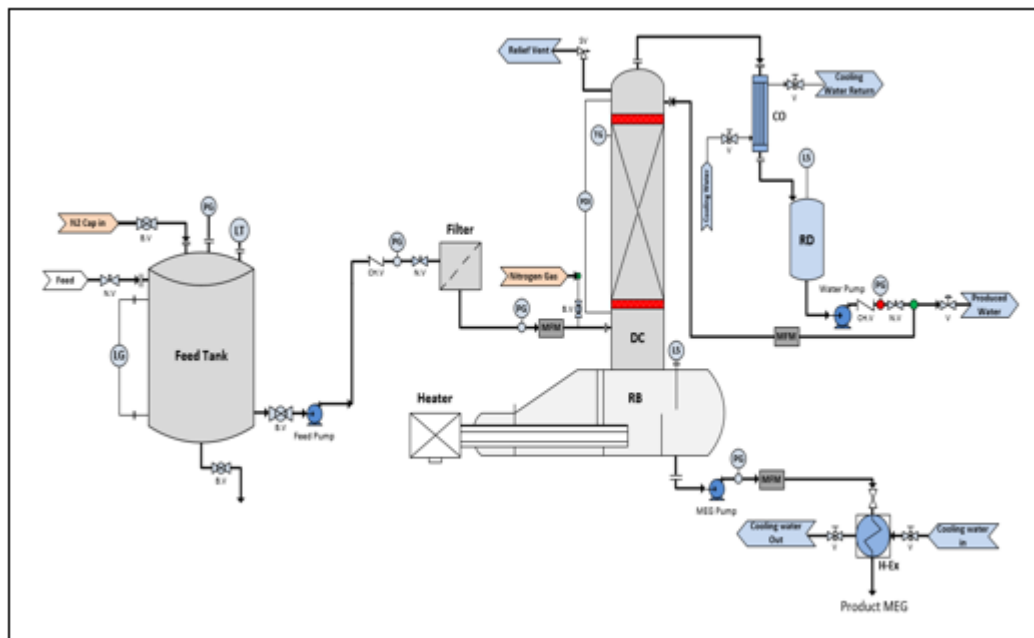


Figure 4-1: Flow diagram for MEG recovery system [118]

Table 4-2: MEG regeneration flow scheme abbreviations[118]

| B.V | Ball Valve | LS | Level Sensor | PG | Pressure Gauge |
|---|---|---|---|---|---|
| CH.V | Check valve | LT | Level Transmitter | RB | Reboiler |
| CO | Total Condenser | MFM | Mass Flow Meter | RD | Reflux drum |
| DC | Distillation Column | N.V | Needle Vave | ST | Safety Valve |
| H-EX | Heat Exchanger | PDI | Pressure Differential Indicator | TG | Temperature Gauge |
| LG | Level Gauge | V | Valve | | |

## 4.4. Equipment Used

The separation of MEG from water was performed using a structurally packed distillation column constructed by De Dietrich Process Systems GmbH, Germany, (De Dietrich) for MEG processing, based upon specifications developed by the Curtin Corrosion Engineering Industry Centre (CCEIC). The operating conditions and design specifications of the MEG distillation column are summarised in Table 4-3. The distillation column operates using Durapack borosilicate glass 3.3 structured packing provided by De Dietrich, such packing was chosen for its high mass transfer efficiency. Table 4-4 outlines the specifications and dimensions of the structured packing.

Table 4-3: Distillation Column Specifications[118]

| 1 | Feed Rate | Up to 6.5 Kg/hr. |
|---|---|---|
| 2 | Feed Conditions | Temperature: 30°C,  Pressure: 1.4 Bar |
| 3 | Column Design Operating Pressure | (1) – (1.5) Bar |
| 4 | Distillation Design Temperature | (20) – (150) °C |
| 5 | Condenser Type | Total |
| 6 | Reflux Drum Capacity | 5 Litres |
| 7 | Reboiler Type (Capacity) | Kettle type (8 Litres) |
| 8 | Reboiler Power requirements | 5 kW |
| 9 | Column Diameter, $D_T$ | DN 80 (76.2 mm) |
| 10 | Packing height, Z | 900 mm x 2 Sections |
| 11 | Packing material | Borosilicate glass 3.3 Structured Packing |

Table 4-4: Packing Specification[118]

| 1 | Packing Surface Area | $300.0 \ m^2/m^3$ |
|---|---|---|
| 2 | Packing Factor, $F_P$ | $195.3 \ m^2/m^3$ |
| 3 | Packing Void Fraction | 0.824 |
| 4 | Corrugation Base Width | 1.8856 cm |
| 5 | Corrugation Side Dimension | 1.3333 cm |
| 6 | Corrugation Height | 0.94281 cm |
| 7 | Corrugation Angle | 45° |

Partial vaporisation of the bottoms product was performed using a kettle type glass reboiler designed for a liquid volume capacity of eight litres. Operation of the reboiler unit was maintained at 1.3 bar throughout distillation, with the unit operated within a temperature range of 120°C up to 160°C. Operation of the reboiler unit at temperatures above 160°C was not performed due to the possibility of thermal degradation effects of MEG at temperatures reaching its boiling point. A temperature limiter was installed as a safety measure to prevent operation at temperatures above 160°C. Furthermore, the total condenser unit operates in conjunction with a 5 litre capacity reflux drum to provide liquid reflux to the column.

The distillation system was operated using magnetic drive gear pump systems manufactured by Micropump for the feed, bottom and reflux product pumps. The Micropump L15034 pump was employed for pumping of the feed stream with a total capacity of 6.5 kg/hr. Conversely, the reflux and bottom product pumps were designed for a maximum capacity of 4kg/hr using the L21382 Micropump system. The composition of the MEG-Water solution in the feed, distillate and bottom products was measured using a ATAGO PAL-91S refractometer shown in Figure 4-2. The refractometer measures the MEG concentration within a 0-90% concentration range with an accuracy of ±0.4% based upon the refractive index of the solution. The mass flow rate of each stream was measured by Promass A 100 inline mass flow metres manufactured by Endress+Hauser with an accuracy of ±0.1%.

Figure 4-2: ATAGO refractometer (ATAGO)

The pressures of each stream were measured using steel pressure gauges, with tantalum membranes capable of operating between -50°C and 200°C. The pressure within the reflux drum was monitored using a Cerabar PMC71 digital pressure transmitter manufactured by Endress+Hauser. The pressure transmitter is capable of operating in process temperature ranges of -40°C to 150°C and up to 40 bar with an accuracy of ±0.075%. A Deltabar PMD75 was used to measure the differential pressure of the distillation column capable of operating between -40°C to 85°C and 0.25mbar to 40bar with an accuracy of ±0.05%

The top operating temperature within the distillation column was measured using a WIKA model 55 bimetal thermometer installed at the top of the column. The thermometer can measure temperatures within -70°C to 600°C with an accuracy of ±1°C. The liquid level within the reboiler was monitored using a Endress+Hauser level detection Liquiphant FTL51 system utilising 316L stainless steel as the sensor material. The unit can operate between -50°C to 150°C and up to 100bar. Additional measurements including pH, oxygen content and electrical conductivity of the rich MEG were taken during operation. pH measurements are made using a Mettler Toledo InPro 4800 pH sensor. Dissolved oxygen was measured using a Mettler Toledo 6510i dissolved ozone sensor with an operating range of 0-5000ppb (mg/L) and an accuracy of +/-4% or 3ppb. Finally, the conductivity of solution was measured using an InPro 7100 conductivity meter capable of operating between -20°C to 150 °C

## 4.5.    Construction

The assembly of the distillation column used in the recovery of MEG from water was performed by the CCEIC and commenced on May 2015. The main experimental systems of the project were specified by CCEIC; designed and manufactured by De Dietrich and consisted of the equipment outlined by Table 4-5. The construction and installation of the distillation column and its subsystems was performed according to the following procedure with an image of the completed distillation column shown in Figure 4-3:

1. Preparation of the foundation base and Installation of the structural frame.
2. Re-boiler vessel preparation and setup of the liquid level measurement device and thermometer cable.
3. Installation of the first section of column fitting of the first five layers of structured packing.
4. Installation of the second column section on top of the first using a glass joint of 200 mm in length.
5. Installation of the bimetal thermometer at the top of second column.
6. Connection of the second column to the condenser unit by a T-connection, the first end is connected to the relief valve and the second is connected to the condenser unit.
7. Installation of the thermometer cable at the top of condenser.
8. Connection of the condenser unit to the Reflex drum by Polytetrafluoroethylene (PTFE) bellows.
9. Installation of the process pressure gauge, normal pressure gauge and level gauge to the Reflex drum.
10. Installation of the differential pressure gauge that connects the first vent to the bottom of the first column section and from the second vent to the top of the system.
11. Installation of additional column supports anchored to the structural frame to provide support when removing or replacing system components.
12. Installation of the distillation column control system for controlling of the reboiler temperature.

Table 4-5: Equipment supplied by QVF[118]

| 1 | Main distillation system components |
|---|---|
| 2 | Carbon steel frame structure (3618mm height, 1250mm width, 685mm length) |
| 3 | Re-boiler vessel |
| 4 | Re-boiler vessel heating unit |
| 5 | Two glass columns to be connected in series |
| 6 | Relief valve set at 1.5 barg |
| 7 | Condenser unit and reflux drum |
| 8 | Feed, reflux and bottom product pumps |
| 9 | Solid filtration system |
| 10 | Rich MEG tank |
| 11 | Lean MEG tank |
| 12 | Measurement Systems |
| 13 | Differential pressure gauge |
| 14 | Process stream pressure gauges |
| 15 | Reboiler liquid level measurement system |
| 16 | Bi-metal thermometer – stainless steel |
| 17 | Two vessel pressure gauges. |



Figure 4-3: MEG Distillation Column [118]

## 4.6. Operating Procedure

Experimental trials were performed for both batch and continuous operation of the distillation column for varying mass fractions of MEG within the feed and varying reboiler operating temperatures. Prior to operation, the system was flushed with distilled water to clean any residual solution from previous trials and Continuous sparging with high purity nitrogen (99.995%, BOC) ensured minimum oxygen ingress. Operation of the column for both batch and continuous distillation operation was conducted as follows.

During batch operation, the distillation system was prepared by filling the re-boiler and reflux drum with the MEG-Water solution at the desired concentrations shown in Table 4-6. For each run performed, eight kilograms of the MEG-Water solution was

introduced in to the re-boiler, while two kilograms of the solution was introduced into the reflux drum. Once filling of the re-boiler and reflux drum had been completed, the reboilers heating element was initiated. On the first occurrence of vapour evolving from the heated solution, operation of the reflux pump was commenced. The reflux drum was operated under total reflux mode with no product withdrawal to circulate the solution until the desired reboiler temperature, as per Table 4-6 was achieved. The release of the first bubbles are an indication that the unsteady state operation of the column has commenced (see Figure 4-5 and Figure 4-6)

Typically, total reflux circulation was performed for two to three hours until the distillation system had reached steady state mode. Steady state conditions are normally achieved when the re-boiler temperature reaches between 125- 145°C, as shown in the Table 4-6 and Figure 4-4. Operation of the column under total reflux is performed with the condenser unit operating at a constant 15°C. The condenser is maintained at such temperature by cooling water supplied by a chiller unit operating at 15°C.

Sampling from the reboiler and the reflux drum sections were taken at 30 minute intervals to measure the MEG concentrations using the ATAGO refractometer. The concentration of MEG over time was used to determine the time required to reach steady state operation of the distillation column. Once steady state conditions had been achieved indicated by the stabilisation of reboiler and reflux drum MEG concentrations operation of the column was ceased.
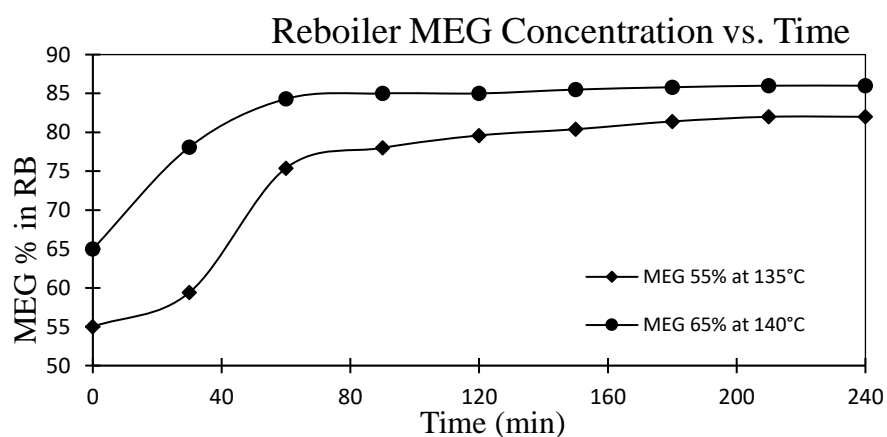


Figure 4-4: Batch Reboiler MEG concentration over time

Table 4-6: Batch and Continues Operating Conditions and Product Composition

| Trial No. | Column Operation Type | Reboiler Temperature (°C) | MEG Feed Mass Fraction | Feed Flow Rate (kg/hr) | Reflux Ratio | Reboiler MEG Mass Fraction | Reflux Drum MEG Concentration (ppm) |
|---|---|---|---|---|---|---|---|
| (1) | Batch | 135 | 0.55 | - | Total | 0.820 | 1500 |
| (2) | Batch | 140 | 0.65 | - | Total | 0.860 | 2000 |
| (3) | Continuous | 130 | 0.50 | 5 | 0.52 | 0.834 | 100 |
| (4) | Continuous | 140 | 0.50 | 5 | 0.44 | 0.864 | 100 |
| (5) | Continuous | 141 | 0.65 | 6 | 0.51 | 0.860 | 100 |
| (6) | Continuous with Salts | 135 | 0.71 | 5.3 | 0.50 | 0.790 | 100 |
| (7) | Continuous with Salts | 140 | 0.73 | 5.3 | 0.51 | 0.800 | 100 |

In a similar manner to batch distillation, operation of the distillation column using continuous operation was prepared by introducing eight kilograms of the MEG-Water solution at the required concentration from the rich MEG feed tank into the reboiler. The reboiler heater was then started while the reflux drum was filled with two kilograms of distilled water. Upon the evolution of vapour from the liquid within the reboiler, the reflux drum circulation rate was set at three kilograms per hour. The column operated under total reflux conditions until the reboiler operating temperature stabilised and steady state conditions were achieved. The feed was then introduced into the columns reboiler at the flow rates shown in Table 4-6 for each case. Operation of the column then proceeded at to the respective reflux ratios. The sampling of reboiler and reflux drum compositions were regularly taken and tested by ATAGO refractometer in a similar manner to the batch operation. Overall, trials were conducted to evaluate the impact of changing reboiler temperature and feed mass fraction on mass fraction of MEG within the bottoms product.



Figure 4-5: Reboiler          Figure 4-6: reflux drum

## 4.7. Operating Results and Calculation

Operating results of sixteen trials utilising both batch and continuous operation are summarised in Table 4-6. Analysis of the results was conducted using the McCabe-Thiele graphical method in conjunction with the Fenske-Underwood-Gilliland short cut distillation column design equations to determine the number of stages required to achieve the experimental separations. As results were recorded in mass fractions they were first converted to mole fractions for the purpose of estimating the number of stages by both methods. Figure 4-8 to Figure 4-10 Present the McCabe Thiele diagrams for Trials (1), (6) and (16) respectively. In addition, the concepts of transfer units and HETP were used to further evaluate the efficiency of the columns packing with the methodology utilised discussed in the subsequent section. A summary of the analysis performed can be found in Table 4-7 for batch and Table 4-8 for continuous experimental trials. Figure 4-4, illustrates the operation of the column during batch operation for trials one and two, it was observed that the system reached equilibrium typically within 60 minutes. Figures six to ten present the McCabe Thiele diagrams for trials, one, three, four and seven.

In order to construct the McCabe-Thiele graphical diagrams, an estimation of the Vapour Liquid Equilibrium (VLE) curve of the MEG-Water binary system was required. Estimation of the curve was performed using partial pressures derived from Antoine coefficients for both water and MEG over the operating temperature of the column. A comparison was also made to literary sources of VLE data and is graphically represented in Figure 4-7. It can be observed that the calculated VLE curve is lower than that of many sources of VLE data, the difference can be attributed to the higher operating temperatures of the column compared to the test conditions the VLE data was obtained at. However, the calculated VLE curve closely matches the data of Trimble and Potts [119] where the data was derived at a similar pressure.

Table 4-7: Analysis Summary of Batch Operation

| Trial No. | McCabe-Thiele | | FUG Method | |
|---|---|---|---|---|
| | Number of Theoretical Stages | Number of Theoretical Plates | Number of Theoretical Stages | Number of Theoretical Plates |
| (1) | 3 | 2 | 2.223(3) | 2 |
| (2) | 3 | 2 | 2.240(3) | 2 |

Table 4-8: Analysis Summary of Continuous Operation

| Trial No. | McCabe-Thiele | | FUG Method | | Transfer Units | | HETP | |
|---|---|---|---|---|---|---|---|---|
| | Number of Theoretical Stages | Number of Theoretical Plates | Number of Theoretical Stages | Number of Theoretical Plates | NTU | HTU (m) | HETP (m) (Z/N) | HETP (m) Estimated |
| (4) | 4 | 3 | 5.325 (6) | 5 | 7.374 | 0.308 | 0.360 | 0.346 |
| (6) | 5 | 4 | 5.762 (6) | 5 | 6.169 | 0.308 | 0.360 | 0.329 |
| (7) | 5 | 4 | 5.516 (6) | 5 | 6.351 | 0.302 | 0.360 | 0.338 |
| (13) | 4 | 3 | 5.332 (6) | 5 | 6.310 | 0.229 | 0.360 | 0.254 |
| (16) | 4 | 3 | 5.395 (6) | 5 | 6.360 | 0.217 | 0.360 | 0.241 |

The operation of the ATAGO refractometer in measuring the MEG mass concentration within the reflux drum was limited to 100ppm. Therefore, the lower concentrations experienced during continuous operation recorded a concentration of zero, as such, a value of minimum value of 100ppm was used in analysis of the continuous trials.
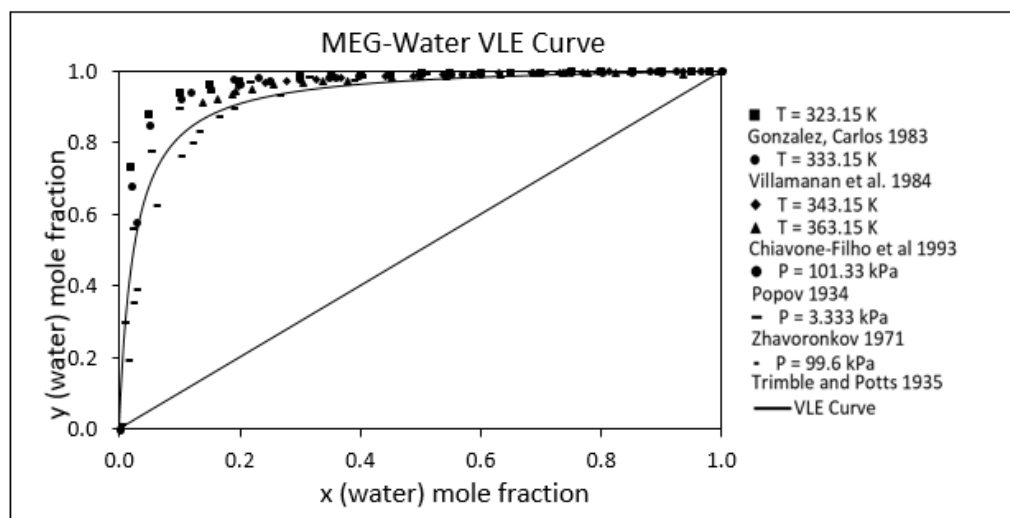


Figure 4-7: Literature MEG- Water VLE data [118]

### 4.7.1 Calculation Equations and Methodology

The required number of stages for each trial experiment was estimated using the Fenske-Underwood-Gilliland (FUG) shortcut design equations. Initially, the minimum number of stages required to achieve a given separation was estimated using the Fenske equation given by eq. (4-1). For trials one and two, operating under batch conditions the minimum number of stages given by the Fenske equation represent the actual number of stages required.

$$N_{min} = \frac{\ln\left[\left(\frac{x_A}{x_B}\right)_{dist}\left(\frac{x_B}{x_A}\right)_{bot}\right]}{\ln \alpha_{AB}} \qquad (4\text{-}1)$$

Due to the binary nature of the MEG-Water system, estimation of the minimum reflux ratio by the multicomponent system Underwood equations was unnecessary. Instead, the minimum reflux was estimated by eq. (4-2) of which is derived from the Underwood minimum reflux equations for binary systems where the liquid feed fraction is equal to one.

$$R_{min} = \frac{1}{\alpha-1}\left[\frac{x_D}{x_F} - \alpha\left(\frac{1-x_D}{1-x_F}\right)\right] \qquad (4\text{-}2)$$

The estimation of the actual number of stages required at a finite reflux was performed using the Gilliland correlation in the form of the modified Molokanov, Korablina [120] equation. Molokanov's correlation is represented by eq. (4-3).

$$\frac{N-N_{min}}{N+1} = 1 - \exp\left[\left(\frac{1+54.4\psi}{11+117.2\psi}\right)\left(\frac{\psi-1}{\psi^{0,5}}\right)\right] \qquad (4\text{-}3)$$

$$\psi = \frac{R-R_{min}}{R+1}$$
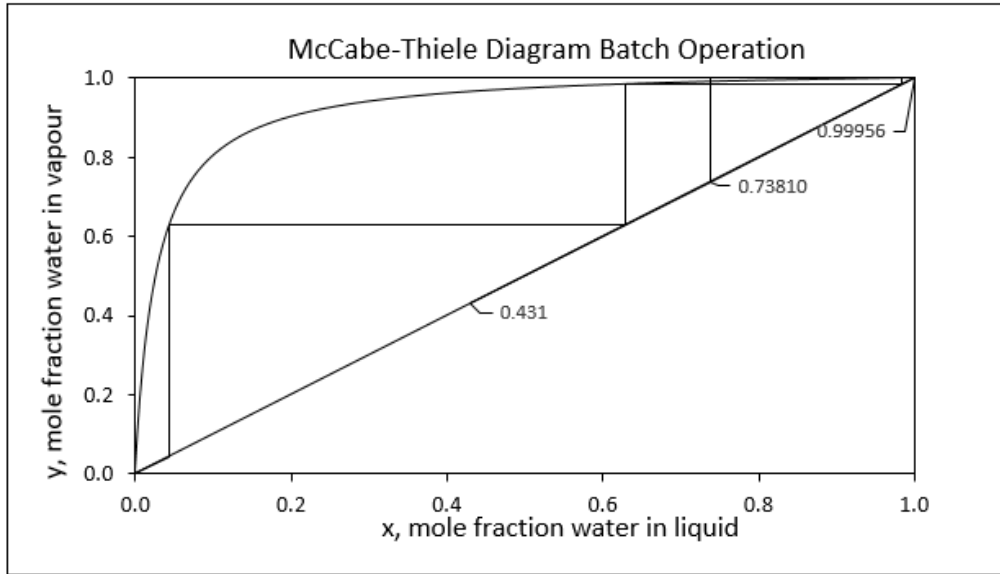
Figure 4-8: McCabe- Thiele diagram, batch trial (1)
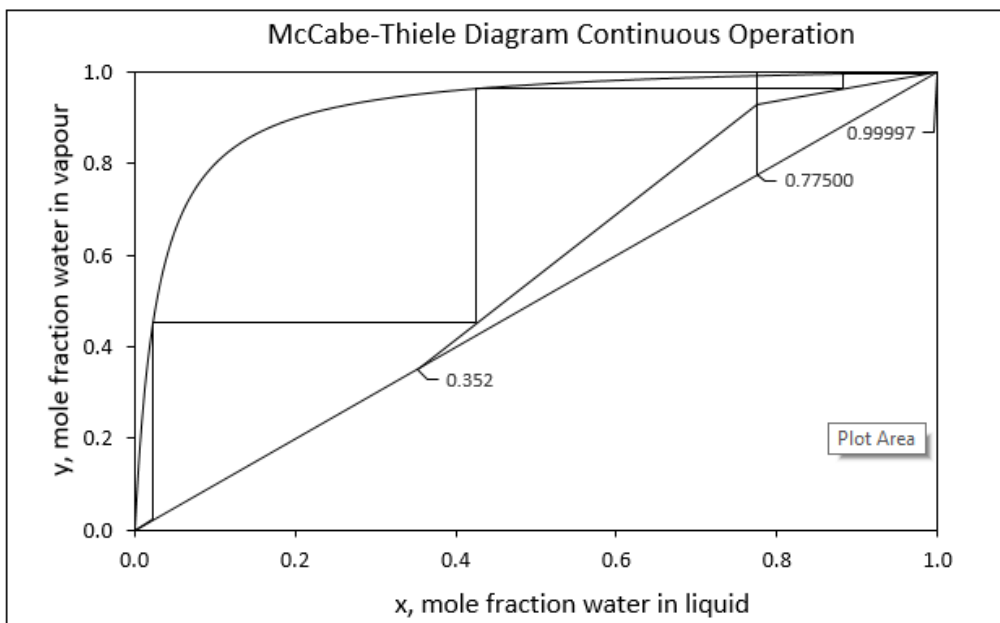


Figure 4-9: McCabe- Thiele Diagram, Continuous Trial (6)
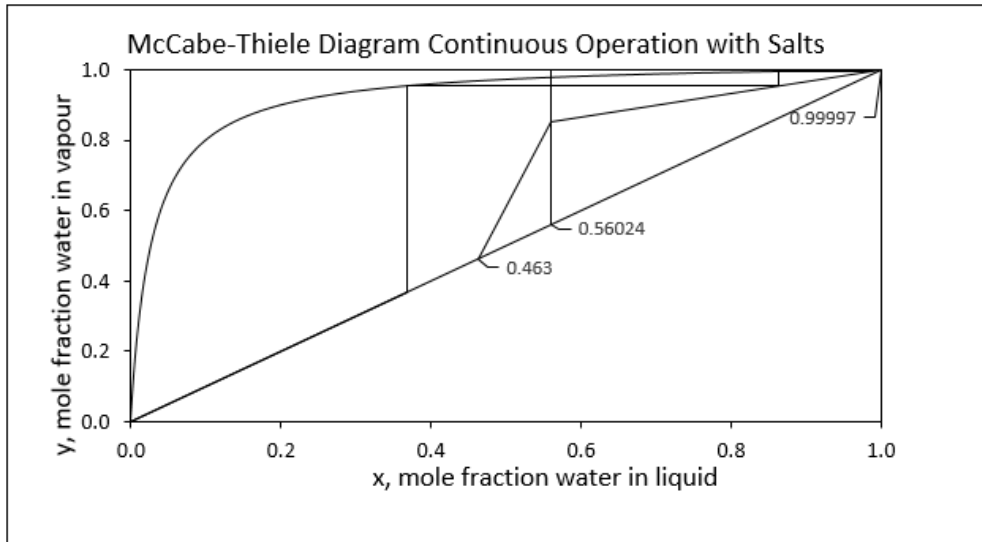
Figure 4-10: McCabe- Thiele Diagram, Continuous Trial (16)

### 4.7.2    Number and Height of Transfer Units

The number and height of transfer units were estimated to provide a secondary estimation of the packed columns performance. The number of transfer units (NTU) required represents the difficulty of the separation whereas the height of transfer units (HTU) is a measure of the effectiveness of the packing [121]. Estimation of the number of transfer units for each trial was performed using eq. (4-4) and evaluated using numerical integration by the Simpson's rule.

$$ NTU = \int_{yB}^{yD} \frac{dy}{y^*-y} \tag{4-4}$$

As described by Dutta [122], the mass transfer exchange between the vapour and liquid phases in distillation is primarily controlled by the vapour phase resistance. As such, the estimation of the HTU was conducted based upon the overall height of the gas phase transfer unit, $H_{OG}$ as per eq. (4-6). The gas and liquid phase transfer units, $H_G$ and $H_L$ can be evaluated from the individual mass transfer coefficients of the gas and liquid phases, $k_G$ and $k_L$ respectively and the effective interfacial area of packing, $a_e$ through eqns. (4-6) and (4-7).

$$ H_{OG} = H_G + \lambda H_L \tag{4-5}$$

$$ H_G = \frac{u_g}{k_G a_e} \tag{4-6}$$

$$H_L = \frac{u_L}{k_L a_e} \tag{4-7}$$

$$\lambda = m\frac{G_m}{L_m} \tag{4-8}$$

### 4.7.3 Height Equivalent to a Theoretical Plate

The height equivalent to a theoretical plate (HETP) represents a correlating factor between the height of packing required and the estimated number of theoretical stages necessary to achieve a desired separation [121]. The concept of HETP is used during column design to allow comparison of efficiencies between packed and plate columns, and is defined by eq. (4-9). Alternately, the HETP can be estimated from experimental results through the $H_{OG}$ by application of eqns (4-10) or (4-11).

$$HETP = Z/N \tag{4-9}$$

$$HETP = \frac{H_{OG}.\ln\left(m\frac{G_m}{L_m}\right)}{m\frac{G_m}{L_m-1}} = H_{OG}.\frac{\ln\lambda}{\lambda-1} \quad \text{for } \lambda \neq 1 \tag{4-10}$$

$$HETP = H_{OG} \text{ for } \lambda = 1 \tag{4-11}$$

### 4.7.4 Mass Transfer Coefficients

In order to determine gas phase transfer unit $H_{OG}$, initial estimation of the gas and liquid phase mass transfer coefficients was required. Estimation was performed using the mass transfer correlations developed by Bravo, Rocha [123] for gauze type structured packing due to its applicability to the structured packing utilised during distillation. Furthermore, the more simplistic nature of the correlations developed by Bravo, Rocha [123] compared to newer correlations as outlined by Wang, Yuan [124] was considered favourable. The gas and liquid phase mass transfer coefficient correlations utilised are outlined by eqns. (4-12) and (4-13) respectively.

$$k_G = 0.0338 \frac{D_G}{d_{eq}} \left[\frac{\rho_g d_{eq}(u_{Le}+u_{Ge})}{\mu_G}\right]^{0.8} Sc_G^{0.33} \tag{4-12}$$

$$k_L = 2\sqrt{\frac{D_L}{\pi s}\left(\frac{9\Gamma^2 g}{8\rho_L\mu_L}\right)^{\frac{1}{3}}} \tag{4-13}$$

$$u_{Ge} = \frac{u_G}{\epsilon \sin \alpha} \tag{4-14}$$

$$u_{Le} = \left(\frac{9\Gamma^2 g}{8\rho_L \mu_L}\right)^{\frac{1}{3}} \tag{4-15}$$

Additional correlations developed by Wilke and Chang [125] and Chapman [126] were utilised in estimation of the liquid and gas phase diffusion coefficients respectively. The liquid phase diffusion coefficient, $D_L$ was estimated through eq. (4-17) utilising an association parameter assumed equal to that of ethanol of 1.5. The gas phase diffusion coefficient, $D_G$ was estimated through eq. (4-16) with the collision integral, $\Omega$ estimated through eq. (4-18) using the corresponding collision integrals reported by Cussler [127]. eq. (4-18) was evaluated using the Lennard-Jones potential parameters reported by Cussler [127] and Ben-Amotz and Herschbach [128] for water and ethylene glycol respectively. The average collision diameter, $\sigma_{12}$ calculated through eq. (4-19) was evaluated using the particle sizes reported by Cussler [127] and Ben-Amotz and Herschbach [128] for water and ethylene glycol respectively.

$$D_G = 1.86 \times \frac{10^{-3} T^{\frac{3}{2}} \left(\frac{M_1 + M_2}{M_1 M_2}\right)^{\frac{1}{2}}}{P \sigma_{12}^2 \Omega} \tag{4-16}$$

$$D_L = \frac{7.4 \times 10^{-8} \left(\sqrt{\phi_2 M_2}\right) T}{\mu_2 V_1^{0.6}} \tag{4-17}$$

$$\frac{\varepsilon_{12}}{k_B T} = \frac{\sqrt{\left(\frac{\varepsilon_1}{k_B}\right)\left(\frac{\varepsilon_2}{k_B}\right)}}{T\,(°K)} \tag{4-18}$$

$$\sigma_{12} = \frac{1}{2}(\sigma_1 + \sigma_2) \tag{4-19}$$

### 4.7.5    Effective Interfacial Area of Packing

The effective interfacial area provided by the packing utilised within the distillation column was estimated using the simple correlation proposed by Bravo and Fair [129] given by eq. (4-20). The interfacial area was estimated assuming a flood percentage, $F_r$ less than 85% based upon the packing surface area, $a_p$ provided in Table 4-4.

$$\frac{a_e}{a_p} = 0.50 + 0.0058 \quad (F_r \leq 0.85) \tag{4-20}$$

## 4.8.    Simulation of MEG- Water System

In order to evaluate the experimental results of each trial, simulations were conducted to model the expected recovery of the MEG-Water distillation system. Simulation of the MEG-Water binary system was performed using the rigorous distillation column models available in Aspen HYSYS and Aspen Plus. As indicated by Table 4-10, separate simulations were performed utilising the HYSYS Peng-Robinson property package, the HYSYS Glycol package and the ELECNRTL package available within Aspen Plus. The Peng-Robinson Equation of State (EOS) was selected for its reliability in simulating a wide range of systems, typically comprised of non-polar light hydrocarbons. Although water and MEG are non-hydrocarbon polar components the Peng-Robinson package was considered suitable as the system to be simulated operates at atmospheric pressure, moderate temperatures and far below the critical properties of each component. Thus, the estimates of vapour properties and component volatility by the package can be considered reliable for initial simulations. The default Peng-Robinson fluid package available within HYSYS was utilised for simulation with no binary parameters associated with the package altered during simulation.

To further improve the capabilities of the developed model, the ELECNRTL Aspen Plus property package was also investigated for its capabilities in simulating electrolytes, such as those commonly experienced industrially during rich MEG regeneration. Initial simulations were performed to evaluate the accuracy of the base property package when simulating only Meg-Water distillation when no dissolved salts were present in order to compare it to the Peng Robinson package. In addition, upon the recommendation of the HYSYS property package selection assistant for systems containing glycols, additional simulations were performed using the available Glycol package.

The experimental operating conditions of the lab-scale MEG recovery column were used as the basis of each simulation. The reboiler operating temperature and reflux ratio of each trial were used as the rigorous columns operating specifications. The feed pressure and temperature for each trial was set at 140 kPa and 30°C respectively with the condenser and reboiler operating pressure maintained at 120 and 130 kPa respectively as per Table 4-3. The main assumptions made in order to develop and simulate the distillation model include:

- Stream flow rates were considered constant and the average flow rate during plant operation was used

- Reboiler temperature remained constant at the specified operating temperature through monitoring and adjustment by the PLC unit.

- Salt free trials consisted of only MEG and water

- Dissolved salt trials consisted of MEG, water and monovalent ions. The majority of divalent ions present within the rich MEG feed are removed prior to distillation during pre-treatment and the impact of remaining divalent ions as given by Table 4-9 are negliable when compared to the monovalent ions Na+ and K+.

- The formation and precipitation of divalent salts during distillation was not simulated due to the low concentration of divalent ions within the rich MEG feed. The formation of monovalent salts was also not considered as they are unlikely to precipitate out within the reboiler unit of a MEG regeneration column.

Table 4-9: Salt Trial Dissolved Salt Compositions

| Dissolved Salts (ppm) | Trial Number | | | | | | |
|---|---|---|---|---|---|---|---|
| | (10) | (11) | (12) | (13) | (14) | (15) | (16) |
| $Na^+$ | 8744 | 8804 | 8021 | 7819 | 8281 | 7243 | 6695 |
| $K^+$ | 3090 | 2715 | 2909 | 3213 | 3121 | 2813 | 2645 |
| $Ca^{2+}$ | 2.9 | 3.5 | 3.88 | 163 | 19.8 | 2.3 | 99 |
| $Mg^{2+}$ | - - | - - | 0.233 | 0.647 | - - | - - | - - |
| $Fe^{3+}$ | 0.346 | 0.445 | 0.347 | 0.109 | 0.255 | 0.43 | 0.127 |
| $Sr^{2+}$ | 0.011 | 0.013 | - | 0.243 | 0.044 | 0.024 | 0.237 |
| $Ba^{2+}$ | 0.504 | 0.367 | 0.273 | 0.574 | 0.452 | 0.295 | 0.615 |

The results of each simulation can be found within Table 4-10 for both salt free and dissolve salt trials for each of the selected fluid packages and their associated average accuracy when compared to the experimental data. Additionally, Figure 4-11 illustrates the relationship between reboiler temperature and lean MEG purity as well as a comparison between experimental and simulated results. Only the Peng-Robinson and ELECNRTL simulation results were illustrated due to the inaccuracy of the results generated by the Glycol fluid package during simulation. The experimental trials involving dissolved salts were also included to visually express the impact of dissolved

salts on the lean MEG purity. Lastly, the impact of MEG mass fraction in the feed upon the lean MEG purity was investigated for constant reboiler temperature trials as Table 4-11. Trials were performed using a constant reboiler temperature of 141°C for feed fractions ranging from 45 to 65% by weight MEG. Lean MEG purities for each trial were subsequently estimated using HYSYS and Aspen Plus with the relationship between feed fraction and lean MEG purity illustrated in Figure 4-12.
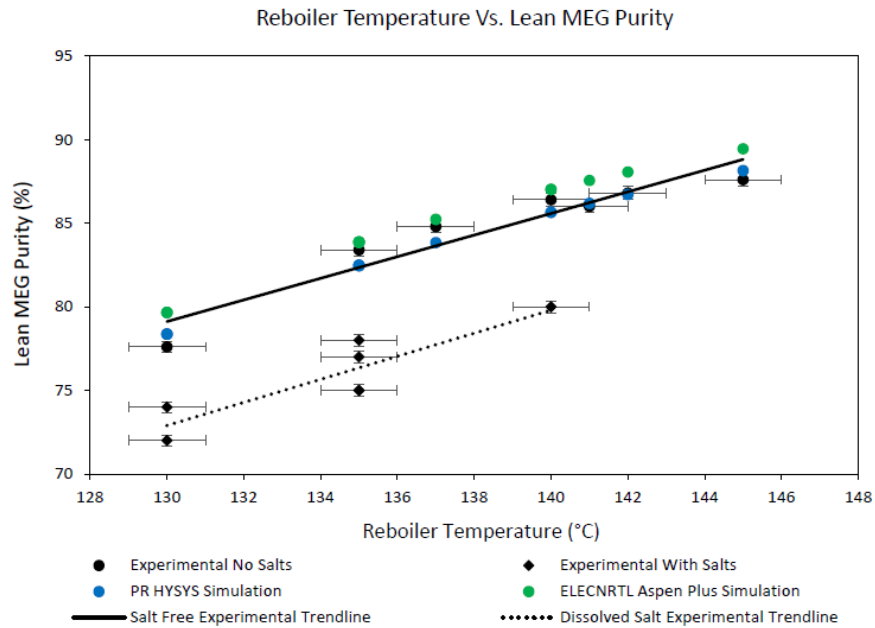


Figure 4-11: Reboiler Temperature vs. Lean MEG Purity (Experimental and Simulated)
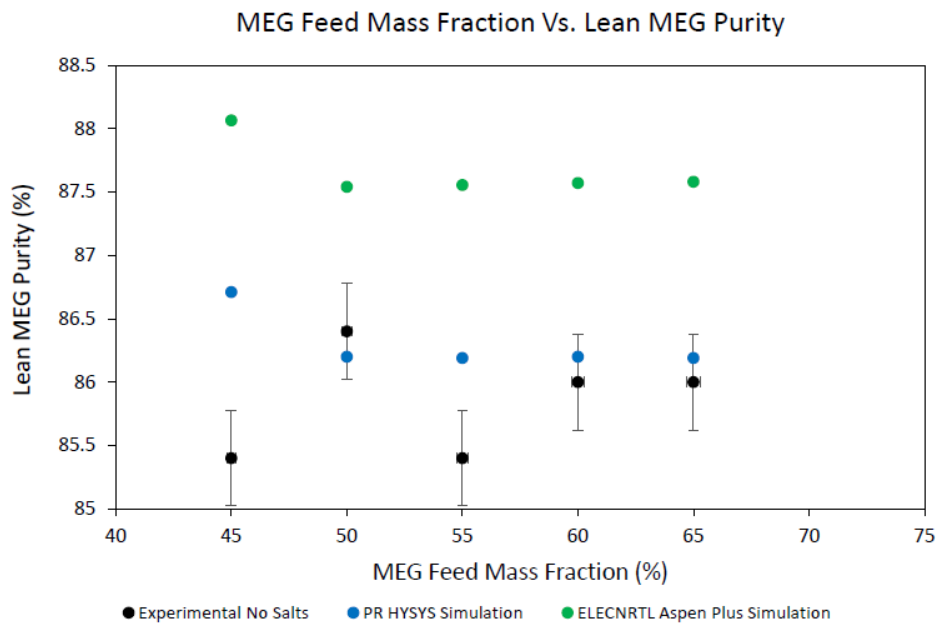


Figure 4-12: Feed MEG Mass Fraction vs. Lean MEG Purity (Experimental and Simulated)

Table 4-10: MEG Water Simulation Results

| Trial No. | Experimental Lean MEG Purity | Simulated Lean MEG Purity | | |
| --- | --- | --- | --- | --- |
| | | Aspen HYSYS | | Aspen Plus |
| | | Peng-Robinson | Glycol Package | ELECNRTL |
| Salt Free Trials | | | | |
| (3) | 0.776 | 0.784 | 0.713 | 0.797 |
| (4) | 0.834 | 0.825 | 0.765 | 0.839 |
| (5) | 0.848 | 0.838 | 0.782 | 0.852 |
| (6) | 0.864 | 0.857 | 0.806 | 0.870 |
| (7) | 0.860 | 0.862 | 0.813 | 0.876 |
| (8) | 0.868 | 0.867 | 0.820 | 0.881 |
| (9) | 0.876 | 0.882 | 0.839 | 0.895 |
| Average Percentage Experimental Deviation | | 0.72% | 6.61% | 1.40% |
| Dissolved Salt Trials | | | | |
| (10) | 0.740 | 0.784 | - | 0.797 |
| (11) | 0.720 | 0.784 | - | 0.797 |
| (12) | 0.750 | 0.827 | - | 0.839 |
| (13) | 0.780 | 0.828 | - | 0.839 |
| (14) | 0.750 | 0.825 | - | 0.839 |
| (15) | 0.770 | 0.825 | - | 0.839 |
| (16) | 0.800 | 0.857 | - | 0.870 |
| (10) | 0.740 | 0.784 | - | 0.797 |
| Average Percentage Experimental Deviation | | 7.79% | - | 9.59% |

Through simulation it was observed that the results obtained using the Peng-Robinson property package were the most consistent with the lean MEG purities obtained through operation of the column when no salts were present. From Table 4-11, the Peng Robinson package was capable of simulating the lean MEG purity within on average 0.72% of the experimentally achieved recovery in comparison to 1.40% by the ELECNRTL package. However, the HYSYS Glycol property package was the least accurate of the tested fluid packages typically estimating a lean MEG purity significantly less than that found experimentally. In contrast, the experimentally obtained lean MEG purities for trials involving dissolved salts were significantly lower than that reported by the respective simulations. The Peng-Robinson and ELECNRTL fluid packages were only capable of simulating salt trials within 7.79% and 9.59% on average respectively, suggesting the dissolved salt content of the rich MEG has a major impact on achievable lean MEG purity during distillation.

Table 4-11: MEG Purity VS. MEG Feed Mass Fraction

| Reboiler Temperature (°C) | MEG Feed Fraction | Lean MEG Purity | HYSYS Estimated Purity | ELECNRTL Estimated Purity |
|---|---|---|---|---|
| 142 | 45 | 0.854 | 0.867 | 0.881 |
| 141 | 50 | 0.864 | 0.862 | 0.875 |
| 141 | 55 | 0.854 | 0.862 | 0.876 |
| 141 | 60 | 0.86 | 0.862 | 0.876 |
| 141 | 65 | 0.86 | 0.862 | 0.876 |

The uncertainty associated with the reported experimental data is expressed within Figure 4-11, Figure 4-12 and Figure 4-13 as uncertainty bars. The uncertainty bars represent the combined uncertainty associated with the measurements made in terms of reboiler operating temperature and the mass fraction of MEG as reported by MEG the refractometer. The errors associated with the reboiler thermometer and MEG refractometer range from $\pm 1°C$ and $\pm 0.4\%$ v/v respectively as per Section 4.4.
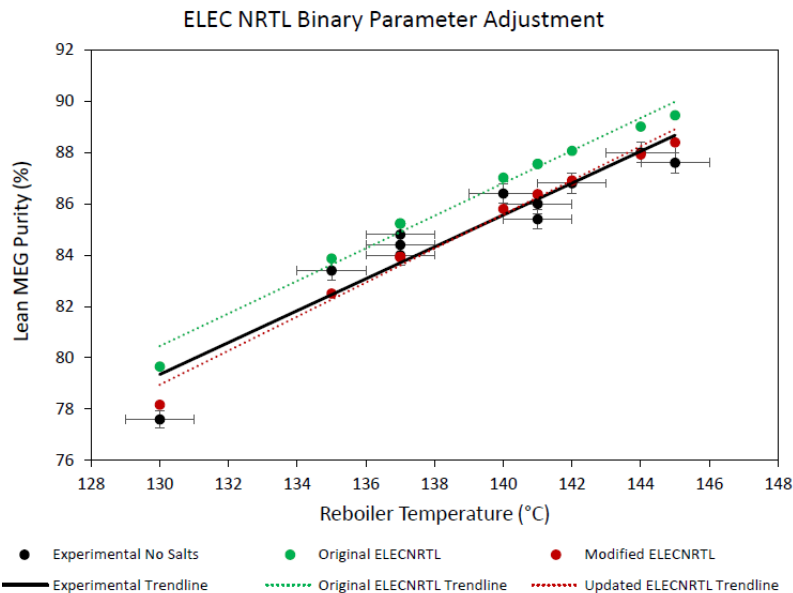


Figure 4-13: Modified ELECNRTL Binary Parameter Simulation Results

In order to improve the accuracy of the ELECNRTL fluid package for simulating salt free trials the binary parameters associated with the package were adjusted using the

data regression function within Aspen Plus. Several sets of isobaric VLE data sets available within the Aspen Plus database were used to regress the MEG and water NRTL binary parameters $\alpha_{ij}$, $b_{ij}$ and $c_{ij}$ to find the best fit with respect to the experimental data. The ELECNRTL property package is consistent with the NRTL-Redlich-Kwong property method utilising the NRTL model given by eq. (4-21) with the temperature dependant parameter, $\tau_{ij}$ given by eq. (4-23). Additional trials not listed in Table 4-6, were used to allow a more accurate fitting of the binary parameters for the ELECNRTL property package. It was found that the VLE data reported by Kamihama et al. [130] provide the best fit for the experimental achieved lean MEG purities within this study.

$$ln y_i = \frac{\sum_j x_j \tau_{ij} G_{ji}}{\sum_k x_k G_{ki}} + \sum \frac{x_j G_{ij}}{\sum_k x_k G_{ki}} \left( \tau_{ij} - \frac{\sum_j x_j \tau_{ij} G_{ji}}{\sum_k x_k G_{ki}} \right)$$ (4-21)

$$G_{ji} = exp\left( -\alpha_{ij} \tau_{ij} \right)$$ (4-22)

$$\tau_{ij} = \alpha_{ij} + \frac{b_{ij}}{T} c_{ij} \ln T$$ (4-23)

The new NRTL binary parameters were regressed using the VLE data by Kamihama [130] as a basis and then further modified to generate the binary components found in Table 4-12 where components $i$ and $j$ are MEG and water respectively. Simulations involving the ELECNRTL package for salt free trials were then reperformed using the newly modified ELECNRTL package with results shown in Table 4-13 and graphically illustrated by Figure 4-13. It was observed that the modified binary parameters allowed a much more accurate estimation on average of the lean MEG purity consistent with experimentally achieved results. Attempts were also made to regress more accurate binary parameters for the Peng Robinson property package within Aspen Plus but it was determined that the default Peng Robinson fluid package within Aspen HYSYS was the most accurate. The VLE curve for the MEG-Water system derived from the modified NRTL binary parameters and the default Peng Robinson EOS available within HYSYS is given by Figure 4-14. The VLE data was generated using the binary analysis capabilities of Aspen Plus and the 'Equilibrium Unit Operation' model within HYSYS at a constant pressure of 130 kPa as per the operating pressure of the reboiler.
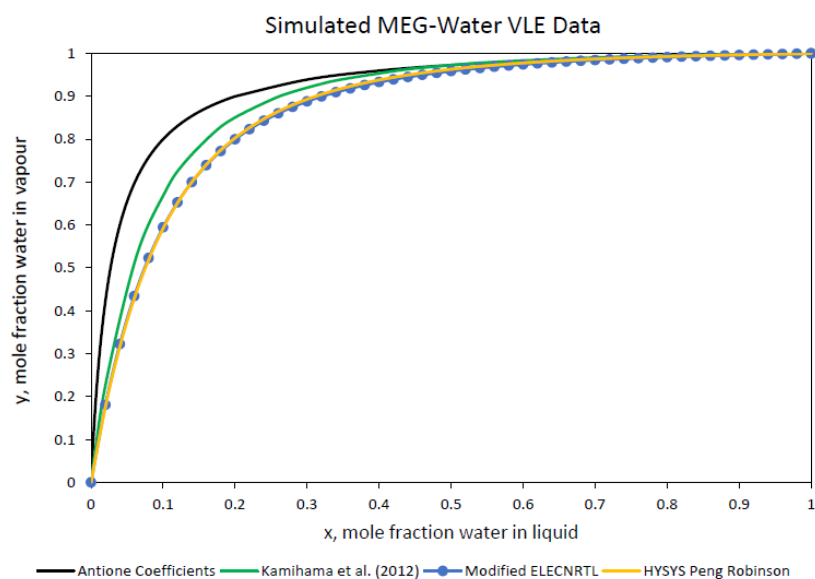
Figure 4-14: Simulated MEG-Water VLE Data

Table 4-12: ELECNRTL Temperature Dependant Binary Parameters

| $A_{ij}$ | $A_{ji}$ | $B_{ij}$ | $B_{ji}$ | $C_{ij}$ |
|----------|----------|----------|----------|----------|
| -1.77 | 1.9479 | 912.662 | -1024.5 | 0.3 |

Table 4-13: Salt Free ELECNRTL MEG-Water Simulation Results with Adjusted

Binary Parameters

| Trial No. | Reboiler Temp | Experimental | Original ELECNRTL | Modified ELECNRTL |
|-----------|---------------|--------------|-------------------|-------------------|
| (3) | 130 | 0.776 | 0.797 | 0.782 |
| (4) | 135 | 0.834 | 0.839 | 0.825 |
| (5) | 137 | 0.848 | 0.852 | 0.839 |
| | 137 | 0.840 | 0.852 | 0.839 |
| | 137 | 0.844 | 0.852 | 0.839 |
| (3) | 140 | 0.864 | 0.870 | 0.858 |
| | 141 | 0.854 | 0.876 | 0.864 |
| (7) | 141 | 0.860 | 0.876 | 0.864 |
| (8) | 142 | 0.868 | 0.881 | 0.869 |
| | 144 | 0.880 | 0.890 | 0.879 |
| (9) | 145 | 0.876 | 0.895 | 0.884 |
| Average Percent Deviation from Experimental | | | 1.45% | 0.63% |

## 4.81.     Simulation of Dissolved Salt Impact upon Operation

Modelling the impact of dissolved salts upon the operation of the distillation column was performed using the salt simulation capabilities of the Aspen Plus ELECNRTL model. The presence of salts within the rich MEG feed to the distillation column was modelled using the dissociation of NaOH and KOH to their respective monovalent cations to produce the salt concentrations listed in Table 4-9 within the feed stream. This was achieved by calculating the amount of NaOH and KOH required using the known concentration of the respective cations, stream flow rates and dissociation reaction stoichiometric ratios. Only the impact of monovalent salt ions, Na+ and K+ were included in the analysis as the majority of divalent cations would be removed in the pre-treatment stage prior to the distillation column in industrial regeneration systems. Thus, due to their low concentration their impact can be considered minimal compared to the much greater presence of monovalent cations within the rich MEG. Furthermore, the formation and precipitation of salts was not modelled as the high solubility of monovalent cations ensures they remain dissolved during distillation to be later removed downstream within the reclaimer unit [64].

The results of dissolved salt simulation are summarised within Table 4-14 of which compares simulation results produced by both the original and modified ELECNRTL fluid packages when dissolved salts are included and compared graphical in Figure 4-15. it can be seen that the ELECNRTL package modified with the reported binary parameters allowed a more accurate estimation of the lean MEG purity in comparison to the original ELECNRTL fluid package when salts where excluded and included. Overall, the Modified ELECNRTL fluid package when salts where incorporated was able to simulate the experimentally determined lean MEG purity within 1.61% on average compared to 9.59% of the simulations reported in Table 4-11. From this it can be determined that the presence of monovalent cations and to an extent divalent cations within the rich MEG feed to MEG regeneration column can have a significant impact on the achievable lean MEG purity and can be modelled with relative accuracy.

Table 4-14: MEG- Water Simulation Results

| Trial No. | Experimental Lean MEG Purity | Original ELECNRTL (No Salts) | Original ELECNRTL (With Salts) | Modified ELECNRTL (With Salts) |
|---|---|---|---|---|
| (10) | 0.74 | 0.797 | 0.725 | 0.715 |
| (11) | 0.72 | 0.797 | 0.724 | 0.714 |
| (12) | 0.75 | 0.839 | 0.777 | 0.765 |
| (13) | 0.78 | 0.839 | 0.774 | 0.763 |
| (14) | 0.75 | 0.839 | 0.774 | 0.763 |
| (15) | 0.77 | 0.839 | 0.782 | 0.771 |
| (16) | 0.80 | 0.870 | 0.819 | 0.808 |
| Average Percentage Experimental Deviation | | 9.59% | 2.02% | 2.02% |
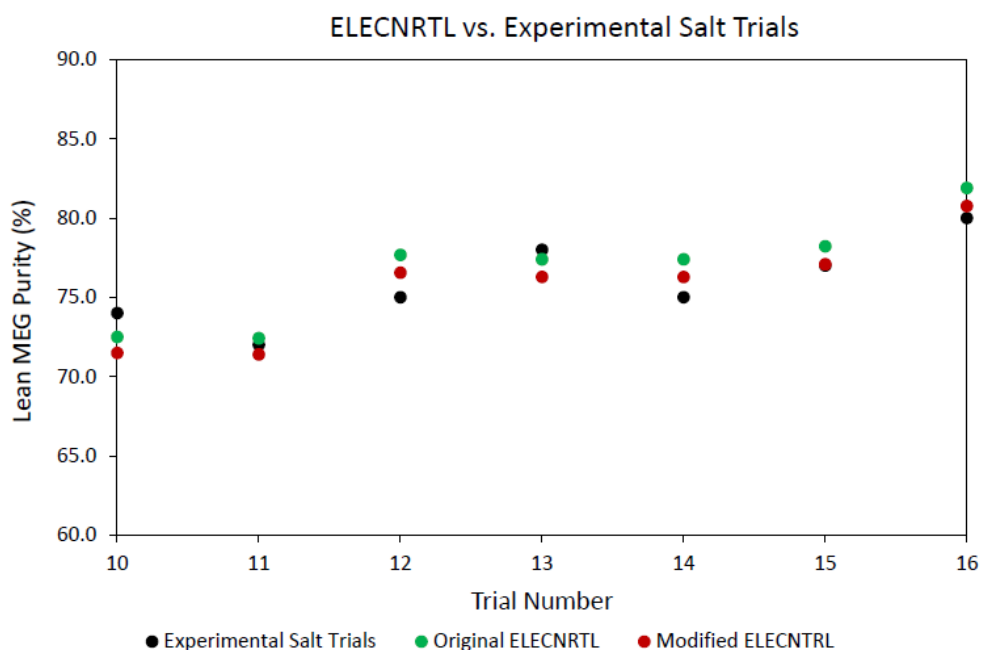


Figure 4-15: ELECNRTL Simulated Dissolved Salt Lean MEG Purities

## 4.9.    Discussion

The design and construction of the MEG distillation column utilised in this study was performed to investigate the recovery of MEG within a pilot scale packed distillation column. Through the experimental trials conducted, the validity of the design for the separation of water from MEG was confirmed. Operation of the distillation column

was successfully performed under varying feed and reboiler conditions with lean MEG purities above 80% by mass achieved. Furthermore, operation of the column was successfully tested upon the introduction of dissolved salts into the rich MEG feed.

One of the primary aspects of this study was to evaluate the design of the MEG distillation column and assess its performance under varying operation conditions. The column was operated using both batch and continuous operation utilising a wide range of both MEG feed mass fractions and reboiler operating temperatures and the impact on lean MEG purity investigated. It was found when operating under batch conditions the number of theoretical stages required to achieve separation was three, of which corresponds to the minimum number of stages required under total reflux. However, when operating at a finite reflux typically between 0.4-0.6 by weight under continuous operation, the actual number of theoretical stages was estimated to be six. It can be observed through Table 4-6 that under both batch and continuous operation when no salts are present within the rich MEG feed, a lean MEG purity above 80% can be achieved when operating the reboiler above 135°C. Although as expected, under batch operation the achievable MEG concentration within the distillate water product was significantly higher than under continuous operation.

Estimation of the number of transfer units for each continuous trial as per Table 4-8, provides a measure of the performance of the column under varying operating conditions. For each trial the number of transfer units indicates the difficulty of the separation and was estimated via numerical integration of eq. (4-4) based upon vapour phase compositions calculated along the stripping and rectifying operating lines and at equilibrium by the VLE curve. The concept of transfer units is considered to be the most accurate way of estimating a columns performance and required height of packing in comparison to other methods including HETP. However, a major problem faced in analysing the experimental results reported using transfer units was the steep nature of the NTU curve as a result of the low mass fraction of MEG in the distillate product (100 ppm). The NTU curve for continuous trial number four is displayed in Figure 4-16 exhibiting the steep NTU curve as the vapour composition reaches one. Due to the steep curve produced, estimation of the number of transfer units by calculation of the area under the curve by both graphical and numerical integration was highly dependent on the step size chosen. As such it was difficult to estimate the number of transfer units accurately and was thus considered a poor representation of

the columns performance in comparison to the number of theoretical stages estimated by the FUG shortcut method.
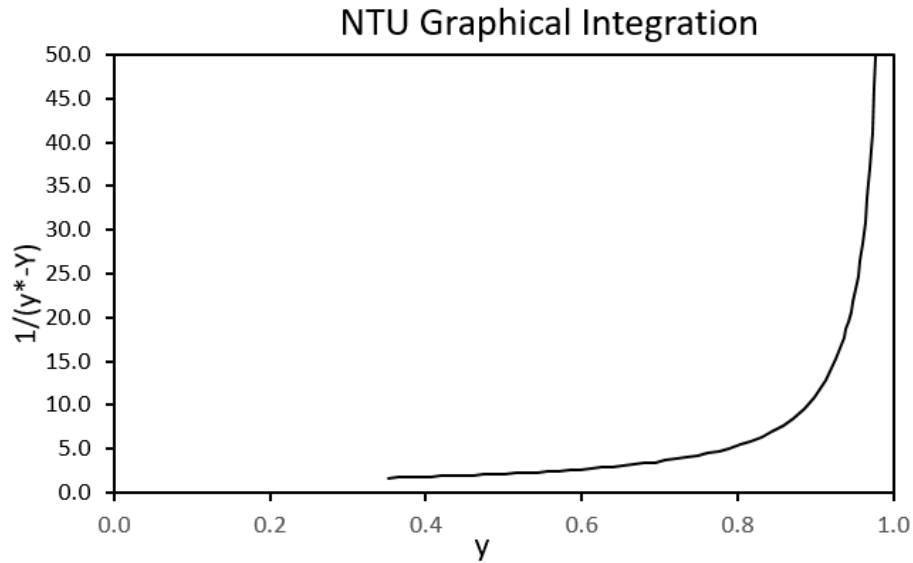


Figure 4-16: Continuous Trial (6) NTU Graphical Integration

Additional calculations were then performed in order to estimate the overall height of the gas phase transfer unit to assess the effectiveness of the packing in separating MEG from water. It was found for continuous trials with no dissolved salts that the average HTU was approximately 0.306 metres, however, when dissolved salts were introduced the HTU decreased to between 0.229-0.217 metres suggesting an increase in packing performance. This directly contradicts what was believed to occur upon the introduction of salts into the rich MEG feed, where the presence of salts was thought to decrease the packings performance. However, through calculation it was observed that the effect of dissolved salts, primarily through increased density and viscosity of the liquid within the reboiler had only a minor impact upon the estimated HTU. Instead, the HTU was primarily influenced by the fraction of MEG within the feed and the relative difference between MEG feed fraction and the final fraction of MEG within the lean MEG product. A lower mass fraction of water within the feed directly resulted in a decreased amount of water boiled within the reboiler and returned to the column as boilup. This was compounded when conducting salt trials due to the lower lean MEG product purity achieved as per Table 4-6. This further reduced the boilup returned to the column as more water was retained within the bottoms product. The combination of these factors ultimately reduced the vapour and liquid throughput of

the column and by extension the vapour and liquid superficial velocities utilised in eqns. (4-6) and (4-7) reducing the estimated HTU. Overall, it can be assumed that the column was not operating at maximum capacity and a lower rate of mass transfer between the liquid and vapour phase occurred.

The HTU for each trial was then used as a basis to estimate the HETP by application of eq.(4-9). It was observed for salt free trials the packing achieved a HETP of approximately 0.33-0.35 metres, slightly lower than that estimated using the known height of packing and estimated number of theoretical plates for each trial by eq.(4-8). From the estimated HETPs the expected height of packing can be calculated, and was estimated at approximately 1.7 metres. This is slightly lower than the height of packing utilised within the column but with additional safety margins and rounding up to the next standard height of a packing section a height of 1.8 metres (900mm×2) is realistic. Again, it was observed that for trials involving dissolved salts within the rich MEG feed the HETP decreased significantly suggesting an increase in column performance when salts are present. However similar to the HTUs estimated, the reduced HETP can be attributed to the reduced liquid and vapour flow rates within the column. Furthermore, estimation of the HTU and HETP for batch trials was not conducted as the column will primarily be operated under continuous conditions.

To further evaluate the operation of the pilot MEG distillation column, simulations were performed using Aspen HYSYS and Plus to investigate how closely simulations conformed to the experimentally determined lean MEG purities. Initial simulations performed using the Peng Robinson fluid package available within Aspen HYSYS was found to provide an accurate estimation of lean MEG purity in comparison to the respective salt free operational trials. As can be seen visually through Figure 4-11, the lean MEG purities estimated through HYSYS simulation closely matched those obtained through experimental means with the estimated trend lines of both the salt free experiments and simulated data points in close agreement. Furthermore, as can be expected, a clear relationship between the operating temperature of the reboiler and the purity of the lean MEG is evident. However, no clear relationship between the fraction of MEG in the feed and experimental lean MEG purities was observed in Figure 4-12 with Aspen HYSYS and Plus both suggesting the lean MEG purity is independent of the feed fraction. This can be attributed to the nature of MEG distillation where there is a large difference in volatility between MEG and water

resulting in an almost 100% pure water distillate. As such, although the salt trials outlined in Table 4-11 were conducted with higher MEG feed fractions, the difference in the lean MEG purities observed in comparison to the salt free trials can be attributed to the presence of dissolved salts.

Likewise, the default ELECNRTL fluid package within Aspen Plus was found to be able to predict the experimentally lean MEG with reasonable but lower accuracy than the HYSYS Peng Robinson EOS. However, with adjustment of the property package's binary parameters, the accuracy of the ELECNRTL package for simulating the MEG-Water system was able to be significantly improved surpassing that of the HYSYS Peng

Robinson EOS. Furthermore, the ELECNRTL package includes the capability of simulating the impact of electrolytes such as dissolved salts that are common in industrial MEG processing after the production of formation water during hydrocarbon production. The NRTL binary parameters found to be suitable for simulating salt free MEG-Water distillation are reported in Table 4-12.

VLE data for the simulated MEG-Water system was also generated using the capabilities of Aspen HYSYS and Plus using the HYSYS Peng Robinson and modified ELECNRTL fluid packages respectively. Figure 4-14 graphically compares the MEG-Water VLE data of that calculated through Antione coefficients as per Figure 4-7, simulation by Aspen HYSYS and Plus and the literature VLE data reported by Kamihama [130] that was used as the basis for NRTL binary parameter regression. It is clear that the VLE data estimated by simulation within this study deviates significantly from that reported in literature and graphed within Figure 4-7. This can be attributed to the different test conditions at which the literature MEG-Water binary VLE data was reported at. These test conditions are not representative of the typical operating conditions at which an industrial MEG distillation column typically operates, namely atmospheric pressure and 120-160°C Psarrou [111]. The VLE data generated within this study was matched to experimental data of a real MEG pilot plant, operating at typical industry conditions and thus can be considered more accurate for future design of such systems compared to previous literature data.

The primary outcome observed during analysis of the experimental results by simulation was the impact of dissolved salts within the rich MEG feed upon the purity

of the final lean MEG product. The purity of lean MEG in trials including dissolved salts deviated significantly from both corresponding salt free trials with similar reboiler operating temperatures and expected results derived from initial simulations when salts were unaccounted for. This phenomenon is observed through the experimentally obtained lean MEG purities reported in Table 4-6 and Figure 4-11 where the purity of salt trials is observed to be notably less than the produced trend lines for both experimental and simulated results. Furthermore, the HETP estimated for trials involving dissolved salts were also noticeably less indicating a poorer separation performance of the column. However, the impact of dissolved salts upon the achieved lean MEG purity during operation was able to be predicted within an average deviation of 1.61% from the experimental results as indicated by Table 4-14. The introduction of Na+ and K+ ions into the simulated rich MEG feed based on experimental concentrations showed noticeable impact upon the lean MEG purity reported during simulation. On average, the inclusion of monovalent cations within the simulation reduced the achieved lean MEG purity by 7.65% for trials with total monovalent concentrations between 10000-12000 ppm.

The impact of the dissolved salts analysed within this work upon the operation of both the pilot MEG column and simulation models can be attributed to the boiling-point elevation of the MEG-Water solution due to the presence of the mono-valent cations, Na+ and K+. The presence of such non-volatile solute within the solution directly reduces the overall vapour pressure of the MEG-Water solution thus requiring a greater reboiler operating temperature for boiling to occur. The effects of various salts on the boiling point of aqueous solutions has been documented by various authors including Bialik [131] and Meranda [132]. Furthermore, the presence of dissolved salts within the MEG-Water solution can have pronounced effects upon the VLE curve of the system. The impact of dissolve salts upon the VLE curve of various binary systems and methods to predict such impacts have been outlined by Aznar [133], Chou [134] and Kumar [135].

The impact of salts on the MEG distillation process was primarily thought to occur through oversaturation of soluble salts, primarily divalent salts including $CaCO_3$ and $FeCO_3$ leading to salt deposition within processing equipment [3, 12]. The process of salt precipitation in industrial regeneration of MEG is a major contributor to poor separation performance due to fouling and the accumulation of suspended solids within the reboiler unit causing reduced heat transfer efficiency. However, the

presence of dissolved mono-valent salt cations within the rich MEG was also found to have significant impact on the achievable lean MEG purity during both experimental operation of the pilot MEG plant and simulated models. To accommodate the impact of dissolved salts a higher reboiler temperature would be required to maintain a constant boil up rate and lean MEG purity compared to salt free operation. However, operating the reboiler at too high of a temperature can lead to thermal degradation of the MEG as per the research performed by AlHarooni, Barifcani [5]. Alternatively, a greater lean MEG purity can be achieved by the reduction of reboiler operating pressure but is generally avoided due to increased operating costs. In addition, due to the inverse soluble nature of some salts including $CaCO_3$ one of the primary salt precipitants experienced in MEG processing, higher operating temperatures may directly lead to increased salt precipitation and reboiler fouling, further reducing separation efficiency.

## 4.10.    Conclusions

The distillation column utilised within this study was designed for the separation of water from MEG when dissolved salts common in MEG systems are present. The primary aim of the experimental trials conducted was to verify the design of the column and to assess its performance in recovering MEG for water. It was estimated through the experimental data obtained through operation of the column that it consists of six equilibrium stages under continuous operation. Under total reflux the minimum number of equilibrium corresponds to two. Further analysis of the column through the concept of HETP evaluated the columns packing as having a HETP of approximately 0.34 metres. Through the estimated HETP in conjunction with the estimated number of theoretical stages for each trial, an estimated height of packing required to achieve separation was found to be approximately 1.7 metres. This corresponds closely with the 1.8 metres of packing utilised within the column thus verifying its design. Secondary estimation of the required packing height can also be made through the estimated HTU and NTUs for each trial, through this method the packing was estimated to be roughly 1.9-2.1 metres. However due to the inaccuracies in estimating the NTU discussed, this estimation is less reliable than that made using the HETP.

The secondary objective of this study was to investigate the impact of dissolved salts upon the recovery of MEG and upon the operational performance of the column. Estimation of the HTU and HETP of the packing for both salt and salt free trials were inconclusive in assessing the columns performance. It was observed that the presence of salts had a significant impact on the perceived performance of the column through the estimated HTUs and HETPs. However, the mass fraction of MEG in the feed and relative difference between feed and lean MEG mass fraction was found to be the underlying factor. Overall the presence of dissolved salts in the rich MEG feed primarily influenced the lean MEG purity that could be achieved during operation. It was observed that for salt trials, the experimentally achieved lean MEG purity was approximately 7.2% less than corresponding salt free trials at equal reboiler operating temperatures.

The conclusions drawn from experimental data were then further investigated through the development of distillation models using Aspen HYSYS and Plus. Of the models developed, the Peng Robinson EOS in HYSYS and the ELECNRTL package with modified binary parameters were found to generate product MEG purities in close agreement with experimental trials when no dissolved salts were present. However, upon the introduction of salts into the feed, the experimental lean MEG purities deviated significantly from the trend lines developed from simulated results for both fluid packages. It was concluded that the impact of dissolved salts upon the MEG distillation process occurred due to an increase in solution boiling point and the resulting impact on the MEG-Water systems VLE. The impact of dissolved salts within the rich MEG feed was able to be predicted with an average deviation of 1.61% from experimental trials using the Aspen Plus ELECNRTL electrolyte simulation capabilities by the inclusion of monovalent cations. Overall, it was established that the impact of dissolved salts is not only limited to the effects of salt precipitation and accumulation within the reboiler unit of a distillation column but also through its impact on the VLE of the system. Therefore, the unexpected presence of dissolved salts within the rich MEG feed stream may require greater reboiler temperature to maintain a constant boil up rate potentially leading to unwanted thermal degradation of the MEG.

# 5. Modelling and optimization of MEG recovery by distillation process

## 5.1 Introduction

First of all, it is worth noting that this chapter has been submitted to a high-quality journal for publication.

In the oil and gas industry, gas hydrate formation can be considered as a serious problem as it leads to blockage of flowlines, which results in operational complications and financial losses [1]. Therefore, developing an effective hydrate inhibition technique to maintain flow assurance and ensure the integrity of transportation pipelines and process facilities, have been the focus of many researchers. Currently there are many techniques implemented to minimize the risk of hydrate formation. These techniques in general involve the removal of elements that are known to cause hydrate formation. One of these elements is wet gas which is caused by the presence of water in the system [136, 137]. Thermodynamic hydrate inhibitors have been injected at wellhead to solve hydrate formation problems. Mono-ethylene glycol (MEG) has been applied to change the equilibrium curve of hydrate toward lower temperatures and higher pressures which make the operating conditions of offshore flowlines different from the hydrate formation conditions [12]. Given the high cost of MEG, its impact on the downstream processes, and the large volume required to achieve a successful hydrate inhibition operation, the process of recovery and regeneration of MEG becomes extremely crucial [5]. The process of MEG regeneration requires heating the water saturated MEG to remove excess water, and to achieve the desired glycol purity of around 80-90% [138]. In practice, MEG is heated up in the distillation column to temperatures ranging from low 95°C to 140-160°C as suggested by Montazaud [139] and Gonzalez [140], respectively. However, the temperature at which MEG begins to show signs of degradation sets the threshold for the operating temperature of the distillation column. Knowing this temperature threshold is extremely crucial to prevent MEG degradation as it produces organic acids such as acetic, glycolic and formic acids due to excessive heat [5]. As regeneration process alone does not remove salts and other contaminants present in the MEG solution, full reclamation process may be carried out whereby "lean MEG" (water free MEG), or "rich MEG" (water-MEG solution) is evaporated, then distilled, to remove

salts and undesired additives such as pipeline corrosion products from MEG. Salts accumulated in the MEG system must be removed by either centrifuging or decanting, or alternatively MEG can be periodically replaced, as high level of salt accumulation in the MEG loop system can cause severe fouling and damage to the equipment and flow lines [2].

It is necessary to enhance the performance of processes and improve the yield without an extra cost. The technique applied to achieve this aim is called optimization [141]. In conventional technique there is a variable change with examined range while keeping the other parameters at fixed values [142]. The main drawback of these methods is missing the synergistic effects among all independent variables [141]. To overcome this disadvantage, optimization with response surface methodology (RSM) can be applied to design experiments and investigate the interactive effects among the variables as well as determine the optimum operating conditions[143]. However, to the best of the author's knowledge, there is no study available to determine optimum operating conditions for MEG recovery by distillation unit.

## 5.2 Experimental Methods

### 5.2.1   Process configuration and description

This can be seen from the process flow diagram in Figure 5-1. The distillation process consists of a feed tank followed by a distillation column. The main purpose of feed tank is to prepare the MEG solution (MEG + Water) which is used in the distillation process. After preparation of the MEG solution, rich MEG feed is preheated by a circulation heater to 25, 30, 35, 40, 45 and 50 °C and pumped through a 10 micro filter to remove the solid particles and then enters the distillation column directly through the reboiler. The distillation column is a traditional tower with 0.01 $m^3$ glass reboiler capacity heated by an immersion heater. The reboiler temperature is varied from 125 to 145 °C.

The distillation column is made from QVF glass with 2.25 m height and structural packing of 80 mm diameter. The column is provided with temperature thermocouples and gauges for temperature monitoring in the reboiler and in the column itself. In

addition, the column consists of a condensation system at the top of the column to condense the vapour top product and a reflux drum to collect the liquid reflux. The reflux is the then fed back to the column through a pump. All operation process is controlled by a programing local control (PLC)
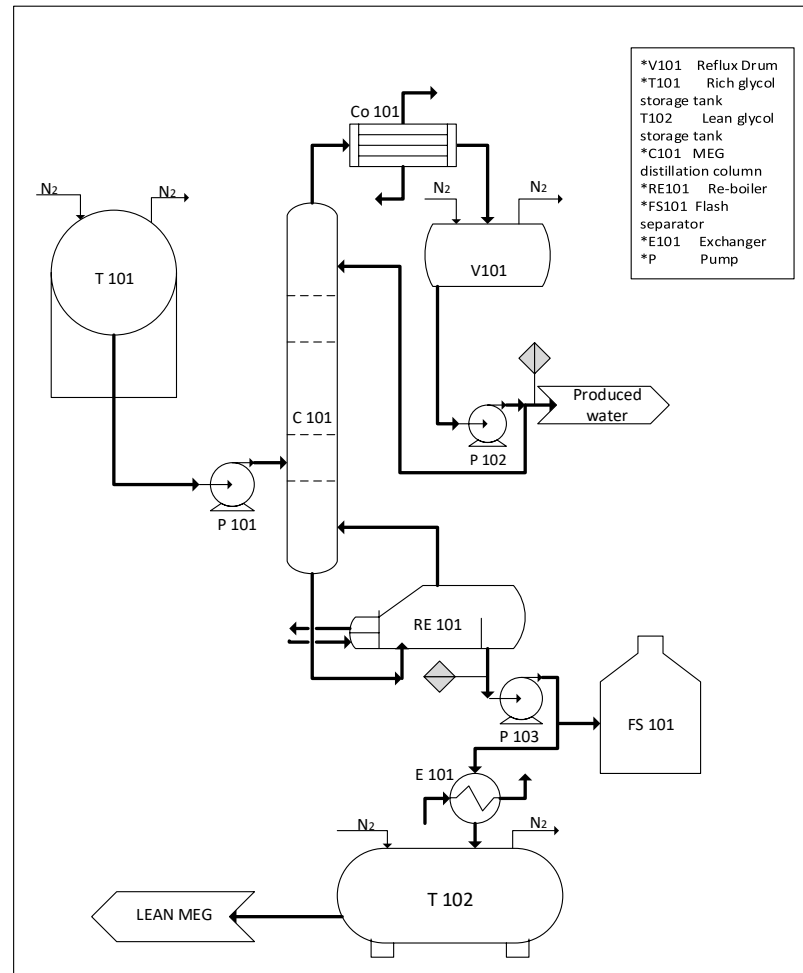


Figure 5-1: Process flow diagram

### 5.2.2 Batch distillation experiments

The batch experiments were performed using the procedure described previously in section (4.6). Every 30 minutes, Samples from the reboiler (RB) and the reflux drum (RD) sections were taken to measure the concentrations by ATAGO refractometer.

### 5.2.3 Continuous distillation experiments

The continuous experiments were accomplished by the procedure described previously in section (4.6). Similar to the batch operation process, samples from the reboiler (RB) and the reflux drum (RD) sections were regularly taken to measure the concentrations using ATAGO refractometer.

### 5.2.4 HYSYS Simulation and Equation of State Selection

In this study, distillation process as in Figure 5-1 has been simulated using Aspen HYSYS V7.2 to find out the best conditions for the process, also to evaluate and compare the results. Aspen HYSYS is considered as one of the most common and comprehensive modelling tools used by the oil and gas producers, refineries and engineering companies for process modelling and optimization. In addition, Peng Robinson equation of state (PR EOS) has been selected as a fluid package for these reasons which will be discussed further in the equation of state part. HYSYS provides various EOS packages for hydrocarbon treatments and sour gases separation. Ping Robinson EOS and Soave Redlich Kwong (SRK) can be considered as the most common fluid packages used in the oil and gas field and petrochemicals application [144, 145]. The PR and Soave Redlich Kwong equations of state have been developed to deal with phase equilibrium calculations for systems ranging from low-temperature cryogenic systems to high-temperature, high-pressure reservoir systems. Moreover, Vitu, Privat [146] found accurate results by using PR EOS to predict the phase equilibria of CO2 and hydrocarbon systems. Jaubert, Privat [147] also tested PR EOS to predict the phase equilibria of syntheses for petroleum fluids (alkanes, aromatics, $CO_2$, $H_2S$, $N_2$ and more) and high accuracy results have been obtained and the model was successful. Despite the fact that PR EOS is more suitable for non-polar compounds $H_2O$ and MEG are polar compounds. The operating conditions in this study are at atmospheric pressure and medium temperature and the process to be simulated far below the critical conditions of MEG [118].

### 5.2.5    Experimental design and regression analysis

Box Behnken designs (BBD) are experimental design for response surface methodology which proposed by Box and Behnken in 1960 [148]. RSM with BBD was used as a tool to optimize MEG recovery by distillation and also investigate interactive effects of three independent factors. Since T (°C) ($X_1$), $XF_{MEG}$($X_2$), and Q (Kg/h) ($X_3$) can significantly impact the MEG recovery process, they were chosen as the critical factors. fifteen experiments were performed by varying T (°C) from 125 to 145 with a central point of 135, the mass percentage of MEG in the feed from 45% to 70% with a central point of 57.5%, and Q (Kg/h) from 5 to 9 with a central point 7. The mass percentage of MEG in the bottom was selected as the response variable. The actual values of independent variables ($X_i$) were calculated as coded values ($x_i$) by applying equation (5-1) [142];

$$x_i = \frac{X_i - X_0}{\Delta X_i} \qquad (5\text{-}1)$$

Where $x_i$ is the coded value of the actual variable ($X_i$), $X_o$ is the actual variable at the centre, and $\Delta x_i$ is the step change value. According to a second-order polynomial equation (5-2) [149], the mass percentage of MEG in the bottom was calculated.

$$Y = \beta_0 + \sum_{j=1}^{k} \beta_j X_j + \sum_{j=1}^{k} \beta_{jj} X_j^2 + \sum_{i=1}^{k-1} \sum_{j=i+1}^{k} \beta_{ij} X_i X_j + \varepsilon \qquad (5\text{-}2)$$

Where $Y$ is the predicted response parameter, $\beta_0$ is the intercept, $i$ and $j$ are the index number, $k$ is the number of variables, and $\beta_j$, $\beta_{jj}$, $\beta_{ij}$ are the calculated constants from the equation of linear, quadratic, and interaction terms, respectively. The actual values of applied variables in BBD matrix with experimental and predicted parameters are shown in Table 1. JMP statistical discovery TM software from SAS (version 13.1.0) was applied to perform BBD experimental design, regression analysis and 3D response surface graphs.

Table 5-1: Actual variables of the Box-Behnken design matrix (BBD) with experimental and predicted response parameters

| Run no. | Actual variables | | | Response variables | |
|---|---|---|---|---|---|
| | $T$ (℃) ($X_1$) | % $XF_{MEG}$ ($X_2$) | $Q$ (Kg/h) ($X_3$) | Experimental vales of % $XB_{MEG}$ | Predicted values of % $XB_{MEG}$ |
| 1 | 125 | 45 | 7 | 74.1 | 74.36 |
| 2 | 125 | 70 | 7 | 83.5 | 83.59 |
| 3 | 145 | 45 | 7 | 87 | 86.91 |
| 4 | 145 | 70 | 7 | 86.2 | 85.94 |
| 5 | 135 | 45 | 5 | 80.9 | 81.40 |
| 6 | 135 | 45 | 9 | 81.5 | 80.83 |
| 7 | 135 | 70 | 5 | 83.2 | 83.88 |
| 8 | 135 | 70 | 9 | 87.1 | 86.60 |
| 9 | 125 | 57.5 | 5 | 80 | 79.24 |
| 10 | 145 | 57.5 | 5 | 87.4 | 86.99 |
| 11 | 125 | 57.5 | 9 | 80.2 | 80.61 |
| 12 | 145 | 57.5 | 9 | 87 | 87.76 |
| 13 | 135 | 57.5 | 7 | 85 | 85.27 |
| 14 | 135 | 57.5 | 7 | 85.2 | 85.27 |
| 15 | 135 | 57.5 | 7 | 85.6 | 85.27 |

## 5.3 Result and discussion

### 5.3.1 Batch experiment

The batch experiments were conducted for the unit at different MEG wt% and different operating boiler temperatures. When 55wt% MEG was introduced to the system as shown in Figure 5-2, the stabilization of the produced MEG occurred after 90 min. This occurred when the boiler temperature was 125 °C and 130 °C which produced 71.4 wt% and 74.4 wt% MEG respectively. However, at 135 °C the MEG product was stabilized after 180 min and the produced MEG was 81.4 wt%. A small percentage of the MEG was produced from the reflux drum as shown in Figure 5-3. When the temperature was 130 ℃ and 135 ℃, after 90 min of operation the wt% of MEG dropped significantly from 55wt% to less than 10wt%. Other MEG wt% have been tested and they all showed similar trends. In Figure 5-4, when the MEG in the feed was 65wt%, the produced MEG in the reboiler required less time to reach 81wt% in comparison with 55 wt%. This is due to less water needing to be evaporated since the MEG has higher boiling point than water so it required less time to reach product stability.
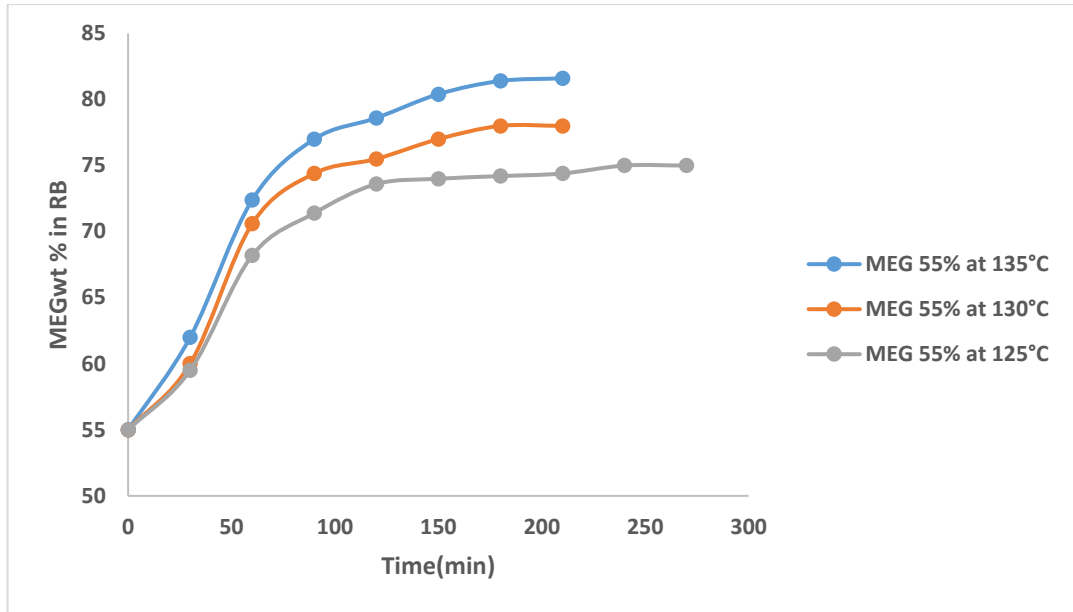
Figure 5-2: Effect of reboiler temperature on MEG wt% in the reboiler at 55 wt% MEG in the feed
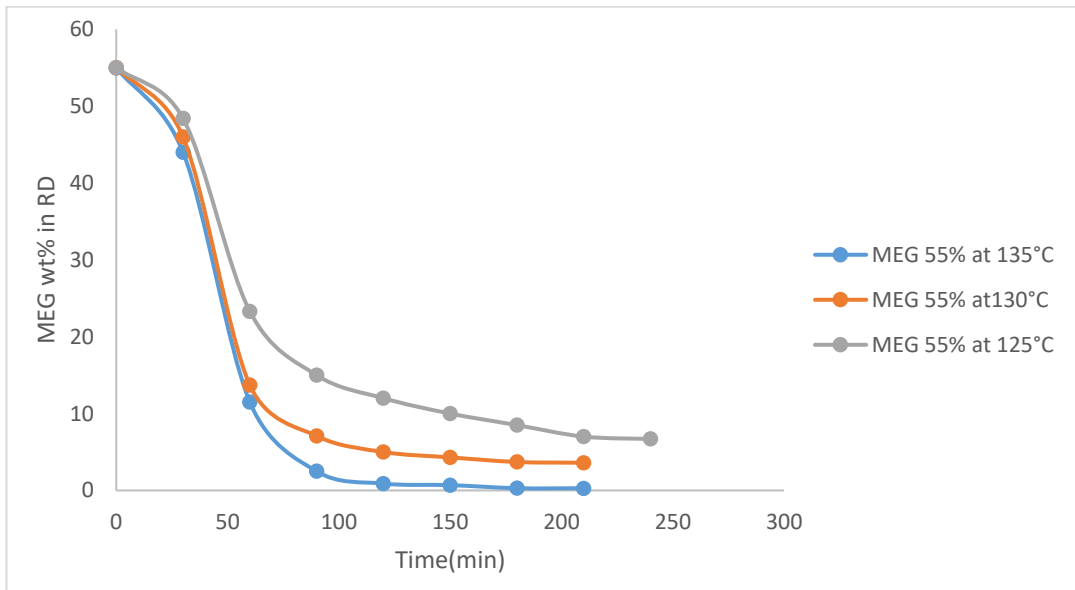


Figure 5-3: Effect of reboiler temperature on MEG wt % in the reflux drum at 55 wt% MEG in the feed
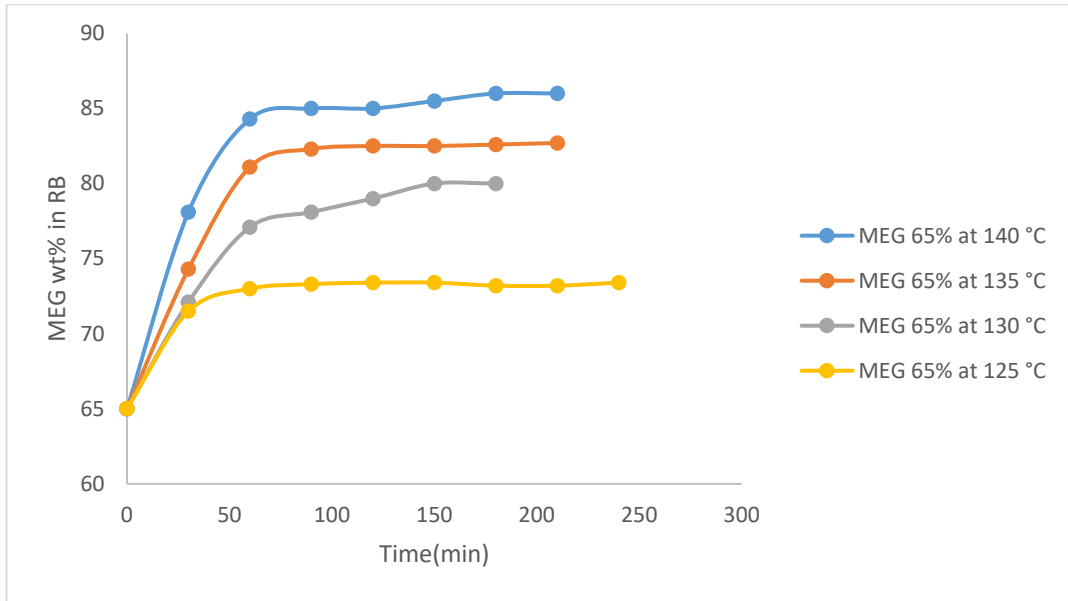
Figure 5-4: Effect of reboiler temperature on MEG % in the reboiler at 65 wt% MEG in the feed

Increasing the MEG wt% above 55 increased the amount of MEG produced from the reflux drum. This is shown in Figure 5-5 to Figure 5-7. At any operating temperature, the 65wt% feed to the batch give more than 25wt% MEG at reflux drum after 210 min while for the 75wt% feed for the batch process produced more than 35wt% MEG at the reflux drum after 200 min as. The temperature has a high effect on the MEG production where it increased with temperature.
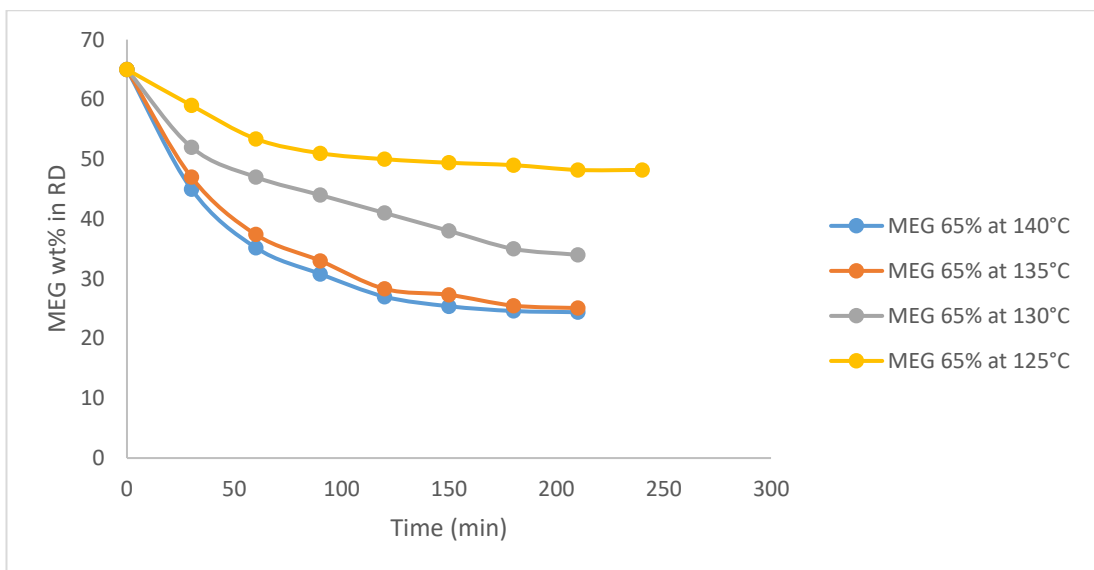


Figure 5-5: Effect of reboiler temperature on MEGwt % in the reflux drum at 65 wt% MEG in the feed
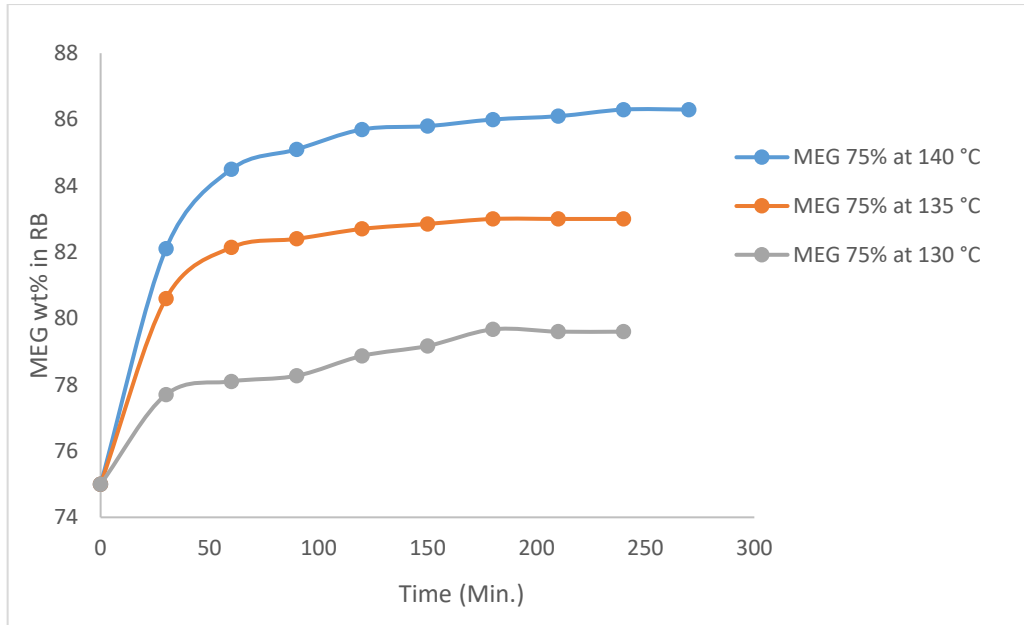
Figure 5-6: Effect of reboiler temperature on MEGwt % in the reboiler at 75 wt% MEG in the feed
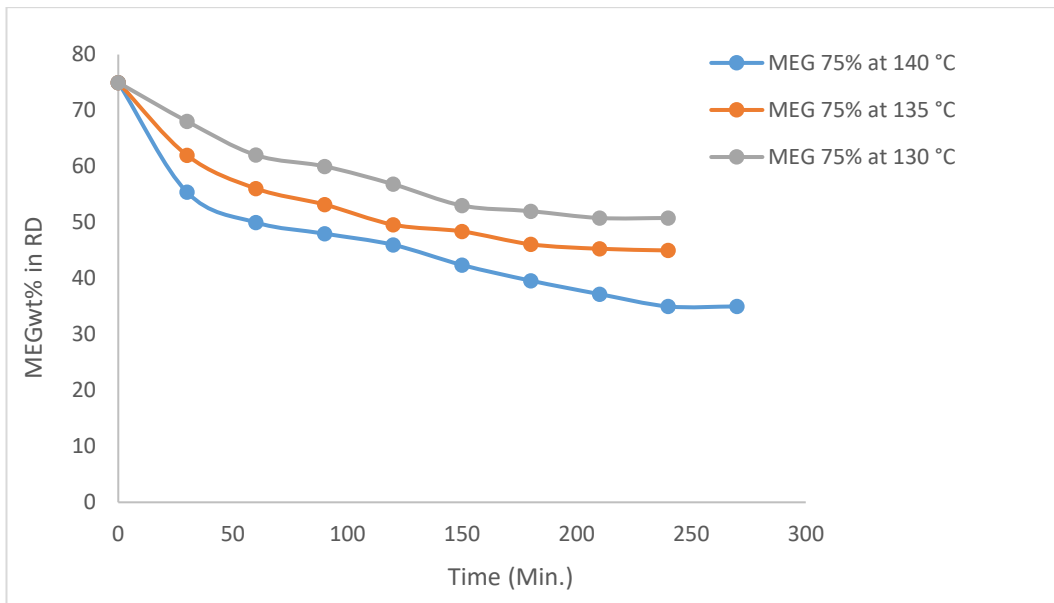


Figure 5-7: Effect of reboiler temperature on MEG wt% in the reflux drum at 75 wt% MEG in the feed

126

### 5.3.2 Continuous experiments

Different variables have been studied in both the HYSYS and the installed unit simultaneously. The comparison between the experimental and the simulated results is important for larger scale production and also to check the conditions that have been made in the study. Table 5-2 to Table 5-4 show the operating conditions.

### 5.3.2.1 Effect of reboiler temperature on MEG product concentration

Both the HYSYS and the experimental results give a similar behaviour for the temperature effect as shown in Figure 5-8. The MEG product concentration increased while increasing the boiler temperature. No degradation in the MEG concentration occurred for all the temperature range which indicates a correct temperature design for the boiler. This is compatible with the temperature range suggested by Diba, Guglielminetti [150]. For a temperature range from 125°C to 135°C the concentration increases from 72.5 wt% to 83.4 wt% at constant rate. At higher temperatures, the concentration was slightly higher. The reboiler temperature were selected at 135 and 145°C as the best temperature to avoid MEG degradation occurring. Table 5-2 shows all the operating conditions and the results in order of changing the reboiler temperature.

Table 5-2: Operation conditions for continuous process at different temperature

| | | HYSYS | | | | | Experimental | | | | |
|---|---|---|---|---|---|---|---|---|---|---|---|
| **Operation Conditions:** MEG wt.% (Feed) = 50%, P = 1.3 bar, Feed = 7 kg/hr | | | | | | | | | | | |
| No. | RB Temp. (°C) | Lean MEG bottom (Kg/hr) | Water Top product (Kg/hr) | Reflux ratio | MEG top Product (ppm) | MEG bottom product (Wt.%) | Lean MEG bottom (Kg/hr) | Water Top product (Kg/hr) | Reflux rate (kg) | MEG top Product (ppm) | MEG bottom product (Wt. %) |
| **1** | **125** | 3.4 | 1.6 | 1 | 0.0 | 72.8 | 3.4 | 1.6 | 1 | 0.0 | 72.5 |
| **2** | **130** | 3.2 | 1.8 | 1 | 0.0 | 78.3 | 3.2 | 1.8 | 1 | 0.0 | 77.6 |
| **3** | **135** | 3.0 | 2.0 | 1 | 0.0 | 82.5 | 3.0 | 2 | 1 | 0.0 | 83.4 |
| **4** | **140** | 2.9 | 2.1 | 1 | 0.0 | 85.6 | 2.9 | 2.1 | 1 | 0.0 | 86.4 |
| **5** | **145** | 2.8 | 2.2 | 1 | 0.0 | 88.1 | 2.8 | 2.2 | 1 | 0.0 | 87.6 |
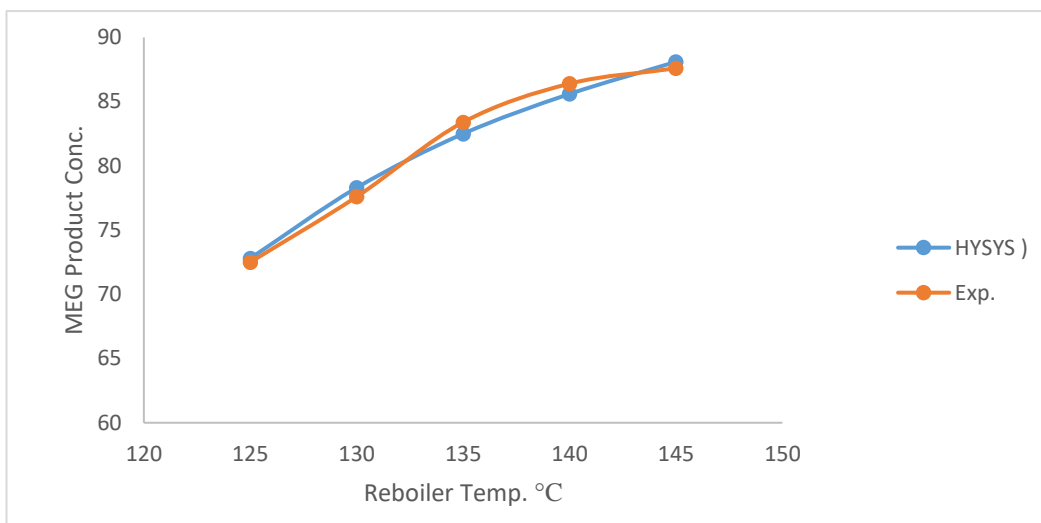
Figure 5-8: The relationship between reboiler temperature and produced MEG wt%

### 5.3.2.2 Effect of MEG feed wt% on MEG product concentration

After studying the boiler temperature in the batch experiments, selecting optimum temperatures is important to then study the MEG wt% to see its effect on the produced MEG. The temperatures selected were 135°C and 140°C and the MEG feed wt% concentration were changed from 45wt% to 70wt% as shown in Figure 5-9. Results were collected from both the simulation and experimental results. Similar behaviour for the experimental and the simulated results is observed for both temperatures, however there is a small difference between them for the low feed wt% from 45wt% to 60wt%. At a feed wt% higher than 60 the difference become smaller.

The MEG product increased when its wt% in the feed was increased at any temperature. Although the increase in temperature was only 5 °C, the MEG product significantly increased at any feed wt%. Table 5-3 and Table 5-4 summarise the operating conditions and the results of changing MEG wt% in the feed at two different reboiler temperatures (135 °C and 140 °C).

Table 5-3: Operation conditions for continuous process at 135 °C and different MEG Conc.

| | | HYSYS | | | | | Experimental | | | | |
|---|---|---|---|---|---|---|---|---|---|---|---|
| No. | Rich MEG Feed inlet (Wt.%) | Lean MEG bottom (Kg/hr) | Water Top product (Kg/hr) | Reflux ratio | MEG top Product (ppm) | MEG bottom product (Wt.%) | Lean MEG bottom (Kg/hr) | Water Top product (Kg/hr) | Reflux rate (kg) | MEG top Product (ppm) | MEG bottom product (Wt.%) |
| 1 | 45/55 | 3.84 | 3.16 | 0.75 | 0.0 | 82.08 | 3.8 | 3.2 | 1 | 0.0 | 81.8 |
| 2 | 50/50 | 4.26 | 2.74 | 0.75 | 0.0 | 82.1 | 4.2 | 2.7 | 1 | 0.0 | 82.0 |
| 3 | 55/45 | 4.7 | 2.3 | 0.75 | 0.0 | 82.13 | 4.6 | 2.3 | 1 | 0.0 | 82.2 |
| 4 | 60/40 | 5.1 | 1.9 | 0.75 | 0.0 | 82.11 | 5 | 2.1 | 1 | 0.0 | 82.4 |
| 5 | 65/35 | 5.3 | 1.7 | 0.75 | 0.0 | 82.09 | 5.5 | 1.5 | 1 | 0.0 | 82.8 |
| 6 | 70/30 | 5.96 | 1.04 | 0.75 | 0.0 | 82.12 | 6 | 1.1 | 1 | 0.0 | 84 |

*Operation Conditions: T=135 °C, P = 1.3 bar, Feed = 7 kg/hr*

Table 5-4: Operation conditions for continuous process at 140 °C and different MEG Conc.

| | | HYSYS | | | | | Experimental | | | | |
|---|---|---|---|---|---|---|---|---|---|---|---|
| No. | Rich MEG Feed inlet (Wt.%) | Lean MEG bottom (Kg/hr) | Water Top product (Kg/hr) | Reflux ratio | MEG top Product (ppm) | MEG bottom product (Wt.%) | Lean MEG bottom (Kg/hr) | Water Top product (Kg/hr) | Reflux rate (kg) | MEG top Product (ppm) | MEG bottom product (Wt.%) |
| 1 | 45/55 | 3.69 | 3.31 | 0.75 | 0.0 | 85.33 | 3.8 | 3.2 | 1 | 0.0 | 85 |
| 2 | 50/50 | 4.1 | 2.9 | 0.75 | 0.0 | 85.33 | 4.2 | 2.7 | 1 | 0.0 | 85.2 |
| 3 | 55/45 | 4.51 | 2.49 | 0.75 | 0.0 | 85.33 | 4.6 | 2.3 | 1 | 0.0 | 85.4 |
| 4 | 60/40 | 4.92 | 2.08 | 0.75 | 0.0 | 85.33 | 5 | 2.1 | 1 | 0.0 | 85.6 |
| 5 | 65/35 | 5.33 | 1.67 | 0.75 | 0.0 | 85.32 | 5.5 | 1.5 | 1 | 0.0 | 85.8 |
| 6 | 70/30 | 5.74 | 1.26 | 0.75 | 0.0 | 85.34 | 6 | 1.1 | 1 | 0.0 | 86 |

*Operation Conditions: T=140°C, P = 1.3 bar, Feed = 7 kg/hr*
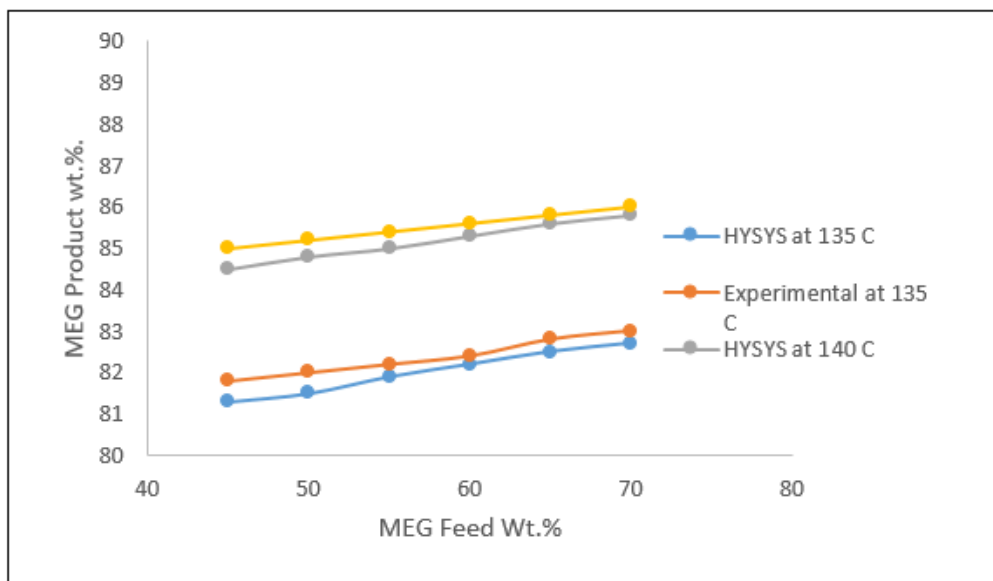


Figure 5-9: The relationship between MEG wt% in Feed and the Produced MEG wt%

5.3.2.3 Effect of feed mass flow rate on MEG product concentration.

The feed mass flow rate was varled and the MEG production measured. As can be seen in Figure 5-10, the product MEG concentration slightly decreased from 83 wt% to 81 wt% when changing the feed mass flow rate from 5 to 9 kg/hr. These results were confirmed by HYSYS when using the same operating conditions (T, P, and RR). Table 5-5 illustrates HYSYS and experimental results for feed mass flowrate changing.
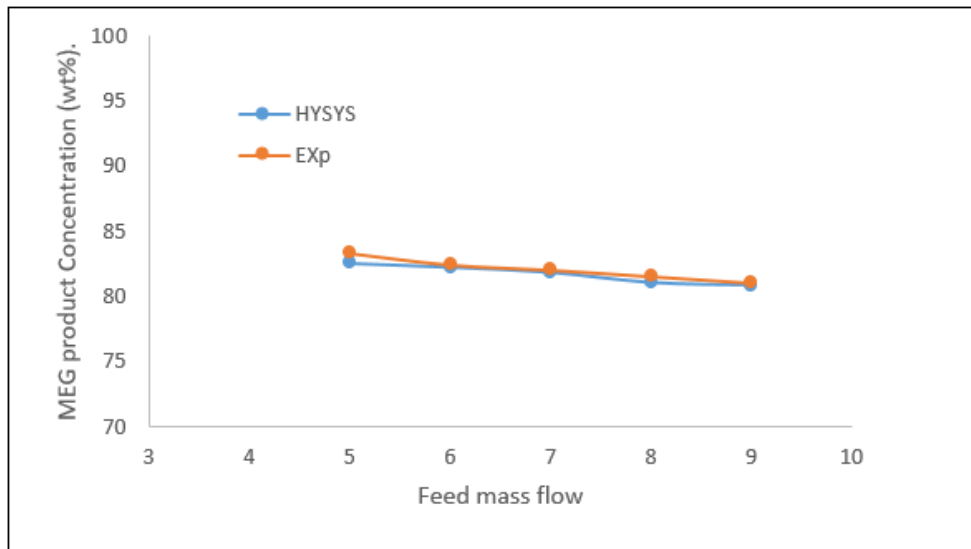


Figure 5-10: Effect of feed mass flowrate on produced MEG

Table 5-5: Operation conditions for continuous process at different feed flowrate

| Operation Conditions: T=135 °C, P = 1.3 bar, MEG wt% = 55 | | | | | | | | | | |
|---|---|---|---|---|---|---|---|---|---|---|
| | | HYSYS | | | | | Experimental | | | |
| No. | Feed (kg/hr) | Lean MEG bottom (Kg/hr) | water Top product (Kg/hr) | Reflux ratio | MEG top Product (ppm) | MEG bottom product (Wt.%) | Lean MEG bottom (Kg/hr) | water Top product (Kg/hr) | Reflux rate (kg) | MEG top Product (ppm) | MEG bottom product (Wt. %) |
| 1 | 5 | 3.0 | 2.0 | 0.75 | 0.0 | 82.5 | 3.0 | 2 | 1 | 0.0 | 85 |
| 2 | 6 | 3.6 | 2.4 | 0.75 | 0.0 | 82.5 | 3.5 | 2.5 | 1 | 0.0 | 85.2 |
| 3 | 7 | 4.2 | 2.8 | 0.75 | 0.0 | 82.5 | 4.0 | 3 | 1 | 0.0 | 85.4 |
| 4 | 8 | 4.85 | 3.15 | 0.75 | 0.0 | 82.5 | 4.8 | 3.2 | 1 | 0.0 | 85.6 |
| 5 | 9 | 5.5 | 3.5 | 0.75 | 0.0 | 82.5 | 5.5 | 3.5 | 1 | 0.0 | 85.8 |

### 5.3.2.4 Reboiler duty

Reboiler duty was calculated at different percentage solutions of MEG with different feed temperatures. The temperature of the feed was varied from 25 ℃ to 50℃ as shown in Figure 5-11. At any feed temperature the reboiler duty increased with the decrease of MEG percentage in the solution. This occurs due to the fact that the specific heat capacity of the solution decreases with the increase of the MEG solution thus decreasing the total heat content. The feed temperature shows a slight change on the reboiler duty. The reboiler duty decreased slightly when the feed temperature was increased from 25 ℃ to 50℃
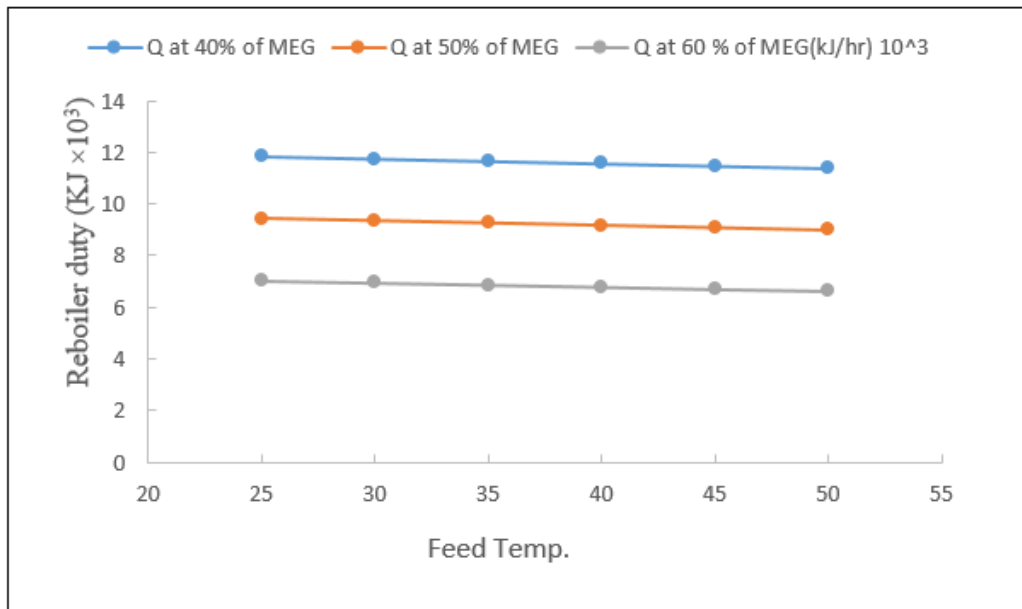


Figure 5-11: Effect of inlet temperature on reboiler duty

### 5.3.3  Modelling of MEG recovery by distillation process

#### 5.3.3.1  Regression analyses

Based on the BBD matrix of actual data Table 5-1, the regression analysis generated a second-order polynomial equation as below;

$$\% \ \mathbf{XB_{MEG}} = 85.26 + 3.725 \ X_1 + 2.06 \ X_2 + 0.5375 \ X_3$$

$$-1.045833 \ X_1^2 \quad -1.520833 \ X_2^2 \quad -0.570833 \ X_3^2$$

$$-2.55 \ X_1 X_2 -0.15 \ X_1 X_3 + 0.825 \ X_2 X_3 \tag{5-3}$$

Where $X_1, X_2$ and $X_3$ are actual values of T (℃), $XF_{MEG}$, and Q (Kg/h), respectively. The determination coefficients ($R^2$) of the **XB$_{MEG}$** regression model was 0.98 show that the predicted values obtained by the above model are in agreement with others obtained by experiments, see Figure 5-12.
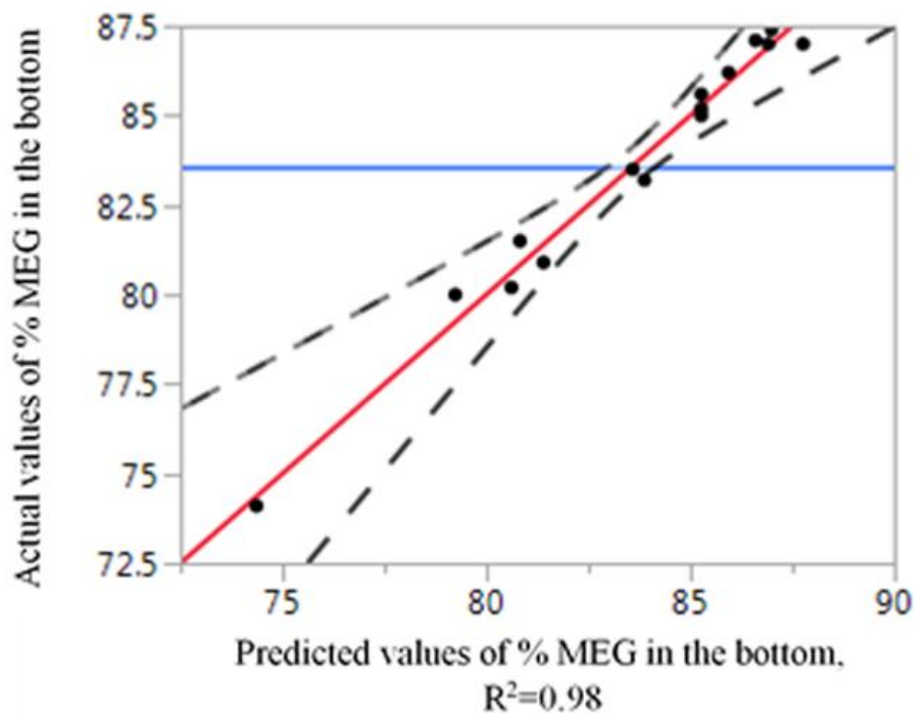


Figure 5-12: Comparison between experimental and predicted values of MEG wt% in the bottom

### 5.3.3.2 Analysis of variance (ANOVA)

Table 5-6 shows analysis of variance (ANOVA) of the second-order polynomial equation as well as the significance of linear, quadratic and interactive terms of model. P-value was applied to check the significance of each term of model and the term with P-value less than 0.05 is a significant term. Based on this value, Table 5-6 indicates that the linear term coefficients of $X_1$(T) , $X_2$ (XF$_{MEG}$), $X_3$(Q) and quadratic term coefficient $X_2^2$ (XF$_{MEG}$. XF$_{MEG}$) significantly influenced the % MEG in the bottom (XB$_{MEG}$). Also, the interactive term coefficient of $X_1$ . $X_2$ (T−XF$_{MEG}$) had significant effects on the XB$_{MEG}$ response. Based on eq. (5-3), the 3D response surfaces plots in Figure 5-13 have been plotted with one independent variable set at coded zero level, while the other two variables were changed within the experimental values. This figure shows the impacts of T (°C), XF$_{MEG}$, and Q (Kg/h) XB$_{MEG}$. In (Figure 5-13a) and (Figure 5-13b), XB$_{MEG}$ increased when temperature extend from 125°C to 145°C. Similarly, XB$_{MEG}$ increased when XF$_{MEG}$ increased from 45 to 70% (Figure 5-13a) and it increased when Q increased from 5 to 9 kg/h. In (Figure 5-13c) shows that XB$_{MEG}$ increased when XF$_{MEG}$ increased from 45 wt% to 60 wt% and then decreased when XF$_{MEG}$ increased from 60 wt% to 70 wt%. Also, XB$_{MEG}$ increased when Q increased from 5 to 7 kg/h and then decrease when Q increased from 7 to 9 kg/h.

Table 5-6: ANOVA analysis by BBD

| Term | Estimate | Standard error | T-value | P-value |
|------|----------|----------------|---------|---------|
| Intercept | 85.26 | 0.465 | 183.06 | <.0001* |
| $X_1$ | 3.72 | 0.285 | 13.06 | <.0001* |
| $X_2$ | 2.06 | 0.285 | 7.23 | 0.0008* |
| $X_3$ | 0.53 | 0.285 | 1.88 | 0.01182* |
| $X_1.X_2$ | -2.55 | 0.403 | -6.32 | 0.0015* |
| $X_1.X_3$ | -0.15 | 0.403 | -0.37 | 0.7252 |
| $X_2.X_3$ | 0.825 | 0.403 | 2.05 | 0.0962 |
| $X_1^2$ | -1.045 | 0.419 | -2.49 | 0.0551 |
| $X_2^2$ | -1.520 | 0.419 | -3.62 | 0.0152* |
| $X_3^2$ | -0.570 | 0.419 | -1.36 | 0.2320 |
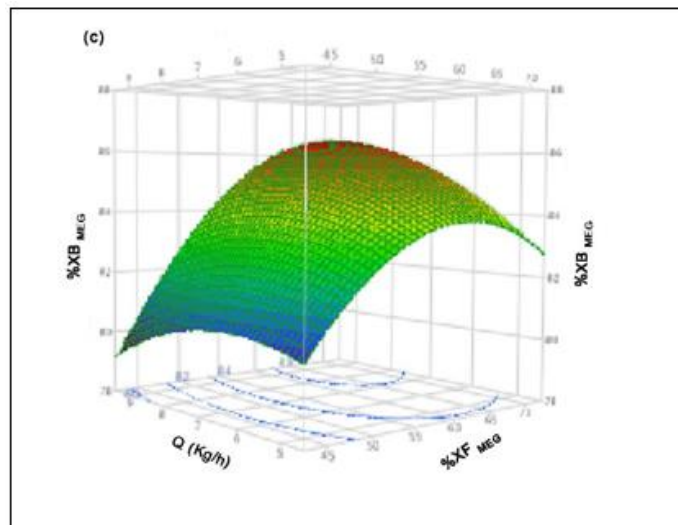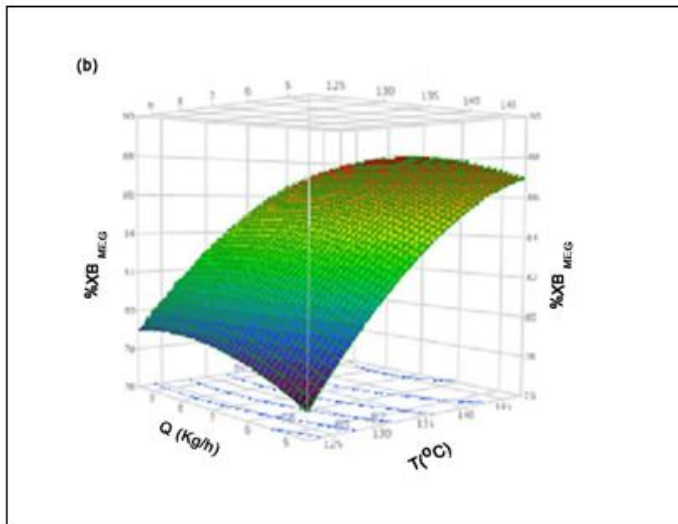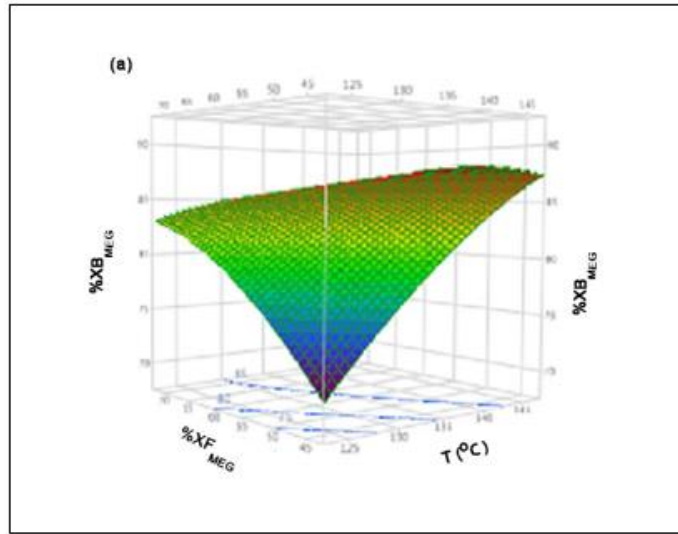
Figure 5-13: Response surface plot of MEG wt% in the bottom

134

### 5.3.3.3 Optimization and validation of the model

The optimum operating conditions for MEG recovery by distillation process were estimated and the ability of regression model to predict optimum value of $XB_{MEG}$ was investigated. The desirability function ranges from zero to one. Zero indicates the response value is unacceptable while one indicates the response value is totally desirable. At 0.99 desirability, the optimum operating conditions were 145℃, 56.45 wt%, and 7.55 kg/h of T, $XF_{MEG}$, and Q, respectively and the predicted value of $XB_{MEG}$ was 88.02 wt%. Under these optimum conditions, experiments were performed in triplicates to validate the optimization accuracy. The obtained $XB_{MEG}$ value from this experiment was in good agreement with the predicted $XB_{MEG}$ value, see Table 5-7. Therefore, it has been concluded that the obtained model by the present study is valid for predicting the $XB_{MEG}$.

Table 5-7: Comparison between experimental and predicted $XB_{MEG}$ at optimum conditions

| Response | Optimum condition | Experimental | Predicted | % error |
|---|---|---|---|---|
| $XB_{MEG}$ | T =145℃ <br> $XF_{MEG}$= 56.45 % <br> Q =7.55 Kg/h | 87.3% | 88.02% | 0.82 |

## 5.4 Conclusions

A MEG separation unit was assembled and successfully operated to separate MEG from water. The operating conditions of the unit were studied and the result compared with HYSYS simulation using PR EOS which gave compatible results for the HYSYS calculation and the experimental data. The response of MEG recovery by distillation to different values of T, $XF_{MEG}$, and Q has been listed. $XB_{MEG}$ is the response parameter for optimization method with RSM and BBD. In the present study, BBD was based on reboiler temperature range of 125℃-145 ℃ along with $XF_{MEG}$ range of 45-70% and Q of 5-9 kg/h. the analysis indicates that all three independent variables (T, $XF_{MEG}$, and Q) were found to have a critical impact on $XB_{MEG}$. The results of present study indicate that the optimum operating conditions were 145℃, 56.45 wt%, and 7.55 kg/h of T, $XF_{MEG}$ and Q, respectively. Under these optimum conditions, $XB_{MEG}$ was 87.3 wt%.

# 6. Case Studies for MEG Distillation System

## 6.1. Introduction

The MEG benchtop facility was used to simulate a number of different scenarios that are likely to occur in the field and this report focusses on the switchover between different corrosion management strategies. Two experiments with respect to switching over between corrosion control strategies have been executed:

1. Gorgon: pH stabilisation using MDEA to film forming corrosion inhibition (FFCI)
2. Gorgon: pH stabilisation using MDEA to film forming corrosion inhibition (FFCI) using an additional HCl dosing point to modify the reboiler feed's pH.

MEG analysis and its dissociated products represent continued challenges for the oil and gas industry field. To better understand these problems, a small MEG plant facility has been constructed simulating the function of a typical MEG regeneration unit at corrosion centre in Curtin University. This research emphasis is providing early ideas for solving some of the issues toward locally operating system in the industrial field.

The MEG plant facility was designed as a MEG regeneration and reclamation closed loop system with a processing capacity of 1-4 kg/hr 90% wt. lean MEG. This facility contains a feed blender (simulating the high shear stresses experienced in pressure reduction valves), a MEG pre-treatment area, a regeneration system, and a reclamation unit.

The MEG plant facility needs to be used for:

1. Simulating the effects of well clean-ups;

2. Simulating the effects of condensate transferral into the MEG pre-treatment vessel;

3. Verifying production chemical additive applicability;

4. Simulating the effects of conversion from one corrosion management strategy to another (e.g. exchanging between film forming corrosion inhibitor and pH stabilisation).

5. Supplying input into methods for an optimum salt condition removal.

This research programme was carried out in partnership with Chevron. As part of this project, research was performed for evaluation of potential start-up and clean-up issues that may arise when operation of the Gorgon wells is started offshore.

### 6.1.1. Corrosion control in field test

A pH stabilisation was used as main corrosion control method in which a base (MDEA) has been added to the lean MEG onshore to increase the pH, reduce the corrosion rate and encourage the formation of a protective $FeCO_3$ scale on the pipeline walls. The pH stabilisation is considered a very effective method to control internal corrosion and reduce the production of corrosion products from the flowline that leads to fouling of downstream equipment. However, the pH stabilisation causes an increase in the scaling risk in the subsea architecture, especially in the choke module and well jumpers. Furthermore, it is not used in case of the breakthrough of formed water or fluid residual due to a scaling risk.

FFCI has been employed as an alternative corrosion control method, when pH stabilisation can't be used because of the scale formation risk (for example, this occurs early in field life when wells are initially opened without cleaning up). Under these conditions, drilling muds might be moved back during the pipeline to shore. FFCIs adsorb into the pipeline wall, forming a protective film to prevent further corrosion. Impacts of FFCI which can be summarised by an increase occurring in risk of emulsion, under deposit corrosion, top of line corrosion and fouling of inlet liquid filters, separators and the rich MEG processing unit.

Switching from pH stabilisation back to FFCI mode may be required, if field-wide formation water production was not managed through alternative means such as production reallocation or scale inhibitor injection. The switchover decision can also

be causing unfavourable conditions resulting from operation in the pH stabilisation mode.

The investigated chemicals in this study were:

- Methyl-Diethanolamine (MDEA) provided the Gorgon pipelines with primary corrosion protection during a pH stabilisation process in which the corrosion rate of gas condensate pipelines can be decreased by increasing the pH artificially. Consequently, this encourages the protective scale formation on the inner pipeline walls of the production flow line.

- Film Forming Corrosion Inhibitor (FFCI) applied to protect against corrosion environments in case of the pH stabilization method.

- Hydrochloric acid (HCl) was added to neutralise MDEA through the switching from pH stabilisation to FFCI corrosion management modes. HCl was injected for pH control in case of NaOH overdose that is used to encourage cation precipitation.

- Sodium hydroxide (NaOH) has been used to precipitate cations during operation in the FFCI mode.

Chemical additives and control loops were installed into the facility to add the chemicals accurately with the correct dosage rates into the system. Therefore, several ProMinnet Micro-dosing/metering pumps (0.05 ml/h to 150 ml/min) were installed. All of these micro-pumps were controlled either by a feedback loop from the respective mass-flow meters (oxygen scavenger, corrosion inhibitor, scale inhibitor, etc.) or by pH control for alkalinity, MEG neutralisation and MDEA addition. Figure 6-1 shows the location of the dosing points.
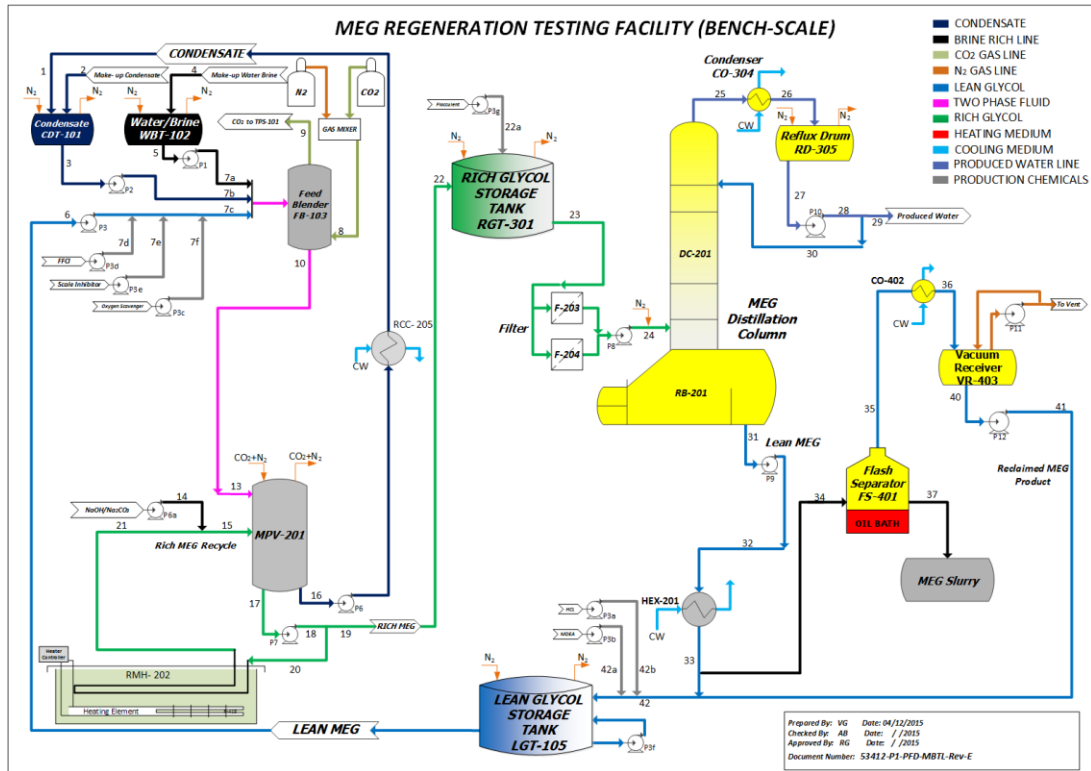
Figure 6-1: PFD of MEG benchtop facility including the dosage points for oxygen scavenger, corrosion inhibitor, scale inhibitor, HCl and MDEA

A measuring residual method from FFCI process in different parts has been developed using a High-Performance Liquid Chromatography (HPLC) system (Thermo Scientific Dionex U3000 HPLC with CAD detector). Furthermore, during operation the concentration of MDEA has been analysed to monitor its consumption and removal rate. Therefore, the Ion Chromatograph at Curtin University has been upgraded to analyse composition of the system including mineral salt ions, organic acids and MDEA. The only disadvantage of this method is it cannot analyse iron concentrations.

### 6.1.2. Objective

Protection of the Gorgon pipelines from internal corrosion can be achieved, using either pH stabilisation method by MDEA or the injection of Film Forming Corrosion Inhibitors (FFCIs) method. The MEG plant facility was employed to simulate switching process between corrosion management strategies for the Gorgon project. The key objectives of the research was to achieve the following:

- Confirm feasibility of switchover procedures, identify potential gaps and improvement opportunities

- Document observations and lessons learned

- Distribution/partitioning of chemicals in the various parts of the system (FFCI and MDEA)

- Removal efficiency of chemicals (FFCI and MDEA)

## 6.2.  Experimental

### 6.2.1.  Matrix Procedure

The experimental matrix was summarised in Table 6-1. Each experiment was repeated twice to obtain reducibility results over several days running. The retention time for the various vessels, concentration of chemicals and pumping capacity for the various pumps has been taken into account during experiment running.

Table 6-1: Experimental matrix for corrosion management strategy switchover

| Test no. | Description | Initial state | | End state | | No. of runs |
|---|---|---|---|---|---|---|
| | | FFCI in lean MEG | MDEA in lean MEG | FFCI in lean MEG | MDEA in lean MEG | |
| 1 | Gorgon MDEA to FFCI | 0 ppm | 580 mM | 3000 ppm | Minimum | 2 |
| 2 | Gorgon MDEA to FFCI | 0 ppm | 100 mM | 3000 ppm | Minimum | 2 |

The switchover was performed according to a series of discrete steps, including MEG chemistry reassessment after each step. Furthermore, in each step, the dosage of each chemical was sequentially changed (increased/decreased) based on the plan. For an example of the theoretical changes in chemical dosage during the switchover see Figure 6-2 and Figure 6-3.

Neutralisation of MDEA was achieved in four stages, to minimise the risk of excessive build-up of neutralised MDEA salts increasing MEG viscosity, and to drop down the

140

risk of HCl overdose that can decrease MEG pH to levels where corrosion rates are significantly high.
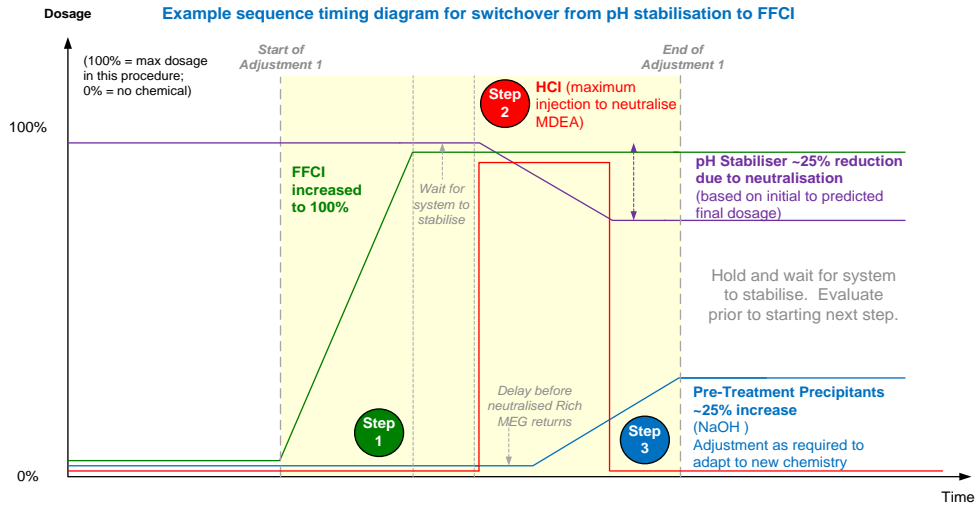


Figure 6-2: Switchover schematic for test
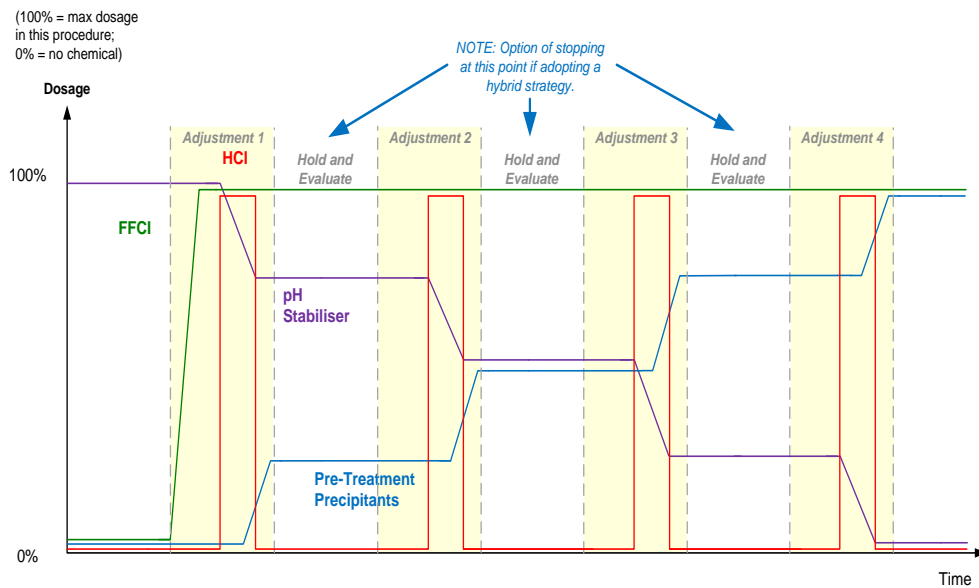


Figure 6-3: Switchover schematic for test
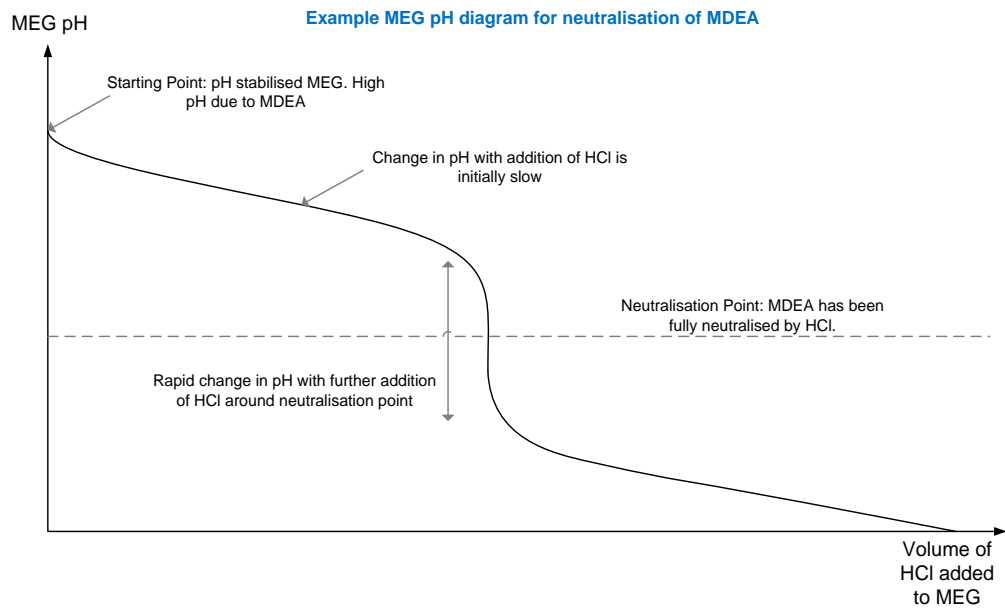
Figure 6-4: Example pH diagram for MDEA neutralisation

The pH was rapidly changed by the neutralisation point of MDEA with HCl as shown in Figure 6-4. To avoid overdose HCl, the injection rate of HCl was performed through pH control to maintain the pH according to the plan of MDEA neutralisation approach.

Test 1 refers to the Gorgon MEG system in operation after formation water breakthrough. After water production formation in pH stabilisation mode, the transition to FFCI mode was performed. The condensed of formation water production and salinities were assumed according to Gorgon MEG Unit Basis of Design (G1-TE-Z-0900-PDB1006). Some of these salts were removed by the reclaimer (operating at maximum capacity to control salt build-up). These assumptions were led to the concentrations summarised in Table 6-2.

Table 6-2: Gorgon fluid compositions at start of experiment for test 2 (MDEA to FFCI) [151].

|  | Brine | Rich MEG | Lean MEG |
|---|---|---|---|
| Na (ppmw) | 266 | 994 | 1601 |
| K (ppmw) | 3.5 | 13 | 21 |
| Ca (ppmw) | 3.4 | 4 | 5 |
| Mg (ppmw) | 0.32 | 1.2 | 1.9 |
| Fe (ppmw) | 0.033 | 0.12 | 0.20 |
| Sr (ppmw) | 0.09 | 0.34 | 0.55 |
| Ba (ppmw) | 0.64 | 2.4 | 3.9 |
| Li (ppmw) | 0.070 | 0.26 | 0.42 |
| Cl (ppmw) | 361 | 1348 | 2172 |
| $HCO_3$ (ppmw) | 118 | 440 | 709 |
| $SO_4$ (ppmw) | 1.1 | 4.0 | 6.4 |
| Acetic acid | 193 | 721 | 1162 |
| Propanoic acid | 17 | 63 | 102 |
| Butanoic acid | 4.1 | 15 | 24 |
| Pentanoic acid | 5.8 | 22 | 35 |
| Phenol (ppmw) | 79 | 293 | 472 |
| Total organic | 299 | 1114 | 1795 |
| MEG (wt%) | 0 | 44 | 80 |

## 6.3. Results and Discussion

.

### 6.3.1. Gorgon Reverse Swithover from pH Stabilisation to FFCI

Reverse switchover from pH stabilisation to FFCI mode may be required if field-wide formation water production is unmanageable through alternative means such as production reallocation or scale inhibitor injection. The decision to switchover may also be driven by unfavourable conditions caused by the operation in pH stabilisation mode. In order to reduce the alkalinity of the injected lean MEG that may lead to scale formation when formation water is being produced. The MDEA present in the lean MEG needs to be neutralised. Leading to the formation of MDEA salts. To avoid the build-up of these highly soluble MDEA salts in the system they must be removed via the reclamation unit. In pure systems, the neutralisation of MDEA will follow a well-defined neutralisation–pH curve as shown in Figure 6-4.

However, in real operation there will be other contributing elements that influence the alkalinity and pH, such as dissolved carbon dioxide, carbonate/bicarbonate ions, and

organic acids. A MEG pH diagram obtained from rich MEG tank is shown in Figure 6-5. The presence of these other species in the rich MEG solution is an advantage, since they provide some buffer capacity and reduce the influence of acid addition near the neutralisation point. This shift in the pH response makes the system less prone to overdosing of HCl, which may result in acidic conditions and potentially corrosion in the MEG facility.
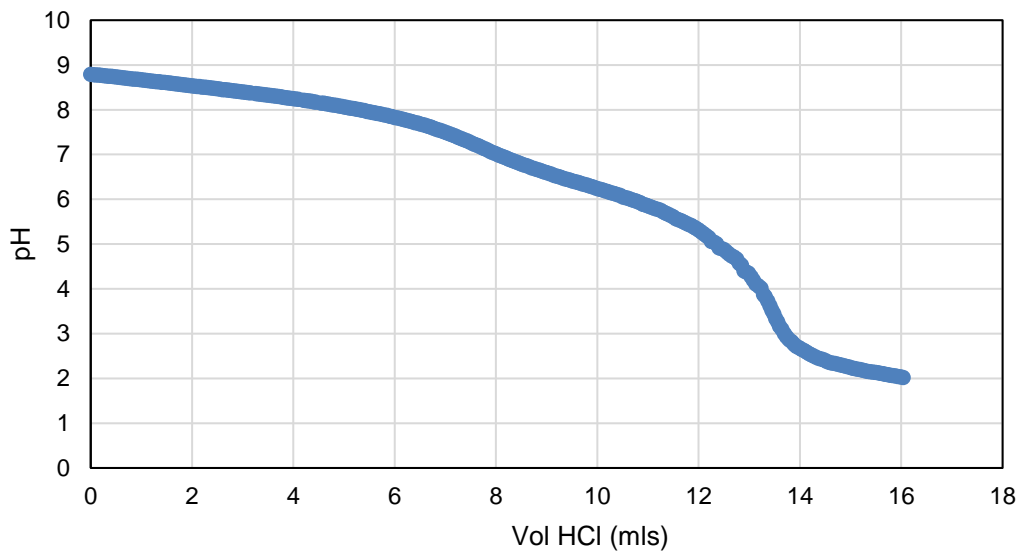


Figure 6-5: Rich MEG pH diagram for neutralisation of MDEA

### 6.3.1.1. Lean glycol Tank (LGT)

MDEA was neutralised by injecting hydrochloric acid into the lean glycol tank in discrete steps for one inventory turnover (one operation day) using pH (uncorrected for MEG) as target: Initial, pH 9.5, pH 9, pH 8.5, pH 8, pH 7.5 and pH 7. Figure 6-6 shows the pH adjustment (corrected for MEG concentration) as function of operation time for the LGT. In the field, it is expected that the pH will be substantially lower. As the MEG facility at Curtin cannot operate under pressure in the feed blending unit, the partial pressure of carbon dioxide was limited to 1 bara. In the real pipeline, which operates at around 100 bara, the partial pressure of $CO_2$ will be much higher at approximately 14 bara.
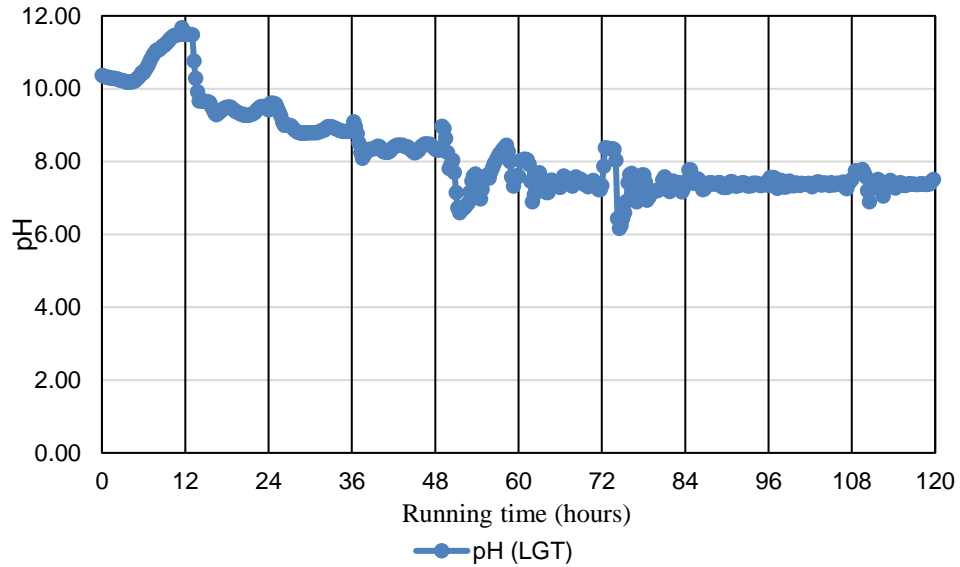
Figure 6-6: pH in the lean glycol tank

### 6.3.1.2. Rich Glycol Tank (RGT)

In the MPV, the pH has been adjusted automatically to a value of 8.3 to 8.5 (corrected for MEG) in order to facilitate the precipitation of calcium and other divalent cations. As expected, magnesium did not precipitate out, see Figure 6-7, since a pH of close to 10 would be required to form magnesium hydroxide. However, significant removal of calcium was achieved resulting in effectively 0 ppm of calcium measured within the RGT.
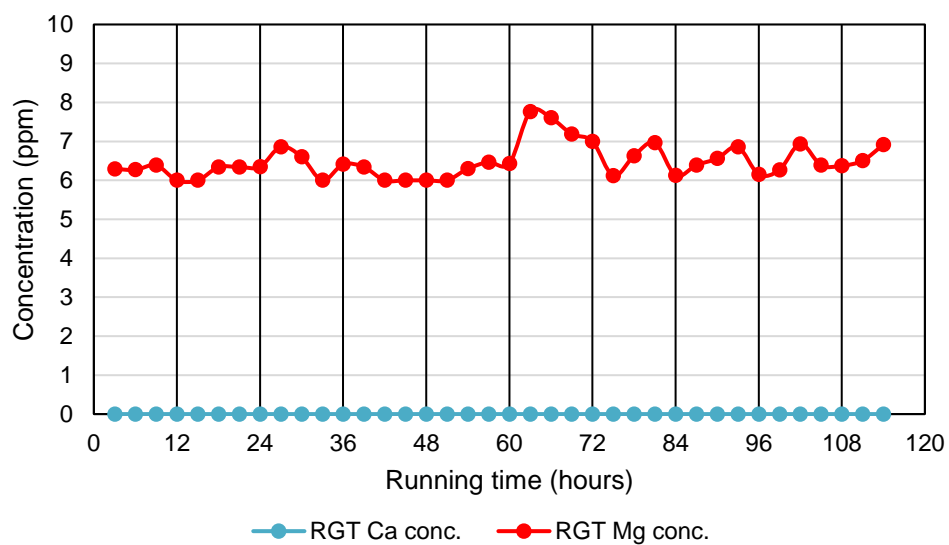


Figure 6-7: Calcium and magnesium concentrations in the rich glycol tank (RGT)

### 6.3.1.3. Regeneration: Reboiler, Produced Lean MEG and Produced Water

It was observed that the pH of the MEG increases considerably when concentrated from rich glycol to lean glycol, see Figure 6-8. The increase in pH is from 8 to ca. 11, as a result of boiling off excess $CO_2$, volatile organic acids, and a concentration effect due to water removal. The pH of the produced water is, consequently, slightly acidic (ca. 4.5 to 6).
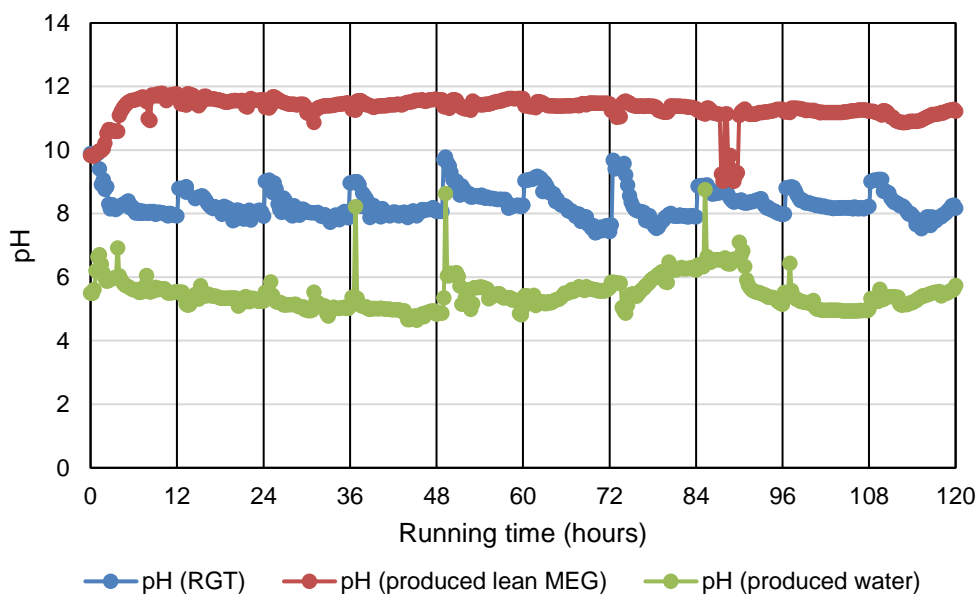


Figure 6-8: pH in feed to distillation column (RGT), produced lean glycol and produced water

No MDEA, FFCI or salts were detected in the produced water, indicating that the reflux ratio of 0.5 was adequate to ensure that no droplet carry-over occurred in the regeneration unit. Another interesting observation was that soon after start up the magnesium concentration inside the reboiler dropped below detection limits, which indicates that magnesium precipitation initiated, see Figure 7-9, which is supported by the high pH in the reboiler (pH >11). The sudden drop in the Mg concentration may be explained by the scale formation mechanism of $Mg(OH)_2$. $Mg(OH)_2$ first precipitates as gelatinous colloid, which does not necessarily form a solid scale on the surfaces (heat exchanger and reboiler vessel). Thus, it would still be detected in the samples analysed, as a colloid would pass through the 2 micron filter used in the

sample preparation process. Once larger crystals are formed these would be filtered out in the sample preparation process.
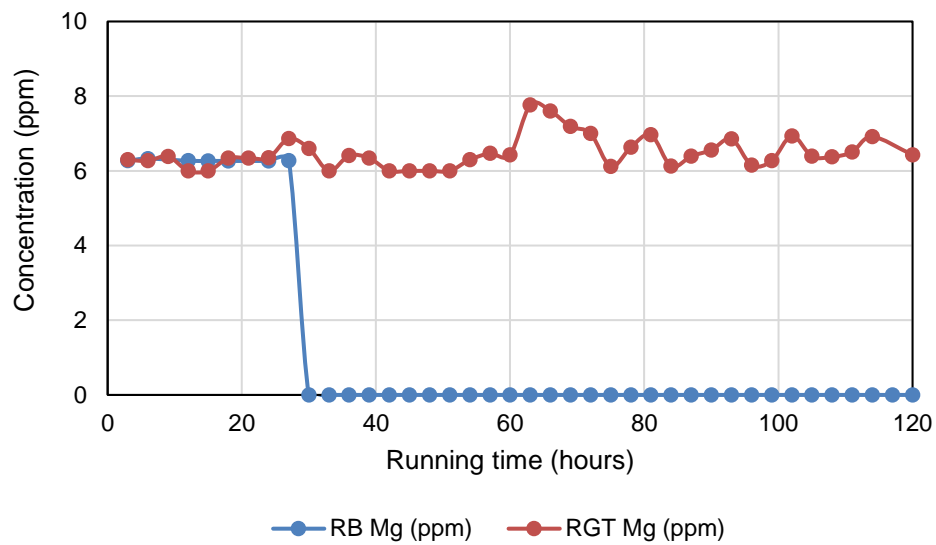


Figure 6-9: Magnesium concentrations in rich MEG feed to reboiler (RGT) and produced lean MEG (RB)

### 6.3.1.4. Scale Formation within Regeneration System

Scale was observed on the reboiler heating bundle (Figure 6-10), glass vessel walls (Figure 6-11) and Scale formation in packed bed column (Figure 6-12). Furthermore, the reboiler sump pump lost efficiency due to scale formation on the inside of the tubing (suction side and pressure side) and inside the pump head.

Figure 6-10: Scale formation on the heater bundle of the reboiler



Figure 6-11: Scale formation on the reboiler glass vessel



Figure 6-12: Scale formation on the packed bed column

148

### 6.3.1.5. Summary of Gorgon Reverse Switchover from MDEA to FFCI

The reverse switchover from MDEA to FFCI corrosion control has a number of challenges in the current plant configuration:

1) The high pH (above pH 8) required in the MPV to remove divalent ions results in a high pH rich glycol feed to the reboiler.

2) Inside the reboiler, the pH of the produced lean MEG increases further due to the boil of excess carbon dioxide. The high pH pushes the equilibrium $MDEA \leftrightarrows MDEA^+ + OH^-$ towards the undissociated organic form that will be reclaimed together with MEG in the reclamation unit.

3) The high pH in the reboiler and reclaimer results in the acetic acid being fully dissociated facilitating its removal within the reclaimer.

4) The high pH in the reclaimer results in poor removal rates for MDEA; based on the benchtop facility results it is estimated that a total of approximately 30 inventory turnovers are needed to reduce MDEA concentration to levels below 5 mM.

Scale formation was observed in the reboiler and on the reboiler heating coil. This was assumed to be magnesium hydroxide scale as magnesium ions present in the feed to the reboiler could not be detected after the regeneration process in the produced lean MEG.

### 6.3.2. Gorgon Switchover from pH Stabilisation to FFCI using a Modified HCl Dosing

Based on the prior experimental results, follow up research on pH stabilisation to FFCI switchover experiments have been conducted with an additional HCl dosing point installed within the RGT system. The aim of this experiment was to verify if reducing the pH of the feed to the reboiler will allow organic acids to boil over into the produced water for removal. The current pH stabilisation to FFCI operational philosophy does not efficiently remove organic acids leading to accumulation within the system. Hence, if not otherwise removed, corrosion issues may arise due to the presence of the accumulating organic acids.

Simultaneously due to a rise in lean MEG pH during the regeneration process, a sufficiently high pH of the regenerated MEG may be achieved to facilitate the removal of MDEA during reclamation whilst also achieving a suitable lean MEG pH without requiring further pH adjustment in the LGT tank. Fast and efficient removal of the MDEA is important during the switch over process as the pH needs to be increased for divalent ion removal in the MPV only to be reduced before re-injection. The longer MDEA is present in the recycled MEG, the longer additional alkalinity and acid will need to be dosed to achieve the desired target pH values, since the excess MDEA will need to protonated (pH increase for RGT) and neutralised in the LGT. Therefore, by installing an additional dosing point, MDEA and organic acids will be removed more effectively during the reverse switchover process compared to the current procedure. The results presented below are focused on the removal or MDEA and acetic acid from the system during the switchover from pH stabilisation to FFCI.

#### 6.3.2.1. Lean Glycol Tank (LGT)

In contrast to the experiment conducted simulating the current plant configuration (refer to Section 6.4.2), the pH of the lean MEG was not adjusted in the LGT. Instead, the pH of the rich MEG feed to the regeneration column was adjusted using HCl to pH 5.7-5.8 within the RGT. The resulting pH changes in the LGT are shown in Figure 6-13 and the resulting total alkalinity is presented in Figure 6-14. The results demonstrate that it is possible to achieve a pH of 7 in the LGT through this method

and to reach the target alkalinity of <10 mM within 5 inventory turnovers. As shown in Figure 6-15, it was also possible to maintain the acetic acid concentration constant throughout the experiment, a significant improvement compared to the current operating philosophy, where the pH of the lean MEG was adjusted in the lean glycol tank and acetic acid accumulation was observed in the system.
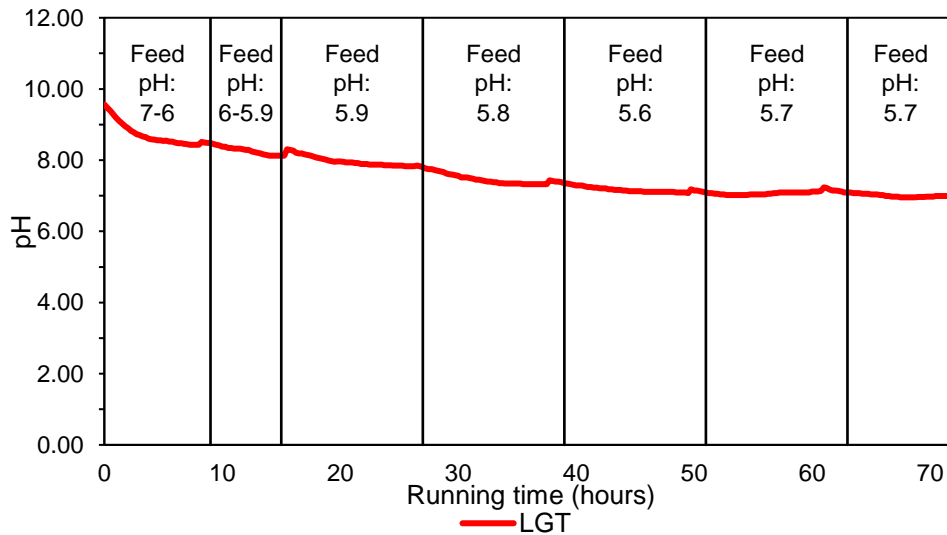


Figure 6-13: The pH in the LGT as result of HClinjection to the rich MEG feed to the Regeneration column
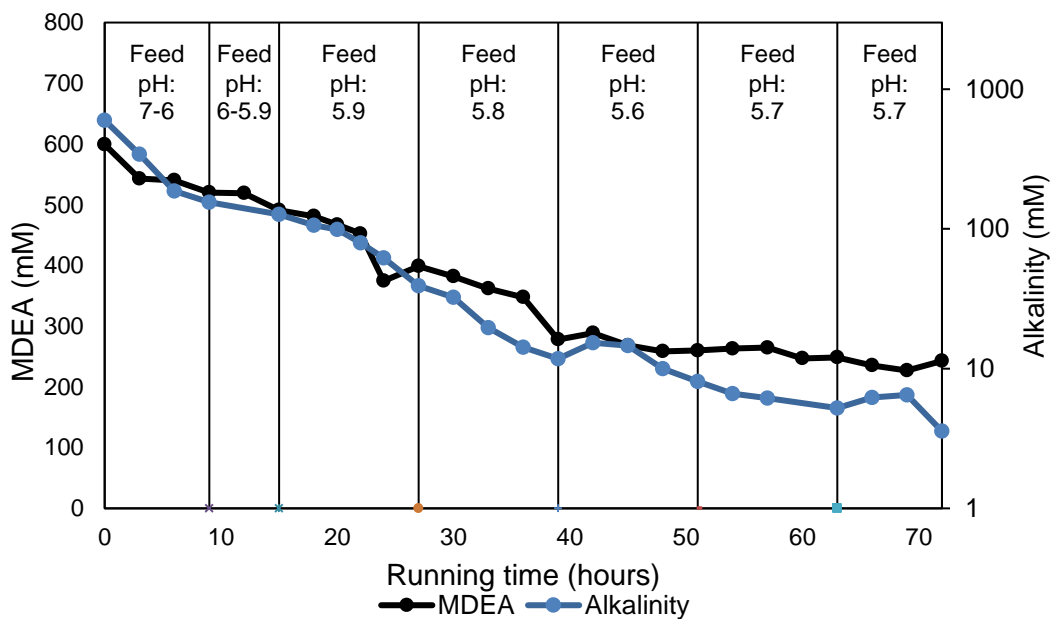


Figure 6-14: Alkalinity and MDEA concentration in the LGT. Each day presents one plant inventory turnover. After 5 inventory turn-overs, the alkalinity in the LGT reached <10 ppm [151].

151
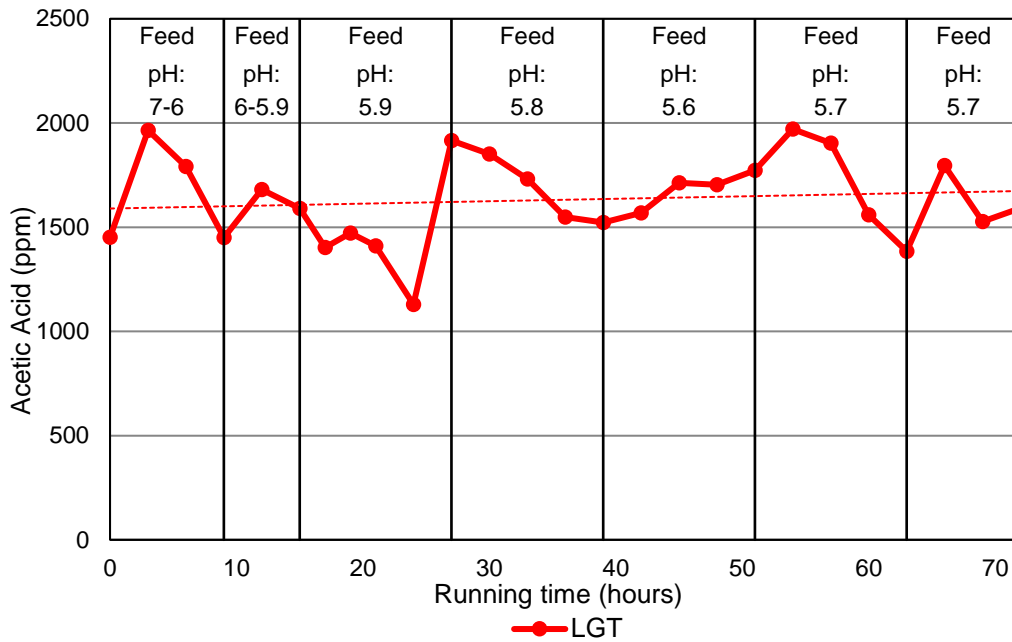
Figure 6-15: Acetic acid concentration stabilised during operation demonstrating that the acetic acid removal in the regeneration column is sufficient to reach steady state [151].

### 6.3.2.2. Rich Glycol Tank (RGT)

Further evidence of the stabilisation of organic acid content (acetic acid) can be observed within the MPV and RGT over the operational period. Figure 6-16 in combination with Figure 6-15 illustrates that the acetic acid concentration within the system has been successfully stabilised via organic acid removal during distillation with the acetic acid removal efficiency further discussed in Section 6.4.4.3. As the simulated brine contains 193 ppm of acetic acid, under normal operation accumulation with the system would occur but has otherwise been prevented by the modified HCl dosing location.

As discussed previously, a pH of 8.0 to 8.3 is required in the MPV to successfully remove calcium from the rich MEG. Although the pH is not only influenced by alkalinity but also dissolved organic acids, as long as the system operates in steady state it is a good measure to ensure that the target alkalinity is reached to precipitate calcium and other divalent ions. From an operational point of view, keeping the pH in the RGT as low as possible reduces the amount of alkalinity that needs to be added to achieve the desired divalent ion concentration, since this alkalinity will need to be

neutralised before re-injection to reduce the risk of scaling (and resulting under-deposit corrosion) in the pipeline.
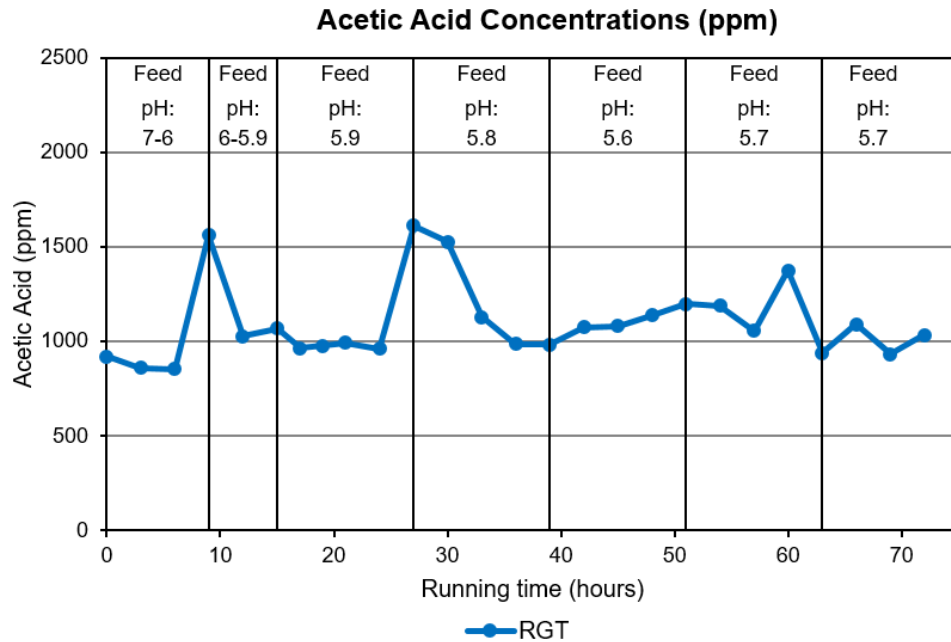


Figure 6-16: Acetic acid concentration (as acetate) measured in the RGT throughout the operation

### 6.3.2.3. Regeneration: Reboiler, Produced Lean MEG and Produced Water

Figure 6-17 shows the acetic acid concentrations in the feed to the reboiler (rich MEG), produced lean MEG and the produced water. For comparison between the acetic acid concentrations of the rich MEG feed and the produced lean MEG, the acetic acid concentration in the produced lean MEG has been converted to the corresponding concentration in rich MEG that has been "diluted". From the graph it can clearly be seen that a proportion of the acetic acid is boiled over into the produced water with acetic acid accumulation occurring with the reflux drum.

Figure 6-18 illustrates the change in pH within the reboiler, reflux drum and rich glycol feed to the reboiler. Over the first two operational days, continuous dosing of HCl into the RGT was maintained to neutralise the initial concentration of MDEA to achieve a pH below 6.0. Following this, HCl dosing was continued to maintain a rich glycol feed pH between 5.7-5.8. Due to the strongly acetic nature of HCl combined with the small volume flows of the bench-top facility, small doses of HCl resulted in large pH changes

explaining the fluctuating pH level. However, in the real plant with higher volumetric flow rates, dosing of HCl will be easier compared to the bench-top facility. Furthermore, the results of this study indicate that it is possible with a rich MEG pH just below 6 (5.7-5.8) to maintain a pH in the reboiler of 7.0, minimising the risk of corrosion of the heater bundle and obtaining a desirable final lean MEG pH around 7.0 (Figure 6-13).
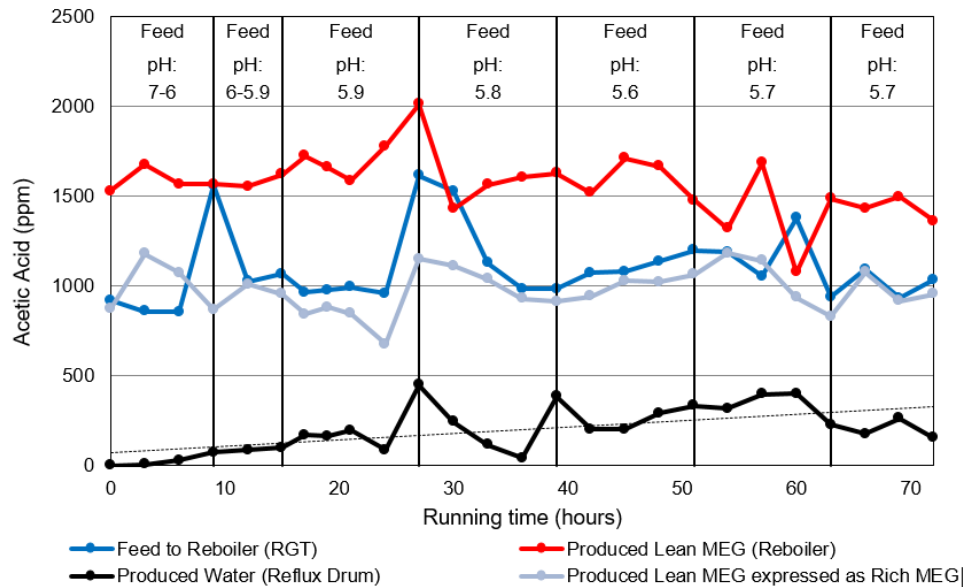


Figure 6-17: Acetic acid concentration in the feed (rich MEG from RGT) to the reboiler, produced lean MEG and produced water.
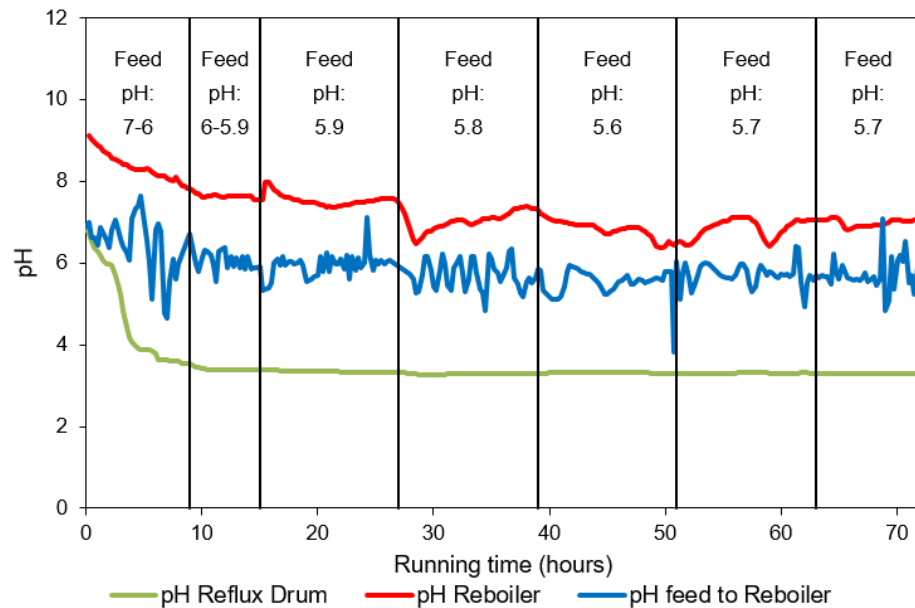


Figure 6-18: pH in the reboiler, reflux drum and feed to reboiler

154

### 6.3.2.4. Sodium Accumulation within Regeneration System

During operation, it was observed that a significant accumulation of sodium ions was occurring within the MEG regeneration loop far greater than that introduced within the brine feed. The accumulation of sodium within the LGT and reboiler is illustrated by Figure 6-19 where a continuous accumulation of sodium within the system is evident. The accumulation of sodium occurs due to the addition of NaOH within the MPV for divalent salt removal. As such, the current reclamation rate is insufficient to provide adequate removal of sodium.
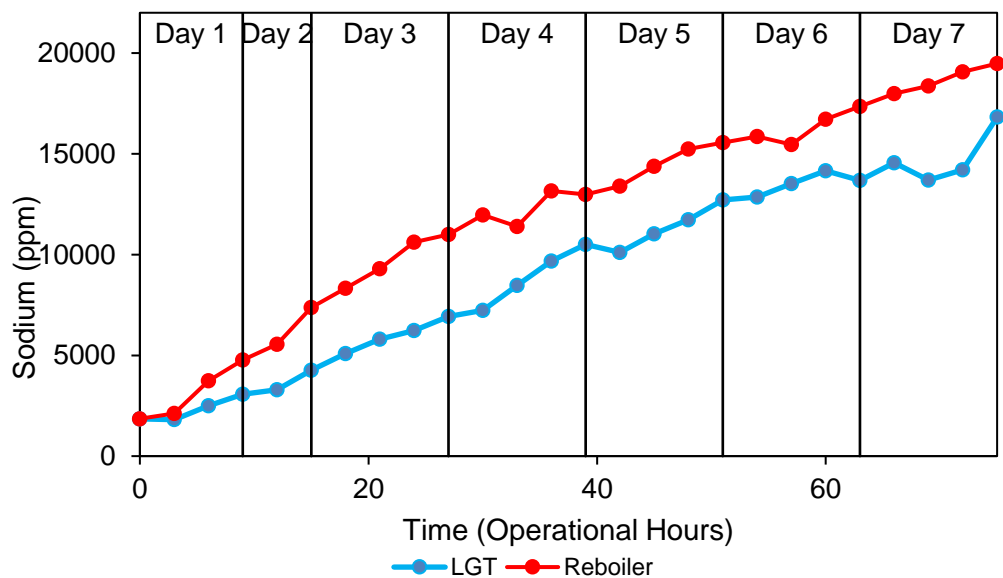


Figure 6-19: Sodium Content within Regeneration System with Time

### 6.3.2.5. Summary of Gorgon reverse Switchover from MDEA to FFCI using Modified HCl Dosing Point

In summary, the experimental results confirm that the reverse switchover from pH stabilisation to FFCI would work much faster and more efficiently if an additional HCl dosng point is installed in the feed to the reboiler and the feed is adjusted to pH 6 or below. A sufficient amount of acetic acid is boiled over into the produced water so that the overall acetic acid concentration remains constant within the system. The efficiency of the MDEA removal from the MEG has also been improved (from ca. 18% to over 85%) due to a lower pH in the feed to the reclaimer.

This is of particular importance for the operational costs during the switchover period. Under normal operation the results from the benchtop facility indicate that it would take for Jansz approximately 25 inventory turnovers and for Gorgon approximately 30 inventory turnovers to remove the MDEA concentration to levels below 10 mM. With the additional dosing point, the same could be expected after 10 inventory turnovers. Furthermore, the required alkalinity (<10 mM) to minimise the risk of scaling in the pipeline has been achieved using the additional dosing point after only 5 inventory turnovers. The comparison in the reduction of total alkalinity in the LGT under Gorgon conditions is provided in Figure 6-20.
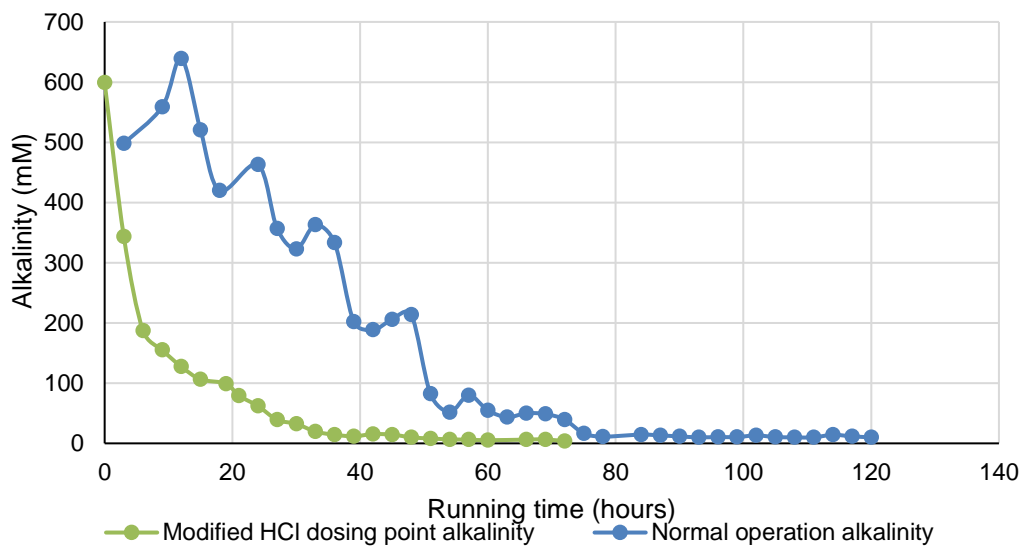


Figure 6-20: Total alkalinity in the lean Glycol tank under Gorgon conditions achieved using normal operation and the additional HCl dosing point.

# 7. Removal of Monoethylene Glycol from Wastewater by Using Zr-metal Organic Frameworks
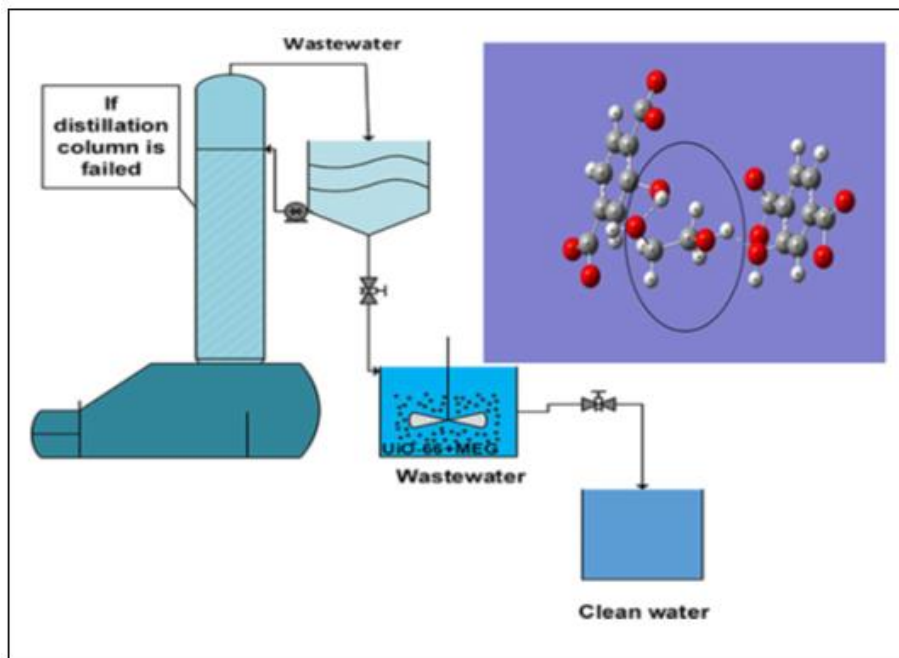
Figure 7-1: Process flow diagram

## 7.1 Introduction

Natural resources have become a hot topic in current scientific research, in an effort to maintain and preserve the Earth's environment for continued human life[152, 153]. In this regard, petroleum pollution is a major global problem [154]. Mono-ethylene glycol (MEG) is a petroleum pollutant, which is a colorless, odorless, and slightly viscous liquid, more hygroscopic than glycerol and miscible with water in all proportions. [155, 156]. The US Environmental Protection Agency has established a standard of less than 7 mg $L^{-1}$ of MEG in drinking water [81, 82]. MEG can cause damage to the kidneys or death at high accumulated concentrations [157]. Natural gas processing produces ethylene glycol-containing wastewater and consequently increases the chemical oxygen demand (COD) in water [80]. Removal of MEG from contaminated water is thus an important consideration in the design of operation units in the petroleum industry [158].

There are three principal treatment processes for removal of MEG from wastewater: filtration [159], biological [160] and adsorption processes [80]. Moreover, nanofiltration and membrane technologies are widely used to separate low molecular organic pollutants (such as MEG) from water [159], but these methods have several challenges such as membrane fouling, chemical resistance and limited lifetime of membranes, insufficient separation, generation of a concentrate and Insufficient rejection for individual compounds [161]. Microorganisms are also used for the removal of MEG, diethylene glycol (DEG), and triethylene glycol (TEG) [162], but biological treatment is incapable of the elimination of the pollutants in a continuous process [163].

Adsorption is a more reliable and economically feasible method in this regard, and has already been used in advanced water treatment [83, 164]. Activated carbon [80, 165, 166] and zeolite [167, 168] are common porous materials used for physical sorption. Recently, metal organic frameworks (MOFs) have been intensively studied for use in water treatment. Many MOFs, such as Zr-MOF (UiO-66) [169], ZIF-67 [170-172], HKUST-1 [173, 174], MIL-101, and MIL-100 [175, 176] have been successfully tested for adsorption of specific contaminants in water. In this unprecedented work, we use modified UiO-66 and UiO-66-2OH with a high pore volume, nano-crystal size and high water stability to effectively capture MEG from wastewater in the case of distillation failure. This batch adsorption process was conducted at different contact time and pH values. Experimental adsorption capacities were obtained for different concentrations in effluent wastewater, and adsorption kinetics and isotherms were studied.

## 7.2 Materials and Methods

All chemicals including N,N-dimethylformamide (DMF, 99%), 1,4-benzenedicarboxylic acid (BDC, 98.9%), ammonium hydroxide (NH4OH, 24%), 2,5-dihydroxyterephthalic acid (DHBDC, 98%), zirconium chloride (ZrCl4, _99.5%), absolute methanol (CH3OH, _99.9%), absolute ethanol (C2H6O, _99.8) and acetic acid (CH3- COOH, _99.7%) were purchased from Sigma Aldrich and used without further purification. Deionized water was supplied from an ultra-high pure water system in the laboratory.

### 7.2.1 Synthesis

UiO-66-2OH was synthesized solvothermally according to a previously reported co-solvent procedure [177]. ZrCl4 (5.150 mmol) and DHBDC (2.63 mmol) were dissolved in DMF (774.93 mmol, 60 mL). After 15 min of mixing, acetic acid (174.68 mmol) and absolute ethanol (171.26 mmol) were added to the mixture. The solution was then transferred in a 125 mL Parr PTFE-lined stainless steel vessel (Parr Instrument Company, USA), which was sealed and heated in a preheating oven at 676 K for 48 h. Greenishyellow crystals were then extracted as a product by vacuum filtration.

For activation of UiO-66-2OH, a solvent exchange method by methanol was used by mixing 100 mg of sample material in 50 mL of absolute methanol for approximately 15 min, and then soaked for 3 d. After that, the product was separated by vacuum filtration and heated at 373 K for 2 h and further heated under vacuum at 453 K for 2 d.

Modified UiO-66 was synthesized solvothermally according to a reported procedure by a single-solvent method [178]. A solution of 405.38 mmol DMF was divided equally into two batches. In the first batch, 2.27 mmol BDC was added and mixed for 15 min and then NH4OH (0.4 mL, 2 M) was added dropwise to this mixture. In the second batch, 2.27 mmol of ZrCl4 was mixed with the solvent for approximately 30 min. After that, both batch solutions were mixed for approximately 20 min. Finally, the resulting solution was placed inside a 45 mL Parr PTFE-lined stainless steel vessel (Parr Instrument Company, USA) and placed in an oven at 393 K for 24 h. After cooling to room temperature, vacuum filtration was used to separate white gel-like materials, which were dried in an oven at 353 K for 24 h. For activation of modified UiO-66, a solvent exchange method by chloroform was used by mixing 100 mg of sample material in 50 mL of chloroform for 30 min, and then soaked for 5 d. Then, the product was filtered by vacuum filtration and dried in the oven at 373 K for 2 h. The final product was heated under vacuum at 473 K for 2d.

### 7.2.2 Characterization

Powder X-ray diffraction (XRD) patterns were obtained by using an XRD diffractometer with CuKa radiation (k = 1.5406 Å) at 2h = 5–70_ to identify the structure of the synthesized material and its structural integrity. Morphological characterization was performed by scanning electron microscopy (SEM; Zeiss Neon 40 EsB FIB/SEM beam). FTIR spectra were obtained using a SpectrumTM 100 FT-IR (PerkinElmer) to investigate the functional groups in UiO-66 over a scan range of 650–4500 cm_1. A Quantachrome instrument (Autosorb-1) was used to determine N2 adsorption/desorption isotherms for pore analysis including pore volume and surface area. A quartz thimble was filled by a 20 mg of sample and then it was preheated in an oven at 393 K for at least 2 h. After that, the sample was degassed at 453 K for 2 d and then transferred to an analysis port for analysis. Thermal stability of MOFs was determined by thermogravimetric analysis (TGA; TGA/ DSC1 STARe system-METTLER TOLEDO). In a typical analysis, 10 mg of sample was loaded into an alumina pan in the TGA furnace and heated under 20 mL_min_1 air flow at a ramping rate of 10 K/ min from room temperature to 1173 K. Zeta potential was determined by a Zetasizer Nano-ZS (Malvern Instruments) at 298 K.

### 7.2.3 Adsorption Studies

Adsorption studies of MEG from wastewater using modified UiO-66 and UiO-66-2OH were conducted using the batch contact adsorption method. Briefly, six samples of MEG were prepared at different concentrations (700, 600, 500, 400, 300, and 150 mg·L$^{-1}$). Then 20 mg of the adsorbents was placed in 40 mL of the MEG solution, which was agitated by a magnetic stirrer for different periods at pH = 7 and 3. A PVDF-0.45 micron syringe filter was used to separate the adsorbents from the aqueous solution and the supernatant solution was measured using an ATAGO refractometer (ATAGO) PAL-Cleaner- 4536.

The adsorbed amount of MEG ($q_t$) and the removal efficiency (R%) were calculated by eqns. (7-1) and (7-2), respectively.

$$q_t = \frac{(C_o - C_t).V}{m} \tag{7-1}$$

$$R\% = \frac{(C_o - C_t).100}{C_o} \tag{7-2}$$

The batch adsorption was also carried out at pH = 3, 5, 8 and 10 for a fixed contact time of 24 h.

Regeneration of the adsorbent was carried out by washing the loaded adsorbents with ultra-high pure water at 373 K for several cycles.

## 7.3  Recycling tests of adsorbents

Modified UiO-66 and UiO-66-2OH were separately suspended in MEG solutions in a ratio of 1:2 using MEG concentration of 600 mg L$^{-1}$ at pH 7 for mixing around 60 min. Then UiO-66 materials were filtered by syringe filter (0.45 µm, PVDF) and supernatant was tested for remaining concentration of MEG to calculate the removal efficiency. The net collected weight was washed by hot water (373 K) three times. Next, the sample was dried in the oven at 393 K for 2 h. The dried adsorbent was used for next cycle of MEG removal. The same procedure was repeated for 5 cycles with carefully adjusting an amount of the solution with a net weight of adsorbents at the same conditions.

## 7.4  Results and Discussion

### 7.4.1   Characterization

Figure 7-2 depicts XRD patterns of UiO-66-2OH and modified UiO-66 after activation, which  were exactly similar to  those of original UiO-66 as shown in previous literature [179]. These MOFs demonstrate robust behavior over a wide pH range (3–10) as shown in Figure 7-3 and Figure 7-4 However, the modified UiO-66 displayed higher water stability than UiO-66-2OH as noted by the absence of some small peaks at high 2θ values on the pattern of UiO-66-2OH after exposure to MEG solution at pH = 10.
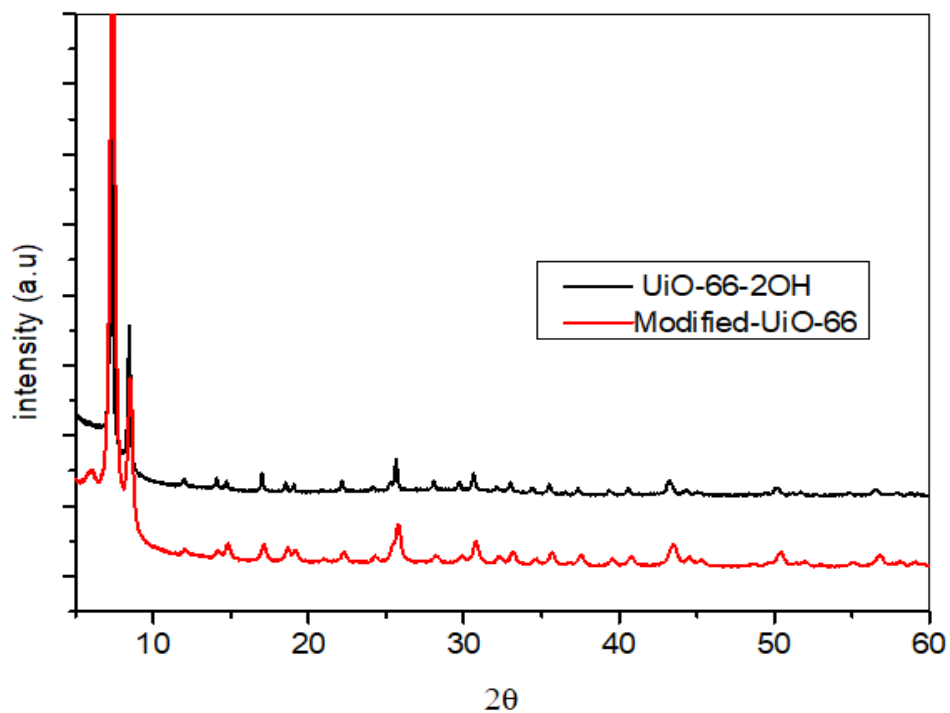
Figure 7-2: XRD patterns of UiO-66-2OH and modified-UiO-66 after activation.
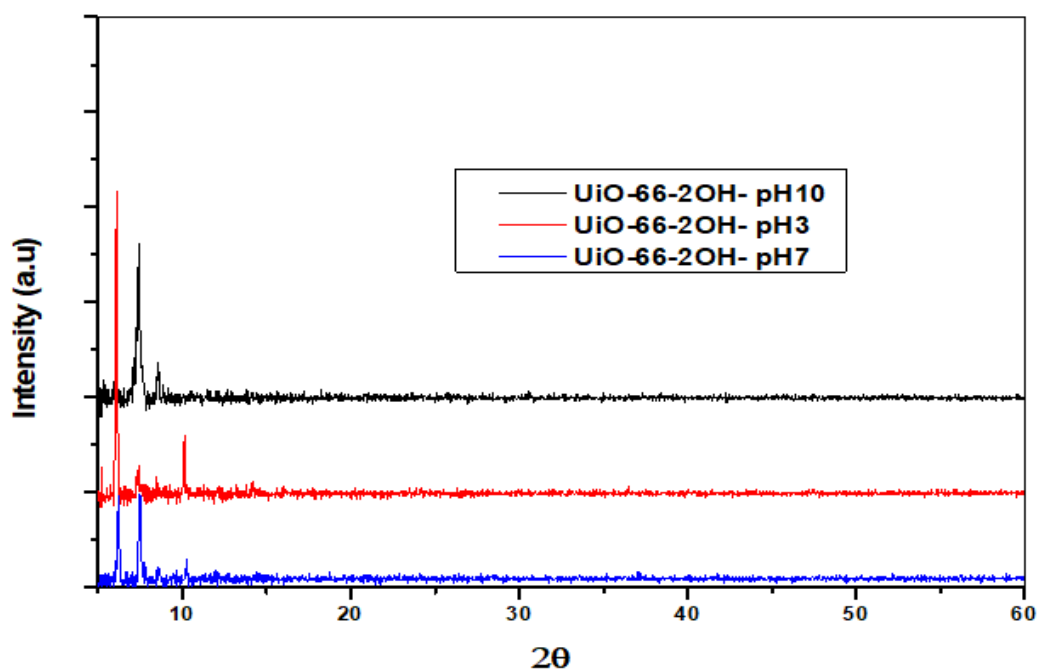


Figure 7-3: FIG.S1 XRD pattern of UiO-66-2OH in different pH values of MEG solution
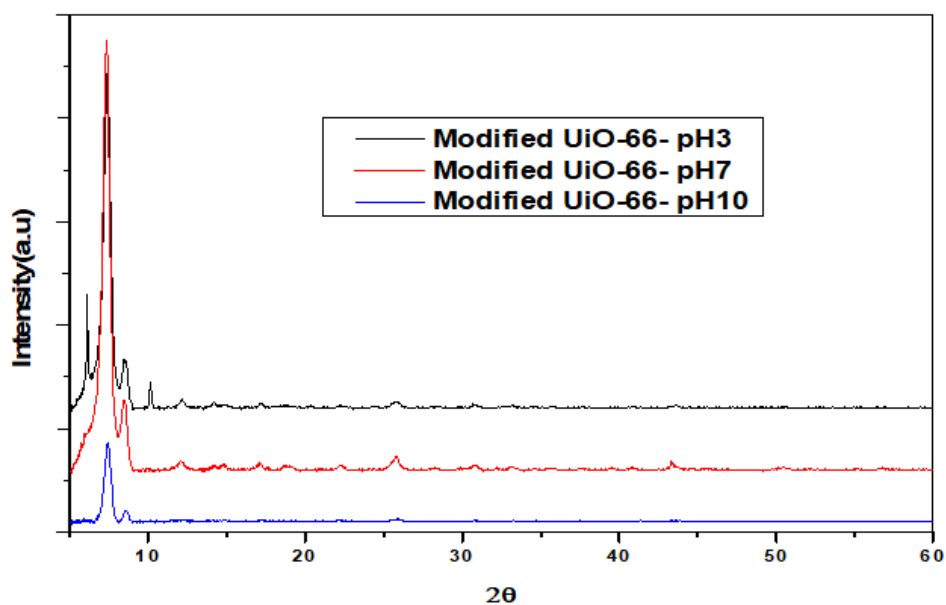
Figure 7-4: XRD pattern of modified UiO-66 in different pH values of MEG solution

The spectra in Figure 7-5 demonstrate the functional groups on modified UiO-66 and UiO-66-2OH. The carboxyl groups (COOH) of BDC and DMF molecules at 1659 cm$^{-1}$ [179] were completely disappeared after activation. In addition, in the spectrum of UiO-66-2OH, two peaks are present for hydroxyl groups at 1460 cm$^{-1}$ and the broad peak at 3000–3680 cm$^{-1}$. Coordinated carboxyl groups of benzene-1, 4,-dicarboxylates with zirconium nodes to form building block units of the structure $(Zr_6O_4)(OH)_4(CO_2)_n$ were present at 1500 and 1380 cm$^{-1}$ [180] in modified UIO-66 and UiO-66-2OH. Figure 7-6 shows the spectra of UiO-66-2OH at pH = 3, 7 and 10 as compared with the spectrum of UiO-66-2OH before adsorption use. The structure of UiO-66-2OH was clearly present based on the decreased peak intensities at 1500 and 1380 cm$^{-1}$. On the other hand, new peaks emerged at 1740–1750 cm$^{-1}$, which are related to carbonyl carbons of UiO-66-2OH conjugated with MEG. Likewise, the peak of hydroxyl groups at 3000–3680 cm$^{-1}$ was more intense, indicating a high amount of loaded MEG in the pores. Figure 7-7 shows spectra of modified UiO-66 used for MEG adsorption at different pH values. All the spectra describe the integrity of the structure, as all peaks in modified UiO-66 prior to MEG adsorption are observed on the spectra of modified UiO-66 after use at pH = 3, 7 and 10. The intensity of hydroxyl groups on the spectrum of used modified UiO-66 was significantly increased due to the high load of MEG

inside the pores. In addition, there is a trace of MEG conjugated with carbonyl carbons of modified UiO-66 after use at pH = 7 and 10, shown by the peak at 1740 cm$^{-1}$.
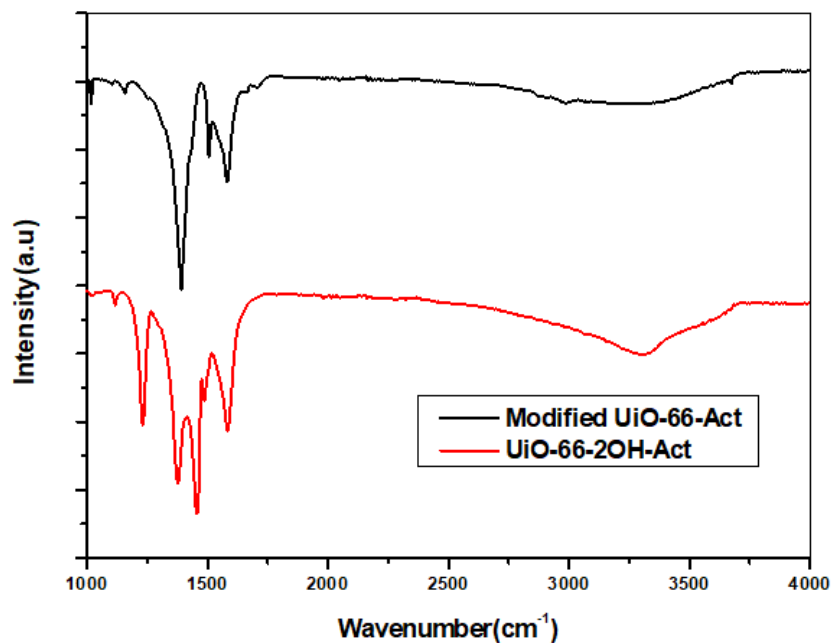


Figure 7-5: FTIR spectra of modified-UiO-66 and UiO-66-2OH after activation.
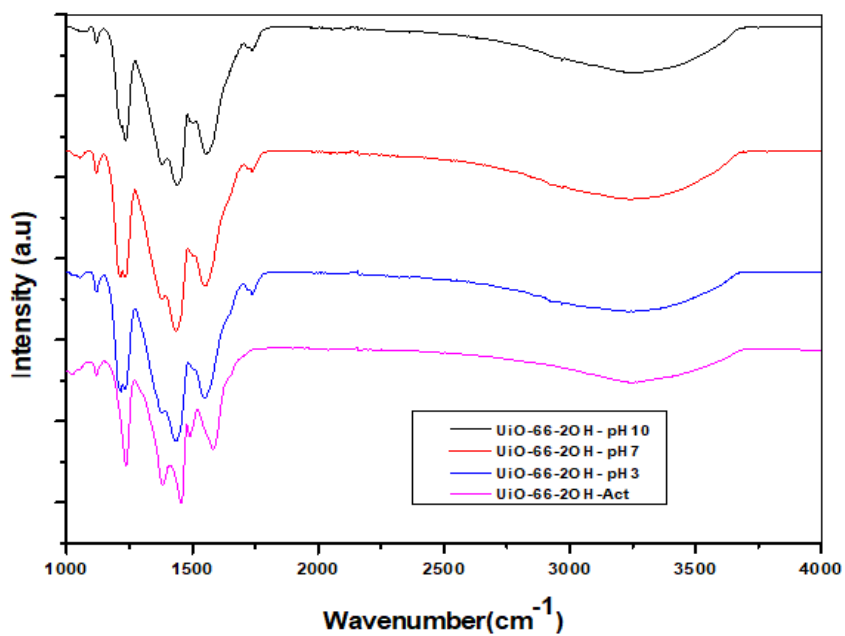


Figure 7-6: FTIR spectra of UiO-66-2OH in different pH values of MEG solution
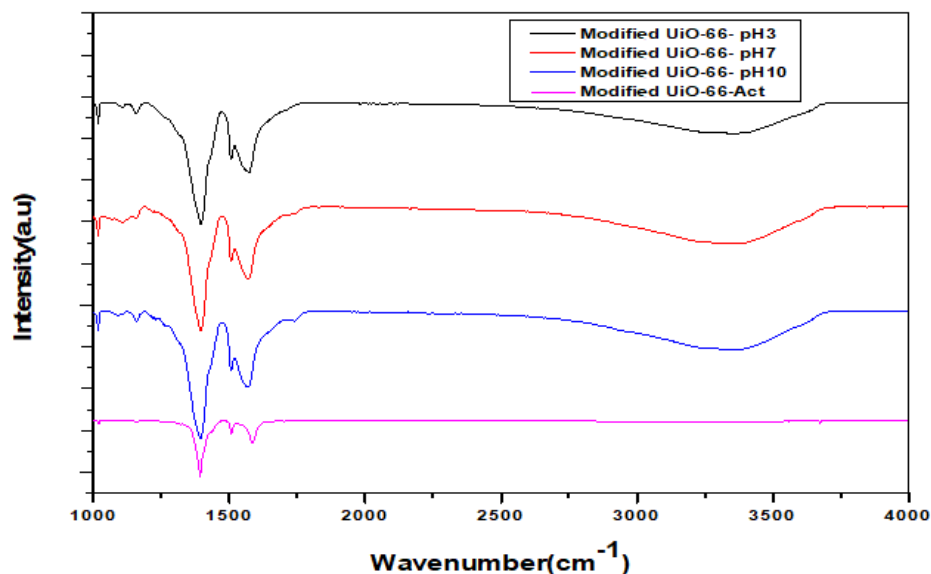
Figure 7-7: FIG.S4 FTIR spectra of Modified UiO-66 in different pH values of MEG solution

$N_2$ adsorption and desorption isotherms of UiO-66-2OH are shown in Figure 7-8 (a), which is of H4 type (IUPAC classification) [181] with a hysteresis loop at a wide range of relative pressure. It was observed, the hysteresis loop is accompanied by capillary condensation in neck bottle pores [182]. UiO-66-2OH is a mostly mesoporous material with several peaks (3.1, 4.8, 7.6, and 12.5 nm) as shown in Figure 7-8 (b). In addition, the micropore distribution was determined with the peak at 2 nm Figure 7-8 (c). The pore volume is approximately 0.63 $cm^3 \cdot g^{-1}$ and the BET surface area is 473 $m^2.g^{-1}$, smaller than those of UiO-66 [183, 184] but slightly higher than those of UiO-66-2OH in a previous study [177]. The external surface area is 289 $m^2.g^{-1}$. Figure 7-9 (a) shows $N_2$ adsorption/desorption isotherms of modified-UiO-66, displaying a narrow hysteresis loop in a wide range of relative pressure. Figure 7-9 (b) shows three mesopore peaks (3.7, 6.7 and 15.4 nm) while Figure 7-9 (c) illustrates the micropore distribution in single peak at 1.4 nm. The BET surface area and pore volume are 1273 $m^2.g^{-1}$ and 1.63 $cm^3.g^{-1}$, respectively, whereas the external surface area is 331 $m^2.g^{-1}$.

The BET surface areas of UiO-66-2OH and modified UiO-66 after adsorption of MEG were reduced, giving 255 and 704 $m^2.g^{-1}$, respectively. The reduction in surface area may attribute to porosity loss [185] as a result of adsorption of MEG and it may also be related to the defect of the structure[186, 187].
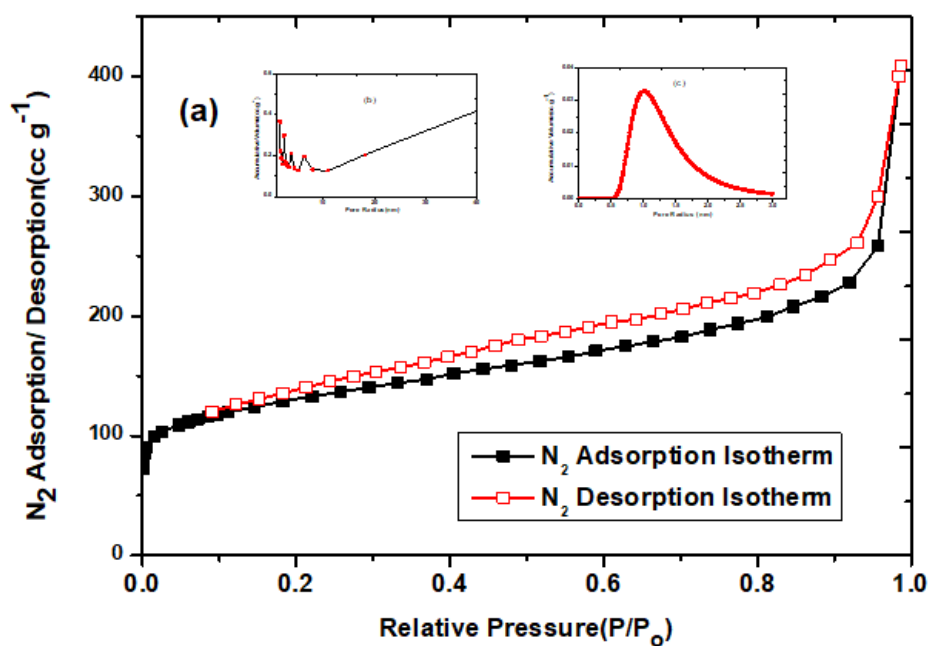
Figure 7-8: a) Adsorption/desorption isotherms of $N_2$ in UiO-66-2OH at 77 K,

b) Mesopore distribution and c) Micropore distribution.
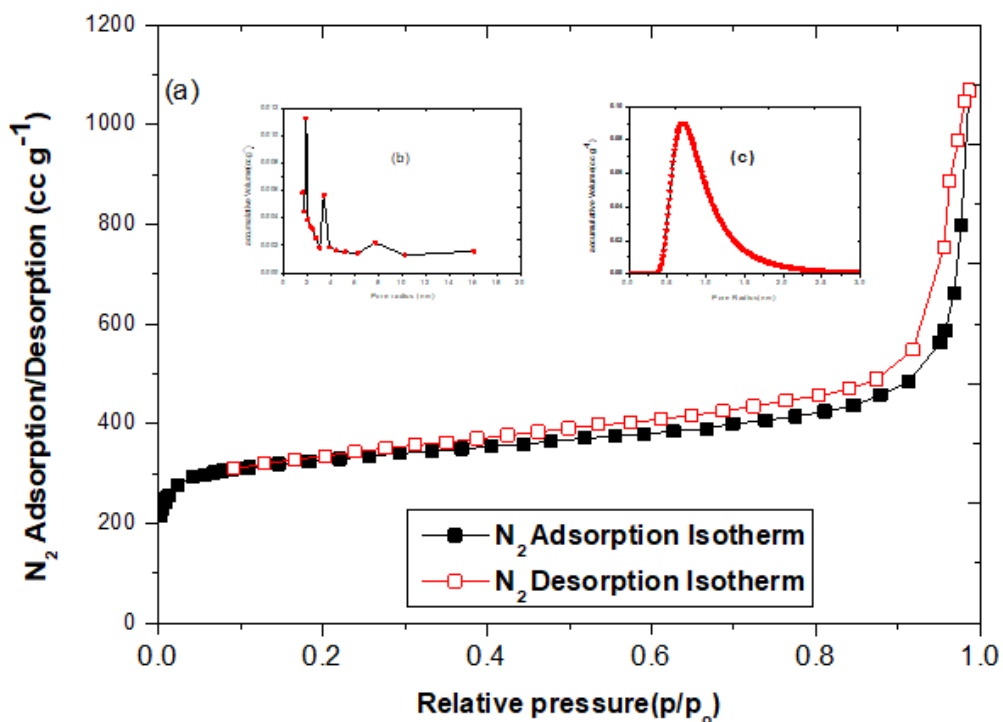


Figure 7-9: a) Adsorption/desorption isotherms of $N_2$ in modified UiO-66 at 77K,

b) Mesopore distribution and c) Micropore distribution after MEG adsorption

Figure 7-10 (a) shows $N_2$ adsorption/desorption isotherm on modified UiO-66 with sharp increasing in relative pressure close to the unity while the hysteresis loop was limited in very narrow range at relative pressure of 0.85, indicating that pore connectivity is high. Figure 7-10 (b) demonstrates a single peak mesopore distribution at 30 nm, which is larger than the mesopore size before the adsorption. The larger mesopore was due to high cavity created during water diffusion. Figure 7-10 (c) displays the micropore diameter of 0.6 nm because of blocking of smaller pores by adsorbate molecules[188].
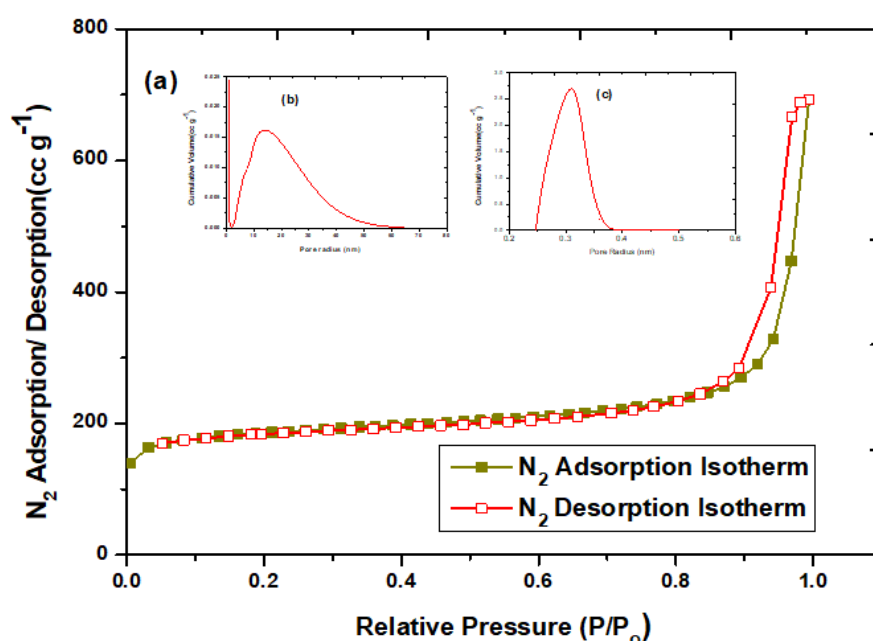


Figure 7-10: Adsorption/desorption isotherms of $N_2$ in modified UiO-66 at 77K, b) Mesopore distribution and c) Micropore distribution after MEG adsorption.

Figure 7-11 (a) shows $N_2$ adsorption/desorption isotherm on UiO-66-2OH. It is similar to that of modified UiO-66, which indicates the majority of meosopore. The mesopore and micropore distributions were represented in single peak at 4 and 0.64 nm as shown in Figure 7-11 (b) and Figure 7-11 (c), respectively. They are smaller than the pore sizes of the adsorbent before the adsorption process, suggesting that the most porous structure was occupied by MEG molecules.
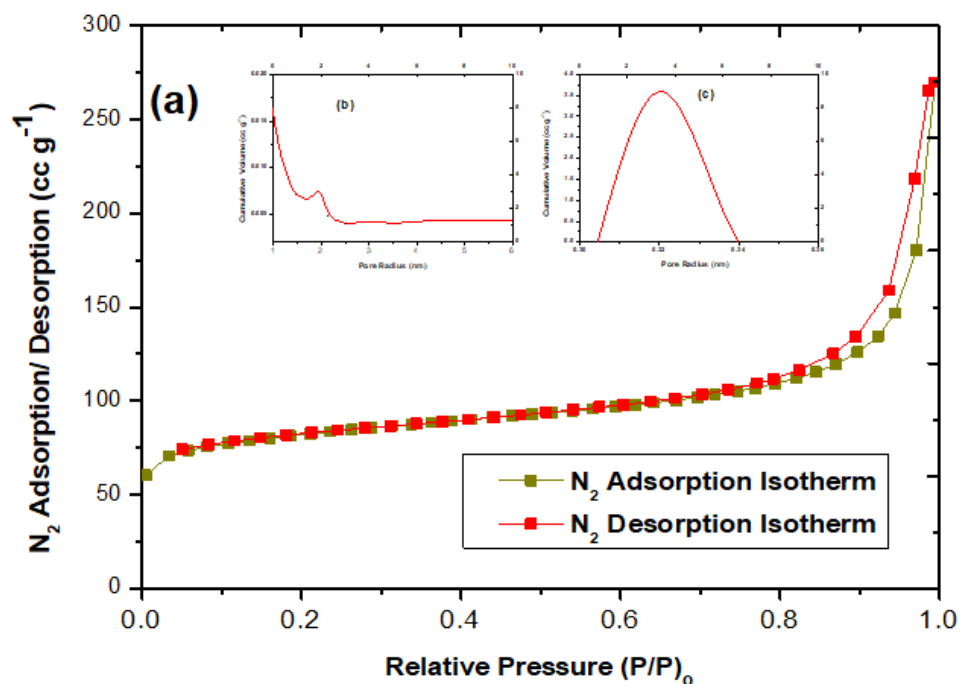
Figure 7-11: Adsorption/desorption isotherms of $N_2$ in UiO-66-2OH at 77K,

b) Mesopore distribution and c) Micropore distribution after MEG adsorption

The SEM images in Figure 7-12 (a) and (b) show the crystal morphology and crystal size of UiO-66-2OH and modified UiO-66, indicating a cubic geometry as the same as the original UiO-66. However, the primary particle size differed significantly. Modified UiO-66 featured nanoscaled crystals < 50 nm in size, while UiO-66-2OH crystals were approximately 100 nm in size. The reduction in crystal size of modified UiO-66 is caused by ammonium hydroxide additives [178], which enhance the solubility of the reactants used during synthesis [189]. Thermal stability of modified UiO-66 and UiO-66-2OH are shown in Figure 7-13, where the thermal stability of modified UiO-66 is higher than that of UiO-66-2OH. The structures of modified UiO-66 and UiO-66-2OH were maintained at temperature up to 740 K and 500 K, respectively. The thermal stability of modified UiO-66 is similar to that of original UiO-66 without modification, as shown in previous literature [190].
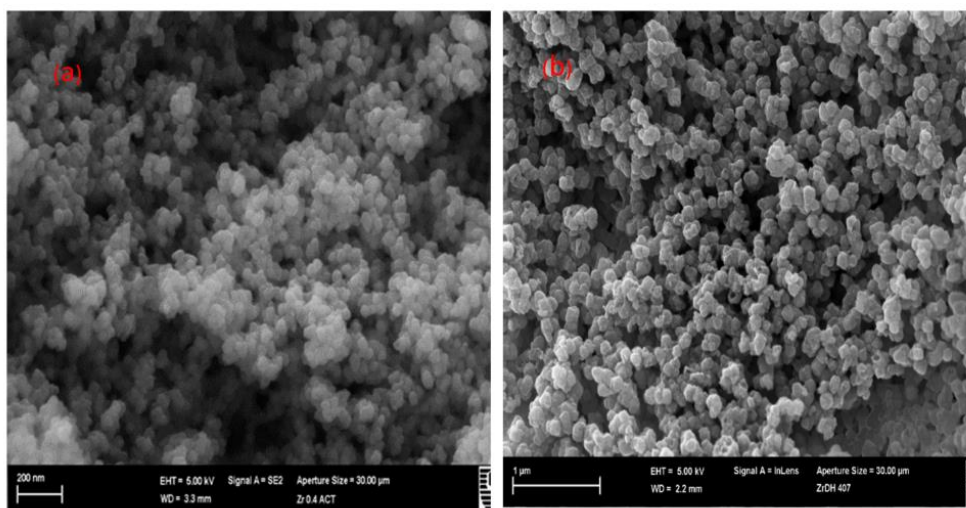
Figure 7-12: SEM images of UiO-66-2OH (a) and Modified UiO-66 (b)
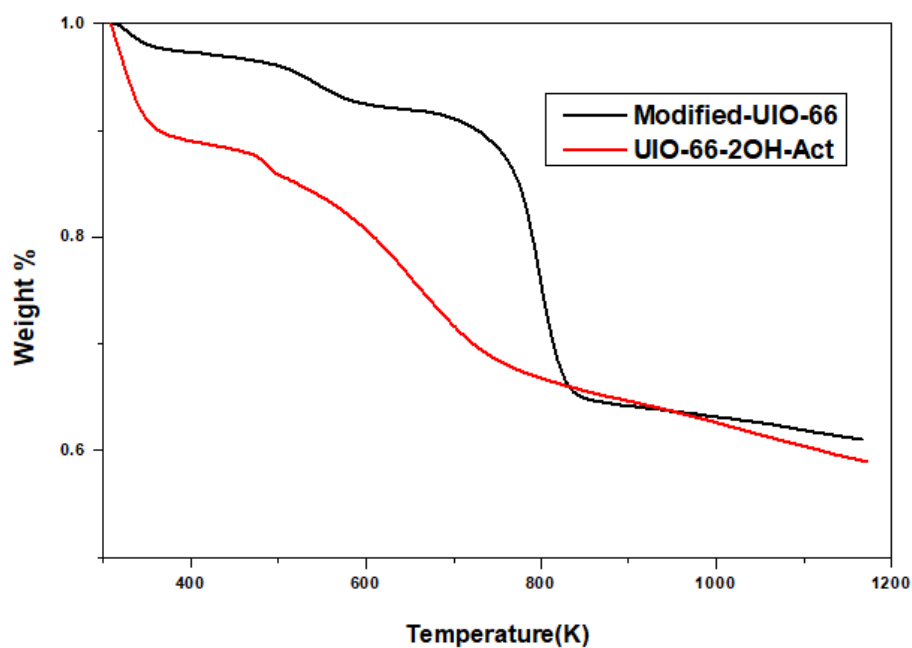


Figure 7-13: TGA profiles of Modified UiO-66 and UiO-66-2OH-Act

### 7.4.2   Adsorption Studies

#### 7.4.2.1  Effect of pH on adsorption

It is important to investigate the effect of acidity on the adsorption of MEG on the surface of modified UiO-66 and UiO-66-2OH. The distribution of acidic or basic molecules in pollutants is strongly dependent on acidity of the aqueous solution, and

consequently their interaction with the surface of an adsorbent through adsorption processes [191]. When the solution is an acidic medium, the attractive force toward the surface of the adsorbent is enhanced. Hence, the adsorption capacity of MEG is increased as the pH decreases from 5 to 3, as shown in Figure 7-14. However, the presence of hydrogen ions in water and their attraction with molecules of MEG can affect the mobility of MEG via its movement toward the surface of adsorbents; this effect is noticed at pH < 5 on modified UiO-66. Neutral solutions (pH = 7) seems to be the best medium for adsorption of MEG. Specifically, UiO-66-2OH can interact via hydrogen bonds between the hydroxyl groups of UiO-66-OH and the hydroxyl groups of MEG. Meanwhile, the interaction between modified UiO-66 and MEG is likely to arise from electrostatic forces. In basic solutions, the adsorption of MEG is decreased, when pH increases from 7 to 8 and 8 to10 in UiO-66-2OH and modified UiO-66 respectively, but in UiO-66-2OH, this influence is minimal at pH > 8.
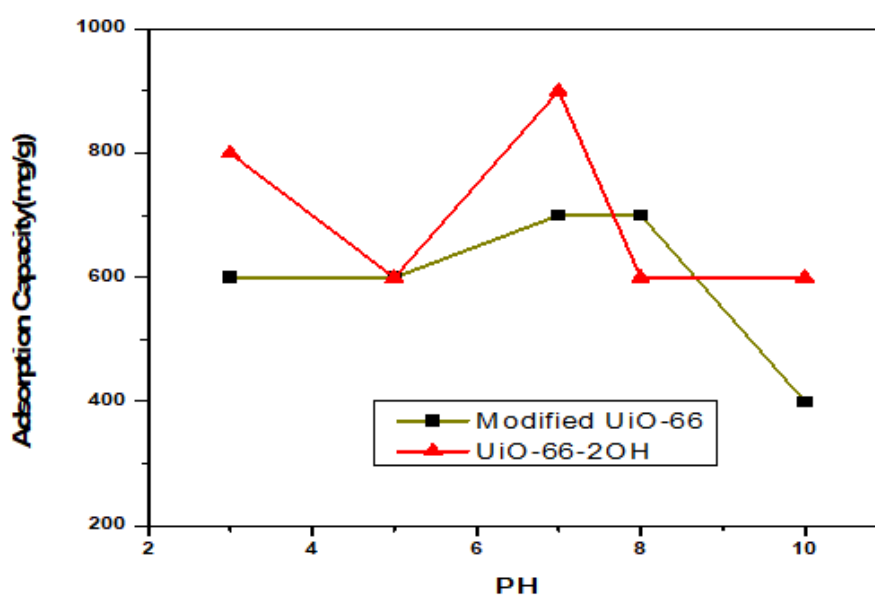


Figure 7-14: Effect of pH on the adsorption capacity of MEG on modified UiO-66 and UiO-66-2OH.

### 7.4.2.2 Kinetic Models

Active water treatment significantly depends on the adsorption kinetics, providing sufficient knowledge on the mechanism of adsorption. In this study, three popular models were investigated and fitted with experimental data. All parameters of the kinetic models are shown in Table 7-1 and Table 7-2.

A pseudo-first order kinetic model (Lagergren) has been suggested for the adsorption of liquid/solid systems, depending on the adsorption capacity of the solid. The general linear form of the pseudo-first order equation [192] is expressed as:

$$\ln(q_e - q_t) = \ln(q_e) - k_f t \qquad (7\text{-}3)$$

Where $q_e$ and $q_t$ are the adsorbed amounts of MEG (mg·g$^{-1}$) on modified UiO-66 or UiO-66-2OH at equilibrium or at time t (min), respectively, and $k_f$ is the rate constant of the first order model (min$^{-1}$).

A pseudo-second order kinetic equation was determined by Ho and Mckay depending on the amount of adsorbate adsorbed on the adsorbent [193]. It can be expressed as:

$$\frac{t}{q_t} = \frac{1}{k_s q_e^2} + \frac{t}{q_e} \qquad (7\text{-}4)$$

Where $k_s$ is the second-order rate constant (g·mg$^{-1}$·min$^{-1}$).

The intra-particle diffusion equation [194] is important for interpreting the adsorption mechanism of MEG on modified UiO-66 and UiO-66-2OH. The linear equation can be described as:

$$q_t = k_d t^{\frac{1}{2}} + C \qquad (7\text{-}5)$$

Table 7-1: Kinetic Parameters for MEG removal by modified UiO-66

| Kinetic Model | | Initial concentration of MEG in aqueous solution | | | |
|---|---|---|---|---|---|
| pH | Parameter | 700 ppm | 600 ppm | 500 ppm | 400 ppm |
| Pseudo-first order kinetic model | | | | | |
| 7 | $K_f$ | 0.018 | 0.017 | 0.014 | 0.0132 |
| | $q_e$ | 818.5 | 737.4 | 623.6 | 523.1 |
| | $R^2$ | 0.969 | 0.962 | 0.993 | 0.913 |
| 3 | $K_f$ | 0.0174 | 0.015 | 0.0137 | 0.0151 |
| | $q_e$ | 647.4 | 617.1 | 515.5 | 419.2 |
| | $R^2$ | 0.979 | 0.942 | 0.931 | 0.985 |
| Pseudo-second order kinetic model | | | | | |
| 7 | $q_e$ | 1000 | 909.1 | 769.2 | 769.2 |
| | $K_s$ | $1.55 \times 10^{-05}$ | $1.40 \times 10^{-05}$ | $1.428 \times 10^{-05}$ | $8.24 \times 10^{-06}$ |
| | $R^2$ | 0.969 | 0.959 | 0.953 | 0.845 |
| 3 | $q_e$ | 833.33 | 833.3 | 769.2 | 555.6 |
| | $K_s$ | $1.79 \times 10^{-05}$ | $1.15 \times 10E^{-05}$ | $8.471 \times 10^{-06}$ | $1.80 \times 10^{-05}$ |
| | $R^2$ | 0.969 | 0.934 | 0.929 | 0.935 |
| Intraparticle diffusion | | | | | |
| 7 | $K_d$ | 88.5 | 79.7 | 61.3 | 62.1 |
| | C | 220.1 | 233.4 | 165.8 | 260.1 |
| | $R^2$ | 0.986 | 0.992 | 0.964 | 0.962 |
| 3 | $K_d$ | 87.3 | 70.9 | 60.1 | 46.9 |
| | C | 285.0 | 246.8 | 230.7 | 157.0 |
| | $R^2$ | 0.978 | 0.986 | 0.963 | 0.994 |

Table 7-2: Kinetic Parameters for MEG removal by UiO-66-2OH

| Kinetic Model | | Initial concentration of MEG in aqueous solution | | | |
|---|---|---|---|---|---|
| pH | Parameter | 700 ppm | 600 ppm | 500 ppm | 400 ppm |
| Pseudo-first order kinetic model | | | | | |
| 7 | $K_f$ | 0.023 | 0.021 | 0.015 | 0.012 |
| | $q_e$ | 980.3 | 879.3 | 796.9 | 704.6 |
| | $R^2$ | 0.992 | 0.990 | 0.989 | 0.938 |
| 3 | $K_f$ | 0.013 | 0.007 | 0.009 | 0.008 |
| | $q_e$ | 896.9 | 824.1 | 716.9 | 617.7 |
| | $R^2$ | 0.926 | 0.981 | 0.980 | 0.991 |
| Pseudo-second order kinetic model | | | | | |
| 7 | $q_e$ | 1111 | 1000 | 1000 | 1111 |
| | $K_s$ | 0.000027 | $3.28 \times 10^{-05}$ | $1.47 \times 10^{-05}$ | $5.59 \times 10^{-06}$ |
| | $R^2$ | 0.984 | 0.985 | 0.981 | 0.880 |
| 3 | $q_e$ | 1250 | 1250 | 1111 | 1000 |
| | $K_s$ | $6.63 \times 10^{-06}$ | $5.18 \times 10^{-06}$ | $4.56 \times 10^{-06}$ | $4.34 \times 10^{-06}$ |
| | $R^2$ | 0.90 | 0.950 | 0.817 | 0.90 |
| Intraparticle diffusion | | | | | |
| 7 | $K_{id}$ | 127.2 | 82.9 | 76.1 | 80.2 |
| | $C$ | 263.3 | 47.9 | 140.7 | 315.6 |
| | $R^2$ | 0.935 | 0.997 | 0.966 | 0.967 |
| 3 | $K_{id}$ | 109.0 | 76.1 | 67.3 | 54.5 |
| | $C$ | 417.2 | 240.7 | 254.1 | 208.6 |
| | $R^2$ | 0.99 | 0.966 | 0.923 | 0.990 |

Table 7-1 and Table 7-2 demonstrate the parameters of the pseudo-first order, pseudo-second order and intra-particle diffusion equations for adsorption of MEG on modified UiO-66 and UiO-66-2OH. The pseudo-first order kinetic model is used to describe the mechanism of adsorption in the case of physisorption and diffusion. More specifically, Table 7-1 and Table 7-2 show that the rate constant $k_f$ is relatively dependent on the initial concentration of MEG. The rate constant of MEG adsorption on modified UiO-66 and UiO-66-2OH was uniformly increased with increasing initial concentration of MEG at neutral acidity (pH = 7) [195]. Interestingly, the rate of diffusion via UiO-66-2OH is faster than that in modified UiO-66. Calculated adsorption capacity values obtained using the pseudo-first order kinetic model are approximately similar to experimental values.

For the adsorption of MEG on modified UiO-66 and UiO-66-2OH, the correlation coefficients ($R^2$) at pH = 7 were 0.969 and 0.992, respectively, at an initial concentration of 700 ppm, while they were 0.913 and 0.938 at an initial concentration of 400 ppm. The fitting of experimental data at pH = 7 with the pseudo-first order

kinetic model is given in Figure 7-15 (a, b). In addition, $R^2$ values at pH = 3 were 0.985 and 0.991, respectively at 400 ppm, and 0.979 and 0.926 at 700 ppm; $R^2$ was increased by decreasing the initial concentration due to the impact of acidity at pH = 3. This can be observed in Figure 7-15 (c, d), where the pseudo-first order kinetic model is in good agreement with the experimental data.
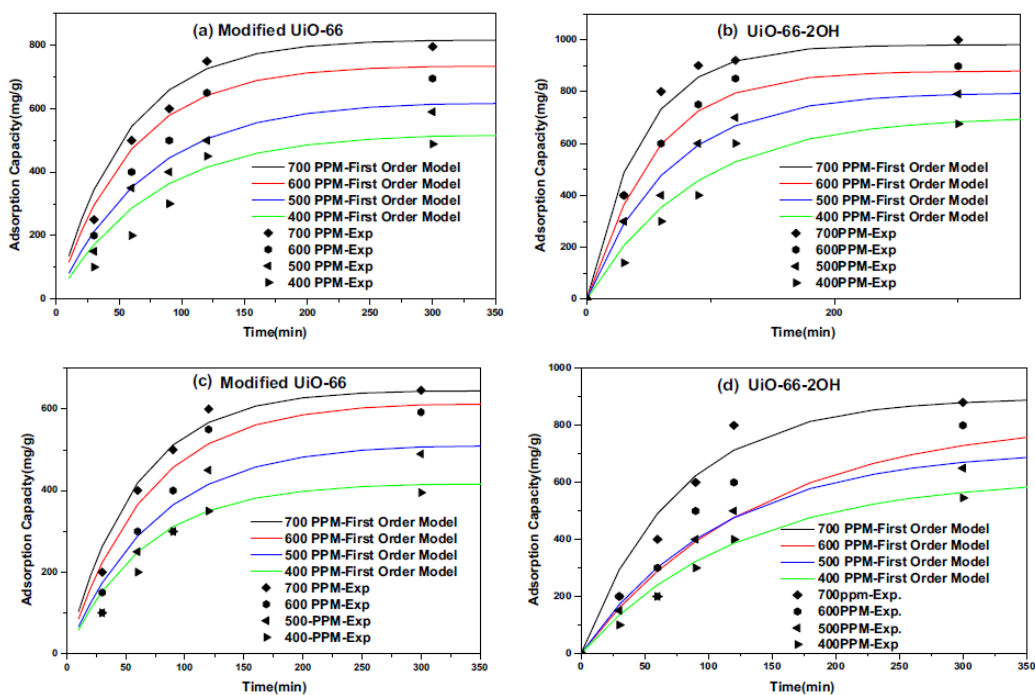


Figure 7-15: Comparison between the measured and pseudo-first order modelled time profiles for adsorption of MEG on modified UiO-66 and UiO-66-2OH at pH = 7 (a,b) and pH = 3 (c, d).

On the other hand, the pseudo-second order rate model was used to refer to chemisorption including valency forces through the sharing or exchange of electrons between adsorbates and adsorbent as covalent forces, and ion exchange [196]. As shown in Table 7-1 and Table 7-2, the calculated values of adsorption capacity are fitted from experimental data. In addition, $K_s$ values are mostly dependent on the initial concentrations of MEG in modified UiO-66 and UiO-66-2OH in acidic and basic conditions. Likewise, the $R^2$ values in the pseudo-second order model are lower than $R^2$ observed in the pseudo-first order model, while they are slightly higher in modified UiO-66 than in UiO-66-2OH at pH = 3, where the average value of $R^2$ is 0.942 in modified UiO-66 and 0.891 in UiO-66-2OH. In contrast, $R^2$ values at pH = 7 are 0.931

and 0.957 for modified UiO-66 and UiO-66-2OH, respectively. The fitting of experimental data to a pseudo-second order rate model in modified UiO-66 and UiO-66-2OH is demonstrated in Figure 7-16 (a, b) at pH = 7, and depicted in Figure 7-16 (c, d) for pH = 3. It seems that this model does not fit well with our experimental data. Based on this, adsorption of MEG on modified UiO-66 and UiO-66-2OH is likely preceded by diffusion and hydrogen bonding.
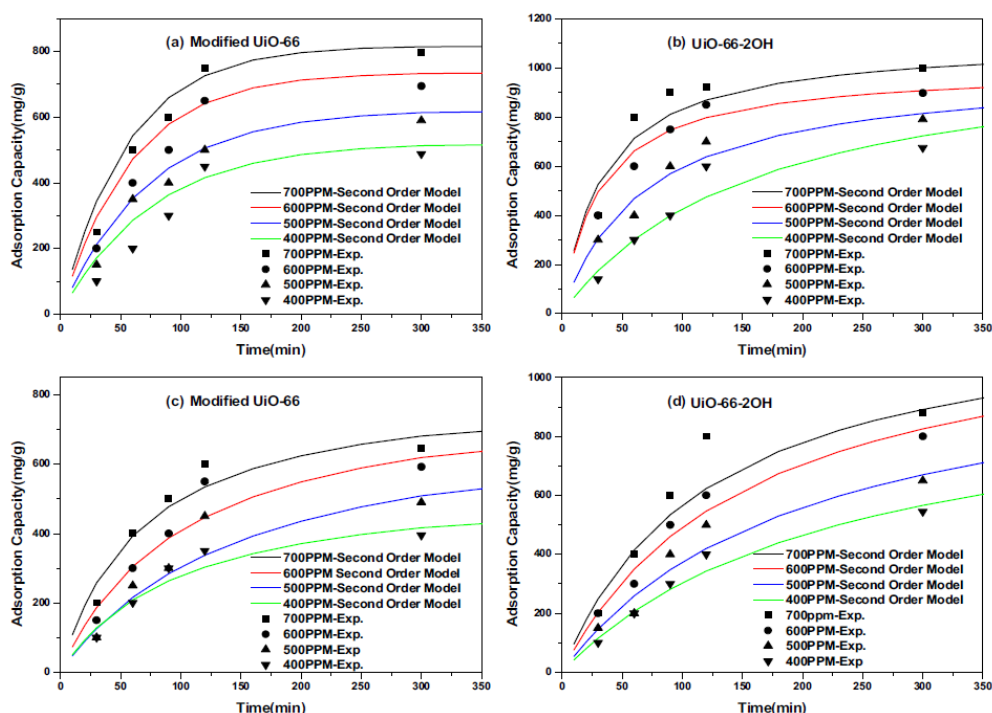


Figure 7-16: Comparison between the measured and pseudo-second order modelled time profiles for adsorption of MEG on modified UiO-66 and UiO-66-2OH at pH = 7 (a,b) and pH = 3 (c, d).

The effect of intra-particle diffusion resistance on the adsorption in this system was explored using eq.(7-3) and the parameters are reported in Table 7-1 and Table 7-2, which were obtained from the slope of the first step on the plot of adsorption capacity (mg/g) at any time against the square root of time (min$^{0.5}$), as shown in Figure 7-17 (a, b, c, d). Tables 1 and 2 show that the diffusion rate increases with increasing initial concentration due to the high driving force at high initial concentrations [197]. Moreover, UiO-66-2OH is faster than the modified UiO-66 because the diffusion rate is significantly dependent on the polarity of the pores, which is better in UiO-66-2OH due to the presence of hydroxyl groups. In addition, the diffusion rate during the migration of MEG molecules from bulk solution to the surface of the adsorbent [198]

decreases somewhat in acidic solutions, which can be attributed to the increased number of protons ($H^+$) in solution and their attraction with MEG molecules. Three steps are shown in Figure 7-17; the first step is related to the high rate of diffusion for MEG molecules via water toward the adsorbents (besides the diffusion on the external surface of the adsorbents), the second step is the diffusion of MEG molecules inside the pores of modified UiO-66 and UiO-66-2OH, and the third step is a move to equilibrium of the adsorption processes between MEG molecules and adsorbents. The second step in Figure 7-17 (d) also shows that the rate of intra-diffusion inside the pores is higher than that in Figure 7-17 (a, b, c). This can be justified according to the enhanced attractive forces for MEG molecules toward the surface of the adsorbent by increasing the concentration of $H^+$ with decreasing pH [198], and consequently the large pores are easily accessed by positive charges. This may enhance the positive charges of electrostatic interactions on the surface of the pores, and the hydrogen bonding interactions (from hydroxyl groups in UiO-66-2OH) may be significantly enhanced.
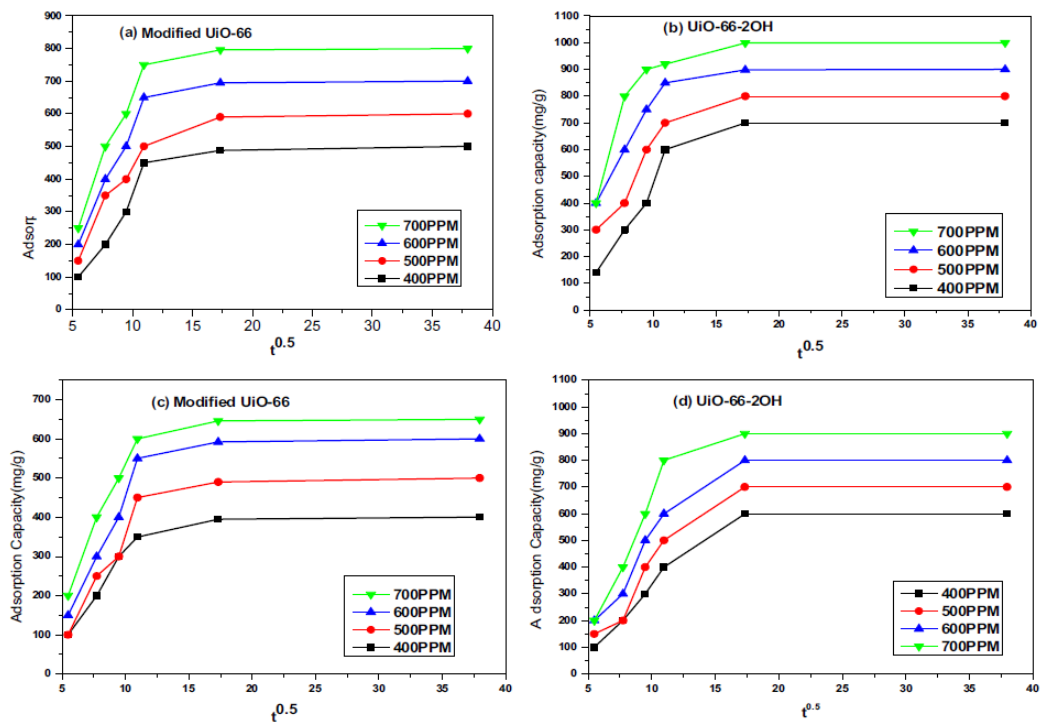


Figure 7-17: Kinetic adsorption represented by the intraparticle model on modified UiO-66 and UiO-66-2OH at pH = 7 (a, b) and pH = 3 (c, d).

Both modified UiO-66 and UiO-66-2OH demonstrated very high affinity to adsorb MEG molecules in neutral aqueous solutions. Both of them had significant adsorption capacity towards MEG, with modified UiO-66 at 800 mg. g$^{-1}$ and UiO-66-2OH at 1000 mg. g$^{-1}$. However, the capacities are reduced in acidic conditions (pH = 3) to 650 and 900 mg. g$^{-1}$, respectively, as shown in Figure 7-17 (a, b, c, d). Although MEG is a non-electrolyte, this high adsorption of MEG is influenced by several factors. First, a large pore size in combination with a high pore volume increases the chance of interactions between MEG molecules and the adsorption sites. Nanoscaled particles of modified UiO-66 and UiO-66-2OH may also enhance the adsorption capacity due to the increase in interparticle pores and external surface area with a decrease in particle size [198, 199]. In addition, the highest adsorption was seen on UiO-66-2OH due to its high external surface area and also the presence of hydroxyl groups in MEG molecules, and UiO-66-2OH enriches their interactions via hydrogen bonding which may lead to an increased adsorption capacity. As a matter of fact, the presence of hydroxyl groups enhanced the zeta potential on the surface of UiO-66-2OH. The Zeta potential was -18.43 mV on UiO-66-2OH while it was -5.92 mV on modified UiO-66. Consequently, the electrostatic attraction can be increased, resulting in a high adsorption capacity of UiO-66-2OH. The removal efficiency of MEG from wastewater during contact time of 24 h depends on the initial concentration and the type of adsorbent. From Figure 7-18, the removal efficiency is at its highest when the initial concentration of MEG is 150 ppm; it was approximately 96% in UiO-66-2OH and 91.6% in modified UiO-66 under the similar conditions (pH = 7, 298 K). Modified UiO-66 also demonstrated lower efficiency than UiO-66-2OH accompanied with variation in the removal rate, as there is a sharp decrease in efficiency when the concentration increases from 300 ppm to 400 ppm [200]. Increasing the initial concentration of MEG may increase the competitive behavior of MEG molecules themselves toward the pore surfaces in modified UiO-66, which does not have attractive functional groups (like hydroxyl groups) as the case of UiO-66-2OH.
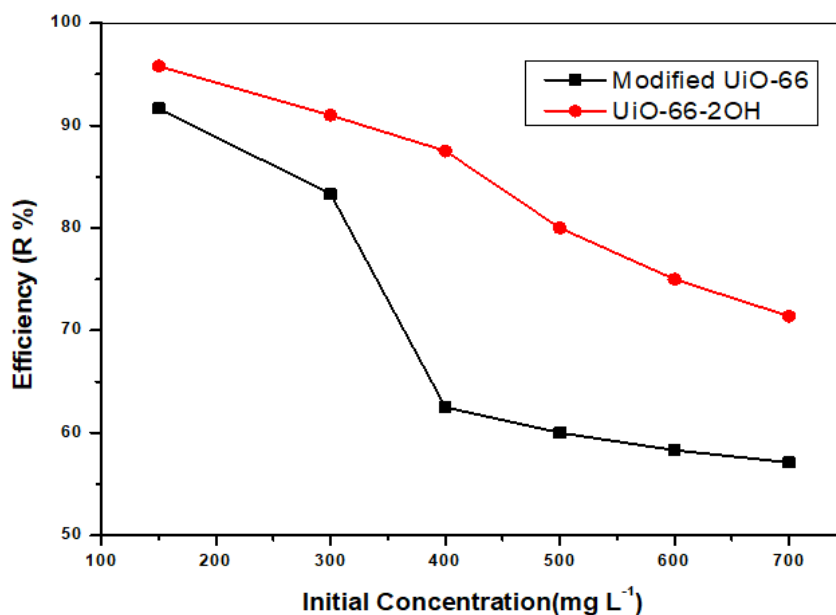
Figure 7-18: Removal efficiency for MEG solutions of different concentrations in aqueous conditions at pH = 7

Figure 7-19 and Figure 7-20 show the removal efficiency of MEG on modified UiO-66 and UiO-66-2OH, respectively, in five cycles. Modified UiO-66 displayed removal efficiency of 42% in the first and second cycles and then stable efficiency at 33.3% in the last three cycles. For UiO-66-2OH, the removal efficiency was 50% in the first three cycles, and then it was dropped to 25% in the fifth cycle. Consequently, the modified UiO-66 and UiO-66-2OH could maintain the removal of MEG from water with relatively strong stability for their practical application.
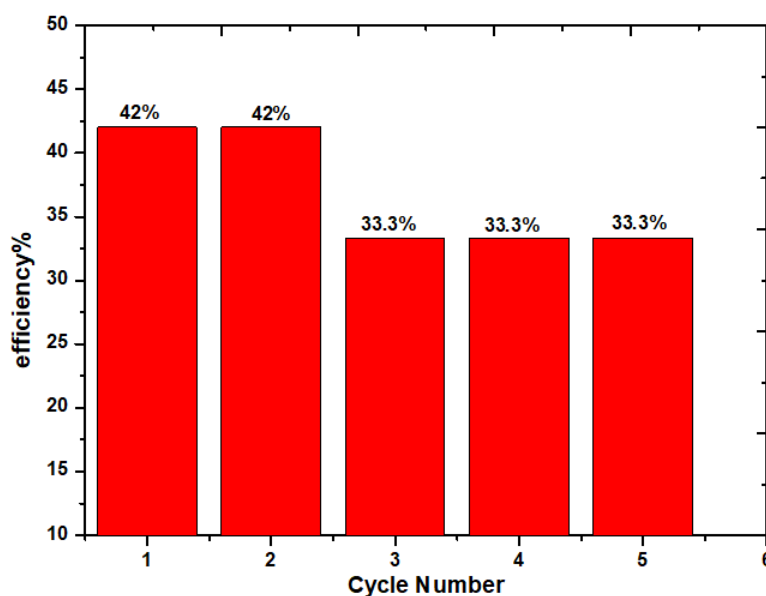


Figure 7-19: Removal efficiency of MEG by modified UiO-66 during 60min in different cycles
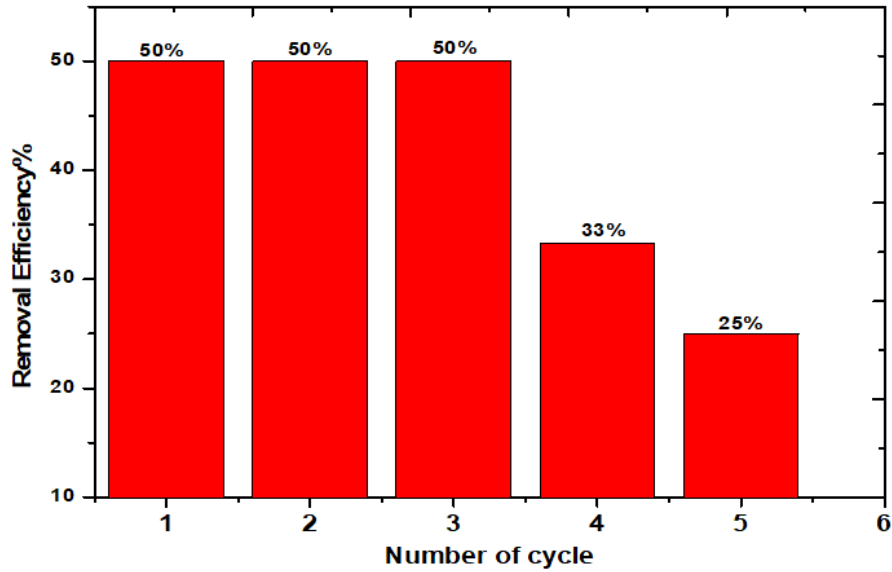
Figure 7-20: Removal efficiency of MEG by UiO-66-2OH during 60min in different cycles

### 7.4.2.3 Sorption Isotherms

It is important to determine the best isotherm that can represent the experimental data. Therefore, two common isotherms were considered when investigating this adsorption isotherm, those being the Langmuir and Freundlich isotherm models. The Langmuir model was derived for the ideal assumption of a uniform homogeneous adsorption surface, while the Freundlich model was designed for application to more heterogeneous surfaces [168].

- Langmuir Model

This model assumes a homogeneous surface where all adsorption sites possess identical affinity for solute, and as such contiguous interactions and steric hindrance are non-existent between adsorbed molecules on neighboring sites [201, 202]. The nonlinear form of the Langmuir adsorption isotherm model can be represented as:

$$q_e = \frac{q_m K_l C_e}{1 + K_L C_e} \tag{7-6}$$

Eq. (7-6) can be transferred to the following linear form to determine the Langmuir adsorption parameters:

$$\frac{1}{q_e} = \frac{1}{q_m} + \frac{1}{q_m K_l C_e} \tag{7-7}$$

179

Where $q_e$ is the amount of MEG adsorbed at equilibrium (mg/g), $q_m$ is a Langmuir constant related to the monolayer coverage capacity (mg/g), $K_l$ is a Langmuir constant for the adsorption energy, and $C_e$ is the concentration of MEG at equilibrium (mg/L). A linear plot of $1/q_e$ versus $1/C_e$ is used to compute Langmuir isotherm constants in Eq. (7-6)

Another equilibrium parameter for the Langmuir isotherm, called the separation factor, may be expressed as $R_L$ (dimensionless) which is related to the adsorption nature [203, 204] as:

$$R_L = \frac{1}{1 + K_L C_o} \tag{7-8}$$

Where $C_o$ is the initial concentration of MEG (mg/L).

- Freundlich Model

This model applies primarily to multilayer adsorption on heterogeneous surfaces with different affinities and adsorption heats for the solute. It is normally used to describe non-ideal and reversible adsorption of inorganic and organic components in solution [165, 196], and can be expressed as:

$$q_e = K_f C_e^{\frac{1}{n}} \tag{7-9}$$

Eq. (7-9) can be rearranged in the following linear form

$$ln\ q_e = lnK_f + \frac{1}{n} lnC_e \tag{7-10}$$

Where $K_f$ is the Freundlich isotherm constant, which is a rough indicator of adsorption capacity (mg/g), $C_e$ is the equilibrium constant of MEG (mg/g), and $n$ is the adsorption intensity. The magnitude of $n$ may indicate the favorability of an adsorption process, where $n > 1$ indicates favorable normal adsorption while $n < 1$ denotes cooperative adsorption [203, 205, 206].

Table 3 shows the parameters of the Langmuir and Freundlich models for adsorption of MEG molecules on modified UiO-66 and UiO-66-2OH. Fitting of the experimental data for MEG on modified UIO-66 to the Langmuir isotherm model in Table 7-3 indicates that $q_m$ is 2.5 times higher than $q_e$ in neutral solution. However, it is 1.4 times

the value of $q_e$ in acidic solution. From the correlation parameters ($R^2$) in Table 7-3, the experimental data for MEG adsorption on modified UiO-66 at pH = 7 were better fitted to the Langmuir adsorption isotherm model ($R^2$= 0.99) compared to the Freundlich isotherm model ($R^2$=0.90). Therefore, the monolayer coverage is dominant on the external surface area of modified UiO-66 at pH = 7. Conversely, the Freundlich isotherm model had $R^2$= 0.98 at pH = 3, suggesting multilayer coverage of MEG on modified UIO-66 in acidic aqueous solutions of MEG. This behavior is apparent in Figure 7-21, and may be attributed to uneven distribution of $H^+$ on the surface of the adsorbent. On the other hand, adsorption of MEG on UiO-66-2OH was fitted well by the Langmuir isotherm model in neutral and acidic conditions, with $R^2 = 0.94$ compared to $R^2 = 0.92$ for the Freundlich model (Table 7-3 and Figure 7-22). However, the calculated values of $q_m$ were higher than the corresponding experimental values. The best fit for the adsorption of MEG was observed on modified UiO-66 and UiO-66-2OH using the Langmuir isotherm model in neutral aqueous conditions.

Table 7-3: Isotherm parameters for MEG removal on modified UiO-66 and UiO-66-2OH at pH = 3 and 7.

| Adsorbent | Langmuir Isotherm | | | Freundlich Isotherm | | | |
|---|---|---|---|---|---|---|---|
| Modified UiO-66 | | | | | | | |
| | $q_m$ $(mg{\cdot}g^{-1})$ | $K_l$ $(L{\cdot}mg^{-1})$ | $R^2$ | $\dfrac{1}{n}$ | $n$ | $K_f$ $(mg{\cdot}g^{-1})$ | $R^2$ |
| pH 3 | 909.09 | 0.00593 | 0.94 | 0.75 | 1.33 | 11.38 | 0.986 |
| pH 7 | 2000 | 0.002258 | 0.99 | 0.53 | 1.88 | 27.75 | 0.906 |
| UiO-66-2OH | | | | | | | |
| pH 3 | 10000 | 0.0004 | 0.94 | 0.92 | 1.08 | 6.35 | 0.902 |
| pH 7 | 2500 | 0.0047 | 0.92 | 0.56 | 1.78 | 47.11 | 0.836 |
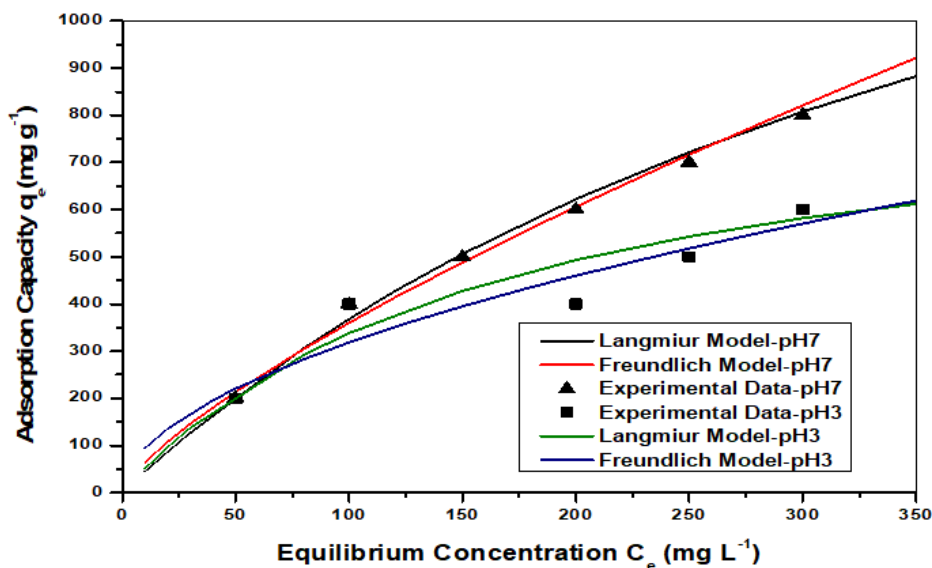
Figure 7-21: Experimental MEG adsorption isotherms on modified UiO-66 and modelled results using Langmuir and Freundlich model.
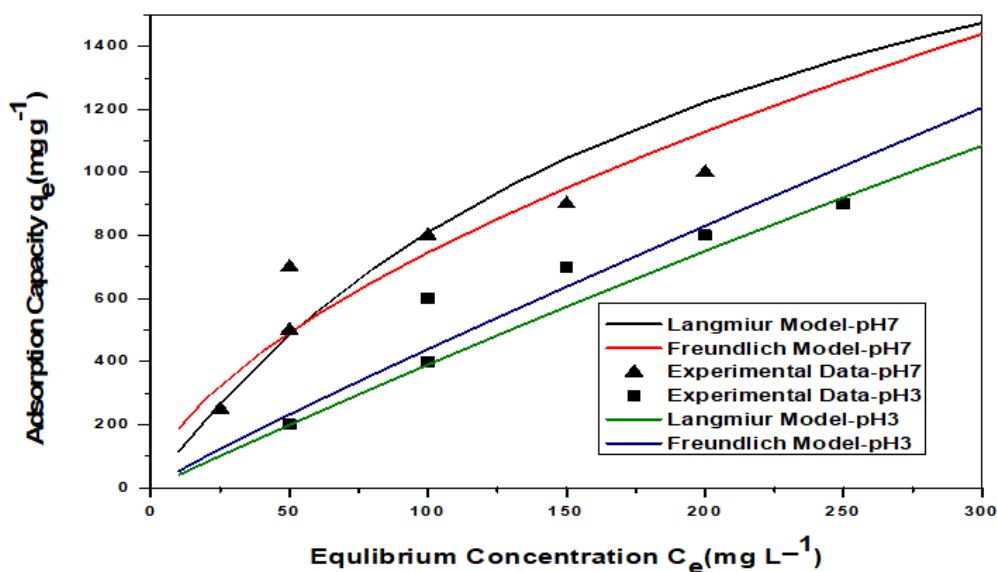


Figure 7-22: Experimental MEG adsorption isotherms on UiO-66-2OH and modelled results using Langmuir and Freundlich models

Figure 7-23 and Figure 7-24 show the separation factor of the Langmuir constant $R_L$, which indicates the nature of adsorption onto the adsorbents. Here, $0 < R_L < 1$ denotes favorable normal adsorption over the whole range of initial concentrations used in this study. However, the behavior of MEG molecules differed for adsorption on modified UiO-66 and UiO-66-2OH, based on the acidity of the aqueous MEG solution. $R_L$ for adsorption of MEG on modified UiO-66 is higher in neutral solutions than in acidic

solutions, while the highest value is demonstrated by the adsorption of MEG on UiO-66-2OH in acidic conditions. This is caused by the enhanced attractive force for MEG molecules toward the surface of UiO-66-2OH at increasing concentrations of $H^+$ which are associated with lower pH values.
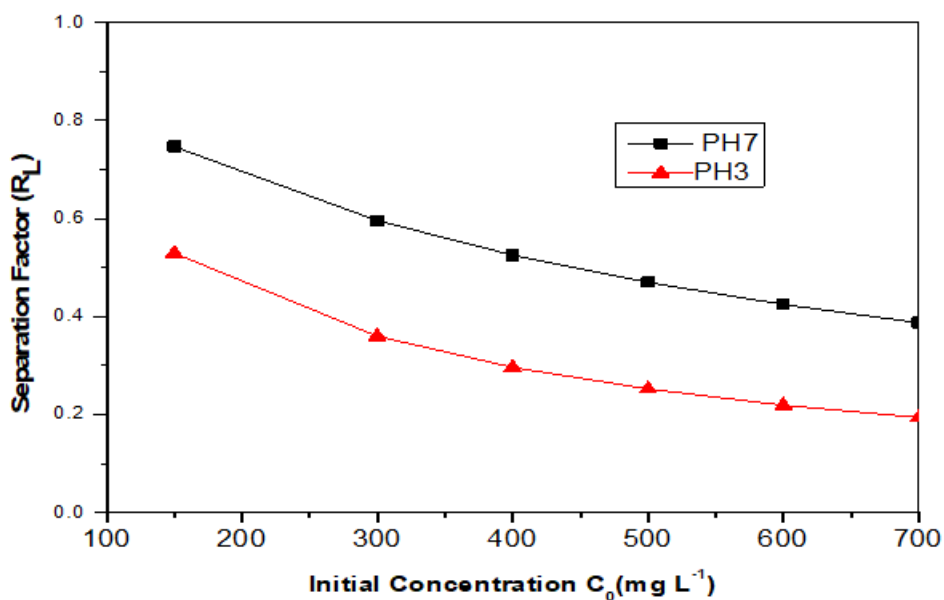


Figure 7-23: Langmuir isotherm parameter (RL) for adsorption of MEG on modified UiO-66
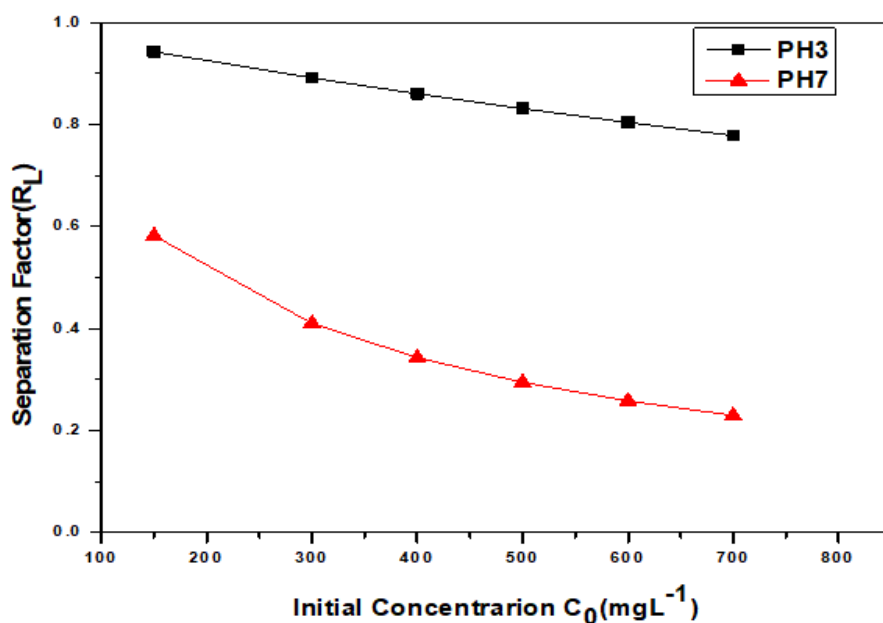


Figure 7-24: Langmuir isotherm parameter (RL) for adsorption of MEG on UiO-66-2OH

## 7.5 Conclusions

MEG exhibits exceptional affinity for adsorption on UiO-66-2OH and modified UiO-66-2OH. The best removal efficiency was achieved on UiO-66-2OH compared to modified UiO-66. The adsorption kinetics were best represented using a pseudo-first order model, while the Langmuir isotherm model suggested monolayer adsorption of MEG on UiO-66-2OH and modified UiO-66. These metal-organic frameworks were unprecedentedly removed this pollutant from wastewater and they will make for better adsorbents for the capture of MEG in the effluent wastewater produced in the petroleum industry. The results in this study by using MOFs as adsorbent to remove MEG from wastewater have never been seen in previous literatures. It can be recommended that dynamic adsorption by breakthrough experiments should be intensively investigated by using these types of MOFs for MEG removal from wastewater and compared with different metal-based MOFs.

# 8. Conclusions & Recommendation

## 8.1. Conclusions

The main objectives of the research can be divided into two main parts with the switchover corrosion experiments, and MEG adsorption on UiO-66-2OH, modified UiO-66-2OH which were also investigated. The main aim was to assemble and design a distillation system part of a MEG bench Scale pilot plant and check its performance for the separation of MEG from water. The number of equilibrium stages estimated for continuous operation was six. Two stages were required calculation by under total reflux condition. The column height based on the HETP values was 0.34 metres while the height of the packing required was approximately 1.7 metres. According to the HTU and NTUs trial method for the packing height estimation, the column height was between 1.9-2.1 metres but by the HETP method it was more accurate. The other aim of the experiment was to study the effect of dissolved salts on the recovery of the MEG. Overall the presence of dissolved salts in the rich MEG feed was primarily influenced the lean MEG purity. The impact of dissolved salts within the rich MEG feed was predictable with an average deviation of 1.61% from experimental trials using the Aspen Plus ELECNRTL electrolyte simulation by the inclusion of monovalent cations. Overall, it was established that the impact of dissolved salts is not only limited to the effects of salt precipitation and accumulation within the reboiler unit of a distillation column but also through its impact on the VLE of the system. Therefore, the unexpected presence of dissolved salts within the rich MEG feed stream may require greater reboiler temperature to maintain a constant boil up rate potentially leading to unwanted thermal degradation of the MEG. HYSYS simulation software was used for calculations, the software results for the operating conditions were compatible with the experimental data using PR EOS. The study for the independent variables (T, $XF_{MEG}$, and Q) was found to have a critical effect on $XB_{MEG}$. The results of the present study indicate that the optimum operating conditions were 145℃, 56.45 %, and 7.55 kg/h of T, $XF_{MEG,}$ and Q, respectively. Under these optimum conditions, $XB_{MEG}$ was 87.3 %. $XB_{MEG}$. In the present study, BBD was based on the reboiler temperature for the range of 125-145 ℃ along with $XF_{MEG}$ range of 45-70% and Q of 5-9 kg/h.

The reverse switchover experiments from MDEA to FFCI corrosion control proved to be more problematic in the current plant set-up for Gorgon. This pH needs to be

increased to values of 8.0 to 8.3 in the RGT in order to effectively precipitate calcium ions from the solution. Magnesium was not removed under these conditions, since it required an even higher pH to form magnesium hydroxide (>10). The pH from the RGT will carry over into the regeneration and reclamation units. The amount of NaOH needed to raise the pH of the rich MEG in the MPV is proportional to the MDEA concentration present. The results of the switchover experiments and benchtop facility operation observations have suggested that with the installation of an additional HCl doing point in the feed line to the reboiler or within the RGT so that the itself, removal of organic acids can be achieved within the regeneration column whilst also improving the MDEA removal rate in the reclaimer. A proof of concept experiment has validated this proposed change in operation during the switchover period. Once the MDEA was removed to sufficiently low levels, the additional dosing point could be switched off and the current operation continued. The additional dosing point significantly aided in the removal of MDEA and reduces the alkalinity in the lean glycol tank much faster compared to the current operation philosophy. This in turn will have a significant impact on the quantities of chemicals required to perform the required pH adjustments. A rough estimate shows that to neutralise the facility inventory (16,000 m3 MEG containing 580mM of MDEA) about 770 m3 of concentrated HCl (37%) will be required initially. In order to increase the pH in the RGT to about 8 to 8.3 from the neutral point about 2.6 g/L NaOH need to be added (41.6 t for 16,000 m3), which in turn will need to be neutralised with 5.4 ml/L HCl (ca. 87 m3 for 16,000 m3).

The MEGhas a unique affinity to be adsorbed on UiO-66-2OH and modified UiO-66-2OH. UiO-66-2OH has a better removal efficiency than the modified UiO-66. A pseudo-first order model was developed for the adsorption kinetic. Since a monolayer adsorption of MEG on UiO-66-2OH and modified UiO-66 the Langmuir isotherm model was used. These metal-organic frameworks have the ability to remove wastewater as well as MEG in the petroleum industry. The consequence of this study was the usage of MOFs as adsorbent to remove MEG from wastewater for the first time. It is recommended that a dynamic adsorption be added to the unit also other types of MOFs for MEG removal are suggested for wastewater treatment.

## 8.2. Recommendation

Based on the conclusions in the previous section, several areas of improvement have been identified for future works which are as follows

1. Analysing saving energy in distillation tower for Recovery of mono-ethylene glycol.
2. Use different packing and study the effect of these packings during the processing of MEG recovery with the structure packing used.
3. The economical aspects of MEG plant should be considered to identify the feasibility of the proposed optimisation approach. This approach permits the actual cost sources at the equipment level to be recognized such as the capital, operating, maintenance costs and cost linked with the exergy loss.
4. Consider scaling up the existing MEG plant to test the distillation column efficiency in terms of MEG recovery and energy consumption.
5. Testing continuous process in water treatment and compare the results with the batch results that were obtained in this thesis.

# References

1. Sloan Jr, E.D. and C. Koh, *Clathrate hydrates of natural gases*. 2007: CRC press.

2. Son, K.V. and C. Wallace, *Reclamation/regeneration of glycols used for hydrate inhibition.* Deep Offshore Technology, 2000.

3. Bikkina, C., et al. *Development of MEG regeneration unit compatible corrosion inhibitor for wet gas systems*. in *SPE Asia Pacific Oil and Gas Conference and Exhibition*. 2012. Society of Petroleum Engineers.

4. John, C., *Natural gas hydrates: A guide for engineers*. 2009, Elsevier incorporated.

5. AlHarooni, K., et al., *Inhibition effects of thermally degraded MEG on hydrate formation for gas systems.* Journal of Petroleum Science and Engineering, 2015. **135**: p. 608-617.

6. Zarinabadi, S. and A. Samimi, *Problems of hydrate formation in oil and gas pipes deals.* Journal of American Science, 2012. **8**(8).

7. Jonassen, A.H., *DISTRIBUTION OF ALCOHOLS AND GLYCOLS BETWEEN OIL, GAS AND WATER PHASES IN HYDRATE PREVENTION.*

8. Time, R., *Flow Assurance and Mulitple Flow Part 2.* Department of Petroleum Engineering, University of Stavanger, Norway, 2011.

9. Haghighi, H., et al., *Experimental and thermodynamic modelling of systems containing water and ethylene glycol: Application to flow assurance and gas processing.* Fluid Phase Equilibria, 2009. **276**(1): p. 24-30.

10. Speight, J.G., *Ullmann's Encyclopedia of Industrial Chemistry.* Petroleum Science and Technology, 1999. **17**(3-4): p. 445-445.

11. Global, S., *Mono-Ethylene Glycol. Shell Global, Global data sourced from PCI Xylenes and Polyesters Ltd Accessed 21/04.* http://www.shell.com/business-customers/chemicals/factsheets-speeches-and-articles/factsheets/mono-ethylene-glycol.html, 2015.

12. Latta, T.M., M.E. Seiersten, and S.A. Bufton. *Flow assurance impacts on lean/rich MEG circuit chemistry and MEG regenerator/reclaimer design*. in *Offshore Technology Conference*. 2013. Offshore Technology Conference.

13. Bahadori, A., *New model calculates solubility of light alkanes in triethylene gycol.* Petroleum Chemistry, 2009. **49**(2): p. 171-179.

14. Brustad, S., K.-P. Løken, and J.G. Waalmann. *Hydrate Prevention using MEG instead of MeOH: Impact of experience from major Norwegian developments on technology selection for injection and recovery of MEG*. in *Offshore Technology Conference*. 2005. Offshore Technology Conference.

15. Kister, H.Z., *Distillation design*. Vol. 1. 1992: McGraw-Hill New York.

16. Coker, A.K., *Ludwig's applied process design for chemical and petrochemical plants: Fourth edition*. Vol. 2. 2010. 1-961.

17. McCabe, W.L., J.C. Smith, and P. Harriott, *Unit operations of chemical engineering*. Vol. 5. 1993: McGraw-Hill New York.

18. Stichlmair, J.G. and J.R. Fair, *Distillation: principles and practices*. 1998: Wiley-VCH New York.

19. Coulson, J. and R. Sinnott, *Coulson & Richardson's Chemical Engineering: Chemical Engineering Design (Chemical Engineering Vol. 6 by RK Sinnot).* Butterworth-Heinemann, 2005.

20. Towler, G.P., *Chemical engineering design : principles, practice, and economics of plant and process design / Gavin Towler, Ray Sinnott*. 2nd ed.. ed, ed. R.K. Sinnott. 2013, Oxford ; Waltham, MA: Oxford ; Waltham, MA : Butterworth-Heinemann.

21. Sinnott, R. and G. Towler, *Separation Columns (Distillation, Absorption and Extraction).* RK Sinnott, Coulson and Richardson's Chemical Engineering, 1999. **6**.

22. Sorel, E., *Distillation et rectification industrielles*. 1899: G. Carré et C. Naud.

23. Lewis, W.K., *The Theory of Fractional Distillation.* Industrial & Engineering Chemistry, 1909. **1**(8): p. 522-533.

24. Seader, J., *The BC (Before Computers) and AD of Equilibrium-Stage Operations.* Chemical Engineering Education, 1985. **19**(2): p. 88-103.

25. Fenske, M.R., *Fractionation of Straight-Run Pennsylvania Gasoline.* Industrial &amp; Engineering Chemistry, 1932. **24**(5): p. 482-485.

26. Wankat, P.C., *Separation process engineering : includes mass transfer analysis / Phillip C. Wankat*. 3rd ed.. ed. 2012, Upper Saddle River, NJ: Upper Saddle River, NJ : Prentice Hall.

27. Gilliland, E., *Multicomponent rectification estimation of the number of theoretical plates as a function of the reflux ratio.* Industrial & Engineering Chemistry, 1940. **32**(9): p. 1220-1223.

28. Liddle, C., *Improved shortcut method for distillation calculations.* Chem. Eng, 1968. **75**(23): p. 137-142.

29. Molokanov, Y.K., et al., *An approximate method of calculating the basic parameters of a multicomponent fractionation.* Chemistry and Technology of Fuels and Oils, 1971. **7**(2): p. 129-133.

30. Kirkbride, C.G., *Process design procedure for multicomponent fractionators.* Petroleum Refiner, 1944. **23**(9): p. 321-336.

31. Erbar, J. and R. Maddox, *Latest score: reflux vs. trays.* Petroleum Refiner, 1961. **40**(5): p. 183-188.

32. Smallwood, I.M., *Solvent recovery handbook*. 2002: CRC Press.

33. Henley, E.J. and J.D. Seader, *Equilibrium-stage separation operations in chemical engineering*. 1981: Wiley.

34. Fischer, L., U. Bühlmann, and R. Melcher, *Characterization of high-performance structured packing.* Chemical Engineering Research and Design, 2003. **81**(1): p. 79-84.

35. Foust, A.S., et al., *Principles of unit operations*. 2008: John Wiley & Sons.

36. Dutta, B.K., *Principles of mass transfer and seperation processes*. 2007: PHI Learning Pvt. Ltd.

37. Richardson, J.F., *Particle technology and separation processes / J.F. Richardson and J.H. Harker with J.R. Backhurst*. 5th ed.. ed, ed. J.H. Harker, J.R. Backhurst, and J.M. Coulson. 2002, Oxford: Oxford : Butterworth-Heinemann.

38. Wang, G., X. Yuan, and K. Yu, *Review of mass-transfer correlations for packed columns.* Industrial & engineering chemistry research, 2005. **44**(23): p. 8715-8729.

39. Bravo, J.L., J. Rocha, and J. Fair, *Mass transfer in gauze packings.* Hydrocarbon processing, 1985. **64**(1): p. 91-95.

40. Harrison, M.E. and J.J. France, *Distillation column troubleshooting-part 2: Packed columns.* Chemical Engineering, 1989. **96**(4): p. 121.

41. Green, D., *Perry's chemical engineers' handbook.-Prepared by a staff of specialists under the editorial direction of Don W. Green, editorin-chief, Robert H. Perry, late editor.* 2008.

42. Nawrocki, P., Z. Xu, and K. Chuang, *Mass transfer in structured corrugated packing.* The Canadian Journal of Chemical Engineering, 1991. **69**(6): p. 1336-1343.

43. Billet, R. and M. Schultes, *Predicting mass transfer in packed columns.* Chemical Engineering & Technology: Industrial Chemistry-Plant Equipment-Process Engineering-Biotechnology, 1993. **16**(1): p. 1-9.

44. Hanley, B., B. Dunbobbin, and D. Bennett, *A unified model for countercurrent vapor/liquid packed columns. 2. Equations for the mass-transfer coefficients, mass-transfer area, the HETP, and the dynamic liquid holdup.* Industrial and Engineering Chemistry Research, 1994. **33**: p. 1222-1222.

45. Rocha, J.A., J.L. Bravo, and J.R. Fair, *Distillation columns containing structured packings: a comprehensive model for their performance. 2. Mass-transfer model.* Industrial & engineering chemistry research, 1996. **35**(5): p. 1660-1667.

46. Brunazzi, E. and A. Paglianti, *Liquid-film mass-transfer coefficient in a column equipped with structured packings.* Industrial & engineering chemistry research, 1997. **36**(9): p. 3792-3799.

47. Shetty, S. and R.L. Cerro, *Fundamental liquid flow correlations for the computation of design parameters for ordered packings.* Industrial & engineering chemistry research, 1997. **36**(3): p. 771-783.

48. Olujić, Ž., A. Kamerbeek, and J. De Graauw, *A corrugation geometry based model for efficiency of structured distillation packing.* Chemical Engineering and Processing: Process Intensification, 1999. **38**(4-6): p. 683-695.

49. Xu, Z., A. Afacan, and K. Chuang, *Predicting mass transfer in packed columns containing structured packings.* Chemical Engineering Research and Design, 2000. **78**(1): p. 91-98.

50. Murch, D., *Height of equivalent theoretical plate in packed fractionation columns.* Industrial & Engineering Chemistry, 1953. **45**(12): p. 2616-2621.

51. Lockett, M. and J. Billingham, *The effect of maldistribution on separation in packed distillation columns.* Chemical Engineering Research and Design, 2003. **81**(1): p. 131-135.

52. Carillo, F., A. Martín, and A. Roselló, *A shortcut method for the estimation of structured packings HEPT in distillation.* Chemical Engineering & Technology: Industrial Chemistry-Plant Equipment-Process Engineering-Biotechnology, 2000. **23**(5): p. 425-428.

53. Shi, M.G., *Effective interfacial area in packed columns.* Ger. Chem. Eng., 1985. **8**: p. 87-96.

54. Fair, J., *Distillation columns containing structured packing.* Chem. Eng. Progr., 1990. **86**: p. 19-29.

55. De Brito, M.H., et al., *Effective mass-transfer area in a pilot plant column equipped with structured packings and with ceramic rings.* Industrial & engineering chemistry research, 1994. **33**(3): p. 647-656.

56. Brunazzi, E., et al., *Interfacial area of mellapak packing: Absorption of 1, 1, 1-trichloroethane by Genosorb 300.* Chemical Engineering & Technology: Industrial Chemistry-Plant Equipment-Process Engineering-Biotechnology, 1995. **18**(4): p. 248-255.

57. Gualito, J., et al., *Design method for distillation columns filled with metallic, ceramic, or plastic structured packings.* Industrial & engineering chemistry research, 1997. **36**(5): p. 1747-1757.

58. Olujic, Z. *Delft model–a comprehensive design tool for corrugated sheet structured packings.* in *Preprints of the Topical Conference on Distillation Tools for the Practicing Engineer, AIChE Spring National Meeting.* 2002.

59. Krell, E., *Handbook of laboratory distillation.* Vol. 2. 1982: Elsevier.

60. Ullmann, F., *Ullmann&#039;s encyclopedia of industrial chemistry / executive editor, Wolfgang Gerhartz*. 5th, completely rev. ed.. ed, ed. W. Gerhartz. 1985, Weinheim, Federal Republic of Germany: Weinheim, Federal Republic of Germany : VCH.

61. Jenkins, S., *Ethylene Glycol Production*. Chemical Engineering, 2015. **122**(10): p. 44-44.

62. Flick, E.W., *Industrial solvents handbook / edited by Ernest W. Flick*. 5th ed.. ed. 1998, Westwood, N.J.: Westwood, N.J. : Noyes Data Corp.

63. Carroll, J.J., *Natural Gas Hydrates: A Guide for Engineers*. 2003. 1-270.

64. Latta, T., et al. *Design Considerations for Mitigating the Impact of Contaminants in Rich MEG on Monoethylene Glycol Recovery Unit MRU Performance*. in *Offshore Technology Conference Asia*. 2016. Offshore Technology Conference.

65. Flaten, E.M., M. Seiersten, and J.-P. Andreassen, *Growth of the calcium carbonate polymorph vaterite in mixtures of water and ethylene glycol at conditions of gas processing*. Journal of Crystal Growth, 2010. **312**(7): p. 953-960.

66. Flaten, E.M., et al. *Impact of Monoethylene Glycol and Fe 2+ on Crystal Growth of CaCO 3*. in *CORROSION 2015*. 2015. NACE International.

67. Dugstad, A. and M. Seiersten. *pH-stabilisation, a reliable method for corrosion control of wet gas pipelines*. in *SPE International Symposium on Oilfield Corrosion*. 2004. Society of Petroleum Engineers.

68. Flaten, E.M., et al. *Precipitation of iron and calcium carbonate in pipelines at varying MEG contents*. in *SPE International Oilfield Scale Conference*. 2008. Society of Petroleum Engineers.

69. Andreassen, J.-P., *Formation mechanism and morphology in precipitation of vaterite—nano-aggregation or crystal growth?* Journal of Crystal Growth, 2005. **274**(1): p. 256-264.

70. Bryce, D.L., E.B. Bultz, and D. Aebi, *Calcium-43 chemical shift tensors as probes of calcium binding environments. Insight into the structure of the vaterite CaCO3 polymorph by 43Ca solid-state NMR spectroscopy*. Journal of the American Chemical Society, 2008. **130**(29): p. 9282-9292.

71. Kaasa, B., K. Sandengen, and T. Ostvold. *Thermodynamic predictions of scale potential, pH and gas solubility in glycol containing systems*. in *SPE International Symposium on Oilfield Scale*. 2005. Society of Petroleum Engineers.

72. Flaten, E.M., M. Seiersten, and J.-P. Andreassen, *Induction time studies of calcium carbonate in ethylene glycol and water*. Chemical Engineering Research and Design, 2010. **88**(12): p. 1659-1668.

73. Figueiredo, C.M.S., et al., *Crystal growth of FeCO3 in mixed monoethylene glycol and water solvent*. Crystal Research and Technology, 2015. **50**(5): p. 354-361.

74. Nasr-El-Din, H. and A. Al-Humaidan. *Iron sulfide scale: formation, removal and prevention*. in *International Symposium on Oilfield Scale*. 2001. Society of Petroleum Engineers.

75. Smith, J. and J. Miller, *Nature of sulphides and their corrosive effect on ferrous metals: a review.* British Corrosion Journal, 1975. **10**(3): p. 136-143.

76. Seiersten, M., et al. *Development of a simulator for ethylene glycol loops based on solution thermodynamics and particle formation kinetics*. in *CORROSION 2010*. 2010. NACE International.

77. Sandengen, K., *Prediction of mineral scale formation in wet gas condensate pipelines and in MEG (mono ethylene glycol) regeneration plants.* 2006.

78. Baraka-Lokmane, S., et al. *Prediction of mineral scaling in a MEG loop system of a gas production offshore*. in *SPE International Conference on Oilfield Scale*. 2012. Society of Petroleum Engineers.

79. Guan, H., G. Cole, and P.J. Clark, *Inhibitor Selection for Iron-Scale Control in MEG Regeneration Process.* SPE Production & Operations, 2009. **24**(04): p. 543-549.

80. Aworn, A., P. Thiravetyan, and W. Nakbanpote, *Preparation of CO 2 activated carbon from corncob for monoethylene glycol adsorption.* Colloids and Surfaces A: Physicochemical and Engineering Aspects, 2009. **333**(1): p. 19-25.

81. Esmaeili, A. and K. Loghmani, *Removal of Monoethylene Glycol from Gas Field Wastewater Using Aspergillus tubingensis and a New Bioreactor.* Waste and Biomass Valorization, 2016. **7**(1): p. 151-156.

82. Aguilar-Arteaga, K., J. Rodriguez, and E. Barrado, *Magnetic solids in analytical chemistry: a review.* Analytica Chimica Acta, 2010. **674**(2): p. 157-165.

83. Mohan, D. and C.U. Pittman, *Arsenic removal from water/wastewater using adsorbents—a critical review.* Journal of hazardous materials, 2007. **142**(1): p. 1-53.

84. Yangui, R.B.E., *Removal of water pollutants by adsorption on actvated carbon prepared from olive-wast cakes and by biological treatment using ligninolytic*, in *Biological Engineering department of Chemical engineering*. 2013, Barcelona/University of Sfax. p. Chapter 2.

85. Tsibranska, I. and E. Hristova, *Comparison of different kinetic models for adsorption of heavy metals onto activated carbon from apricot stones.* Bulgarian Chem Commun, 2011. **43**: p. 370.

86. Yuh-Shan, H., *Citation review of Lagergren kinetic rate equation on adsorption reactions.* Scientometrics, 2004. **59**(1): p. 171-177.

87. Guedidi, H., et al., *The effects of the surface oxidation of activated carbon, the solution pH and the temperature on adsorption of ibuprofen.* Carbon, 2013. **54**: p. 432-443.

88. Vakharkar, A.S., *Adsorption studies for arsenic removal using modified chabazite.* 2005.

89. Crittenden, J.C., et al., *MWH's water treatment: principles and design*. 2012: John Wiley & Sons.

90. M800, M.-P.T., *https://www.mt.com/au/en/home/products/Process-Analytics/transmitter/multi-parameter-digital-transmitter-M800.html*.

91. Probe, I.i.p., *https://www.mt.com/au/en/home/products/Process-Analytics/pH-probe/durable-probe/InPro-4850i.html*.

92. sensor, I.i.p.o., *https://www.mt.com/au/en/home/products/Process-Analytics/DO-CO2-ozone-sensor/dissolved-oxygen-meter/InPro-6850.html*.

93. Meter, I.C., *https://www.mt.com/au/en/home/products/Process-Analytics/conductivity-sensor/electrode/probe-InPro-7100.html*.

94. force, M.f.m.C., *https://www.au.endress.com/en/Field-instruments-overview/Flow-measurement-product-overview/Coriolis-mass-flowmeters*.

95. FMI21), L.m.L., *https://www.endress.com/en/Field-instruments-overview/level-measurement/Capacitance-level-Liquicap-FMI21*.

96. PMD75), D.p.D., *https://www.endress.com/en/Field-instruments-overview/pressure/Differential-Pressure-Deltabar-PMD75?highlight=Differential%20pressure%20(Deltabar%20PMD75)*.

97. thermometer, B., *https://en.wika.com/upload/DS_TM5401_en_co_2088.pdf*.

98. FTL85, L., *https://www.endress.com/en/Field-instruments-overview/level-measurement/Vibronic-Liquiphant-FTL85*.

99. Lu, H., A.T. Kan, and M.B. Tomson, *Effects of Monoethylene Glycol on Carbonate Equilibrium and Calcite Solubility in Gas/Monoethylene Glycol/NaCl/Water Mixed Systems.* 2010.

100. Bikkina, C., et al., *Development of MEG Regeneration Unit Compatible Corrosion Inhibitor for Wet Gas Systems*. 2012, Society of Petroleum Engineers.

101. Haque, M.E., *Ethylene Glycol Regeneration Plan: A Systematic Approach to Troubleshoot the Common Problems.* Journal of Chemical Engineering, 2012. **27**(1): p. 21-26.

102. Latta, T.M., M.E. Seiersten, and S.A. Bufton, *Flow Assurance Impacts on Lean/Rich MEG Circuit Chemistry and MEG Regenerator/Reclaimer Design*. 2013, Offshore Technology Conference.

103. Carroll, J.J., *Natural gas hydrates : a guide for engineers / John J. Carroll*. 2003, Amsterdam, Boston: Gulf Professional Pub.

104. Brustad, S., K.P. Løken, and J.G. Waalmann, *Hydrate Prevention using MEG instead of MeOH: Impact of experience from major Norwegian developments on technology selection for injection and recovery of MEG*. 2005, Offshore Technology Conference.

105. Son, K.v. and C. Wallace, *Reclamation/Regeneration of Glycols Used for Hydrate Inhibition*, in *Deep Offshore Technology Conference*. 2000: New Orleans, LA.

106. McCabe, W.L., *Unit operations of chemical engineering / Warren L. McCabe, Julian C. Smith, Peter Harriott*. 5th ed.. ed, ed. J.C. Smith and P. Harriott. 1993, New York: New York : McGraw-Hill.

107. Kister, H.Z., *Distillation design / Henry Z. Kister*. 1992, New York: New York : McGraw-Hill.

108. Diba, K.D., M. Guglielminetti, and S. Schiavo. *Glycol reclaimer*. in *The Offshore Mediterranean Conference and Exhibition*. 2003. Ravenna.

109. Montazaud, T., *Precipitation of carbonates in the pretreatment process for regeneration of ethylene glycol*, in *Chemical Engineering and Biotechnology*. 2011, Norwegian University of Science and Technology. p. 89.

110. Gonzalez, J.J., M.E. Alfonso, and G. Pellegrino. *Corrosion of carbon steels in mono ethylene glycol*. in *Corrosion 2000 NACE International*. 2000.

111. Psarrou, M.N., et al., *Carbon Dioxide Solubility and Monoethylene Glycol (MEG) Degradation at MEG Reclaiming/Regeneration Conditions.* Journal of Chemical & Engineering Data, 2011. **56**(12): p. 4720-4724.

112. Latta, T.M., et al., *Design Considerations for Mitigating the Impact of Contaminants in Rich MEG on Monoethylene Glycol Recovery Unit MRU Performance*. 2016, Offshore Technology Conference.

113. Babu, D.R., et al., *Carbonates precipitation in MEG loops – A comparative study of South Pars and Bass Strait gas fields.* Journal of Natural Gas Science and Engineering, 2015. **27, Part 2**: p. 955-966.

114. Flaten, E.M., et al., *Impact of Monoethylene Glycol and Fe2+ on Crystal Growth of CaCO3*. 2015, NACE International.

115. Figueiredo, C., et al., *Crystal growth of FeCO3 in mixed monoethylene glycol and water solvent.* Cryst. Res. Technol., 2015. **50**(5): p. 354-361.

116. Kaasa, B., K. Sandengen, and T. Ostvold, *Thermodynamic Predictions of Scale Potential, pH and Gas Solubility in Glycol Containing Systems*. 2005, Society of Petroleum Engineers.

117. Smith, J.S. and J.D.A. Miller, *Nature of Sulphides and their Corrosive Effect on Ferrous Metals: A Review.* British Corrosion Journal, 1975. **10**(3): p. 136-143.

118.     Zaboon, S., et al., *Recovery of mono-ethylene glycol by distillation and the impact of dissolved salts evaluated through simulation of field data.* Journal of Natural Gas Science and Engineering, 2017. **44**: p. 214-232.

119.     Trimble, H.M. and W. Potts, *Glycol-Water Mixtures Vapor Pressure-Boiling Point-Composition Relations.* Industrial & Engineering Chemistry, 1935. **27**(1): p. 66-68.

120.     Molokanov, Y., et al., *An approximate method of calculating the basic parameters of a multicomponent fractionation.* Chemistry and Technology of Fuels and Oils, 1971. **7**(2): p. 129-133.

121.     Coker, A.K., *Chapter 14 - Packed Towers*, in *Ludwig's Applied Process Design for Chemical and Petrochemical Plants (Fourth Edition).* 2010, Gulf Professional Publishing: Boston. p. 483-678.

122.     Dutta, B.K., *Principles of mass transfer and separation processes / Binay K. Dutta*. 2007, New Delhi: New Delhi : Prentice-Hall of India.

123.     Bravo, J.L., J.A. Rocha, and J.R. Fair, *MASS TRANSFER IN GAUZE PACKINGS.* Hydrocarbon Processing, 1985. **64**(1): p. 91-95.

124.     Wang, G., X. Yuan, and K. Yu, *Review of mass-transfer correlations for packed columns*, in *Ind. Eng. Chem. Res.* 2005. p. 8715-8729.

125.     Wilke, C.R. and P. Chang, *Correlation of diffusion coefficients in dilute solutions.* AIChE Journal, 1955. **1**(2): p. 264-270.

126.     Chapman, S., *The mathematical theory of non-uniform gases / Sydney Chapman and T.G. Cowling*. 3rd ed / prepared in co-operation with D. Burnett.. ed, ed. D. Burnett and T.G. Cowling. 1970, Cambridge: Cambridge : Cambridge University Press.

127.     Cussler, E.L., *Diffusion : mass transfer in fluid systems / E.L. Cussler*. 2nd ed.. ed. 1997, New York ; Cambridge: New York ; Cambridge : Cambridge University Press.

128.     Ben-Amotz, D. and D.R. Herschbach, *Estimation of effective diameters for molecular fluids.* The Journal of Physical Chemistry, 1990. **94**(3): p. 1038-1047.

129.     Bravo, J.L. and J.R. Fair, *Distillation columns containing structured packing.* Chemical Engineering Progress, 1990. **86**(1): p. 19-29.

130.     Kamihama, N., et al., *Isobaric vapor–liquid equilibria for ethanol+ water+ ethylene glycol and its constituent three binary systems.* Journal of Chemical & Engineering Data, 2012. **57**(2): p. 339-344.

131.     Bialik, M., P. Sedin, and H. Theliander, *Boiling point rise calculations in sodium salt solutions.* Industrial & Engineering Chemistry Research, 2008. **47**(4): p. 1283-1287.

132.     Meranda, D. and W.F. Furter, *Elevation of the boiling point of water by salts at saturation: Data and correlation.* Journal of Chemical and Engineering Data, 1977. **22**(3): p. 315-317.

133. Aznar, M. and A. Telles, *Prediction of electrolyte vapor-liquid equilibrium by UNIFAC-Dortmund.* Brazilian Journal of Chemical Engineering, 2001. **18**(2): p. 127-137.

134. Chou, T.-J. and A. Tanioka, *Predicting the effect of dissolved salt on the vapour-liquid equilibria for alcohol-water-salt systems.* Chemical Engineering Research and Design, 1999. **77**(4): p. 329-334.

135. Kumar, A., *A simple model for predicting the effect of electrolytes on the vapor-liquid equilibrium data of solvent mixtures.* Separation science and technology, 1993. **28**(5): p. 1203-1210.

136. Chapoy, A., et al., *Clathrate hydrate equilibria in mixed monoethylene glycol and electrolyte aqueous solutions.* The Journal of Chemical Thermodynamics, 2012. **48**: p. 7-12.

137. Seo, Y. and S.-P. Kang, *Inhibition of methane hydrate re-formation in offshore pipelines with a kinetic hydrate inhibitor.* Journal of Petroleum Science and Engineering, 2012. **88**: p. 61-66.

138. Carroll, J., *Natural gas hydrates: a guide for engineers*. 2014: Gulf Professional Publishing.

139. Montazaud, T., *Precipitation of carbonates in the pretreatment process for regeneration of ethylene glycol*. 2011, Institutt for kjemisk prosessteknologi.

140. Gonzalez, J.J., M.E. Alfonso, and G. Pellegrino. *Corrosion of carbon steels in monoethylene glycol*. in *CORROSION 2000*. 2000. NACE International.

141. Baş, D. and I.H. Boyacı, *Modeling and optimization I: Usability of response surface methodology.* Journal of food engineering, 2007. **78**(3): p. 836-845.

142. Al-Mohammedawi, H.H., H. Znad, and E. Eroglu, *Synergistic effects and optimization of photo-fermentative hydrogen production of Rhodobacter sphaeroides DSM 158.* International Journal of Hydrogen Energy, 2018.

143. Bezerra, M.A., et al., *Response surface methodology (RSM) as a tool for optimization in analytical chemistry.* Talanta, 2008. **76**(5): p. 965-977.

144. HYSYS, H., *v7.2, User Guide.* Aspen Technology Inc, 2010.

145. Shiflett, M.B., A.M.S. Niehaus, and A. Yokozeki, *Separation of CO2 and H2S using room-temperature ionic liquid [bmim][MeSO4].* Journal of Chemical & Engineering Data, 2010. **55**(11): p. 4785-4793.

146. Vitu, S., et al., *Predicting the phase equilibria of CO 2+ hydrocarbon systems with the PPR78 model (PR EOS and k ij calculated through a group contribution method).* The Journal of Supercritical Fluids, 2008. **45**(1): p. 1-26.

147. Jaubert, J.N., R. Privat, and F. Mutelet, *Predicting the phase equilibria of synthetic petroleum fluids with the PPR78 approach.* AIChE journal, 2010. **56**(12): p. 3225-3235.

148. Aslan, N. and Y. Cebeci, *Application of Box–Behnken design and response surface methodology for modeling of some Turkish coals.* Fuel, 2007. **86**(1-2): p. 90-97.

149. Belhaj, D., et al., *Box-Behnken design for extraction optimization of crude polysaccharides from Tunisian Phormidium versicolor cyanobacteria (NCC 466): partial characterization, in vitro antioxidant and antimicrobial activities.* International journal of biological macromolecules, 2017. **105**: p. 1501-1510.

150. Diba, K.D., M. Guglielminetti, and S. Schiavo. *Glycol reclaimer.* in *Offshore Mediterranean Conference and Exhibition. Offshore Mediterranean Conference.* 2003.

151. Soames, A., et al., *Operation of a MEG pilot regeneration system for organic acid and alkalinity removal during MDEA to FFCI switchover.* Journal of Petroleum Science and Engineering, 2018. **169**: p. 1-14.

152. Maller, C., et al., *Healthy nature healthy people:'contact with nature'as an upstream health promotion intervention for populations.* Health promotion international, 2006. **21**(1): p. 45-54.

153. Orr, D.W., *Earth in mind: On education, environment, and the human prospect.* 2004: Island Press.

154. Da Silva, E.M., et al., *Impact of petroleum pollution on aquatic coastal ecosystems in Brazil.* Environmental Toxicology and Chemistry, 1997. **16**(1): p. 112-118.

155. Harrison, R.M., *An introduction to pollution science.* 2006: Royal Society of Chemistry.

156. Daghetti, A., et al., *Adsorption of aliphatic monoethers of ethylene glycol (alkoxyethanol) at the free water surface and at the Hg/solution interface.* Journal of Electroanalytical Chemistry and Interfacial Electrochemistry, 1986. **204**(1): p. 299-313.

157. Robinson, M., et al., *Subacute and Subchronic Toxicity of Ethylene Glycol Administered in Drinking Water to Sprague-Dawley Rats.* Drug and Chemical Toxicology, 1990. **13**(1): p. 43-70.

158. Devold, H., *Oil and gas production handbook: an introduction to oil and gas production.* 2013: Lulu. com.

159. Orecki, A., et al., *Separation of ethylene glycol from model wastewater by nanofiltration.* Desalination, 2006. **200**(1-3): p. 358-360.

160. Evans, W. and E. David, *Biodegradation of mono-. di-and triethylene glycols in river waters under controlled laboratory conditions.* Water Research, 1974. **8**(2): p. 97-100.

161. Van der Bruggen, B., M. Mänttäri, and M. Nyström, *Drawbacks of applying nanofiltration and how to avoid them: A review.* Separation and Purification Technology, 2008. **63**(2): p. 251-263.

162. Teamkao, P. and P. Thiravetyan, *Bioremediation of MEG, DEG, and TEG: Potential of Burhead Plant and Soil Microorganisms.* World Academy of Science, Engineering and Technology, International Journal of Biological, Biomolecular, Agricultural, Food and Biotechnological Engineering, 2012. **6**(10): p. 947-950.

163. Robinson, T., et al., *Remediation of dyes in textile effluent: a critical review on current treatment technologies with a proposed alternative.* Bioresource technology, 2001. **77**(3): p. 247-255.

164. Ali, I. and V. Gupta, *Advances in water treatment by adsorption technology.* Nature protocols, 2006. **1**(6): p. 2661.

165. Namasivayam, C. and D. Kavitha, *Removal of Congo Red from water by adsorption onto activated carbon prepared from coir pith, an agricultural solid waste.* Dyes and pigments, 2002. **54**(1): p. 47-58.

166. Monser, L. and N. Adhoum, *Modified activated carbon for the removal of copper, zinc, chromium and cyanide from wastewater.* Separation and purification technology, 2002. **26**(2-3): p. 137-146.

167. Wang, S. and Y. Peng, *Natural zeolites as effective adsorbents in water and wastewater treatment.* Chemical Engineering Journal, 2010. **156**(1): p. 11-24.

168. Hui, K., C.Y.H. Chao, and S. Kot, *Removal of mixed heavy metal ions in wastewater by zeolite 4A and residual products from recycled coal fly ash.* Journal of Hazardous Materials, 2005. **127**(1-3): p. 89-101.

169. Lin, K.-Y.A., Y.-T. Liu, and S.-Y. Chen, *Adsorption of fluoride to UiO-66-NH 2 in water: stability, kinetic, isotherm and thermodynamic studies.* Journal of colloid and interface science, 2016. **461**: p. 79-87.

170. Azhar, M.R., et al., *Adsorptive removal of antibiotic sulfonamide by UiO-66 and ZIF-67 for wastewater treatment.* Journal of colloid and interface science, 2017. **500**: p. 88-95.

171. Wang, B., et al., *Highly stable Zr (IV)-based metal–organic frameworks for the detection and removal of antibiotics and organic explosives in water.* J. Am. Chem. Soc, 2016. **138**(19): p. 6204-6216.

172. Li, X., et al., *Mechanistic insight into the interaction and adsorption of Cr (VI) with zeolitic imidazolate framework-67 microcrystals from aqueous solution.* Chemical Engineering Journal, 2015. **274**: p. 238-246.

173. Azhar, M.R., et al., *One-pot synthesis of binary metal organic frameworks (HKUST-1 and UiO-66) for enhanced adsorptive removal of water contaminants.* Journal of colloid and interface science, 2017. **490**: p. 685-694.

174. Lin, K.-Y.A., et al., *Removing oil droplets from water using a copper-based metal organic frameworks.* Chemical engineering journal, 2014. **249**: p. 293-301.

175. Khan, N.A., Z. Hasan, and S.H. Jhung, *Adsorptive removal of hazardous materials using metal-organic frameworks (MOFs): a review.* Journal of hazardous materials, 2013. **244**: p. 444-456.

176. Hasan, Z. and S.H. Jhung, *Removal of hazardous organics from water using metal-organic frameworks (MOFs): plausible mechanisms for selective adsorptions.* Journal of hazardous materials, 2015. **283**: p. 329-339.

177. Rada, Z.H., et al., *Functionalized UiO-66 by Single and Binary (OH) 2 and NO2 Groups for Uptake of CO2 and CH4.* Industrial & Engineering Chemistry Research, 2016. **55**(29): p. 7924-7932.

178. Abid, H.R., H.M. Ang, and S. Wang, *Effects of ammonium hydroxide on the structure and gas adsorption of nanosized Zr-MOFs (UiO-66).* Nanoscale, 2012. **4**(10): p. 3089-3094.

179. Abid, H.R., et al., *Nanosize Zr-metal organic framework (UiO-66) for hydrogen and carbon dioxide storage.* Chemical Engineering Journal, 2012. **187**: p. 415-420.

180. Biswas, S., et al., *Partially fluorinated MIL-47 and Al-MIL-53 frameworks: influence of functionalization on sorption and breathing properties.* Physical Chemistry Chemical Physics, 2013. **15**(10): p. 3552-3561.

181. Haul, R., *Adsorption, Surface Area and Porosity.* Zeitschrift für Physikalische Chemie, 1969. **63**(1_4): p. 220-221.

182. Thommes, M., et al., *Adsorption hysteresis of nitrogen and argon in pore networks and characterization of novel micro-and mesoporous silicas.* Langmuir, 2006. **22**(2): p. 756-764.

183. Cavka, J.H., et al., *A new zirconium inorganic building brick forming metal organic frameworks with exceptional stability.* Journal of the American Chemical Society, 2008. **130**(42): p. 13850-13851.

184. Abid, H.R., et al., *Adsorption of CH4 and CO2 on Zr-metal organic frameworks.* Journal of colloid and interface science, 2012. **366**(1): p. 120-124.

185. Furukawa, H., et al., *Water adsorption in porous metal–organic frameworks and related materials.* Journal of the American Chemical Society, 2014. **136**(11): p. 4369-4381.

186. Canivet, J., et al., *Water adsorption in MOFs: fundamentals and applications.* Chemical Society Reviews, 2014. **43**(16): p. 5594-5617.

187. Ghosh, P., Y.J. Colón, and R.Q. Snurr, *Water adsorption in UiO-66: the importance of defects.* Chemical Communications, 2014. **50**(77): p. 11329-11331.

188. Wang, C.-C., et al., *Adsorption of basic dyes onto montmorillonite.* Journal of Colloid and Interface Science, 2004. **273**(1): p. 80-86.

189. Ryu, M.Y., et al., *Effect of the pH and basic additives on the precipitation of calcium carbonate during carbonation reaction.* Resources Processing, 2007. **54**(1): p. 14-18.

190. Abid, H.R., et al., *Adsorption of CH 4 and CO 2 on Zr-metal organic frameworks.* Journal of colloid and interface science, 2012. **366**(1): p. 120-124.

191. Bernal, V., et al., *Effect of solution pH on the adsorption of paracetamol on chemically modified activated carbons.* Molecules, 2017. **22**(7): p. 1032.

192. Largergren, S., *Zur theorie der sogenannten adsorption geloster stoffe. Kungliga Svenska Vetenskapsakademiens.* Handlingar, 1898. **24**(4): p. 1-39.

193. Ho, Y.-S. and G. McKay, *Pseudo-second order model for sorption processes.* Process biochemistry, 1999. **34**(5): p. 451-465.

194. Graaf, G., et al., *Intra-particle diffusion limitations in low-pressure methanol synthesis.* Chemical Engineering Science, 1990. **45**(4): p. 773-783.

195. de Menezes, E.W., et al., *Ionic silica based hybrid material containing the pyridinium group used as an adsorbent for textile dye.* Journal of colloid and interface science, 2012. **378**(1): p. 10-20.

196. Ho, Y.-S., *Review of second-order models for adsorption systems.* Journal of hazardous materials, 2006. **136**(3): p. 681-689.

197. Dąbrowski, A., et al., *Adsorption of phenolic compounds by activated carbon—a critical review.* Chemosphere, 2005. **58**(8): p. 1049-1070.

198. Kannan, N. and M.M. Sundaram, *Kinetics and mechanism of removal of methylene blue by adsorption on various carbons—a comparative study.* Dyes and pigments, 2001. **51**(1): p. 25-40.

199. Loucks, R.G., et al., *Origin and classification of pores in mudstones from shale-gas systems.* Search and Discovery Article, 2011. **40855**: p. 1-32.

200. Lin, D.-R., et al., *Mechanisms of competitive adsorption organic pollutants on hexylene-bridged polysilsesquioxane.* Materials, 2015. **8**(9): p. 5806-5817.

201. Langmuir, I., *The constitution and fundamental properties of solids and liquids. Part I. Solids.* Journal of the American chemical society, 1916. **38**(11): p. 2221-2295.

202. Chaudhary, N., et al., *Removal of Phenol Using Fly Ash and Impregnated Fly Ash: An Approach to Equilibrium, Kinetic, and Thermodynamic Study.* Separation Science and Technology, 2015. **50**(5): p. 690-699.

203. Dada, A., et al., *Langmuir, Freundlich, Temkin and Dubinin–Radushkevich isotherms studies of equilibrium sorption of Zn2+ unto phosphoric acid modified rice husk.* IOSR Journal of Applied Chemistry, 2012. **3**(1): p. 38-45.

204. Weber, T.W. and R.K. Chakravorti, *Pore and solid diffusion models for fixed-bed adsorbers.* AIChE Journal, 1974. **20**(2): p. 228-238.

205. Mohan, S.V. and J. Karthikeyan, *Removal of lignin and tannin colour from aqueous solution by adsorption onto activated charcoal.* Environmental Pollution, 1997. **97**(1): p. 183-187.

206. Liu, S., *Cooperative adsorption on solid surfaces.* Journal of Colloid and Interface Science, 2015. **450**(Supplement C): p. 224-238.

# Nomenclature

| | |
|---|---|
| $a_e$ | Effective interfacial area of packing, 1/m |
| $a_p$ | Packing specific surface area, 1/m |
| $d_{eq}$ | Equivalent diameter of flow channel, m |
| $D_L$ | Liquid diffusivity, $m^2/s$ |
| $D_G$ | Gas diffusivity, $m^2/s$ |
| g | Gravitational constant, $m/s^2$ |
| $G_m$ | Gas flowrate within the column, kgmole/hr |
| HETP | Height Equivalent to a Theoretical Plate, m |
| $H_G$ | Height of gas phase transfer unit, m |
| $H_L$ | Height of liquid phase transfer unit, m |
| $H_{OG}$ | Overall height of transfer unit in gas phase, m |
| HTU | Height of mass-transfer unit, m |
| $k_G$ | Gas-side mass-transfer coefficient, m/s |
| $k_L$ | Liquid-side mass-transfer coefficient, m/s |
| $L_m$ | Liquid flow rate within column, kgmole/hr |
| m | Average slope of the VLE curve |
| M | Molecular weight, g/gmole |
| N | Number of theoretical stages |
| $N_{min}$ | Minimum number of theoretical stages |
| NTU | Number of transfer units |
| P | Operating pressure, atm/bar |
| $R_{min}$ | Minimum reflux ratio |
| s | Corrugation side length, m |
| u | Superficial fluid velocity, $m/s$ |
| V | Molar volume at normal boiling point |
| x | Mole fraction of component in liquid phase |
| $x_A, x_B$ | Mole fraction of the more volatile and less volatile component respectively |
| y | Vapour phase composition |
| $y^*$ | Equilibrium vapour phase composition |
| Z | Height of packing |

| | |
|---|---|
| α | Relative volatility |
| | Corrugation inclination angle, °deg |
| $\epsilon$ | Packing void fraction |
| $\varepsilon/k_B(°K)$ | Lennard-Jones potential parameters |
| Γ | Liquid flow rate based on perimeter, $kg/m.s$ |
| λ | Ratio of gas to liquid molar flow rates |
| | Stripping factor |
| Ω | Collision integral |
| ψ | Molokanov variable in Equation |
| ρ | Density of vapour or liquid, $kg/m^3$ |
| μ | Viscosity of vapour or liquid kg/m.s |
| ν | Kinematic viscosity of vapour of liquid $m^2/s$ |
| σ | Surface tension of fluid, $N/m$ |
| | collision diameter of particle (Å) |

**List of Abbreviations** (Figure 4-1)

| | |
|---|---|
| B.V | Ball Valve |
| CH.V | Check Valve |
| CO | Total Condenser |
| DC | Distillation Column |
| H-Ex | Heat Exchanger |
| LG | Level Gauge |
| LS | Level Sensor |
| LT | Level Transmitter |
| MFM | Mass Flow Meter |
| N.V | Needle Valve |
| PDI | Pressure Differential Indicator |
| PG | Pressure Gauge |
| RB | Reboiler |
| RD | Reflux Drum |
| SV | Safety Valve |
| TG | Temperature Gauge |
| V | Valve |

Appendix 1: MEG Benchtop Facility Start-up and Shut-Down Procedures.

## A- Start-up and shut-down procedures for distillation column DC-201, Reboiler RB-201 and micro pumps P9 and P10 (Figure 3-2)

1. <u>Distillation column DC-201and Reboiler RB-201 start-up procedure:</u>

1.1.    Ensure that nitrogen dewar have enough pressure to supply nitrogen to the distillation column.

1.2.    Ensure rich glycol tank RGT-301 is lined up (refer to procedure C)

1.3.    Ensure that all valves are correctly positioned;

      1.3.1.   Ensure reboiler RB-201 sample point valve (V-C11) is closed.

      1.3.2.   Ensure nitrogen gas valve V-C9 is open.

1.4.    Introduce nitrogen gas to the inlet of the distillation column (ensure the whole distillation column system is purged with nitrogen)

1.5.    Introduce nitrogen for sparging the reflux tank (RD-201) by:

      1.5.1. Making sure monometer is full with the required water to provide a back pressure of 4.4 Kpa.

      1.5.2. Open the nitrogen dewar valve and adjust pressure regulator to supply nitrogen with a pressure around 20 Kpa (ensure bubbles are coming out of monometer)

1.6.    Fill the reboiler RB-201 with rich MEG from make-up points up to the required level of around 75% (ensure to fill it to a level above the heating elements)

1.7.    Line up the overhead reflux condenser CO-201by:

      1.7.1.   Opening the inlet valve (V-C16)

      1.7.2.   Opening the outlet valve (V-C17)

1.8.    Switch on the water chiller (ensure chiller is full of water)

1.9.    Switch on the reboiler electric heater and set the required temperature from PLC (110 ºC). (Ensure reboiler liquid level is above the heating element).

1.10.   Monitor the reboiler level via the reboiler and the PLC screen.

1.11.   Check for leaks.

1.12.   Switch on the rich glycol tank micro pump P8.

2. Reboiler pump P9 start-up procedure:

2.1. Ensure that distillation column DC-201and Reboiler RB-201 start-Up procedure is completed.

2.2. Ensure that Mass Flow Meter (C19) is lined up and ready to receive liquid from the pump by opening the inlet valve (V-C25) and outlet valve (V-C28).

2.3. Line up the heat exchanger (Hex-301) by;

      2.3.1. Opening inlet water supply (C15) (F4 port)

      2.3.2. Opening outlet water supply valve (C22) (F2 port)

      2.3.3. Opening hotline inlet valve (VC14) (F1 port)

      2.3.4. Opening hotline outlet valve (VC24) (F3 port)

2.4. Open the reboiler outlet valve (V-C10)

2.5. Open and line up the three way valve V-C24 (after the hex-301)

2.6. Ensure that lean glycol tank LGT-105 and/ or reclaimer (Rotary Evaporator) is ready to receive lean glycol from the pump.

2.7. Ensure lean glycol tank inlet valve (V-A13) is open

2.8. Ensure VC23 the inlet valve of the sample baker (SB-302) is closed.

2.9. Open pump discharge valve (VC13)

2.10. Ensure pump back pressure gauge (C21) is reading less than 1.3 Kpa.

2.11. Start the pump and select the required flow rate (using centralised PLC control system).


3. Distillation column pump P10 start-up procedure:

3.1. Ensure that distillation column DC-201and Reboiler RB-201 start-Up procedure is completed.

3.2. Ensure that Mass Flow Meter (C20) is lined up and ready to receive liquid from the pump.

3.3. Ensure VC23 the inlet valve of the sample baker (SB-301) is closed.

3.4. Open the pump discharge valve V-C20.

3.5. Start the pump and select the required flow rate (using centralised PLC control system).

3.6. Ensure pump discharge pressure gauge (C16) is reading less than 0.8 bar.

Note: Make frequent checks of distillation column and reboiler parameters and pump rate during the first few hours of operation.

4. Distillation column DC-201and Reboiler RB-201 shut-down procedure:

4.1.    Ensure the downstream and upstream parts of the distillation column, reboiler, pump P9 and P10 are ready for the liquid stoppage.

4.2.    Close distillation inlet valve (V-C13)

4.3.    Stop the pumps P9 and P10.

4.4.    Close the distillation column outlet valve (V-C22)

4.5.    Close the reboiler outlet three way valve (V-C31)

4.6.    Close the nitrogen gas valve VC9.

5. Pumps P9/P10 shut-down procedure:

5.1.    Ensure the distillation column DC-201and the reboiler RB-201 shut-down procedure is completed.

5.2.    Ensure the downstream and upstream parts of pump P9 and P10 are ready for liquid stoppage.

5.3.    Stop the pumps

# B-Start-up and shut-down procedures for Lean Glycol Tank LGT-105 and micro pump P3

6. Lean Glycol Tank LGT-105 start-up procedure:

6.1.    Ensure that the nitrogen dewar have enough pressure to supply nitrogen to the tank.

6.2.    Ensure that enough lean glycol is available to fill the tank to around 20%  (note: water to be used to fill the tank when commissioning)

6.3.    Ensure that all valves are correctly positioned;

6.3.1.  Ensure the drain valve (V-A14) is closed

6.3.2.  Ensure the nitrogen blanket valve (V-A11) is open

6.3.3.  Ensure the sparging valve (V-A16) is open.

6.3.4. Ensure the lean MEG make up valves from reboiler are open (V-C13, V-C14, and V-C24).

6.4. Fill the tank with lean glycol from make-up point up to the required level of around 20%

6.5. Introduce nitrogen for blanketing and sparging by:

6.5.1. Making sure the monometer is full with the required water to provide a back pressure of 9.8 Kpa.

6.5.2. Open the nitrogen dewar valve and adjust pressure regulator to supply nitrogen with a pressure of around 20 Kpa (ensure bubbles are coming out of monometer)

6.5.3. Open the sparging valve (V-A16)

6.6. Monitor the tank level via the PLC screen.

6.7. Check for leaks


7. Micro pump P3 start-up procedure:

7.1. Ensure that the lean glycol Tank LGT-105 Start-Up procedure is completed.

7.2. Ensure that the Mass Flow Meter (A18) is lined up and ready to receive lean glycol from the pump.

7.3. Ensure that Feed Blending Vessel FB-103 is ready to receive lean glycol from the pump.

7.4. Ensure that the lean glycol Tank LGT-105 outlet valve (V-A15) is open.

7.5. Ensure that the pump discharge valve (V-A24) is open.

7.6. Ensure that valve (V-A25) on the line to the rotary evaporator (reclamation unit)  is at the required position

7.7. Start the pump and select the required flow rate (using centralised PLC control system).

Note: Make frequent checks of the tank level, pressures, pump rate, during the first few hours of operation.

8. Lean glycol Tank LGT-105 shut-down procedure:

8.1. Ensure that the downstream part of the tank and micro pump P3 are ready for the stoppage of the lean glycol.

8.2. Stop the micro pump P3

8.3. Close the outlet valve (V-A15)

8.4.    Close the nitrogen blanket valve V-A11

8.5.    Close the nitrogen sparging valve V-A16

9.  Micro pump P3 shut-down procedure:

9.1.    Ensure that the shutdown procedure of lean glycol tank LGT-105 procedure is completed

9.2.    Ensure that the Feed Blending Vessel FB-103 and rotary evaporator units are ready for the stoppage of the lean glycol.

9.3.    Stop the pump

## C-    Start-up and shut-down procedures for Rich Glycol Tank RGT-301 and dosage pump P8

10. Rich Glycol Tank RGT-301 start-up procedure:

10.1.    Ensure that the nitrogen dewar have enough pressure to supply nitrogen to the tank.

10.2.    Ensure that all the valves are correctly positioned;

    10.2.1. Ensure that drain valve (V-C3) is closed

    10.2.2. Ensure that nitrogen blanket valve (V-C2) is open

    10.2.3. Ensure that rich glycol make up valve (V-C1) is open

    10.2.4. Ensure that sample point valve VC27 is closed.

10.3.    Fill the tank with rich glycol from the make-up point up to the required level of around 20%

10.4.    Introduce nitrogen for blanketing and sparging by:

    10.4.1. Making sure the monometer is full with required water to provide a back pressure of 9.8 Kpa.

    10.4.2. Open nitrogen dewar valve and adjust pressure regulator to supply nitrogen with a pressure of around 20 Kpa (ensure bubbles are coming out of the vmonometer)

10.5.    Monitor the tank level via the PLC screen and the sight glass.

10.6.    Check for leaks.

11. <u>Micro pump P8 start-up procedure:</u>

11.1.    Ensure that the rich glycol Tank RGT-301 Start-Up procedure is completed.

11.2.    Ensure that the required filter (F-301/F302) is lined up by adjusting the three way valves V-C8 and V-C7.

11.3.    Ensure that the Mass Flow Meter (C9) is lined up and ready to receive rich glycol from the pump.

11.4.    Ensure that the distillation column DC-201 and reboiler RB-201 are ready to receive rich glycol from the pump.

11.5.    Ensure that the rich glycol Tank RGT-301 outlet valve (V-C4) is open.

11.6.    Ensure that the pump discharge valve (V-C6) is open.

11.7.    Start the pump and select the required flow rate (using centralised PLC control system).

11.8.    Monitor the filters differential pressure by comparing the pressure at pressure gauge C6 (after P8) and the pressure gauge C29 (after filters).

<u>Note:</u> Make frequent checks of the tank level, pressures, pumping rate, during the first few hours of operation.

12. <u>Rich glycol Tank RGT-301 and Micro pump P8 shut-down procedure:</u>

12.1.    Ensure that the distillation column DC-201 and the reboiler RB-201 and the micro pump P8 are ready for the stoppage of rich the glycol.

12.2.    Close the rich glycol make up valve (V-C1)

12.3.    Stop that the micro pump P8

12.4.    Close the outlet valve (V-C4)

12.5.    Close the nitrogen blanket valve V-C2

## D-    Start-up and shut-down procedures for the rotary evaporator

13. <u>Rotary Evaporator start-up procedure:</u>

13.1.    Ensure that the distillation column DC-201, Reboiler RB-201 and dosage pumps P9 start-up procedure is completed.

13.2.    Switch on the rotary evaporator power.

13.3. Fill the bath of the rotary evaporator with thermal oil to the required level of around 60%.

13.4. Turn on the rotary evaporator unit following the below steps:
- Turn on the rotary evaporator  (using on/off soft key)
- Run menus check list
- Select scale units of vacuum pressure (100 mbar) and temperature (120 $^{\circ}$C)
- Click the menu settings.
- Set date and time (using the soft key arrow)
- Set glassware assembly parameters
- Set flask rotation speed (30 RPM)

13.5. Line up the line of lean MEG form the Lean MEG Tank to the rotary evaporator by open V-A25, V-A16 (recycle line) and starting P3.


14. <u>Rotary Evaporator shut-down procedure:</u>

14.1. Ensure that the downstream part of the rotary evaporator is ready for the liquid stoppage.

14.2. Turn off the unit.

14.3. Close the inlet and outlet valves.
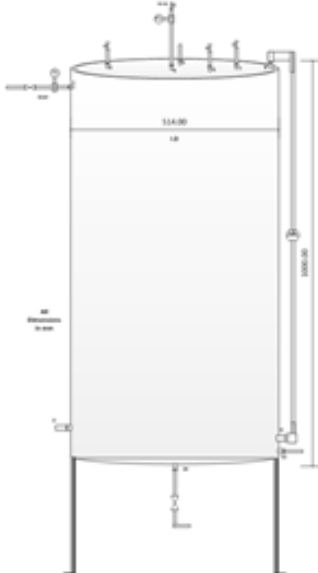
Appendix.2: Equipment Data Sheet (EDS) for Rich & Lean MEG Tanks and Distillation Column.

## 1- Rich MEG Tank

| Material : Stainless steel 316 | | | |
|---|---|---|---|
| Shape :Vertical Cylindrical Vessel | | | |
| **Operating Data** | | | |
| Stream | | *In* | *out* |
| Stream Number | | 22 | 23 |
| Max Operating Temperature(°C) | | 80 | |
| Max Operating Pressure(bar) | | 1.25 | |
| Mass Flow Rate(Kg/hr) | | 5.062 | 5.062 |
| Density(Kg/m³) | | 1014 | 1014 |
| Volumetric flow rate (cc/min) | | 83.167 | 83.167 |
| Design Temperature(°C) | | 120 | |
| Design Pressure(bar) | | 1.8 | |

**Mechanical Design Details**

| **Shell** | | **Head (Flanged)** | |
|---|---|---|---|
| Material | S.S 316 | Material | S.S 316 |
| Type | | Type | Flat |
| Diameter(m) | 0.514 | Thickness | TBC by fabricator |
| Height(m) | 1 | Joint Factor | 1 |
| Orientation | Vertical | Radiography% | 100 |
| Thickness(mm) | | **Bottom (welded)** | |
| Corrosion Allowance(mm) | N/A | Material | S.S 316 |
| Joint Factor | 1 | Type | Hemispherical |
| Weight Of Vessel (N) | | Thickness | TBC by fabricator |
| **Support** | | Joint Factor | 1 |
| Type of Support | Legs | Radiography% | 100 |
| Thickness | TBC by fabricator | **Overall** | |
| **Insulation** | | Design Code | |

| Painting | Jotun |
|---|---|

**Nozzle Schedule**

| No | Service | Size(mm) | Orientation |
|---|---|---|---|
| 1 | Feed line | 6.35 | Side |
| 2 | N2 line | 6.35 | Top |
| 3 | O2 probe | 12.7 | Side |
| 4 | Pressure relief line | 6.35 | Top |
| 5 | Pressure transmitter | 6.35 | Top |
| 6 | N2 throttling line | 6.35 | Top |
| 7 | Lean MEG make up line | 6.35 | Top |
| 8 | Level gauge | 6.35 | Side |
| 9 | Level gauge | 6.35 | Side |
| 10 | Drain line | 6.35 | Bottom |
| 11 | Product line | 6.35 | Side |
| 12 | Corrosion probe | 25.4 | Side |
| 13 | Conductivity probe | 12.7 | Side |

## 2- Lean MEG Tank

| Material : Stainless Steel 316 | | | | |
|---|---|---|---|---|
| Shape :Vertical Cylindrical Vessel | | | | |
| **Operating Data** | | | | |
| Stream | | In | | Out |
| Stream Number | 41 | 42 | | 6 |
| Max Operating Temperature(°C) | 80 | 80 | | 30 |
| Max Operating Pressure(bar) | 1.7 | 1.8 | | 1.25 |
| Mass Flow Rate(Kg/hr) | 0.8486 | 2.410 | | 2.0821 |
| Density(Kg/m³) | 1075 | 1004 | | 1098 |
| Volumetric flow rate (cc/min) | 13.15 | 40 | | 31.6 |
| Design Temperature(°C) | 120 | | | |
| Design Pressure(bar) | 2.55 | | | |

### Mechanical Design Details

| Shell | | | Head (Flanged) | |
|---|---|---|---|---|
| Material | | S.S 316 | Material | S.S 316 |
| Type | | | Type | Flat |
| Diameter(m) | | 0.514 | Thickness | |
| Height(m) | | 1 | Joint Factor | 1 |
| Orientation | | Vertical | Radiography% | 100 |
| Thickness(mm) | | | **Bottom (welded)** | |
| Corrosion Allowance(mm) | | N/A | Material | S.S 316 |
| Joint Factor | | 1 | Type | Hemispherical |
| Weight Of Vessel (N) | | | Thickness | |
| **Support** | | | Joint Factor | 1 |
| Type of Support | | Legs | Radiograph% | 100 |
| Thickness | | TBC by fabricator | **Overall** | |
| **Insulation** | | | Design Code | |
| Painting | | Jotun | | |

| Nozzle Schedule | | | |
|---|---|---|---|
| No | Service | Size(mm) | Orientation |
| 1 | Feed line | 6.35 | Side |
| 2 | N2 line | 6.35 | Top |
| 3 | O2 probe | 12.7 | Side |
| 4 | Pressure relief line | 6.35 | Top |
| 5 | Pressure transmitter | 6.35 | Top |
| 6 | N2 throttling line | 6.35 | Top |
| 7 | Lean MEG make up line | 6.35 | Top |
| 8 | Level gauge | 6.35 | Side |
| 9 | Level gauge | 6.35 | Side |
| 10 | Drain line | 6.35 | Bottom |
| 11 | Product line | 6.35 | Side |
| | | | |
| | | | |
| | | | |

### 3- MEG Distillation Column

| Distillation Process | Continuous | | |
|---|---|---|---|
| **MEG Distillation Column operating data** | **FEED** | **TOP** | **BOTTOM** |
| Temperature(˚C) | 25 -50 | 20.69 | 125- 145 |
| Pressure(bar) | 1.30 | 1.25 | 1.35 |
| Mass Flow Rate(Kg/hr) | 4-9 | 1-3 | 1.5-5 |
| Component (H$_2$O wt. %: MEG wt. %) | 70:30 – 73:27 | 100:00 | 15: 85 – 13:87 |
| Density(Kg/m$^3$) | 1054 | 1019 | 1004 |
| **QVF Distillation Column Operating Range** | | | |
| Operating Temperature range | -20°C to +150 °C | | |
| Operating Pressure Range | -1 bar to +1.5 bar | | |
| **Mechanical Design Details** | | | |

| **Column – DC201** | | **Packing** | |
|---|---|---|---|
| Material | Borosilicate Glass 3.3 | Material | |
| Nominal Diameter | DN 80 (3 inches ) | Nominal Diameter | DN 80 (3 inches ) |
| Total Height | 3.5 m | **Reflux Drum – RD201** | |
| Packing Height | 2 x 900 mm | Type | Vertical cylindrical vessel |
| **Reboiler – RB201** | | Material | Borosilicate Glass 3.3 |
| Type | Horizontal cylindrical vessel | Nominal Diameter | DN 150 |
| Material | Borosilicate Glass 3.3 | Capacity | 5 litres |
| Nominal Diameter | DN 150 | | |
| Nominal Capacity | 6 litres | | |

| **Support and structure** | |
|---|---|
| Type of Support | Modular (SS 1 ¼" Pipe) |
| Dimensions (w x d x h) | 1500 x 1000 x 3500 mm |

**Nozzle Schedule**

| Qty | Type | Size(mm) | Location |
|---|---|---|---|
| 1 | Feed | | Column |
| | | | |
| 1 | Electrical heater | DN50 | |
| 1 | Column | DN80 | |
| 1 | Level switch | DN25 | Reboiler |
| 1 | Pressure Measuring | DN25 | |
| 1 | Bottom outlet | DN25 | |
| | | | |
| 1 | Reflux from Condenser | DN25 | |
| 1 | To Relief Valve and Vent | DN25 | |
| | | | |
| 1 | Pressure Gauge | DN40 | Reflux Drum |
| 1 | Level Switch | DN50 | |
| 1 | Bottom Outlet | DN25 | |

# Appendices.3: Valves and Fittings List

| Parts | Swagelok part no | Function | Schematic |
|---|---|---|---|
| SS 1-piece 40 series ball valve | SS-43GS4 | Open and close, isolation purpose | |
| SS Poppet 6000 psig(413bar) check valve | SS-CHS4-1 | Prevent backflow | |
| SS integral bonnet needle valve, 0.37Cv, ¼ in regulating stem | 1RS-4 | For regulating purpose | |
| SS Low pressure proportional relief valve, 1/4'' Swagelok tube fitting | RL3S4 | Prevent overpressure the vessel and to be connected to the vent line | |
| SS 1-piece 40 series 3 way ball valve | SS-42GXS4 | For switching flow pattern | |
| Union Tee, 1/4 inch | SS-400-3 | For combining two streams into one or splitting one stream into two | |
| Stainless Steel Pipe Fitting, Pipe Cap, 1/4 in. Female NPT | SS-4-CP | For plugging extra end connections | |
| Union cross, ¼ inch | N/A | For combining or splitting of streams | |
| SAF 2507 Super Duplex Swagelok Tube Fitting, Union Elbow, 1/4 in. Tube OD | 2507-400-9 | For connecting two tubing with an angle of 90 degrees | |
| Alloy 400 Swagelok Tube Fitting, Female Branch Tee, 1/4 in. Tube OD x 1/4 in. Tube OD x 1/4 in. Female NPT | M-400-3-4TTF | For installation of pressure gauges with male thread | |
| SAF 2507 Super Duplex Swagelok Tube Fitting, Union, 1/4 in | 2507-400-6 | For connection of two tubing | |
| 316/316L SS Seamless Tubing, 1/4 in. | SS-T4-S-035-20 | Tubing | |
| 316 SS Nut and Ferrule Set (1 Nut/1 Front Ferrule/1 Back Ferrule) for 1/4 in. | SS-400-NFSET | For connection of tubing, fittings, parts | |

Appendices.4: Features and Benefits for InPro 4850i pH Probe, InPro 6850i polarographic oxygen sensor and InPro 7100 Conductivity Meter

1- InPro 4850i pH Probe

| Dual-membrane; pNa reference system | Long lifetime, hermetically sealed, high accuracy and low maintenance. |
|---|---|
| Solution ground and shielding | Stabilize the signal and enable redox measurement. |
| Digital signal | 100% signal integrity. Immunity to electrical interference and signal distortion ensures stable and accurate data. |

2- InPro 6850i polarographic oxygen sensor

| High measurement stability | The new 3-electrode principle with its separated platinum anode for higher signal stability |
|---|---|
| Enhanced diagnostics | Permanent sensor monitoring with ISM technology reduces the risk sensor failures |
| Predictive maintenance | The enhanced diagnostics allows for better maintenance planning "as few as possible, as often as necessary" |
| High process safety | FDA compliant materials of construction and easy-to-clean high-polished surface (N5 grade) to satisfy increasing regulatory requirements |
| Reduced service time | easy-to-replace membrane body and quick-disconnect interior body. |
| Long sensor lifetime | Durable and rugged sensor design for increased resistance to harsh environments<br>Installation in hazardous zones |

3- InPro 7100 Conductivity Meter

| High versatility | The InPro 7100 is compatible with a wide choice of static (InFit and InDip series) and retractable (InTrac series) housings. |
|---|---|
| WideRange™ technologySaving costs and increasingmeasurement accuracy | WideRange™ technology keeps the sensor design small and easy to install. That allows installation in pipes with small diameters (DN50). |
| Fast response time | The InPro 7100´s response time allows quick detection of process changes, leading to better process control. Benefits are:<br>- Increased yield<br>- High product quality<br>- Cost saving in the production process |
| Easy process integration | The compact design of the InPro 7100 makes it compatible with the wide choice of INGOLD housings, opening a wide range of integration options. |

Appendix.5: Safety Hazop

## Courtyard (Plot Plan Option 2) - **Area 300** - (Refer P&ID MPP-300-C)

| **Description** **From STORGE TANK-201 TO FEED DISTILLATION COLUMN DC-201** The column utilizes structured packing to carry out the separation of MEG and water. Rich MEG is distilled by removing water as the overhead product and lean MEG (>85 wt. %) is collected as bottom product. For versatility and ease in operations, electric immersion heating element has been chosen for the heating requirements in the Re-boiler | | | | | | | | **Equipments:** Rich MEG tank, MEG Distillation column, MEG Reboiler, overhead condenser, reflux drum and associated equipment | | | | | |

| Item N° | Deviation | Causes | Consequences | Inherent Risk | | | | Safeguards | Residual Risk | | | | Recommendations |
|---------|-----------|--------|--------------|-----|-----|-----|------|------------|-----|-----|-----|------|-----------------|
| | | | | Cat | Con | Li | Risk | | Cat | Con | Li | Risk | |
| 1.1 | Fire | . Electrical fault, loss of control at Reboiler, Human error, extreme weather conditions | Personal injury, loss of equipment | | Major | Possible | High Risk | High temperature sensors and alarm at regular intervals on distillation column and MEG Reboiler. Visible warning signs. Meshed floors to prevent build-up of fluid leakage. Fire extinguisher, Personal protective equipment. Avoid operating during extreme weather conditions, CO2 fire extinguishers or Dry powder extinguisher or foam extinguishers, Smoke Detectors, Water Showers and Fire blankets | | Minor | Possible | Medium Risk | Assess potential fire hazards around high temperature equipment. Weekly check-up for fire extinguisher and warning signs. Call 000 for emergency situation and Curtin Emergency Services 08-9266 4444. Fire emergency response training. Upgrade or review building emergency plan. |
| 1.2 | Power failure | Electrical fault. Over consumption of power limit in building 614. Weather conditions. Human error. | Unsteady state in MEG distillation systems. Deviation from normal operating conditions. loss of control system and operation.. | | Moderate | Unlikely | Medium Risk | Provide backup power supply to MEG regeneration process to carry out shut down operation during main power failure. Avoid operating during extreme weather conditions. | | Minor | Unlikely | Low Risk | Regular and scheduled power consumption audits to be conducted. Check for limit and possible overloads on power circuits. Contact Curtin electrical technicians, for faults and emergencies, call Western Power 13 13 51 |
| 1.3 | Electrical short | Overload the power supply, wet condition, human mistake, exposed live wires | Short circuit, personal injury due to electrocution | | Moderate | Unlikely | Medium risk | Surge protectors, fuses, circuit breakers. Curtin's policy and procedures for electrical safety issues. | | Minor | Unlikely | Low risk | Never overload circuits, never operate equipment with wet hands, ensure no exposed live wires |

| No. | Hazard | Cause | Consequence | Severity | Likelihood | Risk | Control Measures | Severity | Likelihood | Risk | Recommendations |
|---|---|---|---|---|---|---|---|---|---|---|---|
| 1.4 | Utility failure | Failure of Utilities pumps, Failure of utilities valves and control system, empty N2 gas cylinders. | Abnormal operating conditions, Loss of Blanketing gas , Loss of feed. | Minor | Unlikely | Low Risk | Safety and redundancy barriers to be implemented for all utilities and associated equipment | Minor | Unlikely | Low Risk | Check for operating ranges for equipment pumps and valves etc. Develop Gas cylinder replacing schedule |
| 1.5 | Equipment failure | Power failure. Faulty equipment, error in design. Human error, Abnormal operating conditions | Deviation from normal operating conditions Personal injury, MEG spillage, Shutdown. | Moderate | likely | Significant Risk | Develop safe work procedure, automatic Emergency shutdown. Only authorized personnel to operate equipment. Annual inspection and certification. | Minor | Unlikely | Low Risk | Checking the maximum lifetime for each equipment (pumps and valves). Regular test of emergency shutdown button |
| 1.6 | Leak-gas (Condensate Vapour, $CO_2$,$N_2$) | Loss in integrity of, piping, seals, equipment's component and valves. Human error, overpressure. | Risk of fire, Personal injury, Deviation from normal operating conditions. | Moderate | Unlikely | Medium Risk | Monitoring system for leak detection, Condensate vapour detector on top section of distillation system . | Minor | Unlikely | Low Risk | Carry our pressure test and validation certificates from vendors. Ensure the workplace is adequately ventilated |
| 1.7 | Chemical Spillage- liquid | Overfill the tank, broken drain valve, leakage in piping component, human mistake | Fire risk, skin irritation if come in contact | Moderate | Unlikely | Medium risk | High level alarm, personal protective equipment. Spillage containment strategies- Strategic use of individual equipment crates to contain spillage. | Minor | Unlikely | Low risk | Ensure spillage kit and power water wash is available. Use absorbent such as soil, sand or other inert material to cover the spill, or just water wash |
| 1.8 | Overpressure | Pressure build up due to Blocked upper section of DC-201 | System overpressure, explosion DC-201, Personal injury, loss of equipment | Moderate | Possible | Significant Risk | Pressure relief valve (SV-B2) , Pressure Alarm in upper DC-201 | Moderate | Unlikely | Medium Risk | Regular inspection and maintenance of equipment for upper pipe DC-201 |
| 1.9 | High temperature | Low level in RB-201. Loss of control of temperature. Extreme weather conditions | Fire risk , Deviation from normal operating conditions, , Personal injury | Moderate | Possible | Significant Risk | Monitor temperature of bulk fluid in RB-201, High temperature alarm on RB-201and emergency shutdown of heating source | Moderate | Unlikely | Medium Risk | Check Control system function and set alarm temperatures accordingly |

| | | | | | | | | | | | |
|---|---|---|---|---|---|---|---|---|---|---|---|
| 2.0 | Area emergency | Fire and weather condition which prevent from work normally, surrounding equipment failure such as gas cylinder used by other labs. always traffic in this area to transfer the equipment labs | Personal injury, loss of equipment | | Moderate | Possible | **Significant Risk** | Maintain sufficient distance from other gas N2 cylinder. Assign safety champion, carry mock drills for emergency situations. Safety training for all operators. Fire extinguisher, Personal protective equipment | Moderate | Unlikely | **Medium Risk** | Ensure a clear access for emergency evacuation. Inform personnel for evacuation. Shutdown all electrical. easy to supply equipment to the project |
| 2.1 | Operator risk | Trip hazards ,Chemical Spill, Gas Leak, Equipment Failure, Extreme weather Conditions | Personal injury | | Moderate | likely | **Significant Risk** | Training of operators. Hazard notification and symbols , Safety training, Personal protective equipment | Moderate | Unlikely | **Medium Risk** | Ensure operators are trained and qualified for operation |
| 2.2 | Pumps | Failure of pump , Cavitation, Operator error: Pump not turn off after the experiment, suction valve closed to the pump | Pump failure | | Minor | Possible | **Medium risk** | Safe work procedures, Safety barriers and Regular inspections. | Minor | Unlikely | **Low risk** | Accommodate for pump failure scenarios in safe work procedures. Sufficient training for operators |

Appendix.6: Operational Hazop for Distillation Column

| Operational Hazop - Area 300 - (Refer P&ID MPP-300-B) | | | | | | | | | | | | | |
|---|---|---|---|---|---|---|---|---|---|---|---|---|---|
| **Description**<br>**From STORGE TANK-201 TO FEED DISTILLATION COLUMN DC-201**<br><br>**The column utilizes structured packing to carry out the separation of MEG and water. Rich MEG is distilled by removing water as the overhead product and lean MEG (>85 wt. %) is collected as bottom product. For versatility and ease in operations, electric immersion heating element has been chosen for the heating requirements in the Re-boiler**<br>**Design Intent:** | | | | | | | | | **Documentation:**<br><br>**Equipments:**<br><br>Rich MEG tank, MEG Distillation column, MEG Reboiler, overhead condenser, reflux drum and associated equipment | | | | |

| Ite m N° | Deviation | Causes | Consequences | Inherent Risk | | | | Safeguards | Residual Risk | | | | Recommend ations |
|---|---|---|---|---|---|---|---|---|---|---|---|---|---|
| | | | | Cat | Con | Li | Risk | | Ca t | Con | Li | Risk | |
| 1.1 | No Flow | Failure of P-B1 | Flooding in (ST) tank, High temperature in theRB-201 | | moderate | possible | significant | Install flow and indicators, Install low flow and low level alarms, Regular inspection and maintenance of valves | | Insignificant | Unlikely | Low Risk | shutdown in RB-201 |
| | | Failure of V-B8 | | | moderate | possible | significant | Install flow and indicators, Install low flow and low level alarms, Regular inspection and maintenance of valves | | Insignificant | Unlikely | Low Risk | = |
| | | Failure of P-B2 | No top product, Damage in the RD-201, High level | | Minor | possible | Medium risk | Install flow and indicators, Install low flow and low level alarms, Regular inspection and maintenance of valves | | Insignificant | Unlikely | Low Risk | = |
| | | Failure of V-B13 | | | Minor | possible | Medium risk | Install flow and indicators, Install low flow and low level alarms, Regular inspection and maintenance of valves | | Insignificant | Unlikely | Low Risk | = |

| 1.2 | More Flow | Faulty of V-B8 | column overload , Reducing Re-Boiler efficiency, Over feed in DC-201, Possible flooding in column | | Minor | possible | Medium risk | 'Install flow and indicators, 'Install high flow and high level alarms, 'Regular inspection and maintenance of valves | | Insignificant | Unlikely | Low Risk | Check the valves |
|---|---|---|---|---|---|---|---|---|---|---|---|---|---|
| | | Faulty of V-B13 | | | Minor | possible | Medium risk | = | | Insignificant | Unlikely | Low Risk | |
| 1.3 | Less Flow | Mis operation of P-B1 | *Reduce the production rate , High temperature in theRB-201 | | moderate | possible | significant | 'Install flow and indicators, Install low flow and low level alarms, Regular inspection and check flow indicator maintenance of valves | | Insignificant | Unlikely | Low Risk | . |
| | | Mis operation of V-B8 | Damage in pump P-B1, Reduce the production rate , High temperature in the RB-201 | | moderate | possible | significant | = | | Insignificant | Unlikely | Low Risk | Shutdown in RB-201 |
| | | Mis operation of P-B2 | *Reducing efficiency of DC-201, High temperature in theRB-201, Damage in the RD-201 | | moderate | possible | significant | = | | Insignificant | Unlikely | Low Risk | |
| | | Mis operation f V-B13 | Reducing efficiency of DC-201, High temperature in theRB-201, Damage in the RD-201 | | moderate | possible | significant | = | | Insignificant | Unlikely | Low Risk | |
| 1.4 | Reverse Flow | N/A | | | | | | | | | | | |
| 1.5 | Mis-Directed Flow | N/A | | | | | | | | | | | |
| 1.6 | More/High Temperature | Problem in RB -201, Problem in CO-201 | Degradation of MEG, Less efficiency, Reducing CO-201 efficiency, | | moderate | Possible | significant | Install high temperature alarm | | Insignificant | Unlikely | Low Risk | Reduce the RB-201 duty |
| | | Low level in RB-201 | = | | moderate | Possible | significant | Regular inspection and maintenance to the condenser and re-boiler | | Insignificant | Unlikely | Low Risk | = |
| | | Failure of RB-201, leak, Pipe | off specs product, Reducing vapour in | | Minor | Possible | | Install low temperature alarm, | | Insignificant | Unlikely | Low Risk | |

| | | | | | | | | | | | | |
|---|---|---|---|---|---|---|---|---|---|---|---|---|
| 1.7 | Less/Low Temperature | Rupture, Failure of CO-201 | DC-201, Less separation | | | | Medium Risk | Regular inspection and maintenance to the condenser and re-boiler | | | Low Risk | |
| 1.8 | More/High Pressure | Top stream blockage | Column over pressure and explode | Major | Possible | High risk | Regular inspection and maintenance of DC--201 | Insignificant | Unlikely | Low Risk | |
| | | Increase in column vapour | off specs product, deviation from normal operating conditions | Minor | Possible | Medium Risk | High pressure relieve valve in outlet of DC-201 Check PDI | Insignificant | Unlikely | Low Risk | |
| | | Overfed of N2 due to faulty V-B2, V-B3 | ST-201 will crack | Minor | Possible | Medium Risk | Install pressure gauge, high pressure alarm and pressure relief valve, check PDI,PAL | Insignificant | Unlikely | Low Risk | |
| 1.9 | Less/Low Pressure | N/A | | | | | | | | | | |
| 1.10 | High level | Mis operation of P-B1 | Flooding in DC-201, Low Temperature, Less efficiency | Minor | Possible | Medium Risk | Regular checking and maintenance | Insignificant | Unlikely | Low Risk | Shutdown in RB-201, Open drain in RB-201, |
| | | Failure of RB-201 | off specs product | Minor | Possible | Medium Risk | Install high flow and high level alarms | Insignificant | Unlikely | Low Risk | = |
| | | Mis operation of CO-201 | Distillation flow rate decreases, off spec product | Minor | Possible | Medium Risk | Regular inspection and maintenance of CO-201 | Insignificant | Unlikely | Low Risk | = |
| | | Blockage in the outlet MEG in RB-201 | Flooding in DC-201 | Minor | Possible | Medium Risk | Regular inspection and maintenance of valves in RB-201 | Insignificant | Unlikely | Low Risk | = |
| 1.11 | Less Level | Failure in P-B1 pipe rupture, leak | off specs product, High Temperature in DC-201& RB-201, less production | moderate | Possible | significant | Install flow and indicators, Install low flow and low level alarms, Regular inspection and maintenance | Insignificant | Unlikely | Low Risk | |
| | | Column leakage | | | | | | | | | |
| | | Failure of CO-201 low feed flow rate | | | | | | | | | |
| 1.12 | Wrong Concentration | N/A | | | | | | | | | | |
| 1.13 | Contamination | N/A | | | | | | | | | | |
| 1.14 | | Human mistake | Loss of operation, personal injury | Major | Possible | Medium Risk | PPE, always follow work procedures | Insignificant | Unlikely | Low Risk | |

| | | Start-up/ Shutdown Hazards | | | | | | | | | | | | |
|---|---|---|---|---|---|---|---|---|---|---|---|---|---|---|
| 1.1 5 | Total power failure | Bad weather, electrical problems | Loss of operation | | insignifica nt | Possible | Low Risk | Regular check operator | | Insignificant | Unlikely | Low Risk | | |
| 1.1 6 | Noise | Operation of pumps, venting | ear injury | | Minor | likely | significant | PPE, follow work procedures | | Insignificant | Unlikely | Low Risk | Terminate operation |

Appendix.7: Environmental Impact Analysis (EIA) of MEG pilot plant

| Type of impact | Definition | Corresponding table colour |
|---|---|---|
| Short term impact | Temporary, likely to occur during construction phase (based on approximates construction time of 12-24 hours. These impacts and their associated effects are expected to no longer exist once construction and assembly are complete | Green |
| Long term impact | Likely to occur frequently, or in sustained manner for certain durations over course of plant's life, as result of activities and operations associated with plant | Yellow |
| Permanent impact | Impacts that cause permanent/irreversible damage to environment surrounding plant, seen well after plant is in-operational | Red |

| Aspect evaluated | Activities likely to cause impact | Aspect impacted | Mitigation strategy |
|---|---|---|---|
| Initial construction activities Facilities and associated preparation and construction | Site preparation, construction of wastewater, waste chemicals management system Rigging of pipe racks, equipment, pipeline installation and construction | Disturbance to flora/fauna around designated area, hazard due to moving cranes, forklifts, welding, electrical wires | Selective placement of activities so it does not disturb surrounding flora/fauna. Proper isolation of location for construction work. Use of good site practices and traffic management plans designed in accordance with the Main Roads Western Australia Traffic Management for Works on Roads Code of Practice Section 5.2 |
| Site Utilities<br><br>Compressed gas cylinders<br><br>Cooling water system<br><br>Hot glycol system<br><br>Wastewater management system | High pressure gas from BOC cylinders<br><br>The cooling of water to be generated using onsite chiller.<br><br>High temperature glycol at MEG rebolier.<br><br>Potential wastewater discharge containing chemicals | Associated toxic gas emissions due to leaks, mis-operation. Localized temperature increase due to heat emission | Ensure lab personnel are well trained by BOC GasCare (compressed gas training)<br><br>Ensure adequate air ventilation and use of good working procedures.<br><br>Use of spill pallets to contain chemical spills.<br><br>Follow waste management plan and ensure chemicals are appropriately disposed. |
| Pipelines | Pipeline installation, pressure leak testing using inert gas | Potential noise due to leaks | Ensure lab personnel are well trained by Swagelok Tube Fitting and Installation Training. |
| Housing | Any solid waste such as used containers, plastic bags, papers, dry leaves and tree branches | Improper disposal could result in impact to flora/fauna, blockage of sewage system, unhygienic working environment to lab personnel. Flammable items might catch fire due to extreme weather. | Maintain clean and cluster free environment. Implement and follow housing rules. Carry out timely inspections and carry out cleans up if necessary. |
| Air quality | Associate emissions ( light hydrocarbons , Carbon dioxide, Glycol Vapour/mist ) | Air quality around designated area and potential flammable gas emissions | Sufficient height shall be provided for all venting lines. Emission of toxic gas fumes shall be monitored and handled according to safety hazards. |
| Noise level | Equipment which consist of moving parts such as pumps. Vibration of pipelines due to flowing of gas and liquids. Daily operation activities such as hammering, drilling, moving gas cylinders, etc | Noise level around designated area and potential impact to human hearing system | Always ensure ear protection equipment is available and other personal protective equipment. |

Appendices.8: Recovery of mono-ethylene glycol

https://www.sciencedirect.com/science/article/pii/S1875510017301762

# Recovery of mono-ethylene glycol by distillation and the impact of dissolved salts evaluated through simulation of field data

Sami Zaboon*, Adam Soames, Varun Ghodkay, Rolf Gubner, Ahmed Barifcani

*Chemical Engineering Department, Curtin University of Technology, Perth, W.A, Australia*

**ABSTRACT**

This study was conducted to investigate the operation of a packed distillation column and analyse its performance during the separation of mono-ethylene glycol from water. The column was designed and constructed by the Curtin Corrosion Engineering Industry Centre (CCEIC) and operated in collaboration with a reputable oil company to generate experimental field data. A secondary investigation was then performed into the impacts of dissolved salts within the rich MEG feed upon the purity of the lean MEG product. It was observed through application of the FUG shortcut distillation design equations that six equilibrium stages were required to attain the experimental separations reported under continuous operation of the column. It was further determined that the packing utilised within the column had a Height Equivalent to a Theoretical Plate (HETP) of approximately 0.34 m when no dissolved salts were present corresponding to an estimated packing height of approximately 1.7 m.

The impact of dissolved salts upon the performance of the column was evident through lower lean MEG purities observed during experimental operation of the column in comparison to salt free trials. The reduction in column performance was reaffirmed by Aspen HYSYS and Aspen Plus simulations of the field data, where salt trials resulted in lean MEG purities noticeably less than corresponding salt free experimental trials and simulated predictions. Overall, it was observed that the presence of dissolved salts during operation led to a reduction in MEG mass fraction of the final lean MEG product by on average 7.2%. The impact of dissolved salts on lean MEG purity was successfully predicted by Aspen Plus simulation with an average accuracy of 1.61% through the inclusion of monovalent salt cations using the ELECNRTL equation of state with modified binary parameters. The reduction in lean MEG purity was attributed to boiling point elevation of the MEG-Water solution and the impact of the dissolved salts on the systems vapour liquid equilibrium.

© 2017 Elsevier B.V. All rights reserved.

## 1. Introduction

Mono-ethylene glycol (MEG) is an important raw material having numerous research and industrial applications, one such example is its application as a hydrate inhibitor in the hydrocarbon processing industry (Lu et al., 2010). MEG is one of the most favoured thermodynamic hydrate inhibitors used in hydrocarbon transportation pipelines and processing facilities due to its low volatility, low toxicity, low flammability, favourable thermodynamic behaviour, simple and proven technology requirements and high availability (Bikkina et al., 2012; Haque, 2012). Furthermore, the preference for using MEG over other traditional thermodynamic hydrate inhibitors such as methanol stems from several operational, environmental and safety issues imposed by the use of methanol and MEG's ability to be effectively recovered, regenerated and reused (AlHarooni et al., 2015; Haghighi et al., 2009). Due to the high cost of MEG and significant volumes required to provide effective hydrate control, following the hydrate inhibition process it is essential to separate MEG from the produced water so that it can be recycled and reused to minimize operating costs.

The most prevalent MEG recovery methods have been broadly categorised into two main process types, (i) reconcentration and (ii) regeneration (Bikkina et al., 2012). The reconcentration process is the most basic MEG recovery method and is comprised of a simple distillation column where the water rich MEG is concentrated to form lean MEG by vaporisation of the excess water. Typically, the distillation column is operated to regain a MEG purity within the

* Corresponding author.
  *E-mail address:* s.zaboon@postgrad.curtin.edu.au (S. Zaboon).

225

Appendices.9: Removal of monoethylene glycol from wastewater

https://www.sciencedirect.com/science/article/pii/S0021979718303400
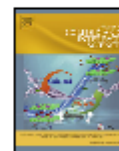
Regular Article

# Removal of monoethylene glycol from wastewater by using Zr-metal organic frameworks ☆
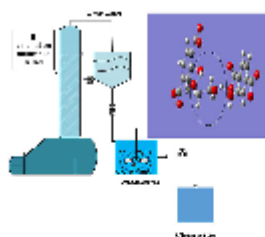
Sami Zaboon[a], Hussein Rasool Abid[a,b,*], Zhengxin Yao[a], Rolf Gubner[a], Shaobin Wang[a], Ahmed Barifcani[a]

[a] Department of Chemical Engineering, Curtin University, GPO Box U1987, Perth, WA 6845, Australia
[b] Environmental Health Department, Faculty of Applied Medical Science, University of Kerbala, Karbala, Iraq

GRAPHICAL ABSTRACT

ABSTRACT

Mono-ethylene glycol (MEG), used in the oil and gas industries as a gas hydrate inhibitor, is a hazardous chemical present in wastewater from those processes. Metal-organic frameworks (MOFs) (modified UiO-66* and UiO-66-2OH) were used for the effective removal of MEG waste from effluents of distillation columns (MEG recovery units). Batch contact adsorption method was used to study the adsorption behavior toward these types of MOFs. Adsorption experiments showed that these MOFs had very high affinity toward MEG. Significant adsorption capacity was demonstrated on UiO-66-2OH and modified UiO-66 at 1000 mg·g$^{-1}$ and 800 mg·g$^{-1}$ respectively. The adsorption kinetics were fitted to a pseudo first-order model. UiO-66-2OH showed a higher adsorption capacity due to the presence of hydroxyl groups in its structure. A Langmuir model gave the best fitting for isotherm of experimental data at pH = 7.
© 2018 Elsevier Inc. All rights reserved.

## 1. Introduction

Natural resources have become a hot topic in current scientific research, in an effort to maintain and preserve the Earth's environment for continued human life [1,2]. In this regard, petroleum pollution is a major global problem [3]. Mono-ethylene glycol (MEG) is a petroleum pollutant, which is a colorless, odorless, and slightly viscous liquid, more hygroscopic than glycerol and miscible with water in all proportions [4,5]. The US Environmental Protection Agency has established a standard of less than 7 mg L$^{-1}$ of MEG in drinking water [6,7]. MEG can cause damage to the kidneys or death at high accumulated concentrations [8]. Natural gas processing produces ethylene glycol-containing wastewater and consequently increases the chemical oxygen demand (COD) in water [9]. Removal of MEG from contaminated water is thus an important consideration in the design of operation units in the petroleum industry [10].
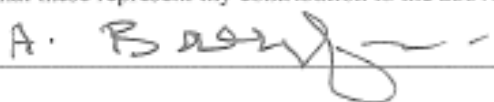
# Appendices.10: Attribution of Authorship

Paper: "Recovery of mono-ethylene glycol by distillation and the impact of dissolved salts evaluated through simulation of field data" Journal of Natural Gas Science and Engineering, 44, 214-232.

Authors and full affiliations: Sami Zaboona[a,b], Adam Soames[a], Varun Ghodkay[a], Rolf Gubner[a], Ahmed Barifcani[a]

[a] WA School of Mines: Minerals, Energy and Chemical Engineering, Curtin University, Bentley Western Australia 6102, Australia

[b] University of Baghdad, college of Engineering, Department of Chemical engineering, Baghdad, Iraq.

| | Conception and design | Acquisition of data and method | Data conditioning and manipulation | Analysis and statistical method | Interpretation and discussion | Final approval |
|---|---|---|---|---|---|---|
| Adam Soames | * | | | | | |
| I acknowledge that these represent my contribution to the above research output. | | | | | | |
| Varun Ghodkay | | * | | | | |
| I acknowledge that these represent my contribution to the above research output. | | | | | | |
| Rolf Gubner | | | | | | * |
| I acknowledge that these represent my contribution to the above research output. | | | | | | |
| Dr. Ahmed Barifcani | * | | | | | * |
| I acknowledge that these represent my contribution to the above research output. Signature: | | | | | | |

# Appendices.11: Attribution of Authorship

Paper: "Removal of monoethylene glycol from wastewater by using Zr-metal organic frameworks" Journal of Colloid and Interface Science, 523, 75-85.

Authors and full affiliations: Sami Zaboona[a,b], Hussein Rasool Abid[a,c], Zhengxin Yao[a], Rolf Gubner[a], Shaobin Wang[a], Ahmed Barifcani[a]

[a] WA School of Mines: Minerals, Energy and Chemical Engineering, Curtin University, Bentley Western Australia 6102, Australia

[b] University of Baghdad, college of Engineering, Department of Chemical engineering, Baghdad, Iraq.

[c] Environmental Health Department, Faculty of Applied Medical Science, University of Kerbala, Karbala, Iraq

| | Conception and design | Acquisition of data and method | Data conditioning and manipulation | Analysis and statistical method | Interpretation and discussion | Final approval |
|---|---|---|---|---|---|---|
| Hussein Rasool Abid | | | | * | * | |
| I acknowledge that these represent my contribution to the above research output. | | | | | | |
| Zhengxin Yao | * | | | | | |
| I acknowledge that these represent my contribution to the above research output. | | | | | | |
| Rolf Gubner | | | | | | * |
| I acknowledge that these represent my contribution to the above research output. | | | | | | |
| Shaobin Wang | | | | | | * |
| I acknowledge that these represent my contribution to the above research output. | | | | | | |
| Dr. Ahmed Barifcani | * | | | | | * |
| I acknowledge that these represent my contribution to the above research output. | | | | | | |
| Signature: A. Barif___ | | | | | | |